

**Nature's Hidden Code:
Unraveling Hydrogen Isotope
Fractionation in Plant Carbohydrates**

Philipp Schuler

**Dissertation for the degree of Doctor of
Sciences**

Diss. ETH No. 29511



ETH zürich

DISS. ETH NO. 29511

**NATURE'S HIDDEN CODE: UNRAVELING
HYDROGEN ISOTOPE FRACTIONATION IN
PLANT CARBOHYDRATES**

A thesis submitted to attain the degree of
DOCTOR OF SCIENCES
(Dr. sc. ETH Zurich)

presented by
PHILIPP SCHULER

M. Sc. in Environmental Geosciences, University of Basel

Born on 29 October 1986

Accepted on the recommendation of
Prof. Dr. Nina Buchmann
Dr. Marco M. Lehmann
Prof. Dr. Arthur Gessler
Prof. Dr. James Ehleringer

2024

“After all, science is essentially international, and it is only through lack of the historical sense that national qualities have been attributed to it.”

Marie Curie

Content

Abstract.....	1
Zusammenfassung	5
Chapter 1.....	9
Introduction	9
Isotopes: General information.....	9
Stable isotopes in time and space	10
The isotopes of hydrogen.....	11
Current knowledge of hydrogen isotope fractionation in plants	11
Thesis objectives.....	13
Thesis outline.....	13
Contribution to the studies	15
References.....	16
Chapter 2.....	21
A high-temperature water vapor equilibration method to determine non-exchangeable hydrogen isotope ratios of sugar, starch and cellulose	21
Abstract.....	22
Introduction	23
Materials and methods	25
Cellulose, starch, and sugar standards	25
Plant species, growing conditions, and sampling	26

Cellulose and starch nitration, and isotopic analysis of the nitrated products	27
Preparation of leaf cellulose and NSC for $\delta^2\text{H}_{\text{ne}}$ analysis.....	28
$\delta^2\text{H}_{\text{ne}}$ analysis of cellulose and NSC using a hot water vapor equilibration method.....	29
Calculation of non-exchangeable hydrogen isotope ratio ($\delta^2\text{H}_{\text{ne}}$).....	31
Results and Discussion.....	32
A hot water vapor equilibration method for determining $\delta^2\text{H}_{\text{ne}}$ of sugar, starch, and cellulose.....	32
Application of the method for analysis of $\delta^2\text{H}_{\text{ne}}$ in plant-derived compounds	36
Acknowledgements	41
References.....	41
Supporting Information.....	51
Chapter 3.....	57
Hydrogen isotope fractionation in carbohydrates of leaves and xylem tissues follows distinct phylogenetic patterns: A common garden experiment with 73 tree and shrub species	57
Abstract.....	58
Introduction	59
Materials and methods	63
Site description.....	63
Sampling of plant material	64
Extraction of leaf and twig water, cellulose and sugars	64
$\delta^2\text{H}$ analysis of twig xylem water ($\delta^2\text{H}_{\text{xw}}$) and leaf water ($\delta^2\text{H}_{\text{LW}}$).....	65
$\delta^2\text{H}_{\text{ne}}$ analyses of sugars and cellulose using a hot water vapor equilibration method.....	65

Calculation of the non-exchangeable hydrogen isotope ratio ($\delta^2\text{H}_{\text{ne}}$), ϵ_{HA} and ϵ_{HE}	67
Statistical analyses	68
Results	69
$\delta^2\text{H}$ of plant water and carbohydrates in angiosperms and gymnosperms	69
Relationship between $\delta^2\text{H}$ of plant water and carbohydrates	72
Phylogenetic analysis of the observed $\delta^2\text{H}$ patterns	74
Discussion	79
Phylogenetic pattern in the $\delta^2\text{H}_{\text{ne}}$ of plant carbohydrates, ϵ_{HA} and ϵ_{HE}	79
Potential drivers of autotrophic and heterotrophic ^2H fractionation	82
^2H fractionation as a proxy for plants' metabolic properties	86
Conclusion	86
Acknowledgements	87
Author contributions	87
References	88
Supporting Information	98
Chapter 4	111
Hydrogen isotope fractionation in plants with C_3 , C_4 , and CAM CO_2 fixation	111
Abstract	112
Introduction	112
Materials and methods	117
Growing conditions, and sampling of leaf material	117
Extraction of leaf water, sugars, and cellulose	118
$\delta^2\text{H}$ analysis of leaf water	119

$\delta^2\text{H}$ analysis of sugar and cellulose using a hot water vapor equilibration method.....	119
Calculation of the isotope ratio ($\delta^2\text{H}$).....	121
Statistical analyses	123
Results.....	123
General patterns of ^2H fractionation within and between plants with C_3 , C_4 , and CAM CO_2 fixation.....	123
Species specific $\delta^2\text{H}$ response to changes in temperature and VPD.....	129
Drivers of the observed $\delta^2\text{H}$ values and ^2H fractionation factors	136
Discussion.....	138
The biochemical drivers of autotrophic ^2H fractionation among C_3 , C_4 and CAM CO_2 fixation	138
Patterns and drivers of the heterotrophic ^2H fractionation ϵ_{H}	145
Compound specific ^2H response to changes in temperature and VPD is highly species specific.....	147
Conclusions.....	148
Acknowledgements	148
References.....	148
Supporting Information.....	158
Chapter 5.....	167
Hot and Hungry: High temperatures induced carbohydrate depletion in leaves - insights from triple isotope fractionations	167
Abstract.....	168
Main.....	169
Results.....	173

Temperature response of the leaf gas exchange and the functioning of PSII	173
Changes in non-structural carbohydrate concentration in response to rising temperatures	177
The triple isotope response to rising temperature.....	179
Drivers underlying the temperature-induced changes in the apparent ^{13}C , ^{18}O , and ^2H fractionation.....	181
Discussion.....	187
Methods.....	191
Experimental design and plant growing conditions	191
Measurement of CO_2 and $\delta^{13}\text{CO}_2$	192
Plant physiological measurements	192
Sampling of plant material	193
Extraction of leaf water and sugars	193
$\delta^2\text{H}$ and $\delta^{18}\text{O}$ analyses of leaf water ($\delta^2\text{H}_{\text{LW}}$ and $\delta^{18}\text{O}_{\text{LW}}$).....	194
$\delta^2\text{H}$ analyses of sugars and cellulose using a hot water vapor equilibration method.....	194
Calculation of the non-exchangeable hydrogen isotope ratio ($\delta^2\text{H}_{\text{ne}}$), ϵ_{HA} and ϵ_{HE}	195
Leaf-level non-structural carbohydrates analysis	197
Statistical analyses	198
References.....	198
Supporting Information.....	206
Chapter 6.....	226
General discussion	226

The ^2H fractionation during CO_2 fixation ϵ_{HA} is driven by enzymatic reactions, reflects the phylogeny of trees and shrubs, and varies between different types of CO_2 fixation.....	227
The post-photosynthetic ^2H fractionation in carbohydrates	228
Outlook.....	228
References	229
Acknowledgements	231
Curriculum Vitae	235

Abstract

Measuring the fractionation of stable isotopes in organic compounds can provide information on various physical, biochemical and plant physiological processes during their formation. This can be particularly useful, for example, when climatic information of a particular area is lacking, or to track water, nutrient and carbon fluxes within an organism or even an entire ecosystem. However, in order to correctly interpret the measured isotope values, it is necessary to unveil the drivers behind the isotope fractionation.

Deuterium (^2H ; D), the heavier isotope of hydrogen, contains a neutron in addition to the proton in its nucleus, unlike the main hydrogen isotope protium (^1H). This almost doubles its mass and affects several other properties of this element and its ion (H^+). For example, the bond energy of the O–H bond in H_2O is lower than that of the corresponding O–D bond, and the bond length of O–H is greater than that of O–D. Thus, the bond of a water molecule containing deuterium is more stable, and D_2O is more viscous than H_2O . Deuterium slows down biochemical reactions. If 25% of an animal's body water is replaced with D_2H , it may become sterile and eventually die from cytotoxic syndrome if 50% of its body water is replaced with D_2H .

It is clear, therefore, that various biological, enzyme-driven ^2H fractionation processes take place that shape the hydrogen isotope composition we find in plant organic compounds such as sugars and cellulose. However, due to the complexity of the carbohydrate metabolism of plants, it is necessary to study various aspects, such as CO_2 fixation, respiration and cellulose synthesis, to unravel the different drivers and their interaction with the environment. This requires the analysis of many samples, which has been a major bottleneck in gaining a deeper understanding of hydrogen isotope fractionation. This is where my doctoral thesis comes in.

In **Chapter 1**, I present the background and previous knowledge on isotope fractionation in general and more specifically on hydrogen isotope fractionation in plant carbohydrates.

In **Chapter 2** I describe the high-throughput water vapor equilibration method developed to accurately measure the carbon-bound, non-exchangeable hydrogen isotope composition of cellulose, starch and sugars. This was necessary because only this hydrogen carries information about the conditions during the synthesis of the compound, while the exchangeable oxygen-bound hydrogen is constantly exchanging with hydrogen from the surrounding water.

Being now able to analyse a large enough number of samples, I conducted a study in **Chapter 3** to determine if we could detect a phylogenetic pattern behind the hydrogen isotope fractionation in leaf water, leaf sugars and twig xylem cellulose. I chose this unusual approach to investigate the level of complexity behind ^2H fractionation: a strong phylogenetic pattern would indicate a relatively simple, probably monocausal, enzymatic driver, whereas a reduced or absent phylogenetic pattern would suggest more complex causes involving multiple factors. Through my research, I have shown that the strong phylogenetic pattern observed in leaf sugars indicates a relatively simple underlying ^2H fractionation process, whereas the reduced phylogenetic pattern in twig xylem cellulose indicates more complex ^2H fractionation processes.

In **Chapter 4**, I used a climate chamber experiment to investigate the differences in ^2H fractionation from leaf water to leaf sugars of plants with C_3 , C_4 and CAM CO_2 fixation, how this signal is transferred from leaf sugars to leaf cellulose, and how this is affected by changes in temperature and vapour pressure deficit (VPD) of the air. By comparing these three types of CO_2 fixation, I was able to narrow down the possible biochemical reaction behind the observed photosynthetic ^2H fractionation. I showed that the heterotrophic ^2H enrichment from sugar to cellulose in C_3 plants cannot be caused by isotope exchange with source water during cellulose synthesis.

In addition, I showed that the climate response of ^2H fractionation differs in different C_3 and CAM plant species, indicating drivers that respond species-specific to the environment.

By stressing seven plant species with temperatures ranging from 10 °C to 40 °C under constant VPD in **Chapter 5**, I was able to identify the physiological drivers behind the apparent ^2H fractionation between leaf sugar and leaf water. In order to obtain a complete picture of the plant physiological temperature response and how this is reflected in the isotopic composition of leaf sugars, I also measured the leaf sugar carbon ($\delta^{13}\text{C}$) and oxygen ($\delta^{18}\text{O}$) isotopic composition, as well as gas exchange, chlorophyll fluorescence and non-structural carbohydrates. I was able to show that the ^2H fractionation is driven by the carbohydrate balance of a C_3 leaf, as C_3 CO_2 fixation is leading to highly ^2H depleted sugars, while a temperature-driven increase in respiration enriches the remaining sugar pool with ^2H by preferentially respiring ^2H depleted sugars.

In **chapter 6** I summarise the achievements of the last four years: We now have a method to accurately measure the $\delta^2\text{H}$ of all plant carbohydrates. My thesis has revealed two main drivers of the biochemical ^2H fractionation processes in plants with C_3 , C_4 and CAM CO_2 fixation. More specifically, this thesis has uncovered the photosynthetic ^2H depletion in C_3 leaves, which is species-specific and probably occurs in a process associated with thylakoids in chloroplasts, and the respiratory ^2H enrichment. The latter could result from a preferential respiratory uptake of sugars with the lighter ^1H isotope, leading to a ^2H enrichment in the remaining sugar pool. This knowledge will enable the scientific community to understand and interpret the measured $\delta^2\text{H}$ of plant carbohydrates. For example, ^2H enrichment in tree-rings may indicate a decrease in net primary production due to an increase in respiration relative to the gross photosynthesis. However, this is likely to be species-specific, reflecting, for example, the ability of a plant species to acclimate to higher temperatures or different light conditions.

Further studies are needed to explore how these ^2H -enriching respiratory processes operate over time and in different tissues, such as the carbohydrate pools of stems and roots, and to investigate potential additional physiological and metabolic processes involved in ^2H fractionation in plants.

Zusammenfassung

Die Messung der Fraktionierung stabiler Isotope in organischen Verbindungen kann uns Aufschluss über verschiedene physikalische, biochemische und pflanzenphysiologische Prozesse während ihrer Entstehung geben. Dies kann besonders nützlich sein, wenn z. B. klimatische Informationen für ein bestimmtes Gebiet fehlen oder um Wasser-, Nährstoff- oder Kohlenstoffflüsse innerhalb eines Organismus oder sogar eines ganzen Ökosystems zu verfolgen. Um die gemessenen Isotopenwerte richtig zu interpretieren, müssen jedoch zunächst die Ursachen für die Isotopenfraktionierung entschlüsselt werden.

Deuterium (^2H ; D), das schwerere Wasserstoffisotop, enthält im Gegensatz zum Hauptwasserstoffisotop Protium (^1H) zusätzlich zum Proton ein Neutron in seinem Kern. Dies führt zu einer annähernden Verdoppelung seiner Masse und wirkt sich auf verschiedene andere Eigenschaften dieses Elements und seines Ions (H^+) aus. So ist beispielsweise die Bindungsenergie der O-H-Bindung in H_2O niedriger als die Bindungsenergie der entsprechenden O-D-Bindung, und die Bindungslänge von O-H ist größer als die von O-D. Daher ist die Bindung eines Wassermoleküls, das Deuterium enthält, stabiler, und D_2O ist zähflüssiger als H_2O . Deuterium verlangsamt biochemische Reaktionen. Wenn 25 % des Körperwassers eines Tieres durch D_2H ersetzt wird, kann es steril werden, und wenn 50 % des Körperwassers durch D_2H ersetzt werden, stirbt es schließlich aufgrund des zytotoxischen Syndroms.

Es ist also klar, dass verschiedene biologische ^2H -Fraktionierungsprozesse an der Wasserstoffisotopenzusammensetzung beteiligt sind, die wir in organischen Pflanzenverbindungen wie Zucker und Zellulose finden. Aufgrund der Komplexität dieser Prozesse im Kohlenhydratstoffwechsel der Pflanzen müssen jedoch verschiedene Aspekte untersucht werden, z. B. die Photosynthese, die Atmung und die Zellulosesynthese, um die verschiedenen Faktoren und ihre Wechselwirkung mit der Umwelt zu entschlüsseln. Dies erfordert die Analyse vieler Proben, was bisher ein

Hauptengpass war, um ein tieferes Verständnis der Wasserstoffisotopenfraktionierung zu erlangen. Und an diesem Punkt kommt meine Doktorarbeit ins Spiel.

In **Kapitel 1** stelle ich den Hintergrund und das bisherige Wissen über die Isotopenfraktionierung im Allgemeinen und speziell über die Wasserstoffisotopenfraktionierung in Kohlenhydraten von Pflanzen vor.

In **Kapitel 2** beschreibe ich die Hochdurchsatz-Wasserdampf-Äquilibrierungsmethode, die entwickelt wurde, um die an Kohlenstoff gebundene, nicht austauschbare Wasserstoff-Isotopenzusammensetzung von Cellulose, Stärke und Zucker genau zu messen. Dies war notwendig, da nur dieser Wasserstoff die Information über die Bedingungen während der Synthese der Verbindung trägt, während der austauschbare, an Sauerstoff gebundene Wasserstoff ständig mit Wasserstoff aus dem umgebenden Wasser ausgetauscht wird.

Da ich nun in der Lage war, eine ausreichend große Anzahl von Proben zu analysieren, habe ich in **Kapitel 3** eine Studie durchgeführt, um festzustellen, ob sich hinter der Wasserstoffisotopenfraktionierung in Blattwasser, Blattsucker und Zweig-Xylem-Zellulose ein phylogenetisches Muster erkennen lässt. Ich wählte diesen ungewöhnlichen Ansatz, um den Grad der Komplexität hinter der ^2H -Fraktionierung zu untersuchen: Ein starkes phylogenetisches Muster würde auf eine relativ einfache, wahrscheinlich monokausale enzymatische Ursache hinweisen, während ein geringeres oder fehlendes phylogenetisches Muster auf komplexere Ursachen mit mehreren Faktoren hindeuten würde. Durch meine Forschung konnte ich nachweisen, dass das bei Blattsucker beobachtete starke phylogenetische Muster auf einen relativ einfachen zugrundeliegenden ^2H -Fraktionierungsprozess hindeutet, während das geringere phylogenetische Muster bei Zweig-Xylem-Zellulose auf komplexere ^2H -Fraktionsierungsprozesse hindeutet.

In **Kapitel 4** untersuchte ich in einem Klimakammerexperiment die Unterschiede in der ^2H -Fraktionierung von Blattwasser zu Blattsucker bei

Pflanzen mit C_3 -, C_4 - und CAM- CO_2 Fixierung, wie dieses photosynthetische Signal vom Blattzucker auf die Blattzellulose übertragen wird und wie dies durch Änderungen der Temperatur und des Dampfdruckdefizits (VPD) der Luft beeinflusst wird. Durch den Vergleich dieser drei Arten der CO_2 Fixierung konnte ich die mögliche biochemische Reaktion hinter der beobachteten photosynthetischen 2H -Fraktionierung eingrenzen. Zudem konnte ich zeigen, dass die heterotrophe 2H -Anreicherung von Zucker zu Zellulose in C_3 -Pflanzen nicht durch einen Isotopenaustausch mit dem Gewebewasser während der Zellulosesynthese verursacht werden kann. Darüber hinaus konnte ich zeigen, dass die Klima-Reaktion der 2H -Fraktionierung bei verschiedenen C_3 - und CAM-Pflanzenarten unterschiedlich ausfällt, was auf Faktoren hinweist, die artspezifisch auf die Umwelt reagieren.

Durch die Belastung von sieben Pflanzenarten mit Temperaturen zwischen $10\text{ }^\circ\text{C}$ und $40\text{ }^\circ\text{C}$ bei konstanter VPD in **Kapitel 5** war ich in der Lage, die pflanzenphysiologischen Triebkräfte hinter der scheinbaren 2H -Fraktionierung zwischen Blattzucker und Blattwasser zu ermitteln. Um ein vollständiges Bild der pflanzenphysiologischen Temperaturreaktion zu erhalten und wie sich diese in der Isotopenzusammensetzung des Blattzuckers widerspiegelt, habe ich auch Messungen der Isotopenzusammensetzung des Blattzuckers in Bezug auf Kohlenstoff ($\delta^{13}C$) und Sauerstoff ($\delta^{18}O$) sowie des Gasaustauschs, der Chlorophyllfluoreszenz und der nicht-strukturellen Kohlenhydrate einbezogen. Ich konnte zeigen, dass die 2H -Fraktionierung durch die Kohlenhydratbilanz eines C_3 -Blattes bestimmt wird, da die CO_2 Fixierung zu stark 2H -abgereichertem Zucker führt, während eine temperaturbedingte Zunahme der Atmung den verbleibenden Zuckerpool mit 2H anreichert, indem der 2H -abgereicherte Zucker bevorzugt veratmet wird.

In **Kapitel 6** ziehe ich ein Fazit über die Errungenschaften der letzten vier Jahre: Wir haben jetzt eine Methode, mit der wir den δ^2H -Wert aller pflanzlichen Kohlenhydrate genau messen können. Meine Dissertation hat zwei Haupttreiber der biochemischen 2H -Fraktionierungsprozesse in

Pflanzen aufgedeckt: die C₃-, C₄- und CAM CO₂ Fixierung. Im Einzelnen konnte diese Arbeit die photosynthetische ²H-Abreicherung in C₃-Blättern besser erklären, die artspezifisch ist und wahrscheinlich während eines mit den Thylakoiden in den Chloroplasten verbundenen Prozesses auftritt, sowie die ²H-Anreicherung bei der Atmung. Letztere könnte auf eine vorzeitige respiratorische Aufnahme von Zucker mit dem leichteren ¹H-Isotop zurückzuführen sein, was zu einer ²H-Anreicherung im verbleibenden Zuckerpool führt. Dieses Wissen wird es der wissenschaftlichen Gemeinschaft ermöglichen, das gemessene δ²H von Pflanzenkohlenhydraten zu verstehen und zu interpretieren. So könnte eine ²H-Anreicherung in Baumringen auf eine abnehmende Nettoprimärproduktion aufgrund einer Zunahme der Atmung im Verhältnis zur Bruttoassimilationsrate hinweisen. Dies ist jedoch wahrscheinlich artspezifisch, da es z. B. die Fähigkeit einer Pflanzenart widerspiegelt, sich an höhere Temperaturen oder andere Lichtverhältnisse anzupassen.

Weitere Studien werden erforderlich sein, um zu erforschen, wie diese ²H-anreichernden Atmungsprozesse im Laufe der Zeit und in verschiedenen Geweben wirken, z. B. in den Kohlenhydratpools von Stängeln und Wurzeln, und um mögliche zusätzliche physiologische und metabolische Prozesse zu untersuchen, die an der ²H-Fraktionierung in Pflanzen beteiligt sind.

Chapter 1

Introduction

Isotopes: General information

Isotopes are variations of an element that differ in the number of neutrons in their nuclei. Usually the most common isotope of an element has the same number of neutrons as protons. However, the nuclei of different isotopes of an element may contain fewer or more neutrons than protons. For example, the three naturally occurring carbon isotopes ^{12}C , ^{13}C , and ^{14}C have mass numbers of 12, 13 and 14 dalton (da), respectively. As the atomic number is defined by the number of protons in the nucleus, the atomic number of each carbon is 6. Thus the neutron numbers for these three carbon isotopes are 6, 7 and 8 respectively. Isotopes can be divided into stable and unstable isotopes, the latter decaying and emitting radioactive radiation (Curie & Lippmann, 1898). In the case of carbon, the ^{12}C , ^{13}C isotopes are stable and account for 98.9% and 1.06% of the carbon isotopes on Earth. On the other hand, the carbon isotope ^{14}C is unstable, meaning that one of its neutrons fuses with an electron to form a proton by β^- decay, producing the nitrogen isotope ^{14}N , while emitting an electron and an electron antineutrino (Loveland *et al.*, 2017). Due to this decay, the ^{14}C isotope has a natural half-life time of approximately 5,730 years, meaning that the analysis of the ^{14}C content in organic material can be used to date its time of formation. Because of this decay, it contributes to only about 1 part per trillion to the total amount of carbon on Earth, and must be constantly regenerated by the primary natural source of ^{14}C on Earth: the interaction of cosmic rays with nitrogen in the Earth's atmosphere.

The ratios between the isotopes of an element (δ) are calculated according to Coplen (2011):

$$\delta = \frac{R_{\text{Sample}} - R_{\text{Standard}}}{R_{\text{Standard}}},$$

where R is the ratio of the rarer to the more abundant isotope (for instance, $^2\text{H}/^1\text{H}$ in the case of hydrogen) of the sample (R_{Sample}) to an internationally accepted standard (R_{Standard} , in the case of hydrogen Vienna Standard Mean Ocean Water VSMOW2) as the standard defining the international isotope scale. To express the resulting δ values in parts per million (‰), the results are normally multiplied by 1000.

Stable isotopes in time and space

The processes known to be involved in isotope fractionation operate from very large (from a human perspective) to very small scales. For example, the natural spatial distribution of stable isotopes is not even and changes with time. On a galactic scale, ^{13}C is known to be more abundant near the centre of galaxies because more stars have already been formed near the centre due to higher star formation activity (Penzias, 1980). Within solar systems, the overall isotopic composition of an astronomical object, such as a planet like Earth, depends on its formation history. For hydrogen, the isoscape (i.e. the geographical variation of isotopes) of our solar system, which might better be called isospace, is strongly influenced by the temperature distribution within the protoplanetary nebula, which affects the chemodynamic deuterium fractionation (Albertsson *et al.*, 2014). Furthermore, the further away a planet is located from our sun in our solar system, the more ^{15}N enriched it becomes, as the solar wind is highly ^{15}N depleted (Füri & Marty, 2015).

On the planetary scale of an active planet like Earth, isotopic fractionation processes are constantly taking place, affecting the distribution of isotopes both in the interior and at the surface. As water evaporates, it becomes depleted of the heavier ^2H isotope, but this fractionation process is temperature dependent. For example, at 15 °C and under equilibrium conditions, water vapor is approximately 85‰ depleted in ^2H compared to the isotopic composition of liquid water (West *et al.*, 2008; West *et al.*, 2010). Temperature, relative humidity, altitude and latitude affect the $\delta^2\text{H}$ of precipitation (Bowen, 2010; Cernusak *et al.*, 2016). Thus, the isotopic

composition of rain varies geographically and over time (Araguás-Araguás *et al.*, 2000; West *et al.*, 2008). After plants have taken up the water, its hydrogen isotopes may be subject to further fractionation processes.

The isotopes of hydrogen

Hydrogen is one of the elements where the most common isotope contains less neutrons than protons: ^1H , also called protium, which contributes to about 99.9855% of the total hydrogen on Earth. In addition, there are two more hydrogen isotopes: the stable ^2H isotope deuterium, which in addition to the proton contains one neutron in its nucleus and contributes to about 0.0145% of the Earth's hydrogen. The third hydrogen isotope is the unstable ^3H isotope tritium, with two neutrons in its nucleus and a half-life time of approximately 12.3 years, that decays into ^3He by β^- decay (Kondev *et al.*, 2021). However, I am focussing only on stable isotopes in my thesis, with the focus on the hydrogen isotope deuterium.

Current knowledge of hydrogen isotope fractionation in plants

It is assumed that water uptake by roots does not have a ^2H fractionation effect (White, 1989). However, after water has been transported to the leaf, ^2H is enriched by evaporation (Flanagan *et al.*, 1991; Farquhar *et al.*, 2007), and mixed with the isotopic signal of atmospheric water vapour and rain (Lehmann *et al.*, 2018; Kagawa, 2020; Cernusak *et al.*, 2022). ^2H fractionation processes in plant water are mainly the result of physical processes and can be well modelled (Cernusak *et al.*, 2016), with existing models for the transfer of leaf water $\delta^2\text{H}$ to tree-ring cellulose $\delta^2\text{H}$ (Roden & Ehleringer, 2000; Roden *et al.*, 2000). In contrast, metabolic ^2H fractionation processes that shape the $\delta^2\text{H}$ in plant carbohydrates are poorly understood.

Differences in the strength of ^2H fractionation leading to different $\delta^2\text{H}$ values of plant carbohydrates can be found between different CO_2 fixation pathways (Luo & Sternberg, 1991; Schmidt *et al.*, 2003; Schuler *et al.*, 2022).

These studies may provide insight into the main ^2H fractionation processes driving species-specific differences in $\delta^2\text{H}$ of plant carbohydrates. During CO_2 fixation, the autotrophic hydrogen isotope fractionation (ϵ_{HA}) in C_3 plants and thus in most tree species, water molecules are split in chloroplastic' thylakoids during the light-dependent reactions of CO_2 fixation, producing protons (H^+) that are then used to generate energy and reducing equivalents for the Calvin-Benson-Bassham (CBB) cycle that takes place in the same chloroplasts' stroma. This process establishes a high concentration of H^+ inside the thylakoid with a simultaneous low concentration of H^+ on the other side of the thylakoid membrane inside the chloroplast stroma during the light-dependent reactions (Heldt *et al.*, 1973; Falkner *et al.*, 1976; Heldt, 1980). This water splitting process probably discriminates against the heavier H isotope, resulting in a strongly ^2H depleted pool of reducing equivalents such as NADPH (Luo *et al.*, 1991). This process, together with other reactions such as active H^+ transport across the thylakoid membrane, leads to a ΔH^+ of $2.7 \mu\text{M}$ between the two compartments (Heldt *et al.*, 1973). This water splitting process could alter the $\delta^2\text{H}$ values of the water in the chloroplast stroma, and thus be responsible for the highly ^2H depleted H^+ pool (Luo *et al.*, 1991; Schmidt *et al.*, 2003; Hayes, 2018), and thus those of new assimilates. Spatial and temporal variations in CO_2 uptake, assimilation and biochemical reactions in C_4 and CAM lead to significant metabolic changes and ^2H -enrichment in plant carbohydrates compared to C_3 plants (Luo & Sternberg, 1991; Schuler *et al.*, 2022). It can be speculated that some of these processes may help to explain the $\delta^2\text{H}$ variations in carbohydrates of C_3 plants.

The heterotrophic processes involved in ^2H fractionation (ϵ_{HE}) appear to be complex and multifactorial (Lehmann *et al.*, 2022; Schönbeck & Santiago, 2022). For instance, increasing $\delta^2\text{H}$ in tree-ring cellulose indicates stressful growing conditions and may indicate mobilisation of carbohydrate reserves (Lehmann *et al.*, 2021; Vitali *et al.*, 2023). Thus, the $\delta^2\text{H}$ variation in plant organic compounds is driven by carbon metabolism (Holloway-Phillips *et al.*, 2022), and differs between various organic compounds (Baan *et al.*,

2023a; Baan *et al.*, 2023b). However, current knowledge of hydrogen isotope fractionation and models for predicting $\delta^2\text{H}$ of tree-ring cellulose are not able to explain the variability we find in the tree-ring records (Vitali *et al.*, 2022). A better understanding of the underlying biochemical processes, their interactions with plant physiology and climate behind ^2H fractionation is urgently needed to develop a better understanding and improved models.

Thesis objectives

The overall aim of this thesis was to investigate the biological hydrogen isotope fractionation within the carbohydrate metabolism of plants. For this purpose, I developed a new method and performed experiments in a common garden and under controlled climatic conditions with different plant species, including different photosynthetic types. The following detailed objectives were addressed:

- (i) Development of a high-throughput water vapour equilibration method for the accurate determination of the non-exchangeable $\delta^2\text{H}$ of sugar, starch, and cellulose. The results of the method development are presented in **Chapter 2**.
- (ii) Investigation of the main biochemical drivers of ^2H fractionation during and after CO_2 fixation using an innovative phylogenetic approach in **Chapter 3**.
- (iii) Investigation and comparison of the climate response of the ^2H fractionation of plants with C_3 , C_4 and CAM CO_2 fixation in **Chapter 4**.
- (iv) Investigation of the interaction between the biochemical and plant physiological drivers of ^2H fractionation in bulk leaf sugar in **Chapter 5**.

Thesis outline

This thesis was carried out within the frame of the SNSF Ambizione project “TreeCarbo”. The method development (Chapter 2) was carried out in the isotope laboratories of the Swiss Federal Institute for Forest, Snow and Landscape Research WSL in Birmensdorf, Switzerland. The new method was

verified on a wide range of sugar, starch, and cellulose of different origin, as well as on samples from leaves of various plant species with C₃, C₄ and CAM CO₂ fixation grown in climate chambers. Sampling for the phylogenetic study (Chapter 3) was carried out over two days in August 2020 in the Kannenfeldpark, Basel, Switzerland. We sampled leaf and twig material from 73 Northern Hemisphere tree and shrub species, including both angiosperms and gymnosperms, for leaf water, leaf bulk sugar and twig xylem cellulose extraction. The first climate chamber experiment (Chapter 4) was carried out in two large walk-in climate chambers at the Swiss Federal Institute for Forest, Snow and Landscape Research WSL in Birmensdorf, Switzerland. Different plant species with C₃, C₄, and CAM CO₂ fixation were grown under different climatic conditions (20 °C and a VPD of 1.2 kPa, 30 °C and a VPD of 1.3 kPa, and 30 °C and a VPD of 2.6 kPa). The second climate chamber experiment (Chapter 5) was conducted in a smaller climate chamber capable of operating over a wide range of temperature and humidity at the Swiss Federal Institute for Forest, Snow and Landscape Research WSL in Birmensdorf, Switzerland. Six C₃ and one C₄ plant species were exposed to increasing temperatures from 10 °C to 40 °C at constant VPD. Leaf samples were taken for analysis of water and bulk sugar, as well as leaf gas exchange, chlorophyll fluorescence and concentration of non-structural carbohydrates.

Following the introduction in Chapter 1, the method development is presented in Chapter 2. The phylogenetic study of ²H fractionation is presented in Chapter 3. In Chapter 4, I present the influence of different types of CO₂ fixation (C₃, C₄, CAM) to investigate the differences in ²H fractionation related to their different biochemical pathways. The biochemical and plant physiological drivers of ²H fractionation in bulk leaf sugar are investigated in Chapter 5. Finally, Chapter 6 consolidates and integrates the findings of the previous chapters and discusses the contributions of this study to our understanding of biological ²H fractionation within the carbohydrate metabolism of plants.

Contribution to the studies

I conceived and designed the studies presented in this thesis with the help of Marco M. Lehmann. I also collected and analyzed the data and supervised the writing of the four manuscripts presented below.

References

- Albertsson T, Semenov D, Henning T. 2014.** Chemodynamical deuterium fractionation in the early solar nebula: The origin of water on earth and in asteroids and comets. *The Astrophysical Journal* **784**(1): 39.
- Araguás-Araguás L, Froehlich K, Rozanski K. 2000.** Deuterium and oxygen-18 isotope composition of precipitation and atmospheric moisture. *Hydrological Processes* **14**(8): 1341-1355.
- Baan J, Holloway-Phillips M, Nelson DB, Kahmen A. 2023a.** The metabolic sensitivity of hydrogen isotope fractionation differs between plant compounds. *Phytochemistry* **207**: 113563.
- Baan J, Holloway-Phillips M, Nelson DB, Kahmen A. 2023b.** Species and biosynthetic effects cause uncorrelated variation in oxygen and hydrogen isotope compositions of plant organic compounds. *Geochimica et Cosmochimica Acta* **352**: 1-13.
- Bowen GJ. 2010.** Isoscapes: spatial pattern in isotopic biogeochemistry. *Annual Review of Earth and Planetary Sciences* **38**: 161-187.
- Cernusak LA, Barbeta A, Bush RT, Eichstaedt R, Ferrio JP, Flanagan LB, Gessler A, Martín-Gómez P, Hirl RT, Kahmen A. 2022.** Do ^2H and ^{18}O in leaf water reflect environmental drivers differently? *New Phytologist* **235**(1): 41-51
- Cernusak LA, Barbour MM, Arndt SK, Cheesman AW, English NB, Feild TS, Helliker BR, Holloway-Phillips MM, Holtum JAM, Kahmen A, et al. 2016.** Stable isotopes in leaf water of terrestrial plants. *Plant, Cell & Environment* **39**(5): 1087-1102.
- Coplen TB. 2011.** Guidelines and recommended terms for expression of stable-isotope-ratio and gas-ratio measurement results. *Rapid Communications in Mass Spectrometry* **25**(17): 2538-2560.
- Curie M, Lippmann. 1898.** Rayons émis par les composés de l'uranium et du thorium. *Note de M. Curie. C.R. T.126*: (1898) 1101-1103 .

- Falkner G, Horner F, Werdan K, Heldt HW. 1976.** pH changes in the cytoplasm of the blue-green alga *Anacystis nidulans* caused by light-dependent proton flux into the thylakoid space. *Plant Physiology* **58**(6): 717-718.
- Farquhar GD, Cernusak LA, Barnes B. 2007.** Heavy Water Fractionation during Transpiration. *Plant Physiology* **143**(1): 11-18.
- Flanagan LB, Comstock JP, Ehleringer JR. 1991.** Comparison of modeled and observed environmental influences on the stable oxygen and hydrogen isotope composition of leaf water in *Phaseolus vulgaris* L. *Plant Physiology* **96**(2): 588-596.
- Füri E, Marty B. 2015.** Nitrogen isotope variations in the Solar System. *Nature Geoscience* **8**(7): 515-522.
- Hayes JM 2018.** 3. Fractionation of Carbon and Hydrogen Isotopes in Biosynthetic Processes. *Stable Isotope Geochemistry*: De Gruyter, 225-278.
- Heldt H 1980.** [57] Measurement of metabolite movement across the envelope and of the pH in the stroma and the thylakoid space in intact chloroplasts. *Methods in Enzymology* **69**: 604-613.
- Heldt HW, Werdan K, Milovancev M, Geller G. 1973.** Alkalization of the chloroplast stroma caused by light-dependent proton flux into the thylakoid space. *Biochimica et Biophysica Acta (BBA)-Bioenergetics* **314**(2): 224-241.
- Holloway-Phillips M, Baan J, Nelson DB, Lehmann MM, Tcherkez G, Kahmen A. 2022.** Species variation in the hydrogen isotope composition of leaf cellulose is mostly driven by isotopic variation in leaf sucrose. *Plant, Cell & Environment* **45**(9): 2636-2651.
- Kagawa A. 2020.** Foliar water uptake as a source of hydrogen and oxygen in plant biomass. *Tree Physiology* **42**(11): 2153-2173.

- Kondev F, Wang M, Huang W, Naimi S, Audi G. 2021.** The NUBASE2020 evaluation of nuclear physics properties. *Chinese Physics C* **45**(3): 030001.
- Lehmann MM, Goldsmith GR, Schmid L, Gessler A, Saurer M, Siegwolf RT. 2018.** The effect of ¹⁸O-labelled water vapour on the oxygen isotope ratio of water and assimilates in plants at high humidity. *New Phytologist* **217**(1): 105-116.
- Lehmann MM, Schuler P, Cormier M-A, Allen ST, Leuenberger M, Voelker S 2022.** The Stable Hydrogen Isotopic Signature: From Source Water to Tree Rings. Chapter in **Siegwolf R. T., Brooks J. R., Roden J., Saurer M. 2022: *Stable Isotopes in Tree Rings: Inferring Physiological, Climatic and Environmental Responses*: Springer: 331-359.**
- Lehmann MM, Vitali V, Schuler P, Leuenberger M, Saurer M. 2021.** More than climate: Hydrogen isotope ratios in tree rings as novel plant physiological indicator for stress conditions. *Dendrochronologia* **65**: 125788.
- Loveland WD, Morrissey DJ, Seaborg GT. 2017.** *Modern Nuclear Chemistry*: John Wiley & Sons.
- Luo Y-H, Steinberg L, Suda S, Kumazawa S, Mitsui A. 1991.** Extremely low D/H ratios of photoproduced hydrogen by cyanobacteria. *Plant and Cell Physiology* **32**(6): 897-900.
- Luo Y-H, Sternberg L. 1991.** Deuterium heterogeneity in starch and cellulose nitrate of CAM and C₃ plants. *Phytochemistry* **30**(4): 1095-1098.
- Penzias AA. 1980.** Nuclear processing and isotopes in the galaxy. *Science* **208**(4445): 663-669.
- Roden JS, Ehleringer JR. 2000.** Hydrogen and oxygen isotope ratios of tree ring cellulose for field-grown riparian trees. *Oecologia* **123**(4): 481-489.

- Roden JS, Lin G, Ehleringer JR. 2000.** A mechanistic model for interpretation of hydrogen and oxygen isotope ratios in tree-ring cellulose. *Geochimica et Cosmochimica Acta* **64**(1): 21-35.
- Schmidt H-L, Werner RA, Eisenreich W. 2003.** Systematics of ²H patterns in natural compounds and its importance for the elucidation of biosynthetic pathways. *Phytochemistry Reviews* **2**(1): 61-85.
- Schönbeck LC, Santiago LS. 2022.** Time will tell: towards high-resolution temporal tree-ring isotope analyses. *Tree Physiology* **42**(12): 2401-2403.
- Schuler P, Cormier MA, Werner RA, Buchmann N, Gessler A, Vitali V, Saurer M, Lehmann MM. 2022.** A high temperature water vapor equilibration method to determine non-exchangeable hydrogen isotope ratios of sugar, starch, and cellulose. *Plant, Cell & Environment* **45**(1): 12-22
- Vitali V, Martínez-Sancho E, Treydte K, Andreu-Hayles L, Dorado-Liñán I, Gutierrez E, Helle G, Leuenberger M, Loader NJ, Rinne-Garmston KT. 2022.** The unknown third - Hydrogen isotopes in tree-ring cellulose across Europe. *Science of The Total Environment* **813**: 152281.
- Vitali V, Peters RL, Lehmann MM, Leuenberger M, Treydte K, Büntgen U, Schuler P, Saurer M. 2023.** Tree-ring isotopes from the Swiss Alps reveal non-climatic fingerprints of cyclic insect population outbreaks over the past 700 years. *Tree Physiology* **43**(5): 706-721.
- West JB, Kreuzer HW, Ehleringer JR. 2010.** Approaches to plant hydrogen and oxygen isoscapes generation. *Isoscapes: Understanding movement, pattern, and process on Earth through isotope mapping*. Springer: 161-178.
- West JB, Sobek A, Ehleringer JR. 2008.** A simplified GIS approach to modeling global leaf water isoscapes. *PloS one* **3**(6): e2447.

White J. 1989. Stable hydrogen isotope ratios in plants: a review of current theory and some potential applications. Chapter in **Rundel PW, Ehleringer JR, Nagy KA. 1989.** *Stable isotopes in ecological research.* Springer: 142-162.

Chapter 2

A high-temperature water vapor equilibration method to determine non-exchangeable hydrogen isotope ratios of sugar, starch and cellulose

Philipp Schuler^{1,2}, 2, Marc-André Cormier³, Roland A. Werner², Nina Buchmann², Arthur Gessler^{1,2}, Valentina Vitali¹, Matthias Saurer¹, Marco M. Lehmann¹

¹Forest dynamics, Swiss Federal Institute for Forest, Snow and Landscape Research WSL, Birmensdorf, Switzerland

²Department of Environmental Systems Science, ETH Zurich, Zurich, Switzerland

³Department of Earth Sciences, University of Oxford, Oxford, United Kingdom

This chapter has been published in the peer-reviewed journal “Plant, Cell & Environment”

Schuler P., Cormier MA, Werner RA, Buchmann N, Gessler A, Vitali V, Saurer M, Lehmann MM (2022). A high-temperature water vapor equilibration method to determine non-exchangeable hydrogen isotope ratios of sugar, starch and cellulose. *Plant, Cell & Environment*. 45 (1), 12-22. <https://doi.org/10.1111/pce.14193>

Abstract

The analysis of the non-exchangeable hydrogen isotope ratio ($\delta^2\text{H}_{\text{ne}}$) in carbohydrates is mostly limited to the structural component cellulose, while simple high-throughput methods for $\delta^2\text{H}_{\text{ne}}$ values of non-structural carbohydrates (NSC) such as sugar and starch do not yet exist. Here we tested if the hot vapor equilibration method originally developed for cellulose is applicable for NSC, verified by comparison with the traditional nitration method. We set up a detailed analytical protocol and applied the method to plant extracts of leaves from species with different photosynthetic pathways (i.e., C_3 , C_4 , CAM). $\delta^2\text{H}_{\text{ne}}$ of commercial sugars and starch from different classes and sources, ranging from -157.8 to +6.4‰, were reproducibly analyzed with a precision between 0.2 and 7.7‰. Mean $\delta^2\text{H}_{\text{ne}}$ values of sugar are lowest in C_3 (-92.0‰), intermediate in C_4 (-32.5‰), and highest in CAM plants (6.0‰), with NSC being ^2H -depleted compared to cellulose and sugar being generally more ^2H -enriched than starch. Our results suggest that our method can be used in future studies to disentangle ^2H -fractionation processes, for improving mechanistic $\delta^2\text{H}_{\text{ne}}$ models for leaf and tree-ring cellulose, and for further development of $\delta^2\text{H}_{\text{ne}}$ in plant carbohydrates as a potential proxy for climate, hydrology, plant metabolism and physiology.

Introduction

The isotopic composition of carbohydrates, which are the primary building blocks of plant biomass, is well known as a useful proxy for hydro-climatic conditions and plant physiological processes that have occurred during their biosynthesis (Saurer *et al.*, 1997; McCarroll & Loader, 2004; Sass-Klaassen *et al.*, 2005; Saurer *et al.*, 2012; Gessler *et al.*, 2014; Porter *et al.*, 2014; Gaglioti *et al.*, 2017; Manrique-Alba *et al.*, 2020). Various high-throughput methods have been developed to study the carbon and oxygen isotopic composition of non-structural plant carbohydrates (NSC; i.e. sugar and starch) (Wanek *et al.*, 2001; Richter *et al.*, 2009; Lehmann *et al.*, 2020), and of structural carbohydrates such as tree-ring or leaf cellulose (Boettger *et al.*, 2007). In contrast, methods to investigate the non-exchangeable hydrogen isotopic composition ($\delta^2\text{H}_{\text{ne}}$) in plant carbohydrates are still mainly limited to cellulose (Epstein *et al.*, 1976; Filot *et al.*, 2006; Sauer *et al.*, 2009; An *et al.*, 2014; Mischel *et al.*, 2015; Arosio *et al.*, 2020b; Nakatsuka *et al.*, 2020; Xia *et al.*, 2020). Existing methods to analyse $\delta^2\text{H}_{\text{ne}}$ values of NSC use site-specific natural isotope fractionation nuclear magnetic resonance spectroscopy (SNIF-NMR) or sample derivatisation prior to isotope ratio mass spectrometry (IRMS) (Dunbar & Schmidt, 1984; Zhang *et al.*, 1994; Schleucher *et al.*, 1999; Augusti *et al.*, 2008; Abraham *et al.*, 2020). These methods are, however, very laborious and limited by their sample throughput and/or produce explosive compounds that are difficult to work with. As a result, publications reporting $\delta^2\text{H}_{\text{ne}}$ values of NSC are rare (Dunbar & Wilson, 1983; Luo & Sternberg, 1991; Ehlers *et al.*, 2015). However, recent studies show the great potential of $\delta^2\text{H}$ values of plant compounds to retrospectively determine hydrological and climatic conditions (Sachse *et al.*, 2012; Gamarra & Kahmen, 2015; Hepp *et al.*, 2015; Anhäuser *et al.*, 2018; Hepp *et al.*, 2019), as well as to disentangle metabolic and physiological processes (Estep & Hoering, 1981; Cormier *et al.*, 2018; Tipple & Ehleringer, 2018; Sanchez-Bragado *et al.*, 2019) such as the proportional use of carbon sources (i.e. fresh assimilates vs. storage compounds) for plant growth (Zhu *et al.*, 2020; Lehmann *et al.*, 2021). Enabling the analysis of $\delta^2\text{H}_{\text{ne}}$ of NSC,

especially sugar at the leaf level, will make it possible to study processes and environmental conditions which are shaping the ^2H -fractionation of carbohydrates at a much higher time resolution compared to the analysis of $\delta^2\text{H}_{\text{ne}}$ of cellulose. New routines and high-throughput analytical methods for $\delta^2\text{H}_{\text{ne}}$ values of NSC are thus needed to enable widespread application in earth and environmental sciences.

The difficulty of establishing reliable methods for $\delta^2\text{H}_{\text{ne}}$ values of NSC and cellulose is mainly caused by the presence of oxygen-bound hydrogen atoms (H_{ex}) that can freely exchange with hydrogen atoms of the surrounding liquid water and water vapor. The interference of H_{ex} greatly affects the analysis of $\delta^2\text{H}_{\text{ne}}$, which retains the useful information on climate, hydrology, metabolism, and physiology. The oldest method of measuring $\delta^2\text{H}_{\text{ne}}$ is to derivatize hydroxyl groups with nitrate esters, using a mixture of either H_2SO_4 or H_3PO_4 with HNO_3 (Alexander & Mitchell, 1949; Epstein *et al.*, 1976; DeNiro, 1981; Boettger *et al.*, 2007). However, the nitration process requires a large sample amount, is labour intensive, uses hazardous derivatisation reactions, and leads to thermally unstable products. A newer derivatisation method to measure $\delta^2\text{H}_{\text{ne}}$ in sugars is by using *N*-methyl-bis-trifluoroacetamide to replace H_{ex} with trifluoroacetate derivatives, which are measured by gas chromatography - chromium silver reduction/high temperature conversion-isotope ratio mass spectrometry (GC-CrAg/HTC-IRMS) (Abraham *et al.*, 2020). This method still relies on a large sample amount of >20 mg extracted NSC, a relatively long measuring time and the limitation of measuring only one element per analysis. Potential alternative methods that work without derivatisation and use smaller amounts of material are based on water vapor equilibration, which sets H_{ex} to a known isotopic composition that allows the determination of $\delta^2\text{H}_{\text{ne}}$ by mass balance (Schimmelmann, 1991; Wassenaar & Hobson, 2000; Filot *et al.*, 2006; Sauer *et al.*, 2009; Cormier *et al.*, 2018). However, established water vapor equilibration methods are mainly calibrated for analysis of $\delta^2\text{H}_{\text{ne}}$ values of complex molecules such as cellulose, keratin and chitin (Schimmelmann *et al.*, 1986; Wassenaar & Hobson, 2000) and whether these methods can also

be used for analysis of $\delta^2\text{H}_{\text{ne}}$ in NSC remains to be shown. The main purpose of this study was therefore to establish a high-throughput hot water vapor equilibration method to determine $\delta^2\text{H}_{\text{ne}}$ of NSC, based on already established protocols for cellulose (Sauer *et al.*, 2009). Nitration of cellulose and starch was additionally applied as an independent method to verify our results. Finally, we used the method to determine $\delta^2\text{H}_{\text{ne}}$ values of NSC and cellulose extracted from leaves of plant species with different photosynthetic pathways (C_3 , C_4 , CAM) grown under the same controlled climatic conditions.

Materials and methods

Cellulose, starch, and sugar standards

As reference materials, we used both commercially available (n=4; spruce cellulose, Fluka, Honeywell International Inc., Morristown, New Jersey, U.S.A., Prod. No. 22181; IAEA-CH-3, International Atomic Energy Agency (IAEA), Vienna, Austria; Merck cellulose (Cellulose native no. 2351, Merck, Darmstadt, Germany), Wei Ming (CYCLOCEL[®] Microcrystalline Cellulose, Wei Ming Pharmaceutical MFG. co., LTD., Taipei City, Taiwan), and in-house produced cellulose standards (n=5; Isonet, spruce, beech, Spain, Siberia), commercially available starch standards (n=4; starch from maize, Fluka, Prod. No. 85652; starch from rice, Calbiochem, Merck KGaA, Darmstadt, Germany, Prod. No. 569380; starch from wheat, Fluka, Prod. No. 85649; starch from potato, Merck, Prod. No. 1.01259.0250), commercially available standards for sugars of different classes (n=6; sucrose, Merck, Prod. No. 1.07687; D-(+)-glucose $\geq 99.5\%$, SIGMA Life Science, St. Louis, Missouri, U.S.A., Prod. No. 49139; D-(-)-fructose $\geq 99\%$, Fluka, Prod. No. 47739; D-(+)-raffinose pentahydrate $\geq 99\%$, Fluka, Prod. No. 83400; D-(+)-trehalose dihydrate $\geq 99\%$, SIGMA Life Science, Prod. No. T9449; myo-Inositol $\geq 99.5\%$, Sigma Life Science, Prod. No. 57569) and two household sugars (Finish sucrose from 2019, Suomalainen Taloussokeri, Kantvik, Finland; Russian sucrose, household sugar from a Russian supermarket supplier). All

reference materials were oven dried at 60 °C for 48 hours and stored in an exicator at low relative humidity (2-5%) until further use.

Plant species, growing conditions, and sampling

Ten plant species with different photosynthetic pathways grown under controlled conditions in walk-in climate chambers (Bouygues E&S InTec Schweiz AG, Zurich, Switzerland) were used to apply the new method, and compare $\delta^2\text{H}_{\text{ne}}$ of cellulose, starch, and soluble sugars. The species selection covered C_3 herbs and grasses (*Abelmoschus esculentus* (L.) Moench, *Cannabis sativa* L., *Hordeum vulgare* L., *Salvia hispanica* L., *Solanum cheesmaniae* (L. Riley) Fosberg), C_4 grasses (*Sorghum bicolor* (L.) Moench, *Zea mays* L.), and CAM plants (*Portulaca grandiflora* Hook., *Kalanchoe daigremontiana* Raym.-Hamet & H.Perrier, *Phalaenopsis* Blume hybrid). Seeds or plantlets were sown or planted in 3 L pots containing potting soil (Kübelpflanzenerde, RICOTER Erdaufbereitung AG, Aarberg, Switzerland). The orchid *Phalaenopsis* was bought in a local supermarket and grown in a special substrate based on bark mulch. The climate chamber conditions were set to 16 daytime hours (30 °C and 40% relative humidity), 8 nighttime hours (15 °C and 60% relative humidity), and a photosynthetically active radiation of 110 $\mu\text{mol m}^{-2} \text{s}^{-1}$ at plant height with uniform fluorescent tubes (OSRAM L 36W 777 Fluora, Osram Licht AG, Munich, Germany). All plants were regularly watered to field capacity with tap water ($\delta^2\text{H} = -79.9 \pm 2.4 \text{ ‰}$ during the experimental period) to avoid any water limitation, except for *Phalaenopsis* that was watered with 50 mL twice a week to keep the substrate moist but prevent root rot due to excess water. The plants were grown for three months to ensure ample leaf material was grown for harvest.

At the sampling day, three samples of fully developed mature leaves, each from individual plants or three pools of leaves of four plants in the case of *H. vulgare*, were sampled after 7 hours of light to allow the plants to synthesize enough sugars and starch on the day of harvest and to guarantee steady-state leaf water enrichment conditions (Cernusak *et al.*, 2016). The leaf samples were immediately transferred to gas-tight 12 ml glass vials

(‘Exetainer’, Labco, Lampeter, UK, Prod. No. 738W), stored on ice until the harvest was complete (\leq two hours), and then at $-20\text{ }^{\circ}\text{C}$ in a freezer until further use (Appendix 1). The sample material was dried using a cryogenic water distillation method (West *et al.* (2006), crumbled with a spatula (dicotyledon species) or cut with scissors (monocotyledon species) into small pieces and 100 mg of the fragmented material was separated for cellulose extraction. The remaining leaf material was then ball-milled to powder (Retsch MM400, Retsch, Haan, Germany) for NSC extraction.

Cellulose and starch nitration, and isotopic analysis of the nitrated products

Nitrates of cellulose and starch without exchangeable H were used as reference material to assess the $\delta^2\text{H}_{\text{ne}}$ values derived from the hot water vapor equilibration method. Nitration of cellulose and starch standards was performed following the method of Alexander and Mitchell (1949), using a mixture of P_2O_5 and 90% HNO_3 . $\delta^2\text{H}$ values of nitrated cellulose and starch were analysed with a TC/EA-IRMS system, using a reactor filled with chromium as described by Gehre *et al.* (2015). Reference materials for $\delta^2\text{H}$ measurements of cellulose and starch nitrates were the IAEA-CH-7 polyethylene foil (PEF; International Atomic Energy Agency, Vienna, Austria) for a first offset correction and the USGS62, USGS63, and USGS64 caffeine standards (United States Geological Survey, Reston, Virginia, U.S.A.) (Schimmelmann *et al.*, 2016) for the final normalization.

All Isotope ratios (δ) are calculated as given in Eq. 1 (Coplen, 2011):

$$\delta = \frac{R_{\text{Sample}} - R_{\text{Standard}}}{R_{\text{Standard}}} \quad \text{Eq. 1}$$

$R = {}^2\text{H}/{}^1\text{H}$ of the sample (R_{Sample}) and of Vienna Standard Mean Ocean Water (VSMOW2; R_{Standard}) as the standard defining the international isotope scale. To express the resulting δ values in permil (‰), results have been multiplied by 1000.

Preparation of leaf cellulose and NSC for $\delta^2\text{H}_{\text{ne}}$ analysis

Every compound (i.e. sugars, starch, and cellulose) was extracted once per sample. Cellulose (hemicellulose) was extracted from 100 mg of the fragmented leaf material in F57 fiber filter bags (made up of polyester and polyethylene with an effective pore size of 25 microns; ANKOM Technology, Macedon NY, U.S.A.). In brief, the samples were washed twice in a 5% sodium hydroxide solution at 60°C, rinsed with deionized water, washed 3 times for 10 hours in a 7% sodium chlorite solution, which was adjusted with 96% acetic acid to a pH between 4-5, and subsequently rinsed with boiling hot deionized water, and dried overnight in a drying oven at 60 °C. The neutral sugar fraction (“sugar”, a mixture of sugars, typically glucose, fructose, sucrose and a sugar alcohol (Rinne *et al.*, 2012)) were extracted from 100 mg leaf powder and further purified using ion-exchange cartridges, following established protocols for carbon and oxygen isotope analyses (Rinne *et al.*, 2012; Lehmann *et al.*, 2020). This is needed to separate the sugar from other water soluble compounds such as amino acids which would alter the resulting $\delta^2\text{H}_{\text{ne}}$ values (Schmidt *et al.*, 2003). Starch was extracted from the remaining pellet of the sugar extraction via enzymatic digestion following the established method for carbon isotope analysis (Wanek *et al.*, 2001; Richter *et al.*, 2009). The same protocol was used to hydrolyse the commercial starch standards. Aliquots of the extracted sugar (including those derived from starch) were pipetted in 5.5x9 mm silver foil capsules (IVA Analysentechnik GmbH & Co. KG, Germany, Prod. No. SA76981106), frozen at -20 °C, freeze-dried, folded into cubes and packed into an additional silver foil capsule of the same type, folded again, and stored in an exicator at low relative humidity (2-5%) until isotope analysis.

$\delta^2\text{H}_{\text{ne}}$ analysis of cellulose and NSC using a hot water vapor equilibration method

One mg of commercial starch or cellulose standard was packed into 3.3x5 mm silver foil capsules (IVA, Prod. No. SA76980506), which led to a total peak area between 20 and 30-volt seconds (Vs) of each IRMS analysis. For sugar standards, one mg was transferred first into a 5.5x9 mm silver foil capsule (IVA), and additionally packed in a second capsule of the same size and folded again. The reason for the double packing was the observation that sugar samples became liquefied and rinsed out of single-packed capsules during the hot water vapor equilibration, which led to a loss of sample and to negative impacts on the analysis of $\delta^2\text{H}_{\text{ne}}$ in sugars. Such rinsing was prevented by double packing and had no negative impact on drying time of the sugars (Appendix 2). The double packing did not have a negative impact on the equilibration itself, as indicated by the high x_e of the sugars (Table 1). All packed samples were stored in an exicator at low relative humidity (2-5%) until isotope analysis.

All samples were equilibrated in a home-built offline equilibration system (Appendix 3), consisting of heating oven with an in-house designed equilibration chamber (Appendix 4) connected to a peristaltic pump (Gilson Incorporated, Middleton, USA). The equilibration chamber consisted of a sampler carousel (Zero Blank Autosampler, N.C. Technologies S.r.l., Milano, Italy) for solid samples with 50 cylindrical sample positions, where samples and reference materials could be placed, inserted into a cubic stainless steel chamber with a heat-stable Viton[®] O-rings (Maagtechnic AG, Dübendorf, Switzerland, Prod. No. 15087359) surrounding the autosampler tray. The top of the chamber was sealed with a stainless steel metal plate using one stainless steel clamp at each corner. In the middle of the top metal plate, one inlet and one outlet connector were installed (Appendix 5). The inlet was connected to a stainless steel tube (i.e. feeding capillary, BGB, Switzerland), which was leading out of the oven where a santoprene pump tubing was fitted into a peristaltic pump (Appendix 6). The end of the

santoprene pump tubing was inserted into a 50 mL falcon tube containing the equilibration water. The peristaltic pump provided a constant flow of the equilibration water (1.7 mL h^{-1}) into the equilibration chamber. The temperature setpoint of the preheated oven was set to a constant 130°C , ensuring immediate evaporation of water after entering the equilibration chamber. The end of the outlet metal tube was inserted into a glass vessel and checked for vapor flow and condensation of the blown out vapor. After 2 hours of equilibration, the feeding capillary was switched to a capillary delivering dry nitrogen gas (N_2 5.0, PanGas AG, Dagmersellen, Switzerland, Prod No. 222 0912) with a pressure of one bar for 2 hours to ensure a complete removal of gaseous water in the chamber, which was still kept at 130°C . The duration of equilibration and drying, as well as the equilibration temperature were step-wise tested for cellulose to ensure maximum equilibration and no residual vapor. However, the high equilibration temperature of 130°C might be important to break down the crystalline structure of sugars and gelatinize starch to enable the access of water vapor (Gudasz *et al.*, 2020). For testing the reproducibility of the adapted method, triplicates of each type of cellulose and sugar samples were equilibrated independently on separate days following a standardised sample sequence (Appendix 7), in total three times with Water 1 ($\delta^2\text{H} = -160\text{‰}$) and three times with Water 2 ($\delta^2\text{H} = -428\text{‰}$). For starch and digested starch, triplicates were equilibrated only once with Water 1 and once with Water 2.

Subsequently, all samples (still hot) were immediately transferred into a Zero Blank Autosampler (N.C. Technologies S.r.l.), which was installed on a sample port of a high-temperature elemental analyzer system. The latter was coupled via a ConFlo III interface to a Delta^{plus} XP IRMS (TC/EA-IRMS, Finnigan MAT, Bremen, Germany). It is crucial to transfer the samples as fast as possible and still hot from the equilibration chamber to the autosampler to avoid any isotopic re-equilibration of the sample with air moisture and water absorption. The autosampler carousel was evacuated to 0.01 mbar and afterwards filled with dry helium gas to 1.5 bar to avoid any contact with ambient water (vapor). The samples were pyrolyzed in a

reactor according to Gehre *et al.* (2004), and carried in a flow of dry helium (150 mL min⁻¹) to the IRMS. Raw $\delta^2\text{H}$ values of standard material (Table 1) were offset corrected using PEF standards (SD of PEF < 0.7‰ within one run). Leaf sugar, starch, and cellulose samples of three biological replicates were prepared as described above for the commercial standard material and equilibrated using identical settings. This corresponded to one equilibration with Water 1 and one with Water 2. Raw $\delta^2\text{H}$ values of plant-derived compounds were offset corrected using PEF. The calculated $\delta^2\text{H}_{\text{ne}}$ of plant extracted sugar and sugar derived from starch (Table 2) were normalized against the $\delta^2\text{H}_{\text{ne}}$ of Finnish, Russian and Merck sucrose from the method implementation (Table 1), while the calculated $\delta^2\text{H}_{\text{ne}}$ of plant extracted cellulose were normalized against the $\delta^2\text{H}$ values of the corresponding nitrocellulose of cellulose from spruce, Spain, and Siberia.

Calculation of non-exchangeable hydrogen isotope ratio ($\delta^2\text{H}_{\text{ne}}$)

According to Filot *et al.* (2006), the %-proportion of exchanged hydrogen during the equilibrations (x_e , Eq. 2) can be calculated as:

$$x_e = \frac{\delta^2\text{H}_{e1} - \delta^2\text{H}_{e2}}{\alpha_{e-w} \cdot (\delta^2\text{H}_{w1} - \delta^2\text{H}_{w2})} \quad \text{Eq. 2}$$

where $\delta^2\text{H}_{e1}$ and $\delta^2\text{H}_{e2}$ are the $\delta^2\text{H}$ values of the two equilibrated samples, $\delta^2\text{H}_{w1}$ and $\delta^2\text{H}_{w2}$ are the $\delta^2\text{H}$ values of the two waters used, α_{e-w} is the fractionation factor of 1.082 for cellulose (Filot *et al.*, 2006). While α_{e-w} needs to be adapted for different compound and fractions with different functional groups (Schimmelmann, 1991), we consider α_{e-w} of cellulose to be transferable to other carbohydrates as they all have the exchangeable hydrogen on hydroxyl groups. The fractionation factor we use in our method lies also within the range proposed in other studies (Schimmelmann *et al.*, 1999; Wassenaar & Hobson, 2000).

$\delta^2\text{H}_{\text{ne}}$ can then be calculated with Eq.3 using one of the two equilibrations (in this example equilibration with Water 1 ($\delta^2\text{H}_{\text{e1}}$ and $\delta^2\text{H}_{\text{w1}}$):

$$\delta^2\text{H}_{\text{ne}} = \frac{\delta^2\text{H}_{\text{e1}} - x_e \cdot \alpha_{\text{e-w}} \cdot \delta^2\text{H}_{\text{w1}} - 1000 \cdot x_e \cdot (\alpha_{\text{e-w}} - 1)}{1 - x_e} \quad \text{Eq. 3}$$

Statistical analyses (one-way ANOVA and Tukey posthoc test) were performed using R version 3.6.3 (R.Core.Team, 2023).

Results and Discussion

A hot water vapor equilibration method for determining $\delta^2\text{H}_{\text{ne}}$ of sugar, starch, and cellulose

Our in-house implementation of the hot water vapor equilibration method for cellulose resulted in precise and accurate measurements of $\delta^2\text{H}_{\text{ne}}$ values of cellulose (Table 1). $\delta^2\text{H}_{\text{ne}}$ values of cellulose, ranging from -44.5 to -70.0‰, were measured with a high precision as indicated by the standard deviations (SD_{e1} and SD_{e2}) ranging between 0.9 and 4.1‰ for both equilibration waters. Also, a high accuracy was found, as indicated by a deviation of -1.0 to +5.7‰ between the $\delta^2\text{H}_{\text{ne}}$ value of the hot water vapor equilibration and the $\delta^2\text{H}$ value of the corresponding cellulose nitrate ($\delta^2\text{H}_{\text{ne}} - \delta^2\text{H}_{\text{nitro}}$), except for two of the commercial cellulose samples from Fluka and Wei Ming, with a deviation of -18.8 and +7.7‰, respectively. For the samples with high accuracy, the calculated x_e ranged between 19.3 and 22.1% compared to a theoretical $x_{\text{e.pot}}$ of 30%. These x_e values are comparable to those $20.5 \pm 0.1\%$ observed in the original implementation of the hot water vapor equilibration for cellulose (Sauer *et al.*, 2009). For the two samples with low accuracy, x_e reached only 16.4%. The reason for the low x_e and the resulting low accuracy of the commercial cellulose from Fluka and the Wei Ming remains elusive. Tentatively, it could be explained by a different extraction method and purification of these cellulose samples, leading to different nanostructures (Jungnikl *et al.*, 2007) or particle sizes, which in turn leads to a different accessibility of water vapor to the cellulose molecule (Chami Khazraji & Robert, 2013). Nevertheless, the results show

that the hot water vapor equilibration is suitable to determine $\delta^2\text{H}_{\text{ne}}$ with high accuracy and precision if the principle of identical treatment (Werner & Brand, 2001) is applied, i.e., all samples are prepared and measured in the same way. Besides, the calculated x_e values of the IAEA-CH-7 reference material without any H_{ex} were close to 0 throughout all measurements, denoting the absence of absorbed water on the surface of each compound, as well as the analytical reproducibility for all $\delta^2\text{H}_{\text{ne}}$ values of cellulose was high as indicated by a standard deviation of 0.8 to 1.9‰ for three repetitions.

Table 1. Results of the hot water vapor equilibrations of cellulose, sugars and starch (including the sugars derived from digested starch) of different classes and origins (referenced against PEF)

	Ref. material	$\delta^2\text{H}_{e1}$ [‰]	SD_{e1}	$\delta^2\text{H}_{e1}$ [‰]	SD_{e2}	x_e [%]	$x_{e.pot}$ [%]	$\delta^2\text{H}_{ne}$ [‰]	$\delta^2\text{H}_{nitro}$ [‰]	$\delta^2\text{H}_{ne^-}$ $\delta^2\text{H}_{nitro}$ [‰]	Rep.
Cellulose	Isonet	-57.1	1.1	-108.2	4.1	20	30	-42.2	-44.5	2.3	0.9
	Beech	-57.7	1.2	-114.3	3.3	20	30	-49.7	-50.8	1.2	1
	Spruce	-40.2	1.7	-96.3	3.3	19	30	-27.9	-30.7	2.7	1.1
	Spain	-49.8	0.8	-114.1	3.7	22	30	-33.4	-27.7	-5.7	N.A.
	Siberia	-164.5	2.2	-224	1.7	21	30	-184.3	-184.9	-0.6	N.A.
	IAEA	-65.1	1	-126	2.8	21	30	-58.2	-57.3	-0.9	1.4
	Merck	-63.5	1	-119.3	2.3	19	30	-56.9	-55.9	-1	1
	Fluka	-72.9	0.9	-120.3	3	16	30	-69.3	-50.5	-18.8	0.8
	Wei Ming	-67	1.8	-114.6	2.1	16	30	-62.3	-70	7.7	1.9
	Sugar	Finn. sucrose	-133.5	3.7	-239.1	1.3	36	36.4	-157.8	N.A.	N.A.
Russ. sucrose		-65	2	-169.7	2.2	36	36.4	-50.3	N.A.	N.A.	4.2
Merck sucrose		-107.5	3.2	-214.2	1.7	37	36.4	-117	N.A.	N.A.	5.8
Glucose		-31.3	2.2	-143.4	3.6	39	41.7	6.4	N.A.	N.A.	4.2
Fructose		-47.6	2.9	-155.3	3.9	37	41.7	-21.9	N.A.	N.A.	4.9
Raffinose		-16.4	1.6	-115.2	3.5	34	34.4	22.2	N.A.	N.A.	4.3
Trehalose		-91.4	2.1	-196.1	3.3	36	36.4	-91.5	N.A.	N.A.	4
Myo-Inositol		-91.5	3.7	-246.6	7.7	54	50	-91.8	N.A.	N.A.	8.6
Starch	Maize	-32.9	1.2	-96.2	0.8	22	30	-16.6	-13.4	-3.1	N.A.
	Maize starch hydrolysed	-41.4	0.5	-132.7	1.8	32	41.7	-18.6	-13.4	-5.1	N.A.
	Rice	-71.6	2	-136.7	0.5	23	30	-65.9	-67.2	1.2	N.A.
	Rice starch hydrolysed	-76.2	1.1	-169.1	1	32	41.7	-69.2	-67.2	-2	N.A.
	Wheat	-58.4	2.1	-110.2	0.2	18	30	-51.3	-53.7	2.3	N.A.
	Wheat starch hydrolysed	-71	0.3	-162.9	0.2	32	41.7	-61.6	-53.7	-8	N.A.
	Potato	-127.1	1.8	-194	4.5	23	30	-137.9	-143.2	5.3	N.A.
	Potato starch hydrolysed	129.1	1.1	-221.8	3.7	32	41.7	-147	-143.2	-3.7	N.A.

The same method was also applied to analyse $\delta^2\text{H}_{ne}$ of NSC (Table 1). $\delta^2\text{H}_{ne}$ values of sugars of different classes, ranging from 6.4 to -157.8‰, were also measured with a high precision as indicated by a SD ranging between 1.3 and 7.7‰ for both equilibration waters, which is comparable to the precision of derivatisation methods (Dunbar and Schmidt (1984): 1.9‰;

Augusti *et al.* (2008): 2 and 10‰; Abraham *et al.* (2020): 0.4 and 3.6‰). As no nitrated sugars were available due to the safety problems with sugar nitration, we could not calculate the accuracy. We, however, can assume that the accuracies for sugars should be in a comparable range as those derived from digested starch (-8.0 and -2.0‰). The reproducibility of the results for all tested commercial sugars ranged between 4.0 to 8.6‰ for three repetitions. The x_e of the different sugars ranged between 34.1 and 53.5% and was thus similar or very close to $x_{e,pot}$, which gives further confidence in the reliability of the method for sugars. The smaller deviation of x_e from $x_{e,pot}$ for sugars than for cellulose might be explained by the dissolution of the sugars during the hot water vapor equilibration, leading to a breakdown of the crystal structure of the sugars. This might have facilitated a complete exchange of H_{ex} with the water vapor in sugars, that is not feasible for cellulose (Schimmelmann, 1991; Sauer *et al.*, 2009).

The δ^2H_{ne} of equilibrated but undigested starch was close to the δ^2H_{ne} of the nitrated starch, measured with a precision ranging between 0.2 to 4.5‰ and an accuracy between -3.1 to +5.3‰. The x_e of the undigested starch was between 17.8 and 23.0%, and thus comparable to the results derived from cellulose. For digested starch, the precision ranged from 0.3 to 3.7‰ and the accuracy between -2.0 and -8.0‰. The x_e of the digested starch ranged between 31.5 and 32.0% and was thus lower than the measured x_e (38.7%) and $x_{e,pot}$ of pure glucose (41.7%). This lower x_e of starch-derived sugar compared to glucose could be explained by an incomplete digestion of the starch to glucose monomers, leading to a mixture of mono- and oligosaccharides.

Overall, our results show that sugars of different classes, as well as sugar derived from digested starch can be measured with high precision, accuracy, and reproducibility. On a daily routine, we were able to measure up to 66 NSC samples and 32 standards. This proves that the method is now a reliable tool that enables high-throughput analysis of δ^2H_{ne} of NSC in plants or in other environmental or biological samples.

Application of the method for analysis of $\delta^2\text{H}_{\text{ne}}$ in plant-derived compounds

The analyses of non-exchangeable hydrogen in sugar, starch and cellulose extracted from leaves of the plants grown in a climate chamber under controlled conditions showed strong differences (Fig. 1, Table 2).

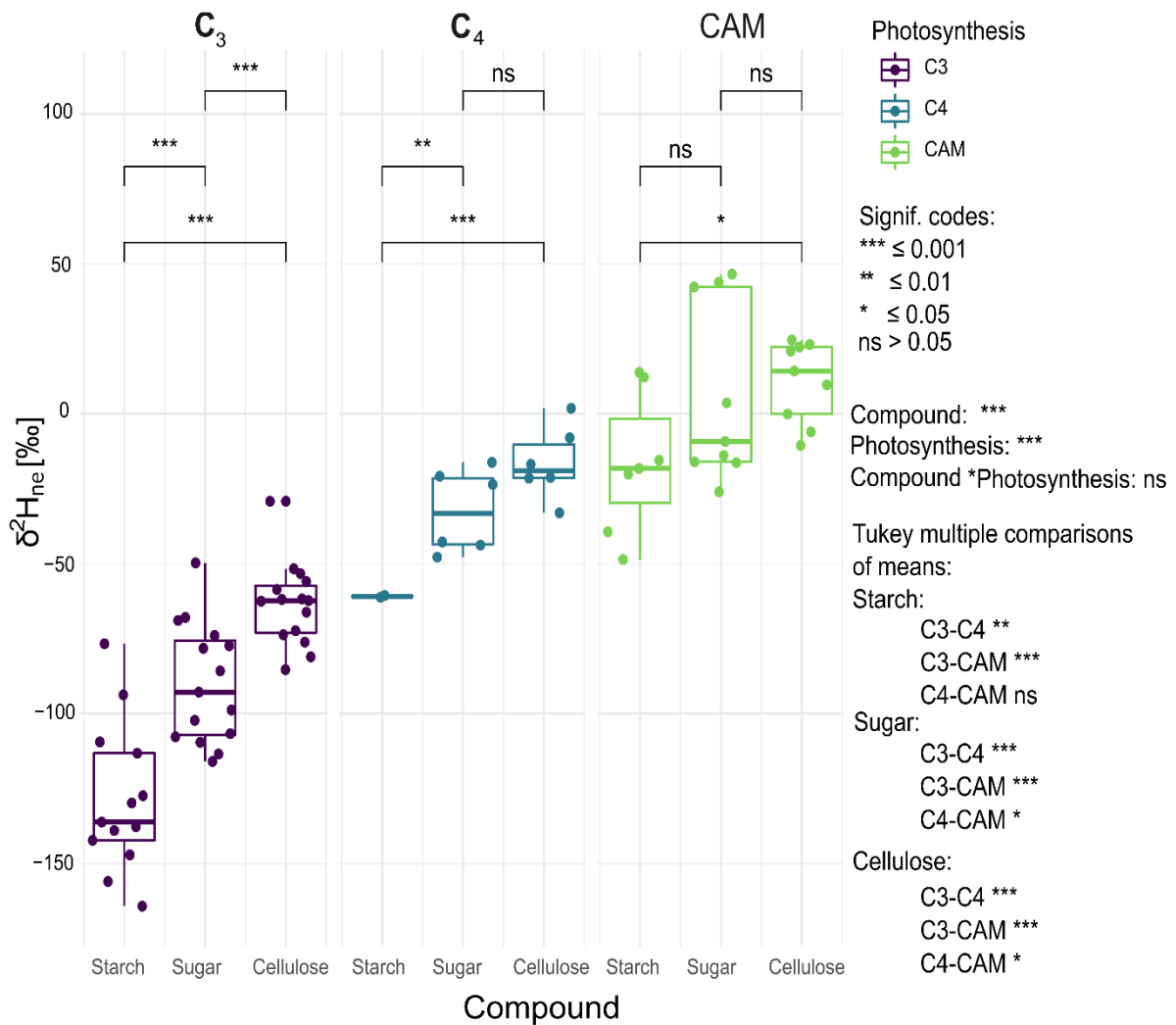


Figure 1: Comparison of $\delta^2\text{H}_{\text{ne}}$ between starch, sugar and cellulose of leaves within and between the three photosynthesis types. The boxplots show the estimated significance levels using a linear model comparing the compounds within the photosynthesis types. On the low-right side, the significant levels of a Tukey posthoc test comparing the photosynthesis types for all three compounds are given

Generally, among all the plant species and photosynthesis pathway types, starch was the most ^2H -depleted compound, followed by sugar, while cellulose was the most ^2H -enriched compound. In C_3 plants, all compounds were significantly different from each other and showed the strongest ^2H -depletion of all photosynthetic types, with a mean $\delta^2\text{H}_{\text{ne}}$ of -121.7‰ for starch, -92.0‰ for sugar, and -61.4‰ for cellulose. In C_4 plants, mean $\delta^2\text{H}_{\text{ne}}$

Table 2: $\delta^2\text{H}_{\text{ne}}$ values of plant-derived sugar, starch and cellulose from leaf material. Plant species differing in photosynthetic pathways were grown under the same controlled conditions.

Species	$\delta^2\text{H}_{\text{ne}}$ Starch [‰]		$\delta^2\text{H}_{\text{ne}}$ Sugar [‰]		$\delta^2\text{H}_{\text{ne}}$ Cellulose [‰]		Difference in $\delta^2\text{H}_{\text{ne}}$ [‰]		
	mean	SD	mean	SD	mean	SD	Cell-Starch	Sugar-Starch	Cell-Sugar
C_3 <i>Cannabis sativa</i>	-125	27.1	-99.4	15.9	-56.1	6.4	68.9	25.6	43.3
<i>Solanum cheesmaniae</i>	-147	17.2	-99.4	6.9	-78.4	6.1	68.6	47.6	21
<i>Salvia hispanica</i>	-133.9	23.3	-75.9	9.1	-50	18.1	83.8	58	25.8
<i>Abelmoschus esculentus</i>	-126.1	12.3	-111	7.3	-63.4	10.6	62.7	15.5	47.1
<i>Hordeum vulgare</i>	-76.7*	*	-74.8	5.1	-59	4.9	17.7	1.9	15.8
mean	-121.7	20	-92	8.9	-61.4	9.2	60.3	29.7	30.6
C_4 <i>Zea mays</i>	-60.6*	*	-44.8	2.6	-7.7	9.3	52.9	15.8	37.1
<i>Sorghum bicolor</i>	-61.2*	*	-20.2	3.7	-25.3	6.7	35.9	41	-5.1
mean	-60.9	*	-32.5	3.2	-16.5	8	44.4	28.4	16
<i>Portulaca grandiflora</i>	-24.8	33.7	-12.8	15.1	14.9	5.7	39.7	11.9	27.7
CAM <i>Kalanchoe daigremontiana</i>	-18	2.3	-13.2	3.6	-5.6	5.3	12.4	4.8	7.6
<i>Phalaenopsis</i>	12.1*	*	44.2	2.2	23.3	1.2	11.2	32.1	-20.9
mean	-10.2	18	6	6.9	10.9	4	21.1	16.3	4.8

* Due to low yields, starch samples of three replicates were pooled for *H. vulgare*, *Z. mays*, *S. bicolor* and *Phalaenopsis*, and thus could be only measured once.

values of -60.9‰ for starch were significantly lower compared to those of -32.5‰ and -16.5‰ for sugar and cellulose and thus reflect intermediate $\delta^2\text{H}_{\text{ne}}$

values compared to C₃ and CAM plants. In CAM plants, only $\delta^2\text{H}_{\text{ne}}$ values of starch and cellulose differed significantly and showed the strongest ²H-enrichment of all photosynthetic types, with a mean $\delta^2\text{H}_{\text{ne}}$ of -10.2‰ for starch, 6.0‰ for sugar, and 10.9‰ for cellulose. The comparison of the $\delta^2\text{H}_{\text{ne}}$ of the same compound between the photosynthetic types resulted in significant differences between C₃ and C₄ and between C₃ and CAM plants. The difference of sugar and cellulose between C₄ and CAM plants were only slightly significant and not significant for starch. Our results go along with studies on $\delta^2\text{H}_{\text{ne}}$ values of organic matter and cellulose, showing also a ²H-enrichment in C₄ and CAM plants compared to C₃ plants (Sternberg *et al.*, 1984b; Leaney *et al.*, 1985). While the observed variation in $\delta^2\text{H}_{\text{ne}}$ of NSC and cellulose among the photosynthetic pathways is unlikely to be explained solely by differences in leaf water ²H enrichment (Leaney *et al.*, 1985; Kahmen *et al.*, 2013), higher leaf water $\delta^2\text{H}$ values might partially contribute to higher $\delta^2\text{H}_{\text{ne}}$ of NSC and cellulose in CAM plants compared to C₃ plants (Smith & Ziegler, 1990). Thus, $\delta^2\text{H}$ measurement of leaf water would be important to disentangle the photosynthetic ²H-fractionation from leaf water to leaf NSC and cellulose within and between the photosynthetic types. However, $\delta^2\text{H}_{\text{ne}}$ difference among photosynthetic pathways and compounds are likely explained by ²H-fractionations in biochemical pathways, including the usage of cytoplasm derived malate as a proton source and glucose precursor in CAM and C₄ plants (Yamori *et al.*, 2014; Zhou *et al.*, 2018), which might overlay the signal of the strongly ²H-depleted NADPH produced via photosystem II (Luo *et al.*, 1991). In summary, the analyses of $\delta^2\text{H}_{\text{ne}}$ in sugars, starch and cellulose might be used to generally distinguish plants with C₃, C₄ and CAM photosynthesis.

Above that, $\delta^2\text{H}_{\text{ne}}$ values in CAM plants may indicate if a facultative CAM plant performs C₃ or C₄ photosynthesis in the absence of water stress (Winter *et al.*, 2008; Guralnick *et al.*, 2020). The higher the contribution of C₃ or C₄ photosynthesis to a CAM plant's total carbon dioxide fixation, the more depleted are the $\delta^2\text{H}_{\text{ne}}$ values of cellulose and NSC (Sternberg *et al.*, 1984a; Luo & Sternberg, 1991), thus indicating absence of water stress.

Within all the tested plant species, the orchid *Phalaenopsis* was the only species with a positive $\delta^2\text{H}_{\text{ne}}$ value in all compounds, and thus likely the only species with no or only a negligible amount of C_3 photosynthesis in mature leaves. However, the observation that *Phalaenopsis* sugars are more ^2H -enriched than cellulose in mature leaves could be explained by the presence of C_3 photosynthesis in the developing leaves (Guo & Lee, 2006), leading to ^2H -depleted cellulose during leaf formation. For the other two CAM species, the C_3 or C_4 photosynthesis contributed a higher fraction to the total carbon dioxide fixation due to the absence of water limitation and thus had lower $\delta^2\text{H}_{\text{ne}}$ values for NSC and cellulose.

The generally lower $\delta^2\text{H}_{\text{ne}}$ values of NSC compared to cellulose (Table 2) can be explained by the ^2H -depletion during photosystem II NADPH formation and the subsequent transfer of the ^2H -depleted H during the reduction of glyceraldehyde-3-phosphate (GAP), continuous enzymatic H-exchange between carbohydrates and water, and kinetic isotope effects during metabolic processes (Cormier *et al.*, 2018; Cormier *et al.*, 2019). Our results are supported by a previous study (Luo & Sternberg, 1991; Schleucher *et al.*, 1999), showing that nitrated starch was more ^2H -depleted than nitrated cellulose within the same autotrophic photosynthetic tissue, which can be interpreted as another proof for the reliability of the new method for $\delta^2\text{H}_{\text{ne}}$ values of NSC. The high variability in ^2H -fractionation in the sequence from sugars to starch to cellulose (Table 2) between all tested species indicate a high variability in common ^2H -fractionation processes, which is also supported by recent studies (Cormier *et al.*, 2018; Sanchez-Bragado *et al.*, 2019). Thus the variability in ^2H -fractionation may find application in future plant physiological studies, investigating stress responses or short- and long-term carbon dynamics. We assume that $\delta^2\text{H}_{\text{ne}}$ of NSC are susceptible to diel or seasonal changes in environmental conditions such as temperature and light intensity due to their short turnover time (Gibon *et al.*, 2004; Fernandez *et al.*, 2017). The variability in ^2H -fractionation between different species might also be important if multiple tree species are used during the

establishment of tree-ring isotope chronologies in dendroclimatological studies (Arosio *et al.*, 2020a).

In conclusion, we show that a hot water vapor equilibration method originally developed for cellulose can be adapted for accurate, precise and reproducible analyses of $\delta^2\text{H}_{\text{ne}}$ in non-structural carbohydrates (NSC) such as sugar and starch. By applying the method for compounds from different plant species, we demonstrated that this analytical method can now be used to estimate ^2H -fractionation among structural and non-structural carbohydrates and to distinguish plant material from plants with different photosynthetic pathways. It should be noted that the method presented herein enables analysis of $\delta^2\text{H}_{\text{ne}}$ of bulk sugar and sugar derived from digested starch and is therefore not compound-specific nor position-specific. Yet, our $\delta^2\text{H}_{\text{ne}}$ method allows to measure NSC samples in high-throughput and we thus expect that it will help to identify important ^2H -fractionation processes. These findings could then eventually be studied in more detail with compound-specific methods (GC-IRMS (Abraham *et al.*, 2020)) or methods giving positional information (NMR (Ehlers *et al.*, 2015)). We therefore expect that the method will find widespread applications in plant physiological, hydrological, ecological and agricultural research to study NSC fluxes and plant performance, and the beverage and food industry, to distinguish between sugars of different origin, which could be applied to check if a certain product is altered by the addition of low-cost supplements. We also expect that the method can help to improve mechanistic models for ^2H distributions in organic material (Yakir & DeNiro, 1990; Roden *et al.*, 2000). The method may further help, in combination with other hydrogen isotope proxies (e.g. fatty acids, n-alkanes or lignin methoxy groups), researchers to better understand metabolic pathways and fluxes, shaping the hydrogen isotopic composition of plant material.

Acknowledgements

We thank Patrick Flütsch at ETH Zurich for technical support, as well as Manuela Laski, Manuela Oettli, Oliver Rehmann, and Neptun at WSL Birmensdorf for laboratory assistance. Our work was supported by the innovative project “HDoor2020” at WSL, by the SNF Ambizione project "TreeCarbo" (No. 179978, granted to M.M.L.), the SNF-project "Isodrought" (No. 182092, granted to MS), and by funding from the UK Biotechnology and Biological Sciences Research Council (received by M.-A.C).

References

- Abraham A, Cannavan A, Kelly SD. 2020.** Stable isotope analysis of non-exchangeable hydrogen in carbohydrates derivatised with N-methyl-bis-trifluoroacetamide by gas chromatography–Chromium silver reduction/High temperature Conversion-isotope ratio mass spectrometry (GC-CrAg/HTC-IRMS). *Food Chemistry* **318**: 126413.
- Alexander W, Mitchell R. 1949.** Rapid measurement of cellulose viscosity by nitration methods. *Analytical Chemistry* **21**(12): 1497-1500.
- An W, Liu X, Leavitt SW, Xu G, Zeng X, Wang W, Qin D, Ren J. 2014.** Relative humidity history on the Batang–Litang Plateau of western China since 1755 reconstructed from tree-ring $\delta^{18}\text{O}$ and δD . *Climate Dynamics* **42**: 2639-2654.
- Anhäuser T, Hook BA, Halfar J, Greule M, Keppler F. 2018.** Earliest Eocene cold period and polar amplification-Insights from $\delta^2\text{H}$ values of lignin methoxyl groups of mummified wood. *Palaeogeography, Palaeoclimatology, Palaeoecology* **505**: 326-336.
- Arosio T, Ziehmer-Wenz M, Nicolussi K, Schlüchter C, Leuenberger M. 2020a.** Larch Cellulose Shows Significantly Depleted Hydrogen Isotope Values With Respect to Evergreen Conifers in Contrast to Oxygen and Carbon Isotopes. *Frontiers in Earth Science* **8**(579).

- Arosio T, Ziehmer MM, Nicolussi K, Schlüchter C, Leuenberger M. 2020b.** Alpine Holocene tree-ring dataset: age-related trends in the stable isotopes of cellulose show species-specific patterns. *Biogeosciences* **17**(19): 4871-4882.
- Augusti A, Betson TR, Schleucher J. 2008.** Deriving correlated climate and physiological signals from deuterium isotopomers in tree rings. *Chemical Geology* **252**(1-2): 1-8.
- Boettger T, Haupt M, Knöller K, Weise SM, Waterhouse JS, Rinne KT, Loader NJ, Sonninen E, Jungner H, Masson-Delmotte V. 2007.** Wood cellulose preparation methods and mass spectrometric analyses of $\delta^{13}\text{C}$, $\delta^{18}\text{O}$, and nonexchangeable $\delta^2\text{H}$ values in cellulose, sugar, and starch: an interlaboratory comparison. *Analytical Chemistry* **79**(12): 4603-4612.
- Cernusak LA, Barbour MM, Arndt SK, Cheesman AW, English NB, Feild TS, Helliker BR, Holloway-Phillips MM, Holtum JAM, Kahmen A, et al. 2016.** Stable isotopes in leaf water of terrestrial plants. *Plant, Cell & Environment* **39**(5): 1087-1102.
- Chami Khazraji A, Robert S. 2013.** Interaction Effects between Cellulose and Water in Nanocrystalline and Amorphous Regions: A Novel Approach Using Molecular Modeling. *Journal of Nanomaterials* **2013**: 409676.
- Coplen TB. 2011.** Guidelines and recommended terms for expression of stable-isotope-ratio and gas-ratio measurement results. *Rapid Communications in Mass Spectrometry* **25**(17): 2538-2560.
- Cormier M-A, Werner RA, Leuenberger MC, Kahmen A. 2019.** ^2H -enrichment of cellulose and n-alkanes in heterotrophic plants. *Oecologia* **189**(2): 365-373.
- Cormier M-A, Werner RA, Sauer PE, Gröcke DR, Leuenberger MC, Wieloch T, Schleucher J, Kahmen A. 2018.** ^2H -fractionations during the

- biosynthesis of carbohydrates and lipids imprint a metabolic signal on the $\delta^2\text{H}$ values of plant organic compounds. *New Phytologist* **218**(2): 479-491.
- DeNiro MJ. 1981.** The effects of different methods of preparing cellulose nitrate on the determination of the D/H ratios of non-exchangeable hydrogen of cellulose. *Earth and Planetary Science Letters* **54**(2): 177-185.
- Dunbar J, Schmidt H-L. 1984.** Measurement of the $^2\text{H}/^1\text{H}$ ratios of the carbon bound hydrogen atoms in sugars. *Fresenius' Zeitschrift für analytische Chemie* **317**(8): 853-857.
- Dunbar J, Wilson A. 1983.** Oxygen and hydrogen isotopes in fruit and vegetable juices. *Plant Physiology* **72**(3): 725-727.
- Ehlers I, Augusti A, Betson TR, Nilsson MB, Marshall JD, Schleucher J. 2015.** Detecting long-term metabolic shifts using isotopomers: CO_2 -driven suppression of photorespiration in C_3 plants over the 20th century. *Proceedings of the National Academy of Sciences* **112**(51): 15585-15590.
- Epstein S, Yapp CJ, Hall JH. 1976.** The determination of the D/H ratio of non-exchangeable hydrogen in cellulose extracted from aquatic and land plants. *Earth and Planetary Science Letters* **30**(2): 241-251.
- Estep MF, Hoering TC. 1981.** Stable Hydrogen Isotope Fractionations during Autotrophic and Mixotrophic Growth of Microalgae. *Plant Physiology* **67**(3): 474-477.
- Fernandez O, Ishihara H, George GM, Mengin V, Flis A, Sumner D, Arrivault S, Feil R, Lunn JE, Zeeman SC. 2017.** Leaf starch turnover occurs in long days and in falling light at the end of the day. *Plant Physiology* **174**(4): 2199-2212.
- Filot MS, Leuenberger M, Pazdur A, Boettger T. 2006.** Rapid online equilibration method to determine the D/H ratios of non-

exchangeable hydrogen in cellulose. *Rapid Communications in Mass Spectrometry* **20**(22): 3337-3344.

Gaglioti BV, Mann DH, Wooller MJ, Jones BM, Wiles GC, Groves P, Kunz ML, Baughman CA, Reanier RE. 2017. Younger-Dryas cooling and sea-ice feedbacks were prominent features of the Pleistocene-Holocene transition in Arctic Alaska. *Quaternary Science Reviews* **169**: 330-343.

Gamarra B, Kahmen A. 2015. Concentrations and $\delta^2\text{H}$ values of cuticular n-alkanes vary significantly among plant organs, species and habitats in grasses from an alpine and a temperate European grassland. *Oecologia* **178**(4): 981-998.

Gehre M, Geilmann H, Richter J, Werner R, Brand W. 2004. Continuous flow $^2\text{H}/^1\text{H}$ and $^{18}\text{O}/^{16}\text{O}$ analysis of water samples with dual inlet precision. *Rapid Communications in Mass Spectrometry* **18**(22): 2650-2660.

Gehre M, Renpenning J, Gilevska T, Qi H, Coplen T, Meijer H, Brand W, Schimmelmann A. 2015. On-line hydrogen-isotope measurements of organic samples using elemental chromium: an extension for high temperature elemental-analyzer techniques. *Analytical Chemistry* **87**(10): 5198-5205.

Gessler A, Ferrio JP, Hommel R, Treydte K, Werner RA, Monson RK. 2014. Stable isotopes in tree rings: towards a mechanistic understanding of isotope fractionation and mixing processes from the leaves to the wood. *Tree Physiology* **34**(8): 796-818.

Gibon Y, Bläsing OE, Palacios-Rojas N, Pankovic D, Hendriks JH, Fisahn J, Höhne M, Günther M, Stitt M. 2004. Adjustment of diurnal starch turnover to short days: depletion of sugar during the night leads to a temporary inhibition of carbohydrate utilization, accumulation of sugars and post-translational activation of ADP-glucose pyrophosphorylase in the following light period. *The Plant Journal* **39**(6): 847-862.

- Gudasz C, Soto DX, Sparrman T, Karlsson J 2020.** A novel method to quantify exchangeable hydrogen fraction in organic matter. *EGU General Assembly Conference Abstracts*. 11630.
- Guo W-J, Lee N. 2006.** Effect of leaf and plant age, and day/night temperature on net CO₂ uptake in *Phalaenopsis amabilis* var. *formosa*. *Journal of the American Society for Horticultural Science* **131**(3): 320-326.
- Guralnick LJ, Gilbert KE, Denio D, Antico N. 2020.** The development of crassulacean acid metabolism (CAM) photosynthesis in cotyledons of the C₄ species, *Portulaca grandiflora* (Portulacaceae). *Plants* **9**(1): 55.
- Hepp J, Glaser B, Juchelka D, Mayr C, Rozanski K, Schäfer IK, Stichler W, Tuthorn M, Zech R, Zech M. 2019.** Validation of a coupled $\delta^2\text{H}$ n-alkane- $\delta^{18}\text{O}$ sugar paleohygrometer approach based on a climate chamber experiment. *Biogeosciences Discussions*: 1-30.
- Hepp J, Tuthorn M, Zech R, Mügler I, Schlütz F, Zech W, Zech M. 2015.** Reconstructing lake evaporation history and the isotopic composition of precipitation by a coupled $\delta^{18}\text{O}$ - $\delta^2\text{H}$ biomarker approach. *Journal of Hydrology* **529**: 622-631.
- Jungnikl K, Paris O, Fratzl P, Burgert I. 2007.** The implication of chemical extraction treatments on the cell wall nanostructure of softwood. *Cellulose* **15**(3): 407.
- Kahmen A, Schefuß E, Sachse D. 2013.** Leaf water deuterium enrichment shapes leaf wax n-alkane δD values of angiosperm plants I: Experimental evidence and mechanistic insights. *Geochimica et Cosmochimica Acta* **111**: 39-49.
- Leaney F, Osmond C, Allison G, Ziegler H. 1985.** Hydrogen-isotope composition of leaf water in C₃ and C₄ plants: its relationship to the hydrogen-isotope composition of dry matter. *Planta* **164**(2): 215-220.

- Lehmann MM, Egli M, Brinkmann N, Werner RA, Saurer M, Kahmen A. 2020.** Improving the extraction and purification of leaf and phloem sugars for oxygen isotope analyses. *Rapid Communications in Mass Spectrometry* **34**(19): e8854.
- Lehmann MM, Vitali V, Schuler P, Leuenberger M, Saurer M. 2021.** More than climate: Hydrogen isotope ratios in tree rings as novel plant physiological indicator for stress conditions. *Dendrochronologia* **65**: 125788.
- Luo Y-H, Steinberg L, Suda S, Kumazawa S, Mitsui A. 1991.** Extremely low D/H ratios of photoproduced hydrogen by cyanobacteria. *Plant and Cell Physiology* **32**(6): 897-900.
- Luo Y-H, Sternberg L. 1991.** Deuterium heterogeneity in starch and cellulose nitrate of CAM and C₃ plants. *Phytochemistry* **30**(4): 1095-1098.
- Manrique-Alba À, Beguería S, Molina AJ, González-Sanchis M, Tomàs-Burguera M, del Campo AD, Colangelo M, Camarero JJ. 2020.** Long-term thinning effects on tree growth, drought response and water use efficiency at two Aleppo pine plantations in Spain. *Science of The Total Environment* **728**: 138536.
- McCarroll D, Loader NJ. 2004.** Stable isotopes in tree rings. *Quaternary Science Reviews* **23**(7-8): 771-801.
- Mischel M, Esper J, Keppler F, Greule M, Werner W. 2015.** $\delta^2\text{H}$, $\delta^{13}\text{C}$ and $\delta^{18}\text{O}$ from whole wood, α -cellulose and lignin methoxyl groups in *Pinus sylvestris*: a multi-parameter approach. *Isotopes in Environmental and Health Studies* **51**(4): 553-568.
- Nakatsuka T, Sano M, Li Z, Xu C, Tsushima A, Shigeoka Y, Sho K, Ohnishi K, Sakamoto M, Ozaki H. 2020.** A 2600-year summer climate reconstruction in central Japan by integrating tree-ring stable oxygen and hydrogen isotopes. *Climate of the Past* **16**(6): 2153-2172.

- Porter TJ, Pisaric MF, Field RD, Kokelj SV, Edwards TW, deMontigny P, Healy R, LeGrande AN. 2014.** Spring-summer temperatures since AD 1780 reconstructed from stable oxygen isotope ratios in white spruce tree-rings from the Mackenzie Delta, northwestern Canada. *Climate Dynamics* **42**(3-4): 771-785.
- R.Core.Team 2023.** R: A language and environment for statistical computing. *R Foundation for Statistical Computing, Vienna, Austria.*
- Richter A, Wanek W, Werner RA, Ghashghaie J, Jäggi M, Gessler A, Brugnoli E, Hettmann E, Göttlicher SG, Salmon Y. 2009.** Preparation of starch and soluble sugars of plant material for the analysis of carbon isotope composition: a comparison of methods. *Rapid Communications in Mass Spectrometry: An International Journal Devoted to the Rapid Dissemination of Up-to-the-Minute Research in Mass Spectrometry* **23**(16): 2476-2488.
- Rinne KT, Saurer M, Streit K, Siegwolf RT. 2012.** Evaluation of a liquid chromatography method for compound-specific $\delta^{13}\text{C}$ analysis of plant carbohydrates in alkaline media. *Rapid Communications in Mass Spectrometry* **26**(18): 2173-2185.
- Roden JS, Lin G, Ehleringer JR. 2000.** A mechanistic model for interpretation of hydrogen and oxygen isotope ratios in tree-ring cellulose. *Geochimica et Cosmochimica Acta* **64**(1): 21-35.
- Sachse D, Billault I, Bowen GJ, Chikaraishi Y, Dawson TE, Feakins SJ, Freeman KH, Magill CR, McInerney FA, Van Der Meer MT. 2012.** Molecular paleohydrology: interpreting the hydrogen-isotopic composition of lipid biomarkers from photosynthesizing organisms. *Annual Review of Earth and Planetary Sciences* **40**: 221-249.
- Sanchez-Bragado R, Serret MD, Marimon RM, Bort J, Araus JL. 2019.** The Hydrogen Isotope Composition $\delta^2\text{H}$ Reflects Plant Performance. *Plant Physiology* **180**(2): 793-812.

- Sass-Klaassen U, Poole I, Wils T, Helle G, Schleser G, Van Bergen P. 2005.** Carbon and oxygen isotope dendrochronology in sub-fossil bog oak tree rings-a preliminary study. *IAWA journal* **26**(1): 121-136.
- Sauer PE, Schimmelmann A, Sessions AL, Topalov K. 2009.** Simplified batch equilibration for D/H determination of non-exchangeable hydrogen in solid organic material. *Rapid Communications in Mass Spectrometry: An International Journal Devoted to the Rapid Dissemination of Up-to-the-Minute Research in Mass Spectrometry* **23**(7): 949-956.
- Saurer M, Borella S, Leuenberger M. 1997.** $\delta^{18}\text{O}$ of tree rings of beech (*Fagus sylvatica*) as a record of $\delta^{18}\text{O}$ of the growing season precipitation. *Tellus B: Chemical and Physical Meteorology* **49**(1): 80-92.
- Saurer M, Kress A, Leuenberger M, Rinne KT, Treydte KS, Siegwolf RT. 2012.** Influence of atmospheric circulation patterns on the oxygen isotope ratio of tree rings in the Alpine region. *Journal of Geophysical Research: Atmospheres* **117**(D5).
- Schimmelmann A. 1991.** Determination of the concentration and stable isotopic composition of nonexchangeable hydrogen in organic matter. *Analytical Chemistry* **63**(21): 2456-2459.
- Schimmelmann A, Deniro MJ, Poulicek M, Voss-Foucart M-F, Goffinet G, Jeuniaux C. 1986.** Stable isotopic composition of chitin from arthropods recovered in archaeological contexts as palaeoenvironmental indicators. *Journal of Archaeological Science* **13**(6): 553-566.
- Schimmelmann A, Lewan MD, Wintsch RP. 1999.** D/H isotope ratios of kerogen, bitumen, oil, and water in hydrous pyrolysis of source rocks containing kerogen types I, II, IIS, and III. *Geochimica et Cosmochimica Acta* **63**(22): 3751-3766.

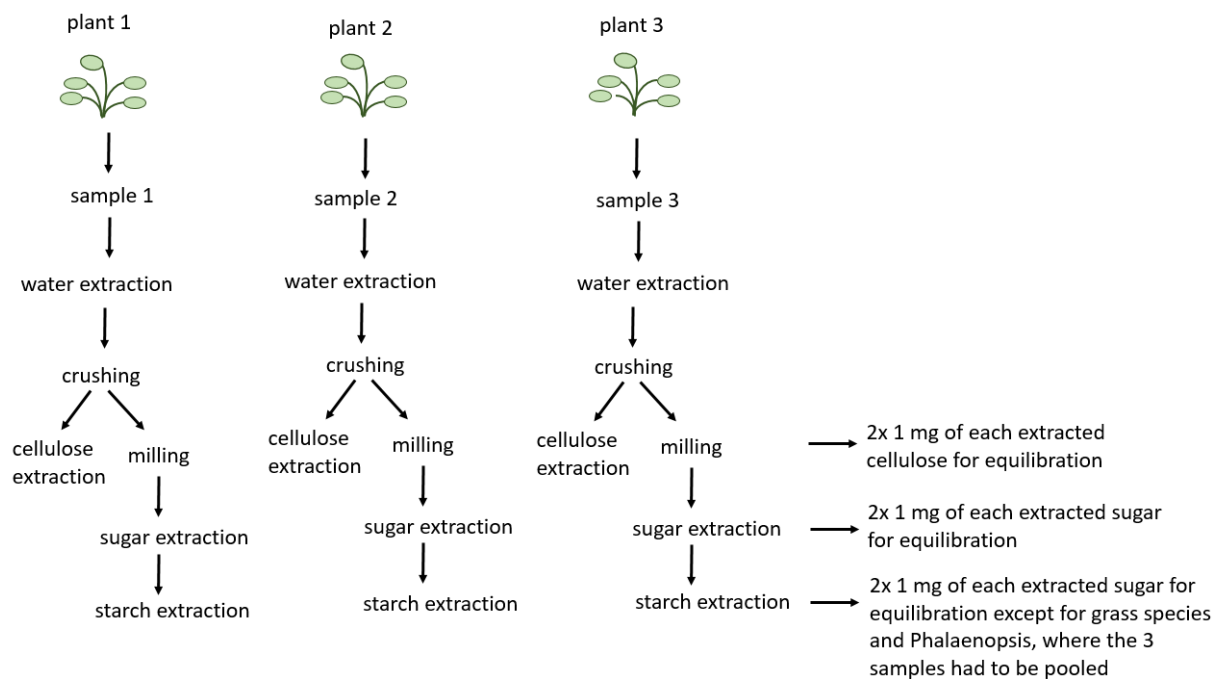
- Schimmelmann A, Qi H, Coplen TB, Brand WA, Fong J, Meier-Augenstein W, Kemp HF, Toman B, Ackermann A, Assonov S. 2016.** Organic reference materials for hydrogen, carbon, and nitrogen stable isotope-ratio measurements: caffeines, n-alkanes, fatty acid methyl esters, glycines, l-valines, polyethylenes, and oils. *Analytical Chemistry* **88**(8): 4294-4302.
- Schleucher J, Vanderveer P, Markley JL, Sharkey TD. 1999.** Intramolecular deuterium distributions reveal disequilibrium of chloroplast phosphoglucose isomerase. *Plant, Cell & Environment* **22**(5): 525-533.
- Schmidt H-L, Werner RA, Eisenreich W. 2003.** Systematics of ^2H patterns in natural compounds and its importance for the elucidation of biosynthetic pathways. *Phytochemistry Reviews* **2**(1): 61-85.
- Smith B, Ziegler H. 1990.** Isotopic fractionation of hydrogen in plants. *Botanica Acta* **103**(4): 335-342.
- Sternberg L, Deniro M, Johnson H. 1984a.** Isotope ratios of cellulose from plants having different photosynthetic pathways. *Plant Physiology* **74**(3): 557-561.
- Sternberg L, Deniro MJ, Ajie H. 1984b.** Stable hydrogen isotope ratios of saponifiable lipids and cellulose nitrate from CAM, C_3 and C_4 plants. *Phytochemistry* **23**(11): 2475-2477.
- Tipple BJ, Ehleringer JR. 2018.** Distinctions in heterotrophic and autotrophic-based metabolism as recorded in the hydrogen and carbon isotope ratios of normal alkanes. *Oecologia* **187**(4): 1053-1075.
- Wanek W, Heintel S, Richter A. 2001.** Preparation of starch and other carbon fractions from higher plant leaves for stable carbon isotope analysis. *Rapid Communications in Mass Spectrometry* **15**(14): 1136-1140.
- Wassenaar LI, Hobson KA. 2000.** Improved method for determining the stable-hydrogen isotopic composition (δD) of complex organic

- materials of environmental interest. *Environmental Science & Technology* **34**(11): 2354-2360.
- Werner RA, Brand WA. 2001.** Referencing strategies and techniques in stable isotope ratio analysis. *Rapid Communications in Mass Spectrometry* **15**(7): 501-519.
- West AG, Patrickson SJ, Ehleringer JR. 2006.** Water extraction times for plant and soil materials used in stable isotope analysis. *Rapid Communications in Mass Spectrometry: An International Journal Devoted to the Rapid Dissemination of Up-to-the-Minute Research in Mass Spectrometry* **20**(8): 1317-1321.
- Winter K, Garcia M, Holtum JA. 2008.** On the nature of facultative and constitutive CAM: environmental and developmental control of CAM expression during early growth of *Clusia*, *Kalanchoë*, and *Opuntia*. *Journal of Experimental Botany* **59**(7): 1829-1840.
- Xia Z, Zheng Y, Stelling JM, Loisel J, Huang Y, Yu Z. 2020.** Environmental controls on the carbon and water (H and O) isotopes in peatland *Sphagnum* mosses. *Geochimica et Cosmochimica Acta*.
- Yakir D, DeNiro MJ. 1990.** Oxygen and hydrogen isotope fractionation during cellulose metabolism in *Lemna gibba* L. *Plant Physiology* **93**(1): 325-332.
- Yamori W, Hikosaka K, Way DA. 2014.** Temperature response of photosynthesis in C₃, C₄, and CAM plants: temperature acclimation and temperature adaptation. *Photosynthesis Research* **119**(1-2): 101-117.
- Zhang BL, Quemerais B, Martin ML, Martin GJ, Williams JM. 1994.** Determination of the natural deuterium distribution in glucose from plants having different photosynthetic pathways. *Phytochemical Analysis* **5**(3): 105-110.

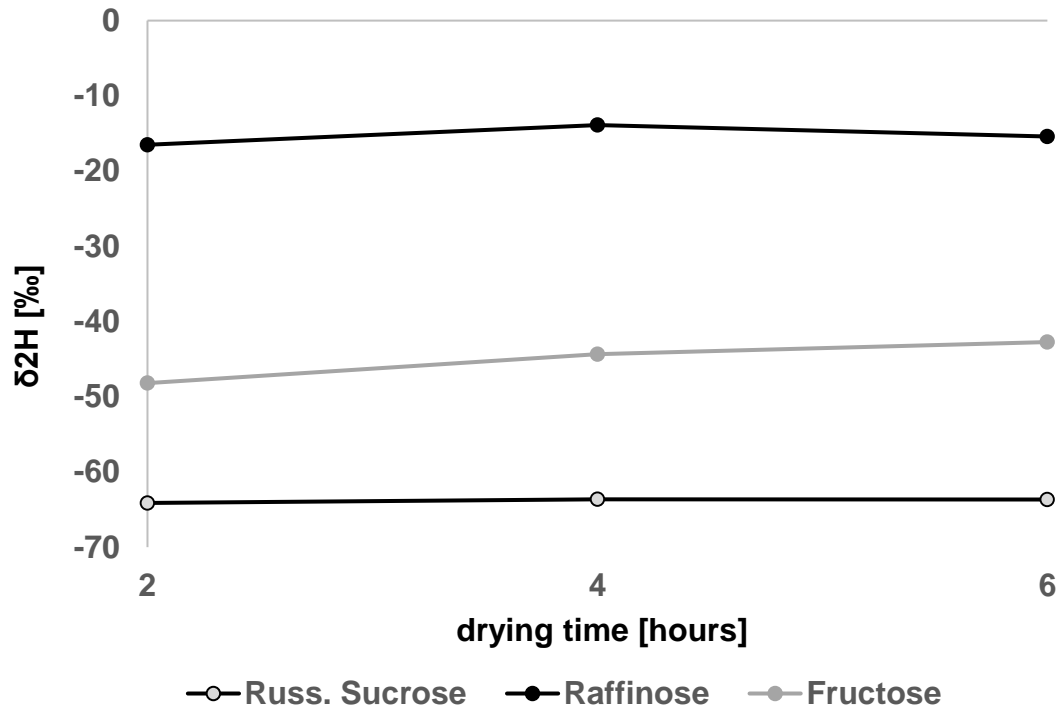
Zhou Y, Zhang B, Stuart-Williams H, Grice K, Hocart CH, Gessler A, Kayler ZE, Farquhar GD. 2018. On the contributions of photorespiration and compartmentation to the contrasting intramolecular ^2H profiles of C_3 and C_4 plant sugars. *Phytochemistry* 145: 197-206.

Zhu Z, Yin X, Song X, Wang B, Ma R, Zhao Y, Rani A, Wang Y, Yan Q, Jing S. 2020. Leaf transition from heterotrophy to autotrophy is recorded in the intraleaf C, H and O isotope patterns of leaf organic matter. *Rapid Communications in Mass Spectrometry* 34(19): e8840.

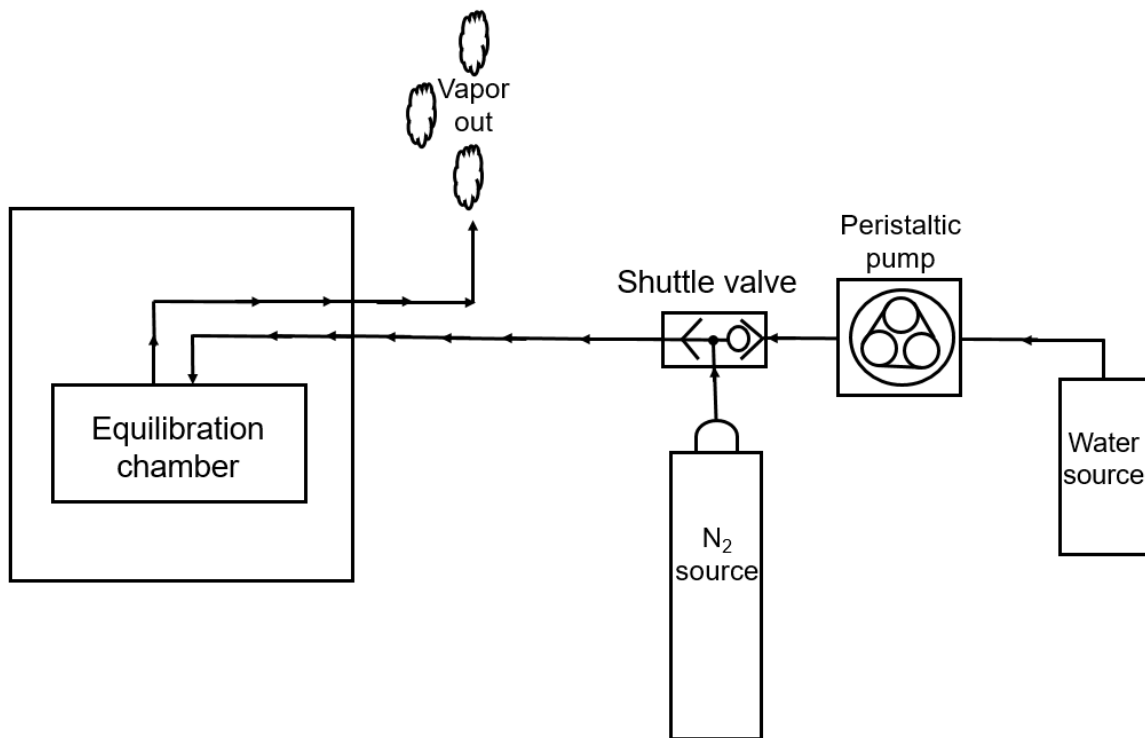
Supporting Information



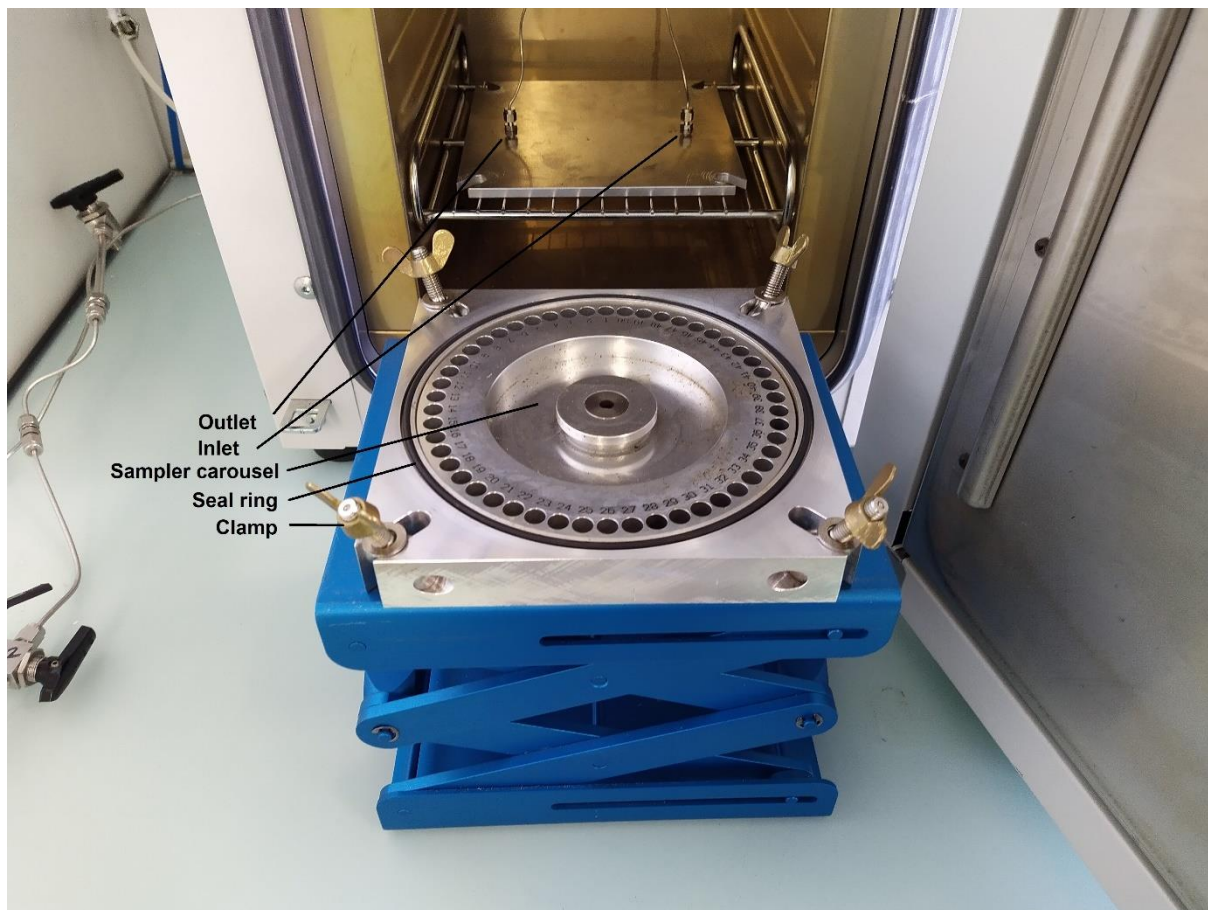
Appendix 1: Overview of the sample processing of the plant derived samples. For *H. vulgare*, the plant 1, 2 and 3 representing individual pools of four plants.



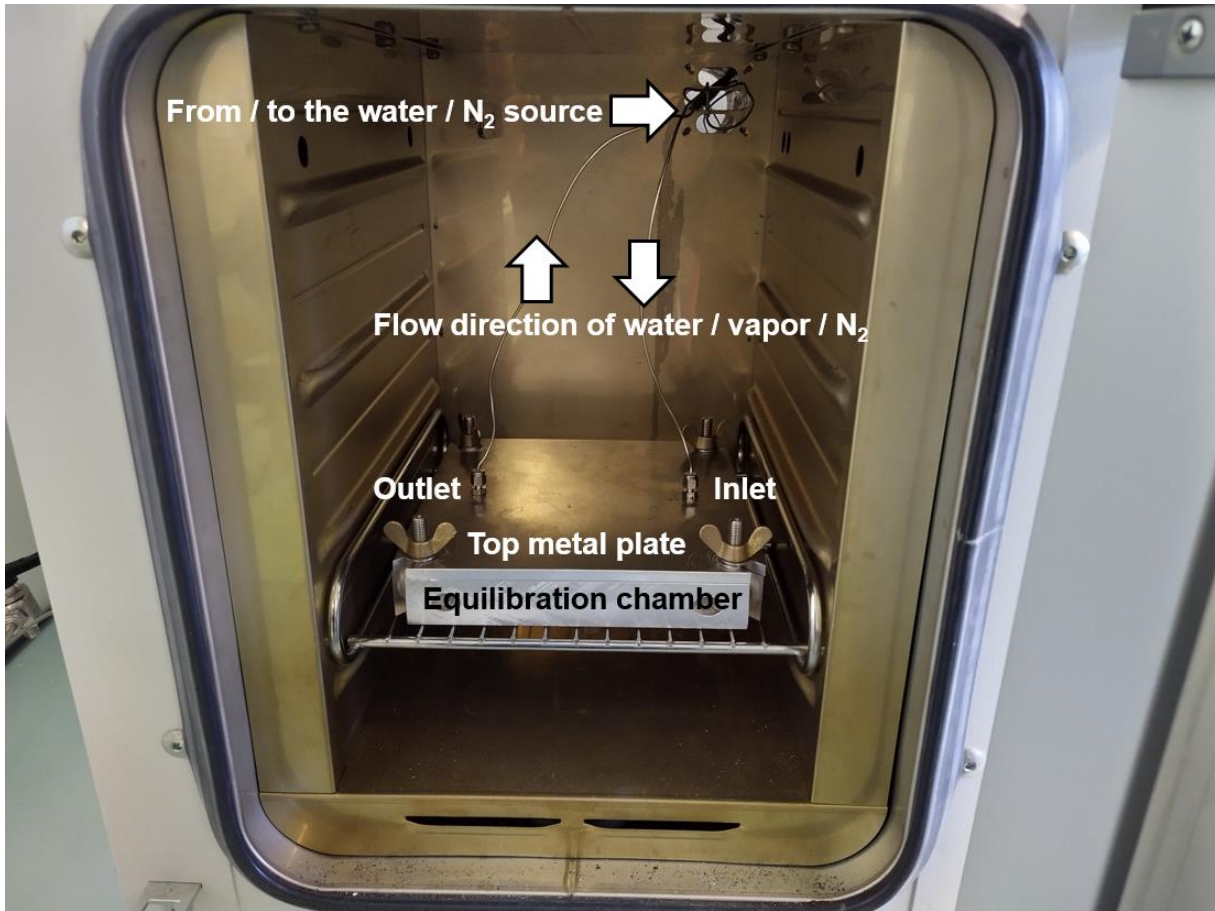
Appendix 2: $\delta^2\text{H}$ measurement of three sugars measured after two, four, and six hours drying with dry nitrogen gas after equilibration



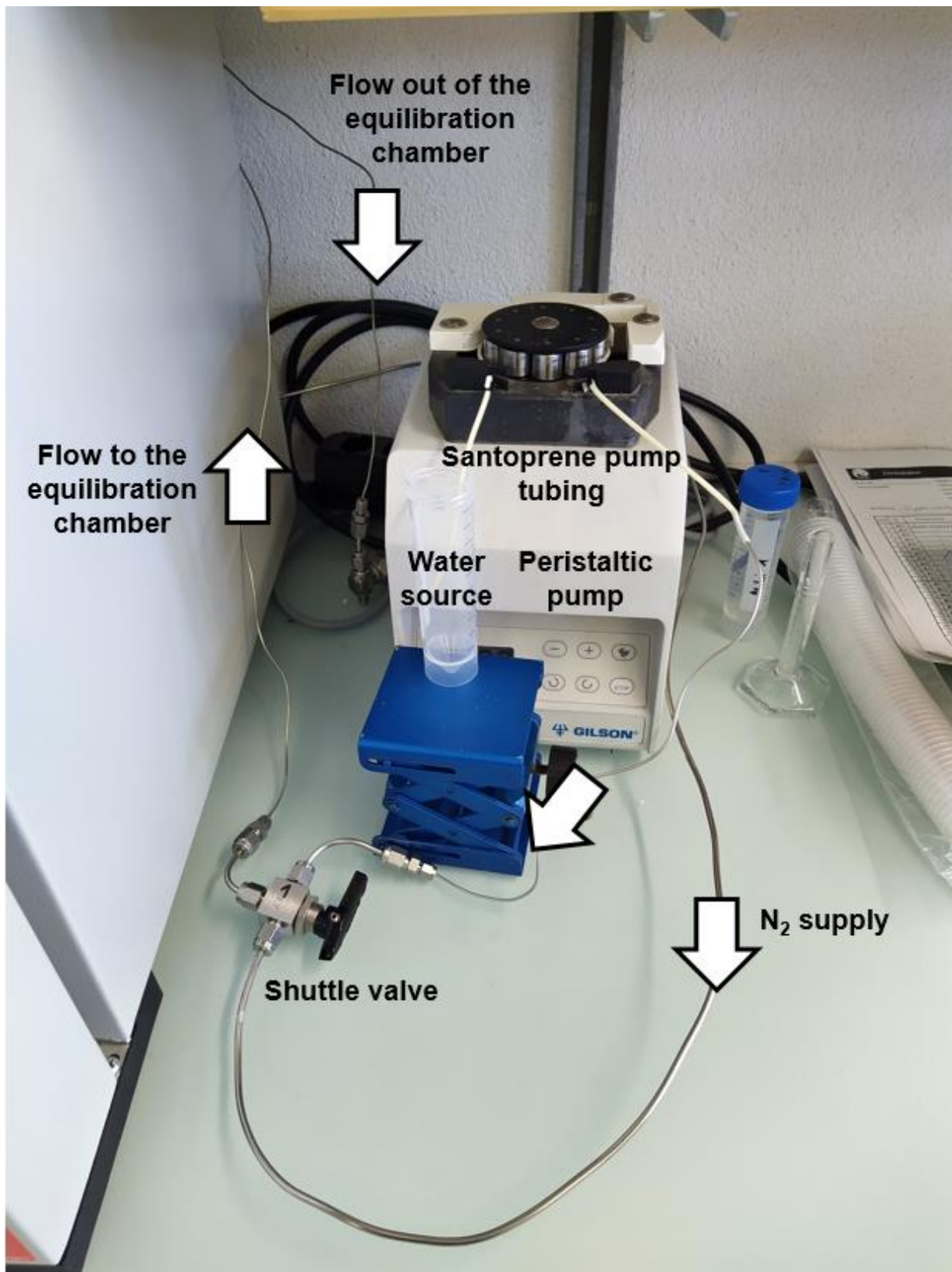
Appendix 3: Overview sketch of the equilibration system



Appendix 4: Inner structure of the equilibration chamber



Appendix 5: Outer structure of the equilibration chamber

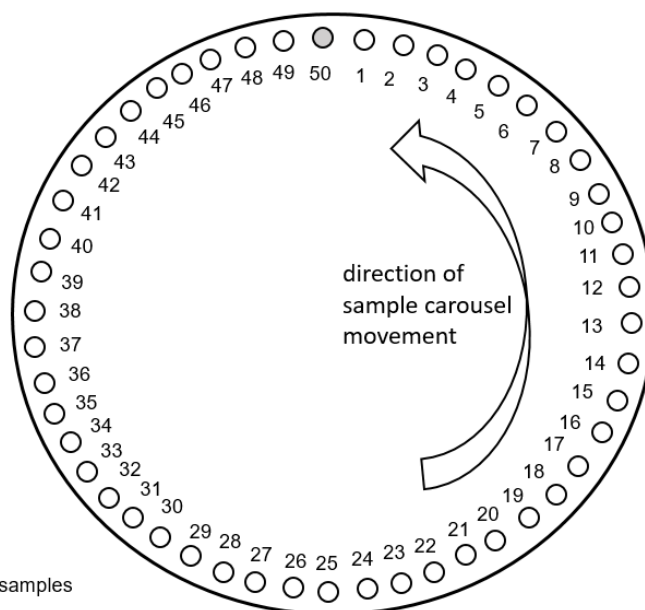


Appendix 6: Water source and dry nitrogen gas connection

Typical loading scheme for one equilibration

- 1-3: polyethylene foil
- 4-6: cellulose or sugar standard 1
- 7-9: cellulose or sugar standard 2
- 10-12: cellulose or sugar standard 3
- 13: polyethylene foil
- 14-24: samples
- 25: polyethylene foil
- 26-36: samples
- 37: polyethylene foil
- 38-48: samples
- 49: polyethylene foil
- 50: zero blank

Total: 7 polyethylene foil, 9 standards for normalization, 33 samples



Appendix 7: Typical loading scheme for one hot water vapor equilibration

Chapter 3

Hydrogen isotope fractionation in carbohydrates of leaves and xylem tissues follows distinct phylogenetic patterns: A common garden experiment with 73 tree and shrub species

Philipp Schuler^{1,2}, Valentina Vitali¹, Matthias Saurer¹, Arthur Gessler^{1,2}, Nina Buchmann², Marco M. Lehmann¹

¹Forest Dynamics, Swiss Federal Institute for Forest, Snow and Landscape Research WSL, 8903 Birmensdorf, Switzerland

²Department of Environmental Systems Science, ETH Zurich, 8092 Zurich, Switzerland

This chapter has been published in the peer-reviewed journal “New Phytologist”

Schuler P, Vitali V, Saurer M, Gessler A, Buchmann N, Lehmann MM (2023). *New Phytologist*. 239 (2), 547-561. <https://doi.org/10.1111/nph.18976>

Abstract

Recent methodological advancements in determining the nonexchangeable hydrogen isotopic composition ($\delta^2\text{H}_{\text{ne}}$) of plant carbohydrates make it possible to disentangle the drivers of hydrogen isotope (^2H) fractionation processes in plants.

Here, we investigated the influence of phylogeny on the $\delta^2\text{H}_{\text{ne}}$ of twig xylem cellulose and xylem water, as well as leaf sugars and leaf water, across 73 Northern Hemisphere tree and shrub species growing in a common garden.

^2H fractionation in plant carbohydrates followed distinct phylogenetic patterns, with phylogeny reflected more in the $\delta^2\text{H}_{\text{ne}}$ of leaf sugars than in that of twig xylem cellulose. Phylogeny had no detectable influence on the $\delta^2\text{H}_{\text{ne}}$ of twig or leaf water, showing that biochemistry, not isotopic differences in plant water, caused the observed phylogenetic pattern in carbohydrates. Angiosperms were more ^2H -enriched than gymnosperms, but substantial $\delta^2\text{H}_{\text{ne}}$ variations also occurred at the order, family, and species levels within both clades. Differences in the strength of the phylogenetic signals in $\delta^2\text{H}_{\text{ne}}$ of leaf sugars and twig xylem cellulose suggest that the original phylogenetic signal of autotrophic processes was altered by subsequent species-specific metabolism.

Our results will help improve ^2H fractionation models for plant carbohydrates and have important consequences for dendrochronological and ecophysiological studies.

Introduction

Isotope ratios of the non-exchangeable hydrogen in plant carbohydrates ($\delta^2\text{H}_{\text{ne}}$; i.e. the hydrogen that is bound to carbon) are becoming an increasingly important proxy for the study of metabolic pathways (Cormier *et al.*, 2018; Sanchez-Bragado *et al.*, 2019; Schuler *et al.*, 2022; Wieloch *et al.*, 2022), the origin of plant water (Kagawa, 2020), plant internal carbohydrate dynamics (Lehmann *et al.*, 2021), and past climatic conditions (Yapp & Epstein, 1982; Augusti *et al.*, 2008). However, the actual ^2H fractionation processes influencing the $\delta^2\text{H}_{\text{ne}}$ of sugars and cellulose in autotrophic and heterotrophic tissues remain elusive (Badea *et al.*, 2021; Schönbeck & Santiago, 2022). Recent studies have highlighted that the transfer of the ^2H signal from leaf sugars to leaf cellulose (Holloway-Phillips *et al.*, 2022) or from source water to tree-ring cellulose (Arosio *et al.*, 2020a; Lehmann *et al.*, 2022; Vitali *et al.*, 2022) varies both within and among species and is also dynamic over time. However, systematic studies on potential phylogenetic effects on $\delta^2\text{H}_{\text{ne}}$ in trees are still missing.

The isotopic composition of source water, which is mostly taken up by plant roots (Ziegler, 1989), depends on the isotopic composition of the rain, which is strongly influenced by air temperature and the distance to the ocean, among other factors (Craig, 1961; Dansgaard, 1964). Although a ^2H fractionation effect was recently observed during root water uptake in *Fagus sylvatica* L. (Barbeta *et al.*, 2020), the observed fractionation process might have been a methodological artefact potentially caused by the small amount of extracted water (Diao *et al.*, 2022). Generally, however, source water uptake by roots is thought to have no distinct ^2H fractionation effect (White, 1989). Subsequently, water is transported into leaves, where ^2H becomes enriched in the leaf water due to evaporative enrichment (Farquhar *et al.*, 2007) and the ^2H signal is mixed with the isotopic signal of atmospheric water vapour and rain (Lehmann *et al.*, 2018; Kagawa, 2020; Cernusak *et al.*, 2022). The ^2H fractionation processes in plant water are mainly the result of physical processes and can be modelled accurately

(Cernusak *et al.*, 2016). Such models consider the transfer of $\delta^2\text{H}$ of source and leaf water to the $\delta^2\text{H}_{\text{ne}}$ of tree-ring cellulose (Roden & Ehleringer, 2000; Roden *et al.*, 2000). In contrast, the metabolic ^2H fractionation processes that shape $\delta^2\text{H}$ in plant carbohydrates are poorly understood. Large variation can occur in the $\delta^2\text{H}$ of different plant organic compounds, caused by different ^2H fractionation processes during their biosynthesis (Luo & Sternberg, 1991; Zhou *et al.*, 2016; Baan *et al.*, 2023). One of the proposed main drivers of a ^2H fractionation in C_3 plants is proton production during the water-splitting process in the light-dependent reactions, which discriminates against the heavier ^2H isotope. This leads to a strongly depleted pool of reducing equivalences, such as NADPH (Luo *et al.*, 1991). Spatial and temporal variation in CO_2 uptake and assimilation in C_4 and CAM plants lead to significant metabolic changes and to a ^2H -enrichment in carbohydrates compared with in C_3 plants (Luo & Sternberg, 1991; Schuler *et al.*, 2022). Some of these processes may help to explain species-specific $\delta^2\text{H}$ variations in the carbohydrates of C_3 plants.

Further, various heterotrophic ^2H fractionation processes occur during plant metabolism (Augusti *et al.*, 2008), altering the initial $\delta^2\text{H}_{\text{ne}}$ of the fresh assimilates (e.g. non-structural carbohydrates (NSCs) in the form of sugar and starch) in the pathway to tree-ring cellulose formation (Kagawa & Battipaglia, 2022; Lehmann *et al.*, 2022). At the leaf level, heterotrophic ^2H fractionation processes within a species seem to be relatively constant under stable climatic conditions, and the $\delta^2\text{H}_{\text{ne}}$ of leaf sucrose can explain more than the half of the $\delta^2\text{H}_{\text{ne}}$ variation in leaf cellulose (Holloway-Phillips *et al.*, 2022). It is currently assumed that, similar to the isotopic exchange of oxygen isotopes between carbohydrates and xylem water during tree-ring formation (Epstein *et al.*, 1977; Cernusak *et al.*, 2005; Gessler *et al.*, 2009), the hydrogen of plants carbohydrates undergoes an isotopic exchange with the xylem water during cellulose formation (Augusti *et al.*, 2006; Augusti *et al.*, 2008). Further, recent findings suggest that fundamental plant traits, such as seasonal leaf shedding behaviour, significantly impact the $\delta^2\text{H}_{\text{ne}}$ of tree-ring cellulose (Arosio *et al.*, 2020a). Such effects may be caused by

differences in ^2H fractionation processes (Lehmann *et al.*, 2022), but the mechanistic basis of these processes are not yet known. Several biochemical pathways probably influence the apparent autotrophic and heterotrophic ^2H fractionation, and they can be summarized as ϵ_{HA} (autotrophic ^2H fractionation, between leaf water and sugar) and ϵ_{HE} (heterotrophic ^2H fractionation, between sugars and cellulose). Due to the complexity of these interactions, it is not well understood which processes drive ϵ_{HA} and ϵ_{HE} , and how this differs among plant species or functional groups.

Phylogenetic (evolutionary) relationships can be inferred by analysing genetic data from different plant species and are usually displayed as phylogenetic trees. Understanding phylogenetic relationships is important for identifying evolutionary patterns, predicting ecological and functional characteristics of plants, and guiding conservation efforts. Phylogenetics also provides insights into the evolution of traits, such as photosynthesis, growth and development, as well as adaptations to different environmental conditions. Phylogenetic relationships among plant species have been investigated by analysing genes coding for proteins, such as the oxygen-evolving complex (De Las Rivas & Roman, 2005), ATP synthase (Recipon *et al.*, 1992), and ferredoxin-NADP⁺ reductase (Karlusich & Carrillo, 2017), which are directly involved in the generation, transport and processing of protons during the light-dependent reactions of photosynthesis. Given that changes in enzyme structure and activity can impact isotope fractionation (Dirghangi & Pagani, 2013), species-related differences in genes coding for enzymes involved in photosystem II (Cameron & Carmen Molina, 2006) may be one reason for the species-specific variations in the $\delta^2\text{H}_{\text{ne}}$ of primary assimilates and cellulose (Fig. 1).

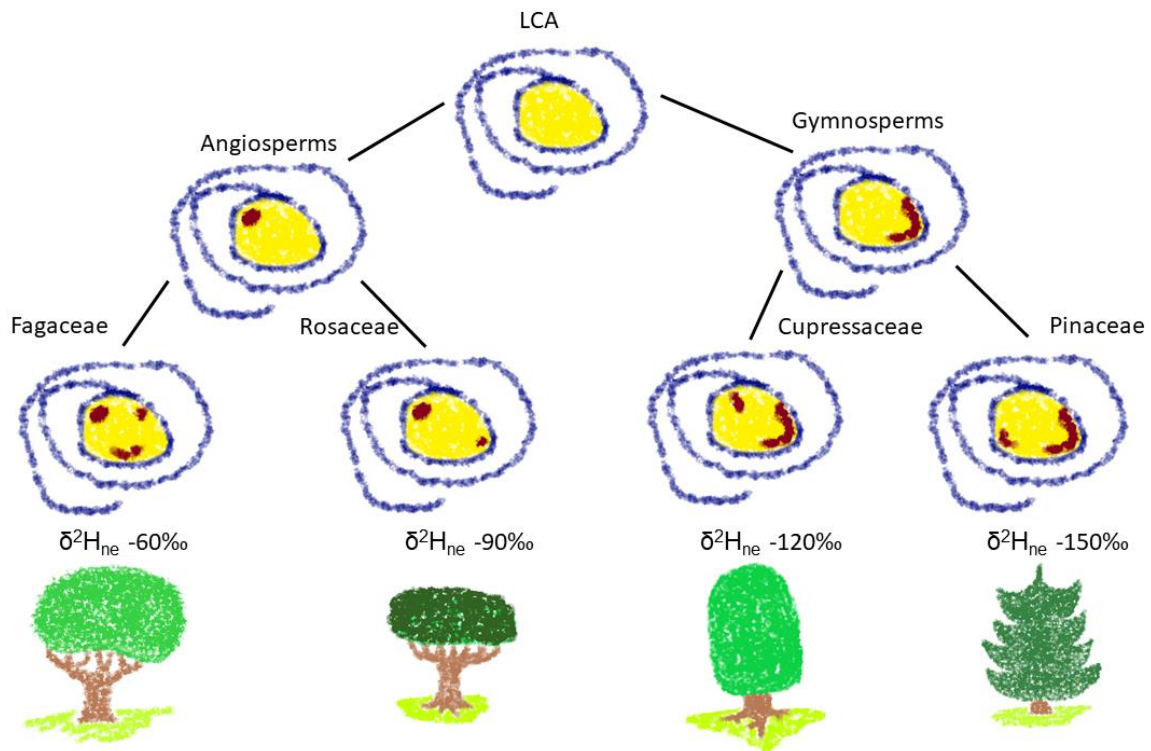


Figure 1: Theoretical framework for the expected phylogenetic signal in the non-exchangeable hydrogen isotopic composition ($\delta^2\text{H}_{\text{ne}}$) of carbohydrates in trees and shrubs. The last common ancestor (LCA) of all tested tree and shrub species had a hypothetical gene coding for a protein important in a distinct biological ^2H fractionation process during photosynthesis. The active region of the protein in the middle is shown in yellow. During the evolutionary separation between angiosperms and gymnosperms, certain genetic mutations lead to structural changes (red) of the active site of the protein, which was passed on to the next generations. During the evolution of the different tree families, additional small mutations occurred within both the angiosperm and gymnosperm families. The sum of all these small mutations has shaped the species-specific ^2H fractionation caused by the protein.

To advance knowledge on species-specific drivers of ^2H fractionation, we conducted a comprehensive and systematic comparison across 152 Northern Hemisphere trees. As all sampled species grew in a common garden, impacts of climate and source water were neglectable. The selected

trees represent 73 species, 48 genera, 19 families, and 12 orders containing both evergreen and deciduous angiosperms and gymnosperms, enabling us to test whether variation ^2H fractionation is driven by phylogenetic effects. We measured the $\delta^2\text{H}_\delta$ of plant water (leaf water and twig xylem water) and $^2\text{H}_{\text{ne}}$ of carbohydrates (leaf sugars and twig xylem cellulose) using a recently developed hot water vapour equilibration technique for the $\delta^2\text{H}_{\text{ne}}$ analysis of plant carbohydrates (Schuler *et al.*, 2022). We tested the following hypotheses: (1) phylogenetic distance is a major descriptor of the variation in ε_{HA} and ε_{HE} , translating to a clear phylogenetic pattern in the $\delta^2\text{H}_{\text{ne}}$ of leaf sugars and twig xylem cellulose. (2) the phylogenetic pattern decreases from sugars to cellulose, as the apparent ^2H fractionation in cellulose reflects more complex metabolic processes.

Materials and methods

Site description

All tree and shrub species (Supporting Information Table S1) were growing in Kannenfeldpark in the city of Basel, Switzerland (0.91 km², 47° 33' 54.216" N, 7° 34' 16.126" E). The small sampling area, uniform site conditions, and flat surface minimize the variability in site conditions, and soil water isotopic signatures are uniform spatially. The mean annual temperature and mean annual precipitation sum for the site were 11.2 °C and 841 mm, respectively, for the period 2000–2019 (IDAweb, MeteoSwiss, Zurich, Switzerland). Mean summer (June to August) temperature was 19.6 °C, and mean summer precipitation was 263 mm over the same period. In the year of the sampling campaign (2019), the mean annual temperature was 11.6 °C and precipitation summed to 786 mm. For the summer period of 2019, the mean temperature was 20.7 °C and precipitation summed to 279 mm. The park is watered regularly during dry periods. Thus, it was assumed that trees and shrubs were not water limited in 2019 and that they used the same water source throughout the growing season.

Sampling of plant material

Leaves and twig material were sampled in summer 2019 from 73 species, 48 genera, 19 families and 12 orders, for a total of 152 trees (minimum of one tree per species; Supporting Information Table S1). Sampling was performed between 10:20 and 16:00 on 29 August and between 09:55 and 13:00 on 30 August to minimize the diel variability in the $\delta^2\text{H}$ of leaf water (Cernusak *et al.*, 2016). The two consecutive sampling days were sunny and warm, i.e. 25.7–28.7 °C (mean 26.6 °C) and 51.3–60.7% relative humidity (mean 57.3%) on 29 August and 24.2–27.2 °C (mean 25.9 °C), and 55.0–70.5% (mean 62.8%) on 30 August (Table S2).

Branches were collected from sun-exposed canopies using pruners. The bark and phloem of ~10 cm from the cut end of the twig samples were removed with a peeler. Whole, fully developed leaves and the separated twig xylem were immediately transferred into individual gas-tight 12 ml glass vials (Prod. No. 738W, Exetainer, Labco, Lampeter, UK), stored on dry ice until the harvest was complete, and then stored in a -20 °C freezer. For the extraction of the current-year twig xylem cellulose, twig material was transferred to paper bags, stored on dry ice, and then oven-dried for 72 h at 60 °C.

Extraction of leaf and twig water, cellulose and sugars

Leaf water and twig water were cryogenically extracted using a hot water bath at 80 °C and a vacuum (10^{-2} mbar) for 2 h (West *et al.*, 2006; Diao *et al.*, 2022), then stored in glass vials at -20 °C until $\delta^2\text{H}$ measurement. The dried leaf material from the cryogenic vacuum distillation was ball-milled (MM400, Retsch, Haan, Germany), and the bulk leaf sugar fraction (i.e. “leaf sugars”) was then extracted from 100 mg of leaf powder following established protocols for carbon and oxygen isotope analysis (Rinne *et al.*, 2012; Lehmann *et al.*, 2020). First, the ground leaf material was mixed with deionized water in a 2 ml reaction vial and the water-soluble content was extracted at 85 °C for 30 minutes. Leaf sugars were then purified from the

water-soluble content using ion exchange cartridges (OnGuard II A, H and P, Dionex, Thermo Fisher Scientific, Bremen, Germany). The remaining sugar solutions were frozen and freeze-dried, and the mass of each sugar sample was measured.

For the extraction of twig xylem holocellulose, the twig xylem tissue from the current year was visually identified, separated manually with scissors, and ball-milled to a powder (Retsch). About 100 mg of the ball-milled material was packed into F57 fibre filter bags (ANKOM Technology, Macedon NY, USA). The samples were washed twice, for 2 h each time, with 5% NaOH at 60°C. The samples were then rinsed three times with boiling deionized water and subsequently incubated three times at 60 °C, for 8 h each time, in a solution of 7% NaClO₂ adjusted with 96% acetic acid to a pH of 4–5. After that, the samples were again rinsed three times with boiling deionized water, squeezed using a spatula, and dried for at least 4 h in a drying oven at 60° C. In a final step, the purified cellulose was mixed with deionized water, homogenized with an ultrasonic transducer (UP200St, Hielscher, Germany), and freeze-dried overnight.

$\delta^2\text{H}$ analysis of twig xylem water ($\delta^2\text{H}_{\text{XW}}$) and leaf water ($\delta^2\text{H}_{\text{LW}}$)

The $\delta^2\text{H}$ of water samples was measured with a high temperature conversion elemental analyser coupled to a DeltaPlus XP isotope ratio mass spectrometer (TC/EA-IRMS; Finnigan MAT, Bremen, Germany). Calibration was done using a range of certified waters of different isotope $\delta^2\text{H}$ ratios, resulting in a precision of analysis of 2‰.

$\delta^2\text{H}_{\text{ne}}$ analyses of sugars and cellulose using a hot water vapor equilibration method

For the $\delta^2\text{H}_{\text{ne}}$ analyses of sugars and cellulose, the previously developed hot water vapor equilibration method was applied (Schuler *et al.*, 2022). The dried sugar samples were dissolved in water, with a target concentration of

1 mg per 20 μ L. The reason for this relatively high target was to reduce sample volume and increase its viscosity, thereby reducing the risk of losing sample material while processing. Two identical sets of each sugar sample, with 1 mg sample material each, were prepared by pipetting 20 μ L into pre-weighed 5 \times 9 mm silver foil capsules (Prod. No. SA76981106, Säntis, Switzerland). Each duplicate was then frozen at -20°C, freeze-dried at -50°C, and packed into a second silver foil capsule to prevent sample loss during the equilibration process when sugars are liquified. Cellulose samples were also prepared in duplicate by transferring 1 mg into 3.3 \times 5 mm silver foil capsules (Prod. No. SA76980506, Säntis). Sugar and cellulose samples were stored in a desiccator at low relative humidity (2-5%) until $\delta^2\text{H}$ measurement.

The two sets of duplicates were then equilibrated with two isotopically distinct water vapours ($\delta^2\text{H}$ water vapour 1 = -160‰ and $\delta^2\text{H}$ water vapour 2 = -428‰) at 130°C in an apparatus consisting of an electrical heating oven (ED23, Binder, Tuttlingen, Germany) into which a specially designed equilibration chamber was inserted (Schuler *et al.*, 2022). After 2 h of equilibration with hot water vapour, the continuous water flow was stopped, the excess water in the line was pumped back and discarded, and the feeding capillary was switched to a capillary delivering dry nitrogen gas (N25.0, Prod. No. 2220912, PanGas AG, Dagmersellen, Switzerland) for 2 h at 130°C. After the samples were equilibrated and dried, they were immediately transferred into a Zero Blank Autosampler (N.C. Technologies S.r.l., Milano, Italy). The latter was coupled via a ConFlo III referencing interface to a Delta^{plus} XP IRMS (TC/EA-IRMS, Finnigan MAT, Bremen, Germany). The autosampler was evacuated to 0.01 mbar and filled with dry helium gas. The samples were pyrolysed in a reactor according to Gehre *et al.* (2004), and carried in a flow of dry helium (150 ml min⁻¹) to the IRMS. Raw $\delta^2\text{H}$ values were offset corrected using PEF standards (IAEA-CH-7 polyethylene foil, International Atomic Energy Agency, Vienna, Austria; SD < 0.7‰ within one run).

Calculation of the non-exchangeable hydrogen isotope ratio ($\delta^2\text{H}_{\text{ne}}$), ϵ_{HA} and ϵ_{HE}

All Isotope ratios (δ) were calculated as given in Eq. 1 (Coplen, 2011):

$$\delta = \frac{R_{\text{Sample}} - R_{\text{Standard}}}{R_{\text{Standard}}}$$

Eq. 1

where $R = ^2\text{H}/^1\text{H}$ of the sample (R_{Sample}) and of Vienna Standard Mean Ocean Water (VSMOW2; R_{Standard}) as the standard defining the international isotope scale. To express the resulting δ in permil (‰), results were multiplied by 1,000.

According to Filot et al. (2006), the %-proportion of exchanged hydrogen during the equilibrations (x_e , Eq. 2) can be calculated as:

$$x_e = \frac{\delta^2\text{H}_{e1} - \delta^2\text{H}_{e2}}{\alpha_{e-w} \cdot (\delta^2\text{H}_{w1} - \delta^2\text{H}_{w2})}$$

Eq. 2

where $\delta^2\text{H}_{e1}$ and $\delta^2\text{H}_{e2}$ are the measured $\delta^2\text{H}$ values of the two equilibrated subsamples, $\delta^2\text{H}_{w1}$ and $\delta^2\text{H}_{w2}$ are the $\delta^2\text{H}$ values of the two waters used, and α_{e-w} is the fractionation factor of 1.082, which is the same for sugars and cellulose (Filot *et al.*, 2006; Schuler *et al.*, 2022). Typical x_e values for sugars are between 0.32 and 0.36, and for cellulose around 0.20 (Schuler *et al.*, 2022).

$\delta^2\text{H}_{\text{ne}}$ can then be calculated with Eq. 3 using one of the two equilibrations (equilibration one in this example, $\delta^2\text{H}_{e1}$ and $\delta^2\text{H}_{w1}$):

$$\delta^2\text{H}_{\text{ne}} = \frac{\delta^2\text{H}_{e1} - x_e \cdot \alpha_{e-w} \cdot \delta^2\text{H}_{w1} - 1000 \cdot x_e \cdot (\alpha_{e-w} - 1)}{1 - x_e}$$

Eq. 3

The results were then calibrated using internal reference material, with three sucrose samples for the equilibrations of leaf sugars and three cellulose samples for the equilibrations of the twig xylem cellulose.

The total leaf water enrichment (LWE) was calculated with Eq. 4, ϵ_{HA} with Eq. 5, and ϵ_{HE} with Eq. 6, using the values for leaf water (δ^2H_{LW}) and xylem water (δ^2H_{XW}):

$$LWE = \delta^2H_{\text{leaf water}} - \delta^2H_{\text{twig xylem water}} \quad \text{Eq. 4}$$

$$\epsilon_{HA} = \delta^2H_{\text{leaf sugar}} - \delta^2H_{\text{leaf water}} \quad \text{Eq. 5}$$

$$\epsilon_{HE} = \delta^2H_{\text{twig xylem cellulose}} - \delta^2H_{\text{leaf sugar}} \quad \text{Eq. 6}$$

To eliminate unnecessary complexity, in agreement with the law of parsimony in explaining observed processes, the two biological fractionation factors were expressed as the actual difference between the δ^2H_{ne} of leaf sugars and the δ^2H of leaf water (ϵ_{HA}), and the actual difference between the δ^2H_{ne} of twig xylem cellulose and the δ^2H of leaf sugars (ϵ_{HE}).

Statistical analyses

Statistical analyses were performed using R version 4.1.2 (R.Core.Team, 2023). The distribution of the data was assessed for normality with Kolmogorov-Smirnov tests. T-tests were performed to evaluate δ^2H fractionation differences between angiosperms and gymnosperms, as well as between deciduous and evergreen species. Analysis of variance (ANOVA), followed by Tukey's post hoc tests, was performed to evaluate differences between clades, orders, families and genera. Linear models, implemented in the R package *ggplot2* (Wickham, 2016), were used to determine the general drivers behind the 2H fractionation processes.. Final assembly of the graphs was done using the R package *patchwork* (Pedersen, 2022). The phylogenetic analyses were performed and the phylogenetic trees were generated using the R package *phytools* (Revell, 2012). Pagel's λ was used to estimate the phylogenetic signal behind the observed δ^2H_{ne} of leaf sugars and twig xylem cellulose and the fractionation factors (ϵ_{HA} and ϵ_{HE}). According to Molina-Venegas and Rodríguez (2017), Pagel's λ measures the

similarity of the covariances among species and the covariances expected for values with a distribution similar to Brownian motion. It is highly robust to incompletely resolved phylogenies and suboptimal branch-length information. A Pagel's λ of 1 indicates a strong phylogenetic signal, where the tested trait is more similar in closely related species than in more distantly related species. In contrast, a Pagel's λ of 0 indicates the absence of a phylogenetic signal, which means that the variability of the tested trait is not affected by the evolutionary relationships of the species. As there was no calibrated phylogenetic tree available containing all the considered species, generic branch lengths were used for the phylogenetic tree: 1 on the species level, 2 on the genus level, 4 on the family level, 8 on the order level, and 16 between angiosperms and gymnosperms. This was done with the aim of reflecting the increasing phylogenetic distance along this sequence. Due to the uneven number of replicates (one to three) within the tested species, mean values per species were used.

Results

$\delta^2\text{H}$ of plant water and carbohydrates in angiosperms and gymnosperms

The measured $\delta^2\text{H}$ and ^3H fractionation factors of carbohydrates and water in angiosperms and gymnosperms were normally distributed (Fig. 2a-d), with mostly unimodal peaks around the mean values, and the mean and median values close to each other. For the ε_{HE} of angiosperms, there was a slightly bimodal but still normal distribution (Fig. 2d), with a secondary accumulation at values about twice as large as the bulk of the ε_{HE} values.

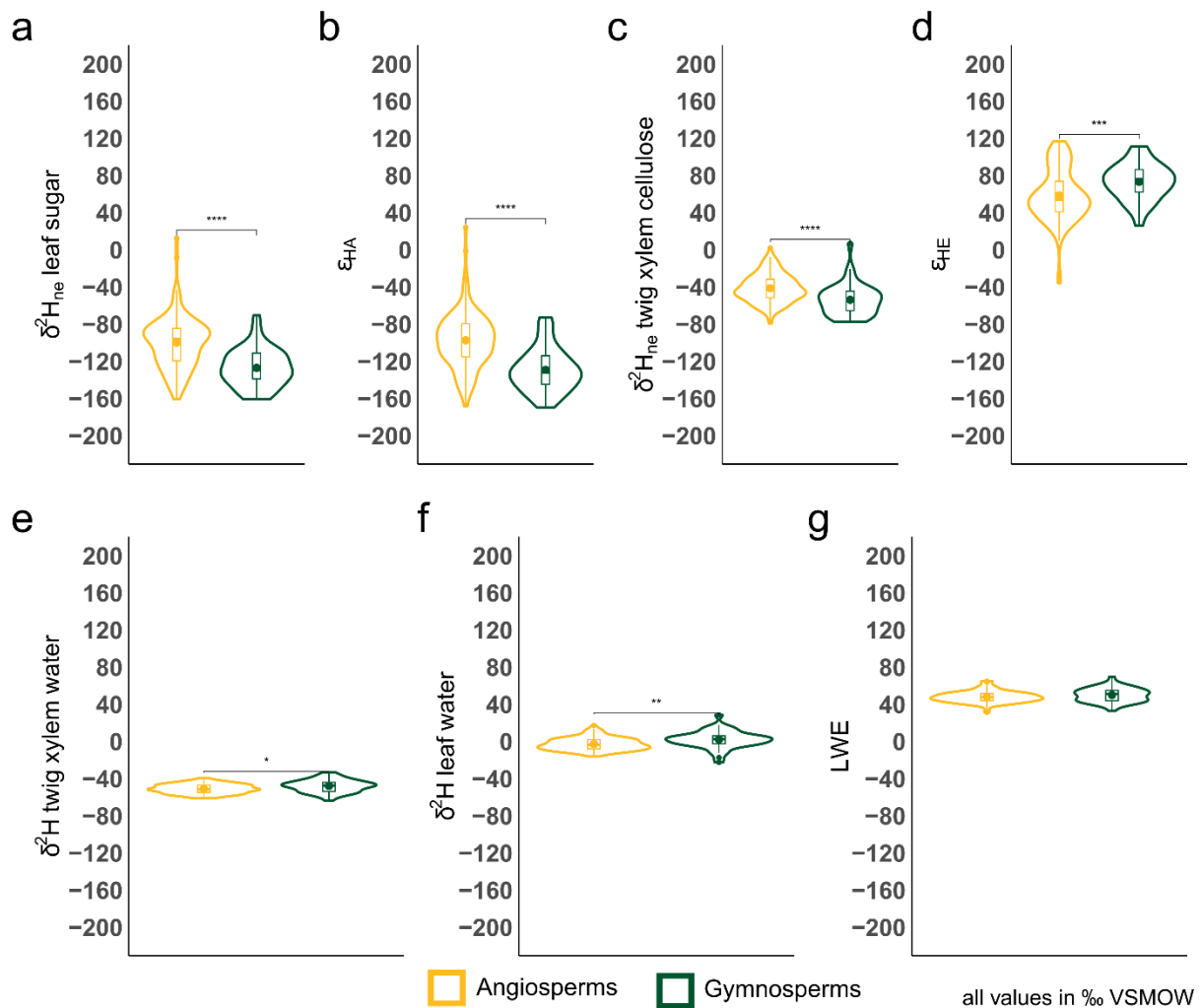


Figure 2: Violin plots of the hydrogen (H) isotope ratios of plant water and carbohydrates and their ^2H fractionation factors across 152 tree and shrub species in a common garden. The boxplots within the violin plots are indicating the mean (points) and median (horizontal line) values. (a) Non-exchangeable H isotopic composition ($\delta^2\text{H}_{\text{ne}}$) of leaf sugar, (b) autotrophic ^2H fractionation factor (ϵ_{HA}), (c) $\delta^2\text{H}_{\text{ne}}$ of twig xylem cellulose, (d) heterotrophic ^2H fractionation factor (ϵ_{HE}), (e) $\delta^2\text{H}$ of twig xylem water, (f) $\delta^2\text{H}$ of leaf water, and (g) leaf water enrichment (LWE). In all panels, angiosperms (yellow) and gymnosperms (green) are compared, with asterisks indicating significant differences (t-test: *, $P \leq 0.05$; **, $P \leq 0.01$; ***, $P \leq 0.001$; ****, $P \leq 0.0001$). VSMOW, Vienna Standard Mean Ocean Water

Among the sampled species and phylogenetic groups (clade, order, family, genus, species), we observed large variability in the $\delta^2\text{H}_{\text{ne}}$ of leaf sugars and

twig xylem cellulose and in the biological fractionation factors ϵ_{HA} and ϵ_{HE} (Fig. 2, Tables 1, S1, S3, S4). For angiosperm carbohydrates, the mean δ^2H_{ne} values of leaf sugars and twig xylem cellulose were -99.9‰ (SD = 28.1‰) and -41.2‰ (SD = 15.2‰), respectively. The observed δ^2H in angiosperms resulted in mean ϵ_{HA} and ϵ_{HE} values of -97.3‰ (SD = 30.5‰) and 58.7‰ (SD = 28.3‰), respectively. For gymnosperm carbohydrates, the mean δ^2H_{ne} values of leaf sugars and twig xylem cellulose were -127.0‰ (SD = 20.5‰) and -53.7‰ (SD = 16.9‰), respectively. The observed δ^2H in gymnosperms resulted in mean ϵ_{HA} and ϵ_{HE} values of -129.1‰ (SD = 23.4‰) and 73.2‰ (SD = 19.6‰), respectively. The ϵ_{HA} values of gymnosperm species were significantly lower than those of angiosperm species ($P \leq 0.0001$), whereas ϵ_{HE} values were significantly higher for gymnosperms ($P \leq 0.001$).

Table 1: Order-level mean values and standard deviations (SD) of δ^2H_{ne} of plant carbohydrates, ϵ_{HA} and ϵ_{HE} , δ^2H of twig xylem water and leaf water, and leaf water enrichment (LWE). The corresponding grouping according to the analysis of variance and Tukey's post hoc tests is shown.

Order	n	δ^2H_{ne} leaf sugar [‰]			ϵ_{HA} [‰]			δ^2H_{ne} xylem cellulose [‰]			ϵ_{HE} [‰]		
		mean	SD	Group	mean	SD	Group	mean	SD	Group	mean	SD	Group
Aquifoliales	3	-15.1	31.7	A	-7.12	34.7	A	-24.3	11.2	ABC	-9.2	38.6	D
Buxales	3	-95.3	4.56	BCDE	-101	2.3	BCD	-43.9	4.3	ABC	51.4	8.7	ABCD
Fabales	5	-134	30.4	DE	-137	34.9	D	-45.2	14.9	BC	88.9	29.3	A
Fagales	47	-100	18.3	C	-99	18.5	C	-46.8	14	BC	53.3	19.9	BC
Lamiales	9	-72.7	25.3	B	-65.5	28.6	B	-16.2	11.4	A	56.6	27.4	ABC
Magnoliales	13	-116	25.2	CDE	-114	27	CD	-40	10.3	BC	75.5	27.2	AB
Malvales	5	-82.6	3.98	BC	-77.6	6.7	BC	-46.8	5.8	BC	35.8	6.6	CD
Rosales	13	-102	25.3	BCDE	-94.7	27	BC	-41.8	12.7	BC	59.8	31	ABC
Sapindales	12	-117	16.2	CDE	-113	19.9	CD	-39.9	13.7	BC	77.2	24.2	AB
Saxifragales	1	-86.6	NA	ABCDE	-91.4	NA	ABCD	-23	NA	ABC	63.6	NA	ABCD
Ginkgoales	2	-96.2	36.5	BCDE	-96.4	33	BCD	-52.1	10.9	ABC	44.1	25.6	ABCD
Pinales	39	-129	18.8	E	-131	22.1	D	-53.8	17.2	C	74.7	18.4	A

Order	n	δ^2H twig xylem water [‰]			δ^2H leaf water [‰]			Leaf water [‰]		
		mean	SD	Group	mean	SD	Group	mean	SD	Group
Aquifoliales	3	-47.7	3.7	AB	-8	3.3	AB	39.7	5.6	B
Buxales	3	-44	2.1	AB	5.3	4	AB	49.2	5	AB
Fabales	5	-54.8	4.4	AB	3.3	10.2	AB	58.1	6.9	A
Fagales	47	-49.4	5.5	AB	-1.2	5.7	AB	48.2	5	B
Lamiales	9	-50.9	3.7	AB	-7.3	5.3	B	43.7	5.9	B
Magnoliales	13	-49.9	2.6	AB	-1.2	6.5	AB	48.7	5.8	AB
Malvales	5	-53.8	3.6	AB	-4.9	5.9	AB	48.9	4.6	AB
Rosales	13	-52.8	4.4	AB	-6.9	5.5	B	45.9	4.8	B
Sapindales	12	-55	3.4	B	-4.5	7.5	AB	50.6	6.7	AB
Saxifragales	1	-47.3	NA	AB	4.8	NA	AB	52.1	NA	AB
Ginkgoales	2	-50.9	4.7	AB	0.2	3.5	AB	51	8.2	AB
Pinales	39	-47.7	6.8	A	2.2	9.6	A	50	7.6	AB

In comparison to the $\delta^2\text{H}_{\text{ne}}$ of sugars and cellulose (Fig. 2 a-d), variability was smaller for $\delta^2\text{H}_{\text{xw}}$, $\delta^2\text{H}_{\text{LW}}$ and LWE (Fig. 2 e-g). In angiosperms, the mean $\delta^2\text{H}$ values of twig xylem water and leaf water were -50.8‰ (SD = 5.0‰) and -2.6‰ (SD = 6.7‰), respectively, leading to a mean isotopic leaf water enrichment (LWE) of 48.2‰ (SD = 6.1‰ ; Fig. 2). In gymnosperms, the mean $\delta^2\text{H}$ values of twig xylem water and leaf water were -47.9‰ (SD = 6.7‰) and 2.1‰ (SD = 9.4‰), respectively, leading to a mean isotopic leaf water enrichment of 50.2‰ (SD = 7.5‰ ; Fig. 2). The $\delta^2\text{H}$ values of xylem and leaf water were significantly higher in gymnosperms than in angiosperms ($P \leq 0.05$), while LWE was not significantly different between the two groups ($P \geq 0.05$).

Within the tested angiosperms, *Ilex aquifolium* L. had the smallest ϵ_{HA} , with a mean of -7.1‰ (SD = 34.7‰), leading to a mean $\delta^2\text{H}_{\text{ne}}$ of leaf sugars of -15.1‰ (SD = 31.7‰). Interestingly, this species was the only one with a negative heterotrophic ^2H fractionation factor ϵ_{HE} (mean = -9.2‰ , SD = 38.6‰), leading to a mean $\delta^2\text{H}_{\text{ne}}$ of twig xylem cellulose of -24.3‰ (SD = 11.2‰). While gymnosperms showed, on average, a stronger ^2H fractionation than angiosperms, the order with the strongest ^2H fractionation, for both ϵ_{HA} and ϵ_{HE} , was the angiosperm Fabales (ϵ_{HA} mean -137.4‰ , SD = 34.9‰ ; ϵ_{HE} mean 88.9‰ , SD = 29.3‰). We observed no significant differences for the tested variables ($\delta^2\text{H}_{\text{ne}}$ of leaf sugar, ϵ_{HA} , $\delta^2\text{H}_{\text{ne}}$ of twig xylem cellulose, ϵ_{HE} , $\delta^2\text{H}$ of twig xylem water, $\delta^2\text{H}$ of leaf water, and LWE) between the deciduous and evergreen species within the angiosperms and within the gymnosperms ($P > 0.05$, Fig. S1).

Relationship between $\delta^2\text{H}$ of plant water and carbohydrates

$\delta^2\text{H}_{\text{ne}}$ of leaf sugars was not or only very weakly ($R^2 < 0.1$) linearly related to $\delta^2\text{H}$ of twig xylem water and of leaf water and to LWE (Fig. 3a, b, c), but it was strongly linearly related to ϵ_{HA} ($R^2 = 0.95$; Fig. 3d) and to ϵ_{HE} ($R^2 = 0.68$; Fig. 3e). For $\delta^2\text{H}_{\text{ne}}$ of twig xylem cellulose, we observed a weak relationship

($R^2 = 0.1$) with $\delta^2\text{H}$ of twig xylem water (Fig. 4a), but no or very weak relationships with $\delta^2\text{H}$ of leaf water and with LWE (Fig. 4b, c). In contrast to values for leaf sugars, $\delta^2\text{H}_{\text{ne}}$ of twig xylem cellulose was only weakly related to ϵ_{HA} ($R^2 = 0.16$; Fig. 4d) and to ϵ_{HE} ($R^2 = 0.19$; Fig. 4e).

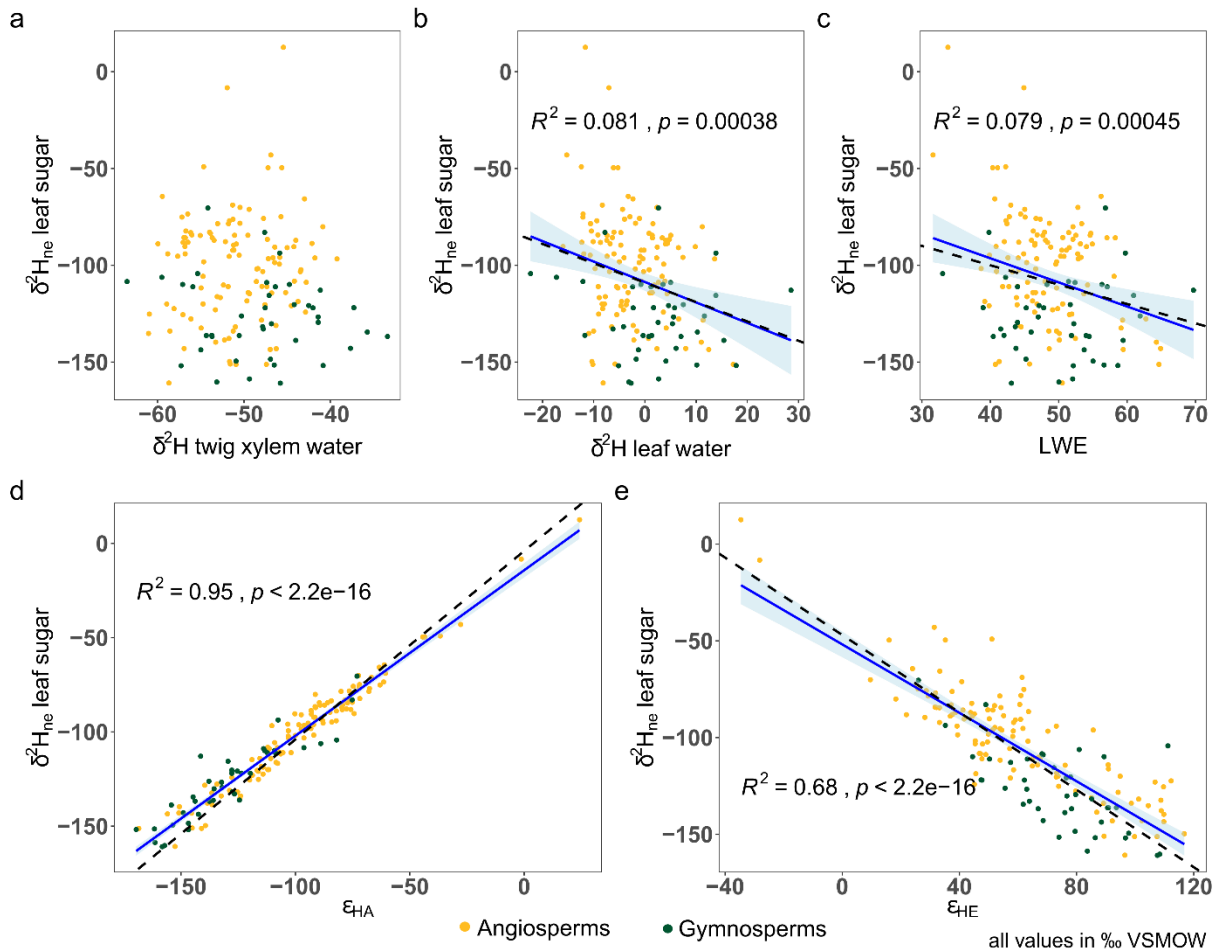


Figure 3: Linear relationships between $\delta^2\text{H}_{\text{ne}}$ of leaf sugars and (a) $\delta^2\text{H}$ of twig xylem water, (b) $\delta^2\text{H}$ of leaf water, (c) leaf water enrichment (LWE), (d) autotrophic ^2H fractionation factor (ϵ_{HA}), and (e) heterotrophic ^2H fractionation factor (ϵ_{HE}). Yellow dots indicate angiosperms, and green dots indicate gymnosperms. The continuous blue line represents the linear model, the light blue shading denotes the 95% confidence level interval for predictions from the linear model, and the dashed black line is the 1 : 1 line. VSMOW, Vienna Standard Mean Ocean Water.

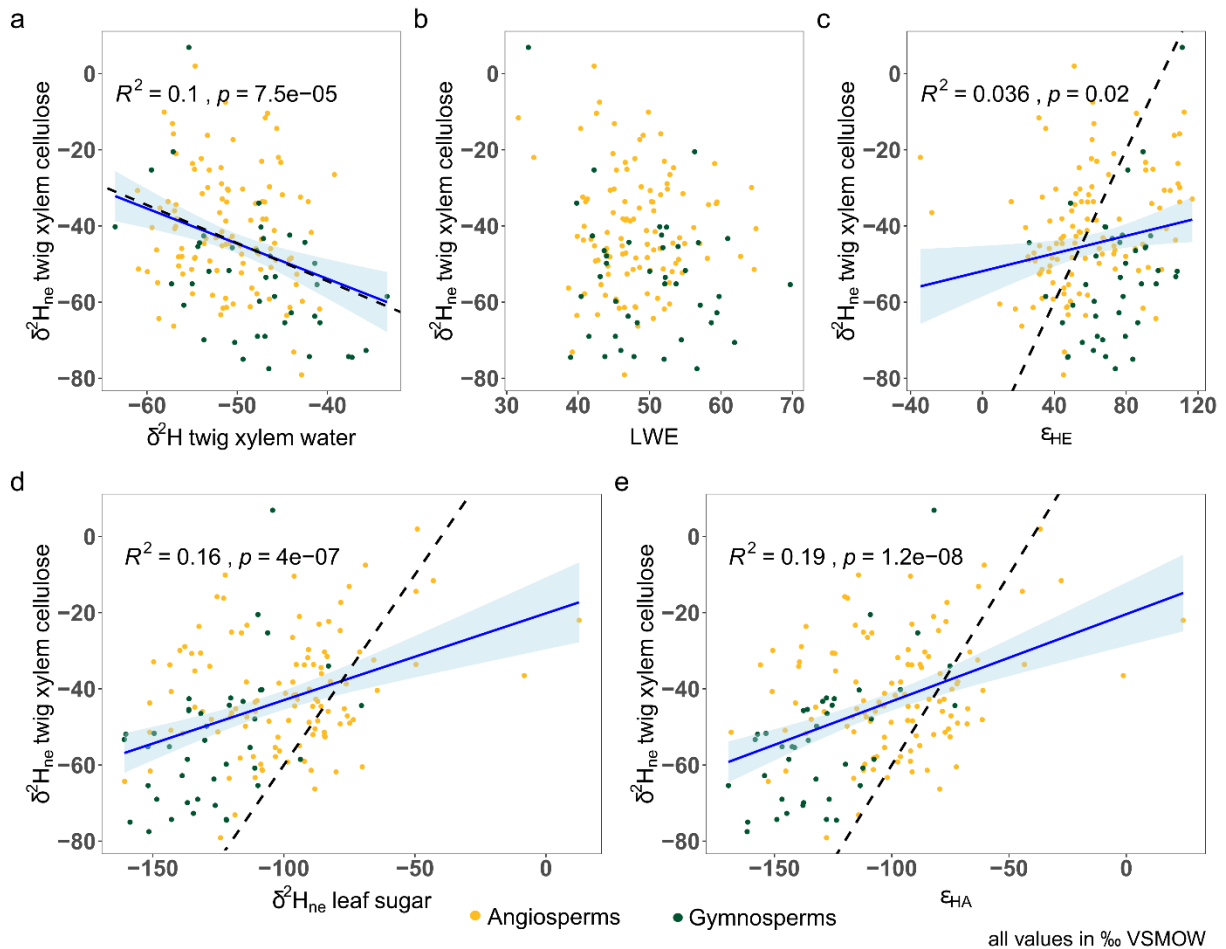


Figure 4: Linear relationship between $\delta^2\text{H}_{\text{ne}}$ of twig xylem cellulose and (a) $\delta^2\text{H}$ of twig xylem water, (b) leaf water enrichment (LWE), (c) heterotrophic ^2H fractionation factor (ϵ_{HE}), (d) $\delta^2\text{H}_{\text{ne}}$ of leaf sugars, and (e) autotrophic ^2H fractionation factor (ϵ_{HA}). Yellow dots indicate angiosperms, and green dots indicate gymnosperms. The continuous blue line represents the linear model, the light blue shading denotes the 95% confidence level interval for predictions from the linear model, and the dashed black line is the 1 : 1 line. VSMOW, Vienna Standard Mean Ocean Water.

Phylogenetic analysis of the observed $\delta^2\text{H}$ patterns

Pagel's λ , a measure of phylogenetic effects, differed among the isotopic variables (Table 2, Figs S2-S4). For $\delta^2\text{H}_{\text{ne}}$ of leaf sugars and for ϵ_{HA} , Pagel's λ values were close to 1, indicating a clear phylogenetic signal. Similarly, a phylogenetic signal was

visible in the $\delta^2\text{H}_{\text{ne}}$ of twig xylem cellulose and in ϵ_{HE} , albeit weaker. No significant phylogenetic signal was observed in the $\delta^2\text{H}$ of xylem water, leaf water or LWE (Table 2).

Table 2: Pagel's λ for $\delta^2\text{H}$ of plant water (leaf water, twig xylem water), $\delta^2\text{H}_{\text{ne}}$ of plant carbohydrates (leaf sugars, twig xylem cellulose), leaf water enrichment (LWE), and the autotrophic (ϵ_{HA}) and heterotrophic (ϵ_{HE}) ^2H fractionation factors. Asterisks indicating significant differences (t-test: *, $P \leq 0.05$; **, $P \leq 0.01$; ***, $P \leq 0.001$).

	Pagel's λ	P
$\delta^2\text{H}_{\text{ne}}$ leaf sugar	0.87	***
ϵ_{HA}	0.88	***
$\delta^2\text{H}_{\text{ne}}$ twig xylem cellulose	0.64	***
ϵ_{HE}	0.61	***
$\delta^2\text{H}$ twig xylem water	0.26	N.S.
$\delta^2\text{H}$ leaf water	0.03	N.S.
LWE	0	N.S.

The phylogenetic trees for $\delta^2\text{H}_{\text{ne}}$ of the carbohydrates and the corresponding fractionation factors (Figs 5, 6), in combination with the ANOVA results (Table S6), indicated distinct patterns among the tested phylogenetic groups. The phylogenetic tree for $\delta^2\text{H}_{\text{ne}}$ of leaf sugars (Fig. 5a) showed lower (more negative) $\delta^2\text{H}_{\text{ne}}$ values for gymnosperms than for angiosperms. Three groups of angiosperms had lower $\delta^2\text{H}_{\text{ne}}$ of leaf sugars compared with the other angiosperms: the family Fabaceae, the genus *Acer* L., and, to a lesser extent, the family Magnoliaceae. The phylogenetic pattern of ϵ_{HA} reflected the phylogenetic relationships of the $\delta^2\text{H}_{\text{ne}}$ of leaf sugars (Fig. 5b), demonstrating that leaf water did not shape the detected phylogenetic pattern. Within the gymnosperms, there were no significant differences for $\delta^2\text{H}_{\text{ne}}$ of leaf sugars and ϵ_{HA} , whereas the ϵ_{HA} of Ginkgoaceae and Taxaceae

were significantly different than the values for Cupressaceae and Pinaceae (Table S6).

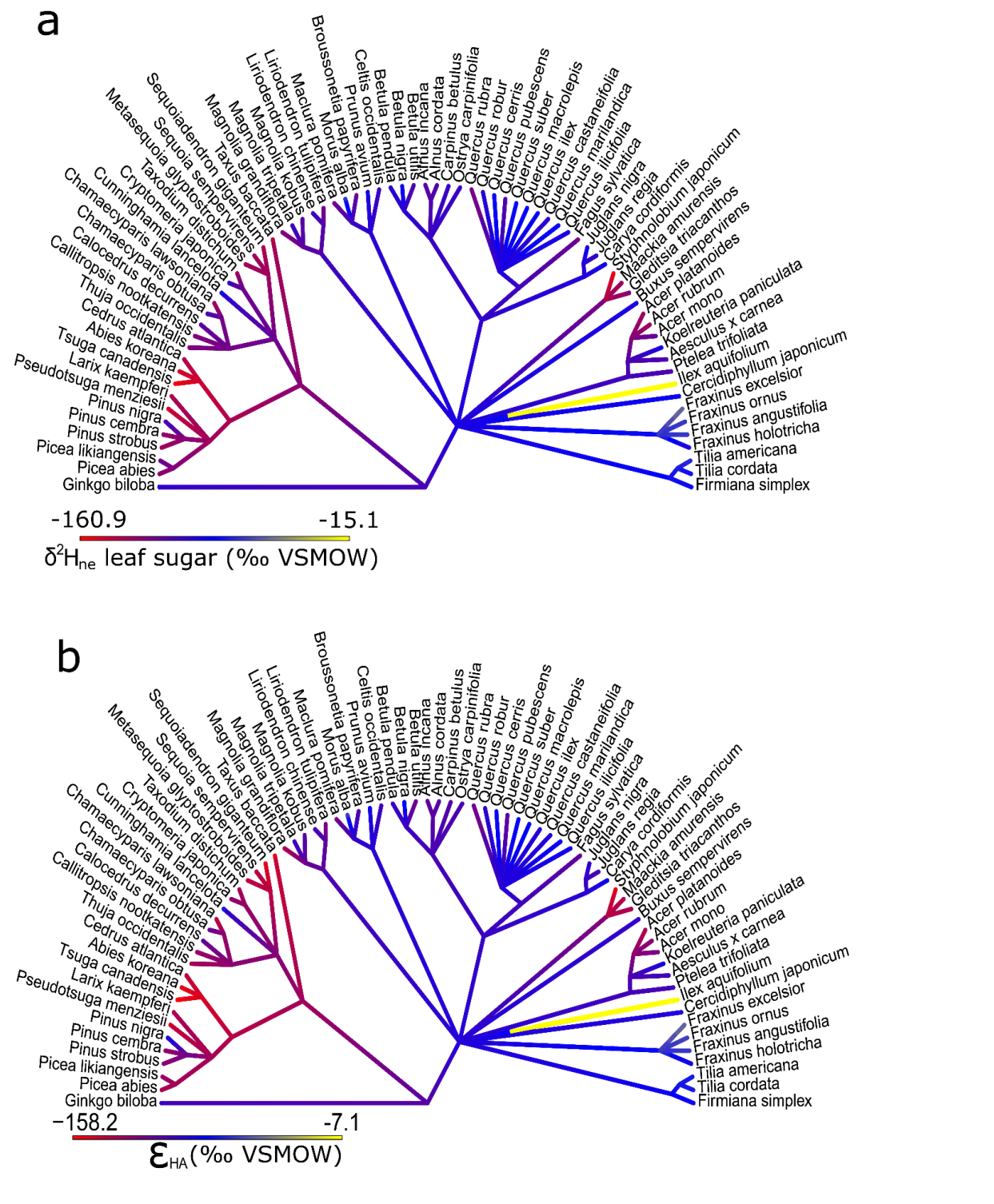


Figure 5: Phylogenetic trees showing (a) the $\delta^2\text{H}_{\text{ne}}$ of leaf sugars and (b) the autotrophic ^2H fractionation factor between leaf water and leaf sugars (ϵ_{HA}) among the tested tree species. Gymnosperms are on the left side and

angiosperms on the right side of the tree. VSMOW, Vienna Standard Mean Ocean Water.

The phylogenetic tree for $\delta^2\text{H}_{\text{ne}}$ of twig xylem cellulose (Fig. 6a) revealed a different and slightly more complex pattern than observed for the $\delta^2\text{H}_{\text{ne}}$ of leaf sugars and for ε_{HA} . While $\delta^2\text{H}_{\text{ne}}$ values were, on average, lower (more negative) in gymnosperms than in angiosperms, we found distinct groups within both angiosperms and gymnosperms. For angiosperms, there were three distinct groups: (1) species of the family Fagaceae (containing *Betula* L., *Alnus* MILL., *Carpinus* L. and *Ostrya* SCOP.) had the lowest $\delta^2\text{H}_{\text{ne}}$ of twig xylem cellulose; (2) species within the genus *Fraxinus* L. had the highest $\delta^2\text{H}_{\text{ne}}$ values, and (3) the remaining species had $\delta^2\text{H}_{\text{ne}}$ values distributed between those of the two other groups. For gymnosperms, species within the family Pinaceae had higher $\delta^2\text{H}_{\text{ne}}$ of twig xylem cellulose than observed for species belonging to the families Cupressaceae and Taxaceae.

For the phylogenetic tree of ε_{HE} (Fig. 6b), angiosperm species were divided into three different groups. Species of the family Fabaceae and the genus *Acer* were distinguished by a stronger ^2H enrichment, caused by ε_{HE} , compared with the other angiosperms. Interestingly, *Ilex aquifolium* was the only species with a negative ε_{HE} , leading to a ^2H depletion from leaf sugars to xylem cellulose. As with ε_{HA} , for ε_{HE} two distinct groups within the gymnosperms were observed (Fig. 6b, Table S6): (1) species within the family Pinaceae, where ε_{HE} caused a strong ^2H enrichment, and (2) species of the families Cupressaceae, Taxaceae and Ginkgoaceae, with much lower ε_{HE} values.

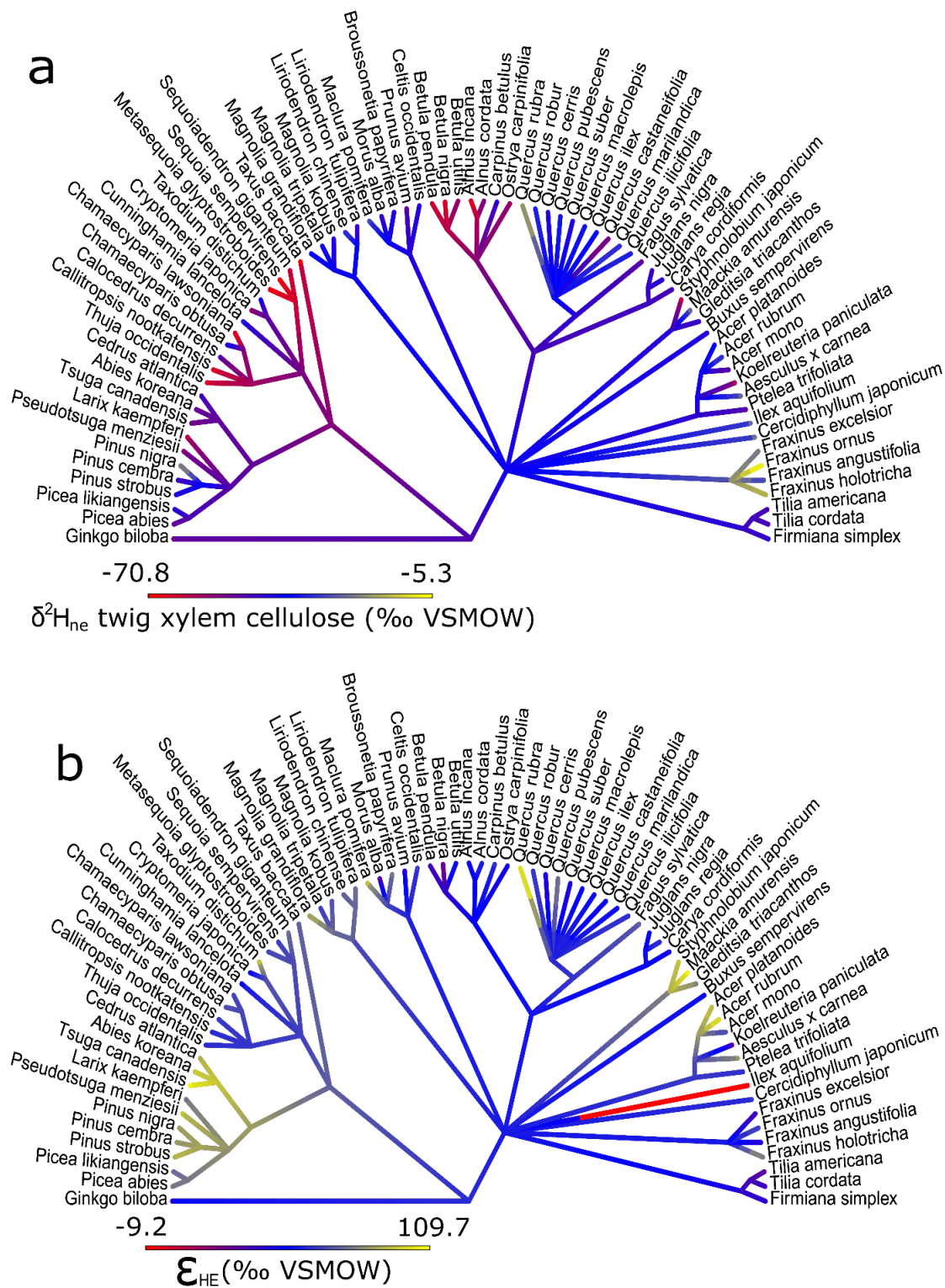


Figure 6: Phylogenetic trees showing (a) the $\delta^2\text{H}_{\text{ne}}$ of twig xylem cellulose and (b) the heterotrophic ^2H fractionation factor between leaf sugars and twig xylem cellulose (ϵ_{HE}) among the tested tree species. Gymnosperms are

on the left side and angiosperms on the right side of the tree. VSMOW, Vienna Standard Mean Ocean Water

Discussion

Phylogenetic pattern in the $\delta^2\text{H}_{\text{ne}}$ of plant carbohydrates, ϵ_{HA} and ϵ_{HE}

Our study revealed a strong phylogenetic signal in the hydrogen isotopic composition of plant carbohydrates (Tables 1, 2, Figs 5, 6, S2, S3). Given that $\delta^2\text{H}$ in twig xylem and leaf water varied less and that species-related trends in plant water were opposite to those in carbohydrates (Figs 2, 3), we conclude that the phylogenetic signal in the $\delta^2\text{H}_{\text{ne}}$ of plant carbohydrates was not driven by source or leaf water (Figs 3, 4), which is in accordance with recent studies (Holloway-Phillips *et al.*, 2022). A strong relationship between the $\delta^2\text{H}$ of the source water and the $\delta^2\text{H}_{\text{ne}}$ of carbohydrates probably only occurs if plants are growing with source water with pronounced differences in their $\delta^2\text{H}$, such as along a geographic gradient along a dividing range (Roden & Ehleringer, 2000), on the continental scale (West *et al.*, 2008; Vitali *et al.*, 2022), or when source water is experimentally enriched or depleted in ^2H (Roden & Ehleringer, 1999). Instead, our results showed that the $\delta^2\text{H}_{\text{ne}}$ of sugars and cellulose and their phylogenetic signal were caused by biological processes, and differed between angiosperms and gymnosperms (Fig. 2). ϵ_{HA} explained 95% of the variation in the $\delta^2\text{H}_{\text{ne}}$ of leaf sugars. The strong relationship between these two variables (Fig. 2d) indicates that the observed $\delta^2\text{H}_{\text{ne}}$ of leaf sugars was representative for the sampled species.

The strong phylogenetic pattern of the $\delta^2\text{H}_{\text{ne}}$ of leaf sugars and ϵ_{HA} was dampened during heterotrophic ^2H fractionation (ϵ_{HE}), as the isotopic signal in leaf sugars was not directly translated into twig xylem cellulose (Figs 3, 4), resulting in a reduced phylogenetic pattern in $\delta^2\text{H}_{\text{ne}}$ of twig xylem cellulose (Figs 6, S3, Table 2). The change in ^2H signal transfer from leaf sugars to cellulose might also be partially explained by a temporal and

spatial separation between ^2H fractionation processes shaping the $\delta^2\text{H}_{\text{ne}}$ of leaf sugars and those shaping the $\delta^2\text{H}_{\text{ne}}$ of twig xylem cellulose. In contrast, drivers of heterotrophic ^2H fractionation and the $\delta^2\text{H}_{\text{ne}}$ of twig xylem cellulose were likely more complex than those influencing ϵ_{HA} . These heterotrophic ^2H fractionation processes might be influenced by the physiological adaptation of a species to its environment, such as the interaction of respiration rate with temperature (Patterson *et al.*, 2018), or by differences in tree internal carbon allocation (Herrera-Ramírez *et al.*, 2020).

An evolutionary development causing the stronger autotrophic ^2H fractionation in gymnosperms could be their faster electron transport of photosystem II compared with angiosperms (Shirao *et al.*, 2013), which might also affect the rate of proton transport, leading to stronger ^2H fractionation. Other known differences between gymnosperms and angiosperms are the higher water use efficiency of the former (Flexas & Carriquí, 2020), as well as differences in their leaf hydraulics and stomatal conductance (Lusk *et al.*, 2003; Brodribb *et al.*, 2005). However, these variables would explain the observed pattern in ^2H fractionation only if the ^2H fractionation were derived from the leaf water, which was not the case in our study (Figs 3, 4). The absence of any relationship between the $\delta^2\text{H}$ of leaf water and the $\delta^2\text{H}_{\text{ne}}$ of carbohydrates might be caused by strong isotopic differences between the water of the whole leaf and the water inside the chloroplasts, which is the isotopically relevant pool during C_3 carbon fixation, due to the photosynthetic proton production inside the chloroplast (Heldt *et al.*, 1973). In this case, the $\delta^2\text{H}$ of the water inside the plants' chloroplasts might be responsible for the phylogenetic relationships detected here. Relationships in the H isotopic signal in leaf and source water and carbohydrates, reported by others (Rodén & Ehleringer, 2000), would only occur if plants of the same species grew with source water with different $\delta^2\text{H}$ values. Nitrogen metabolism is a process that could influence ϵ_{HE} , as gymnosperms have a lower photosynthetic nitrogen use efficiency than angiosperms (Flexas & Carriquí, 2020). However, the nitrogen

metabolism of the tree and shrub species considered here probably did not contribute significantly and consistently to the observed phylogenetic pattern in plants' ^2H fractionation, as the nitrogen-fixing angiosperm species within Fabales and the two *Alnus* species within Fagales had different patterns of autotrophic and heterotrophic ^2H fractionation (Tables S3, S4).

Another potential reason for the difference between our tested angiosperm (mostly deciduous) and gymnosperm (mostly evergreen) species could be related to findings from recent studies showing a ^2H depletion in tree-ring cellulose of deciduous compared with evergreen conifer species (Arosio *et al.*, 2020a; Arosio *et al.*, 2020b), suggesting an influence of leaf shedding behaviour. However, in our data set, which included more species from more genera than previous studies, such differences did not emerge between deciduous and evergreen species for either angiosperms or gymnosperms (Fig. S1). This was the case even when we reduced our data set to the species used by Arosio *et al.* (2020a).

One reason for the differences between our findings and those from previous studies could be related to the plant tissue analysed. While we used current-year twig material for the cellulose extraction, cellulose derived from branch material was investigated in earlier studies. $\delta^2\text{H}_{\text{ne}}$ of twig xylem cellulose from current-year twigs should reflect nearly exclusively stable isotope ratios of fresh assimilates, as the NSC pool in the canopy is largely depleted during leaf flushing (Nabeshima *et al.*, 2018; Palacio *et al.*, 2018; Tixier *et al.*, 2018). In contrast, cellulose synthesis in older branch and stem tissues might use a larger percentage of older carbon reserves, which might be isotopically distinct from fresh NSCs due to heterotrophic fractionations, isotopic mixing, and the integration of larger temporal variations, e.g. in climate. The overall composition of the NSC storage pools of deciduous and evergreen species might also differ in terms of the time of the year when these assimilates were formed. Unlike deciduous species, evergreen species can assimilate throughout the entire year if the climatic conditions are favourable (Hadley, 2000; Schaberg, 2000;

Zhang *et al.*, 2013) and may use isotopically different water sources in different seasons. This might lead to distinct differences in the $\delta^2\text{H}$ of assimilates during summer and winter.

Therefore, the phylogenetic signals in the $\delta^2\text{H}_{\text{ne}}$ of leaf sugars might be overwritten along the path to tree-ring cellulose by other physiological and phenological traits. This possibility needs to be investigated in further studies. Thus, we conclude that any differences in $\delta^2\text{H}$ between deciduous and evergreen tree species under the same climatic conditions, apart from the species specific pattern in ^2H fractionation, were probably tissue specific and caused by the use of different proportions of fresh and old NSCs and by temporal variation in their photosynthetically active period.

Potential drivers of autotrophic and heterotrophic ^2H fractionation

Our results suggested that $\delta^2\text{H}_{\text{ne}}$ was driven by autotrophic ^2H fractionation, as leaf water could be ruled out as an important driver of the $\delta^2\text{H}_{\text{ne}}$ of carbohydrates (Figs 2, 3a and b, 4a and b, Tables 1, 2). A closer look at the biochemical reactions inside the chloroplast with the potential to impact the $\delta^2\text{H}_{\text{ne}}$ of freshly assimilated sugars might narrow down the processes that could cause the observed phylogenetic signal in the ^2H fractionation (ϵ_{HA}) in the leaf sugars of tree and shrub species (Fig. 7).

Photosynthetic carbon (C) fixation is divided into light-dependent (Fig. 7a) and light-independent reactions (Fig. 7b). During the light-dependent reactions (Fig. 7a), H^+ is produced inside the thylakoid lumen (Ferreira *et al.*, 2004) and subsequently transported through the thylakoid membrane into the chloroplast stroma. There, H^+ is used to synthesize NADPH (Nelson and Ben-Shem (2005)). H^+ undergoes continuous exchange reactions with the H of the H_2O (Giguere, 1979), both inside the water pool of the thylakoid lumen and in the chloroplast stroma, causing an additional potential for ^2H fractionation, as relative energies of ^1H and ^2H bonds are affected by their differences in zero-point vibrational energy (Scheiner & Ćuma, 1996). These

light-dependent reactions produce a strong H^+ gradient between the thylakoid lumen and the chloroplast stroma, leading to a ΔpH of 2.3 between the two compartments (Heldt *et al.*, 1973). New sugars are synthesized during the light-independent reactions (Fig. 7b).

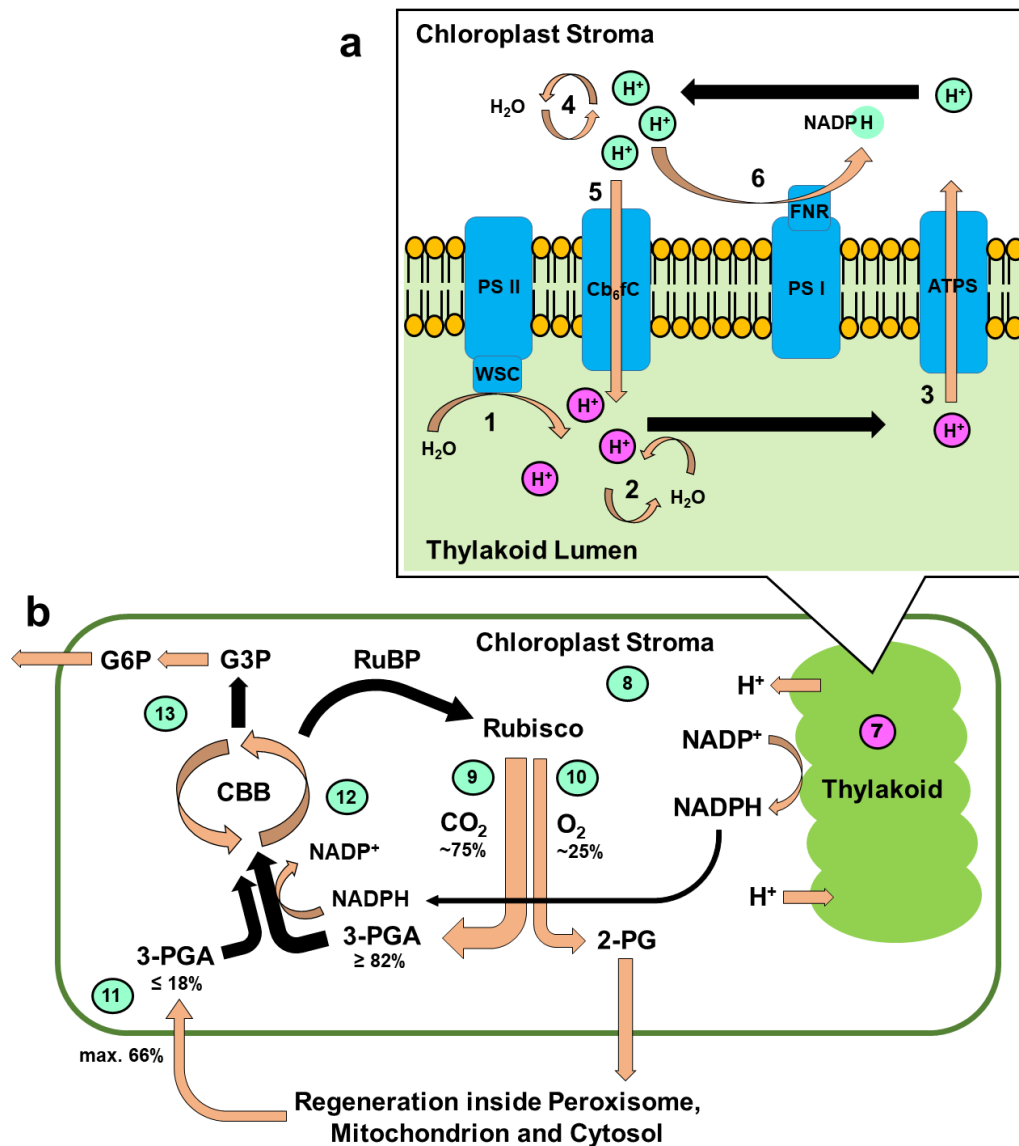


Figure 7: Simplified scheme of photosynthesis, showing only the steps where hydrogen (H, i.e. protons) is directly involved: (a) light-dependent reactions in the thylakoid according to Allen *et al.* (2011), and (b) light-independent reactions in the chloroplasts' stroma according to Busch (2020). Bold numbers indicate reactions where strong 2H fractionation is likely to occur. The proton pool within the thylakoid lumen is shown as pink

circles, while the proton pool in the chloroplast stroma is shown as mint green circles. Arrows indicate proton fluxes, with their color indicating if ^2H fractionation potentially happens (orange) or not (black) during the process. During the light-dependent reactions (1-7), ^2H fractionation can potentially occur during: (1) the splitting of water molecules by the water-splitting complex (WSC) of photosystem II (PSII; Ferreira *et al.* (2004)), which initially produces the protons for the whole reaction chain; (2) the exchange reaction between the free protons and the water molecules of the thylakoid lumen; (3) the proton pump of ATP synthase (ATPS; Seelert *et al.* (2000)), which pumps protons from the thylakoid lumen into the chloroplast stroma as the $\delta^2\text{H}$ of the proton pool in the chloroplast stroma can potentially be influenced by a selective H^+ transport by ATPS; (4) the exchange reaction between the free protons and the water molecules of the chloroplast stroma; (5) the transfer of protons back into the thylakoid lumen by the cytochrome *b₆f* complex (Cb₆fC; Cramer *et al.* (2011)); (6) NADPH synthesis by ferredoxin-NADP⁺ reductase (FNR; Nelson and Ben-Shem (2005)), which is connected to photosystem I (PSI) and uses protons from the pool in the chloroplast stroma. This process is driven by (7) the light-dependent reactions in the thylakoid. During the light-independent reactions (8-13), the $\delta^2\text{H}$ of the (8) proton pool in the chloroplast stroma is incorporated during the carbon dioxide (CO_2) assimilation process and probably further altered by ^2H fractionation. (9) About 75% of RuBisCO binds CO_2 to 3-phosphoglyceric acid (3-PGA). (10) About 25% of RuBisCO binds oxygen (O_2) in a process called photorespiration (Busch, 2020) and needs to be regenerated as 2-phosphoglycolate (2-PG) to form (11) 3-PGA (Bauwe, 2018). At least 82% of the 3-PGA pool comes from direct CO_2 fixation, while a maximum of 18% comes from photorespiration (Busch, 2020). Further biochemical exchange reactions involving H occur during (12) the Calvin-Benson-Bassham cycle (CBB), and (13) the synthesis of glucose-6-phosphate (G6P) out of glyceraldehyde-3-phosphate (G3P).

These sugars have seven C-bound H atoms, which can originate from the NADPH pool (21%), from photorespiration (up to 3% under normal

conditions), RuBP (max. 29%), or from the water inside the chloroplasts' stroma (min. 50%; Cormier *et al.* (2018)). NADPH is formed with protons from the pool in the chloroplast stroma, and thus might have a $\delta^2\text{H}$ similar to that in this water pool. This means, in summary, that up to 71% of the C-bound H in G6P is derived from the water inside the chloroplasts' stroma. Thus, the strong overall ^2H fractionation we observed is most likely driven by processes during the light-dependent reaction of photosynthesis. The most likely protein candidates causing the strong autotrophic ^2H fractionation, leading to ^2H -depleted sugars in C_3 plants, are therefore the water-splitting complex (WSC), ATP synthase (ATPS), the cytochrome b_6f complex (Cb_6fC), and ferredoxin-NADP⁺ reductase (FNR).

The processes behind the heterotrophic ^2H fractionation, which caused the observed ^2H enrichment from leaf sugars to twig xylem cellulose, most likely involve further steps that can be temporally and spatially separated from each other. For instance, trees form their tree rings at night, while sugars are formed during the day (Zweifel *et al.*, 2021). The very weak explanatory power of the $\delta^2\text{H}$ of twig xylem water for the $\delta^2\text{H}_{\text{ne}}$ of twig xylem cellulose ($R^2 = 0.1$) in our study indicates that the ^2H enrichment during cellulose formation was likely not caused by isotopic exchange with source water. Respiration has been identified as one heterotrophic ^2H -enriching process (Holloway-Phillips *et al.*, 2022). As plants respire continuously in all their living tissues, this accumulated respiratory ^2H enrichment in the leaves and twigs we sampled probably cause higher (less negative) $\delta^2\text{H}_{\text{ne}}$ in older pools of active carbohydrates, and with it higher $\delta^2\text{H}_{\text{ne}}$ of the cellulose that is formed from this pool (Lehmann *et al.*, 2021). In addition, trees and shrubs can be classified into so-called "starch" and "fat" trees / shrubs (Kramer & Kozlowski, 1960), with the latter using more lipids, in addition to carbohydrates, for their energy storage (Hoch *et al.*, 2003; Herrera-Ramírez *et al.*, 2021). This variation in the use of storage compounds might explain some of the observed variation in the heterotrophic fractionation. However, as this classification according to storage compounds has not

been done for a large fraction of species, further studies are needed to further explore the impact of such internal C dynamics.

^2H fractionation as a proxy for plants' metabolic properties

The strength of the ^2H fractionation differs between C_3 , C_4 , and CAM photosynthesis pathways (Sternberg *et al.*, 1984; Luo & Sternberg, 1991), with carbohydrates of C_3 plants being ^2H depleted compared with those of C_4 and CAM plants. Within our dataset, the angiosperm species *Ilex aquifolium* stood out, with the highest ϵ_{HA} , and with two out of three sampled trees showing a ^2H enrichment instead of the typical ^2H depletion during sugar formation. Likewise, ϵ_{HE} of *Ilex aquifolium* was the only negative value among our tested species, leading to a more ^2H -depleted cellulose compared with the currently synthesized leaf sugar. A similar pattern has been observed previously in the CAM orchid *Phalaenopsis* BLUME, probably caused by C_3 photosynthesis during leaf formation and a subsequent switch to CAM photosynthesis when the leaves reached maturity (Schuler *et al.*, 2022). Thus, *Ilex aquifolium* might be an overlooked facultative CAM species. As increased respiration rates also correlate with ^2H enrichment (Holloway-Phillips *et al.*, 2022), strong respiration rates in *Ilex aquifolium* might drive the strong ^2H enrichment in its leaf sugars. In any case, the metabolism of this species appeared to be distinct from other tree species and deserves further study. In conclusion, screening $\delta^2\text{H}_{\text{ne}}$ of carbohydrates in different plant species has the potential to reveal unknown metabolic functional groups, such as C_3 -CAM intermediates, which cannot be identified by traditional isotope approaches (Edwards, 2019).

Conclusion

Our study highlights that (1) plant metabolism was the main driver of ^2H fractionation in plant carbohydrates, (2) plants' phylogeny strongly influenced the processes affecting $\delta^2\text{H}_{\text{ne}}$ at the leaf level, (3) ^2H fractionation processes influencing the $\delta^2\text{H}_{\text{ne}}$ of cellulose altered the initial phylogenetic

signal found in $\delta^2\text{H}_{\text{ne}}$ within leaf sugars, (4) species-specific variability in ^2H fractionation must be taken into account if new ^2H fractionation models are to be developed, and (5) studying the ^2H fractionation between leaf water, leaf sugars and twig xylem cellulose could be used as a new tool for large-scale screening of plants' metabolic functioning. Based on our findings, we speculate that investigating the phylogenetic relationships of the proteins involved in the light-dependent reactions (WSC, ATPS, Cb_6fC and FNR) might reveal the steps crucial for autotrophic ^2H fractionation. Finally, further studies are needed to investigate the interaction between ^2H fractionation factors and plant physiological processes, such as gas exchange rates, photorespiration, and plant internal carbon allocation in response to environmental forcing.

Acknowledgements

We thank Yvonne Aellen und Thierry Giegelmann from Basel city gardening (Stadtgärtnerei Basel) for granting us permission to sample the outstanding tree and shrub collection in Kannenfeldpark. We thank Manuela Oettli, Oliver Rehmann and Manuela Gjoka (all at WSL) for their laboratory assistance. We also thank Melissa Dawes (Dawes Scientific Editing) for proof-editing this manuscript. Our work was supported by the Swiss National Science Foundation (SNSF) Ambizione project TreeCarbo (No. 179978, granted to M.M.L.).

Author contributions

P.S. and M.M.L. conceived and designed the study; P.S., V.V., M.S. and M.M.L. collected the samples; P.S. analysed the data and led the writing of the manuscript; V.V. supported the analysis. All authors critically contributed to the manuscript and gave final approval for publication.

References

- Allen JF, de Paula WB, Puthiyaveetil S, Nield J. 2011.** A structural phylogenetic map for chloroplast photosynthesis. *Trends in Plant Science* **16**(12): 645-655.
- Arosio T, Ziehmer-Wenz M, Nicolussi K, Schlüchter C, Leuenberger M. 2020a.** Larch Cellulose Shows Significantly Depleted Hydrogen Isotope Values With Respect to Evergreen Conifers in Contrast to Oxygen and Carbon Isotopes. *Frontiers in Earth Science* **8**(579).
- Arosio T, Ziehmer MM, Nicolussi K, Schlüchter C, Leuenberger M. 2020b.** Alpine Holocene tree-ring dataset: age-related trends in the stable isotopes of cellulose show species-specific patterns. *Biogeosciences* **17**(19): 4871-4882.
- Augusti A, Betson TR, Schleucher J. 2006.** Hydrogen exchange during cellulose synthesis distinguishes climatic and biochemical isotope fractionations in tree rings. *New Phytologist* **172**(3): 490-499.
- Augusti A, Betson TR, Schleucher J. 2008.** Deriving correlated climate and physiological signals from deuterium isotopomers in tree rings. *Chemical Geology* **252**(1-2): 1-8.
- Baan J, Holloway-Phillips M, Nelson DB, Kahmen A. 2023.** The metabolic sensitivity of hydrogen isotope fractionation differs between plant compounds. *Phytochemistry* **207**: 113563.
- Badea S-L, Botoran OR, Ionete RE. 2021.** Recent Progresses in Stable Isotope Analysis of Cellulose Extracted from Tree Rings. *Plants* **10**(12): 2743.
- Barbeta A, Gimeno TE, Clavé L, Fréjaville B, Jones SP, Delvigne C, Wingate L, Ogée J. 2020.** An explanation for the isotopic offset between soil and stem water in a temperate tree species. *New Phytologist* **227**(3): 766-779.

- Bauwe H. 2018.** Photorespiration—Damage Repair Pathway of the Calvin-Benson Cycle. *Annual Plant Reviews* **50**: 293-342.
- Brodribb TJ, Holbrook NM, Zwieniecki MA, Palma B. 2005.** Leaf hydraulic capacity in ferns, conifers and angiosperms: impacts on photosynthetic maxima. *New Phytologist* **165**(3): 839-846.
- Busch FA. 2020.** Photorespiration in the context of Rubisco biochemistry, CO₂ diffusion and metabolism. *The Plant Journal* **101**(4): 919-939.
- Cameron KM, Carmen Molina M. 2006.** Photosystem II gene sequences of psbB and psbC clarify the phylogenetic position of *Vanilla* (Vanilloideae, Orchidaceae). *Cladistics* **22**(3): 239-248.
- Cernusak LA, Barbeta A, Bush RT, Eichstaedt R, Ferrio JP, Flanagan LB, Gessler A, Martín-Gómez P, Hirl RT, Kahmen A. 2022.** Do ²H and ¹⁸O in leaf water reflect environmental drivers differently? *New Phytologist* **235**(1): 41-51
- Cernusak LA, Barbour MM, Arndt SK, Cheesman AW, English NB, Feild TS, Helliker BR, Holloway-Phillips MM, Holtum JAM, Kahmen A, et al. 2016.** Stable isotopes in leaf water of terrestrial plants. *Plant, Cell & Environment* **39**(5): 1087-1102.
- Cernusak LA, Farquhar GD, Pate JS. 2005.** Environmental and physiological controls over oxygen and carbon isotope composition of Tasmanian blue gum, *Eucalyptus globulus*. *Tree Physiology* **25**(2): 129-146.
- Coplen TB. 2011.** Guidelines and recommended terms for expression of stable-isotope-ratio and gas-ratio measurement results. *Rapid Communications in Mass Spectrometry* **25**(17): 2538-2560.
- Cormier M-A, Werner RA, Sauer PE, Gröcke DR, Leuenberger MC, Wieloch T, Schleucher J, Kahmen A. 2018.** ²H-fractionations during the biosynthesis of carbohydrates and lipids imprint a metabolic signal

- on the $\delta^2\text{H}$ values of plant organic compounds. *New Phytologist* **218**(2): 479-491.
- Craig H. 1961.** Isotopic variations in meteoric waters. *Science* **133**(3465): 1702-1703.
- Cramer WA, Hasan SS, Yamashita E. 2011.** The Q cycle of cytochrome bc complexes: a structure perspective. *Biochimica et Biophysica Acta (BBA)-Bioenergetics* **1807**(7): 788-802.
- Dansgaard W. 1964.** Stable isotopes in precipitation. *Tellus* **16**(4): 436-468.
- De Las Rivas J, Roman A. 2005.** Structure and evolution of the extrinsic proteins that stabilize the oxygen-evolving engine. *Photochemical & Photobiological Sciences* **4**(12): 1003-1010.
- Diao H, Schuler P, Goldsmith GR, Siegwolf RT, Saurer M, Lehmann MM. 2022.** On uncertainties in plant water isotopic composition following extraction by cryogenic vacuum distillation. *Hydrology and Earth System Sciences Discussions*: 1-17.
- Dirghangi SS, Pagani M. 2013.** Hydrogen isotope fractionation during lipid biosynthesis by *Haloarcula marismortui*. *Geochimica et Cosmochimica Acta* **119**: 381-390.
- Edwards EJ. 2019.** Evolutionary trajectories, accessibility and other metaphors: the case of C_4 and CAM photosynthesis. *New Phytologist* **223**(4): 1742-1755.
- Epstein S, Thompson P, Yapp CJ. 1977.** Oxygen and hydrogen isotopic ratios in plant cellulose. *Science* **198**(4323): 1209-1215.
- Farquhar GD, Cernusak LA, Barnes B. 2007.** Heavy Water Fractionation during Transpiration. *Plant Physiology* **143**(1): 11-18.
- Ferreira KN, Iverson TM, Maghlaoui K, Barber J, Iwata S. 2004.** Architecture of the photosynthetic oxygen-evolving center. *Science* **303**(5665): 1831-1838.

- Filot MS, Leuenberger M, Pazdur A, Boettger T. 2006.** Rapid online equilibration method to determine the D/H ratios of non-exchangeable hydrogen in cellulose. *Rapid Communications in Mass Spectrometry* **20**(22): 3337-3344.
- Flexas J, Carriqui M. 2020.** Photosynthesis and photosynthetic efficiencies along the terrestrial plant's phylogeny: lessons for improving crop photosynthesis. *The Plant Journal* **101**(4): 964-978.
- Gehre M, Geilmann H, Richter J, Werner R, Brand W. 2004.** Continuous flow $^2\text{H}/^1\text{H}$ and $^{18}\text{O}/^{16}\text{O}$ analysis of water samples with dual inlet precision. *Rapid Communications in Mass Spectrometry* **18**(22): 2650-2660.
- Gessler A, Brandes E, Buchmann N, Helle G, Rennenberg H, Barnard RL. 2009.** Tracing carbon and oxygen isotope signals from newly assimilated sugars in the leaves to the tree-ring archive. *Plant, Cell & Environment* **32**(7): 780-795.
- Giguere PA. 1979.** The great fallacy of the H^+ ion: And the true nature of H_3O^+ . *Journal of Chemical Education* **56**(9): 571.
- Hadley JL. 2000.** Effect of daily minimum temperature on photosynthesis in eastern hemlock (*Tsuga canadensis* L.) in autumn and winter. *Arctic, Antarctic, and Alpine Research* **32**(4): 368-374.
- Heldt HW, Werdan K, Milovancev M, Geller G. 1973.** Alkalization of the chloroplast stroma caused by light-dependent proton flux into the thylakoid space. *Biochimica et Biophysica Acta (BBA)-Bioenergetics* **314**(2): 224-241.
- Herrera-Ramírez D, Muhr J, Hartmann H, Römermann C, Trumbore S, Sierra CA. 2020.** Probability distributions of nonstructural carbon ages and transit times provide insights into carbon allocation dynamics of mature trees. *New Phytologist* **226**(5): 1299-1311.

- Herrera-Ramírez D, Sierra CA, Römermann C, Muhr J, Trumbore S, Silvério D, Brando PM, Hartmann H. 2021.** Starch and lipid storage strategies in tropical trees relate to growth and mortality. *New Phytologist* **230**(1): 139-154.
- Hoch G, Richter A, Körner C. 2003.** Non-structural carbon compounds in temperate forest trees. *Plant, Cell & Environment* **26**(7): 1067-1081.
- Holloway-Phillips M, Baan J, Nelson DB, Lehmann MM, Tcherkez G, Kahmen A. 2022.** Species variation in the hydrogen isotope composition of leaf cellulose is mostly driven by isotopic variation in leaf sucrose. *Plant, Cell & Environment* **45**(9): 2636-2651.
- Kagawa A. 2022.** Foliar water uptake as a source of hydrogen and oxygen in plant biomass. *Tree Physiology* **42**(11): 2153-2173.
- Kagawa A, Battipaglia G. 2022.** Post-photosynthetic Carbon, Oxygen and Hydrogen Isotope Signal Transfer to Tree Rings—How Timing of Cell Formations and Turnover of Stored Carbohydrates Affect Intra-annual Isotope Variations. Chapter in **Siegwolf RT, Brooks JR, Roden J, Saurer M 2022.** *Stable Isotopes in Tree Rings*. Springer: 429-462.
- Karlusich JJP, Carrillo N. 2017.** Evolution of the acceptor side of photosystem I: ferredoxin, flavodoxin, and ferredoxin-NADP⁺ oxidoreductase. *Photosynthesis Research* **134**(3): 235-250.
- Kramer PJ, Kozlowski TT. 1960.** Physiology of trees. *McGraw-Hill Book Company*.
- Lehmann MM, Egli M, Brinkmann N, Werner RA, Saurer M, Kahmen A. 2020.** Improving the extraction and purification of leaf and phloem sugars for oxygen isotope analyses. *Rapid Communications in Mass Spectrometry* **34**(19): e8854.
- Lehmann MM, Goldsmith GR, Schmid L, Gessler A, Saurer M, Siegwolf RT. 2018.** The effect of ¹⁸O-labelled water vapour on the oxygen isotope

- ratio of water and assimilates in plants at high humidity. *New Phytologist* **217**(1): 105-116.
- Lehmann MM, Schuler P, Cormier M-A, Allen ST, Leuenberger M, Voelker S. 2022.** The Stable Hydrogen Isotopic Signature: From Source Water to Tree Rings. Chapter in **Siegwolf RT, Brooks JR, Roden J, Saurer M. 2022: *Stable Isotopes in Tree Rings: Inferring Physiological, Climatic and Environmental Responses*.** Springer:331-359
- Lehmann MM, Vitali V, Schuler P, Leuenberger M, Saurer M. 2021.** More than climate: Hydrogen isotope ratios in tree rings as novel plant physiological indicator for stress conditions. *Dendrochronologia* **65**: 125788.
- Luo Y-H, Steinberg L, Suda S, Kumazawa S, Mitsui A. 1991.** Extremely low D/H ratios of photoproduced hydrogen by cyanobacteria. *Plant and Cell Physiology* **32**(6): 897-900.
- Luo Y-H, Sternberg L. 1991.** Deuterium heterogeneity in starch and cellulose nitrate of CAM and C₃ plants. *Phytochemistry* **30**(4): 1095-1098.
- Lusk CH, Wright I, Reich PB. 2003.** Photosynthetic differences contribute to competitive advantage of evergreen angiosperm trees over evergreen conifers in productive habitats. *New Phytologist* **160**(2): 329-336.
- Molina-Venegas R, Rodríguez MÁ. 2017.** Revisiting phylogenetic signal; strong or negligible impacts of polytomies and branch length information? *BMC evolutionary biology* **17**(1): 1-10.
- Nabeshima E, Nakatsuka T, Kagawa A, Hiura T, Funada R. 2018.** Seasonal changes of δD and $\delta^{18}\text{O}$ in tree-ring cellulose of *Quercus crispula* suggest a change in post-photosynthetic processes during earlywood growth. *Tree Physiology* **38**(12): 1829-1840.

- Nelson N, Ben-Shem A. 2005.** The structure of photosystem I and evolution of photosynthesis. *Bioessays* **27**(9): 914-922.
- Palacio S, Camarero JJ, Maestro M, Alla AQ, Lahoz E, Montserrat-Martí G. 2018.** Are storage and tree growth related? Seasonal nutrient and carbohydrate dynamics in evergreen and deciduous Mediterranean oaks. *Trees* **32**(3): 777-790.
- Patterson AE, Arkebauer R, Quallo C, Heskell MA, Li X, Boelman N, Griffin KL. 2018.** Temperature response of respiration and respiratory quotients of 16 co-occurring temperate tree species. *Tree Physiology* **38**(9): 1319-1332.
- Pedersen TL. 2022.** patchwork: The Composer of Plots.
- R.Core.Team 2023.** R: A language and environment for statistical computing. *R Foundation for Statistical Computing, Vienna, Austria.*
- Recipon H, Perasso R, Adoutte A, Quetier F. 1992.** ATP synthase subunit c/III/9 gene sequences as a tool for interkingdom and metaphytes molecular phylogenies. *Journal of Molecular Evolution* **34**(4): 292-303.
- Revell LJ. 2012.** phytools: an R package for phylogenetic comparative biology (and other things). *Methods in Ecology and Evolution*(2): 217-223.
- Rinne KT, Saurer M, Streit K, Siegwolf RT. 2012.** Evaluation of a liquid chromatography method for compound-specific $\delta^{13}\text{C}$ analysis of plant carbohydrates in alkaline media. *Rapid Communications in Mass Spectrometry* **26**(18): 2173-2185.
- Roden JS, Ehleringer JR. 1999.** Hydrogen and oxygen isotope ratios of tree-ring cellulose for riparian trees grown long-term under hydroponically controlled environments. *Oecologia*: 467-477.
- Roden JS, Ehleringer JR. 2000.** Hydrogen and oxygen isotope ratios of tree-ring cellulose for field-grown riparian trees. *Oecologia* **123**(4): 481-489.

- Roden JS, Lin G, Ehleringer JR. 2000.** A mechanistic model for interpretation of hydrogen and oxygen isotope ratios in tree-ring cellulose. *Geochimica et Cosmochimica Acta* **64**(1): 21-35.
- Sanchez-Bragado R, Serret MD, Marimon RM, Bort J, Araus JL. 2019.** The Hydrogen Isotope Composition $\delta^2\text{H}$ Reflects Plant Performance. *Plant Physiology* **180**(2): 793-812.
- Schaberg P. 2000.** Winter photosynthesis in red spruce (*Picea rubens* Sarg.): limitations, potential benefits, and risks. *Arctic, Antarctic, and Alpine Research* **32**(4): 375-380.
- Scheiner S, Ćuma M. 1996.** Relative stability of hydrogen and deuterium bonds. *Journal of the American Chemical Society* **118**(6): 1511-1521.
- Schönbeck LC, Santiago LS. 2022.** Time will tell: Towards high resolution temporal tree-ring isotope analyses. *Tree Physiology* **42**(12): 2401-2403
- Schuler P, Cormier MA, Werner RA, Buchmann N, Gessler A, Vitali V, Saurer M, Lehmann MM. 2022.** A high temperature water vapor equilibration method to determine non-exchangeable hydrogen isotope ratios of sugar, starch, and cellulose. *Plant, Cell & Environment* **45**(1): 12-22
- Seelert H, Poetsch A, Dencher NA, Engel A, Stahlberg H, Müller DJ. 2000.** Proton-powered turbine of a plant motor. *Nature* **405**(6785): 418-419.
- Shirao M, Kuroki S, Kaneko K, Kinjo Y, Tsuyama M, Förster B, Takahashi S, Badger MR. 2013.** Gymnosperms have increased capacity for electron leakage to oxygen (Mehler and PTOX reactions) in photosynthesis compared with angiosperms. *Plant and Cell Physiology* **54**(7): 1152-1163.
- Sternberg L, Deniro MJ, Ajie H. 1984.** Stable hydrogen isotope ratios of saponifiable lipids and cellulose nitrate from CAM, C₃ and C₄ plants. *Phytochemistry* **23**(11): 2475-2477.

- Tixier A, Orozco J, Roxas AA, Earles JM, Zwieniecki MA. 2018.** Diurnal variation in nonstructural carbohydrate storage in trees: remobilization and vertical mixing. *Plant Physiology* **178**(4): 1602-1613.
- Vitali V, Martínez-Sancho E, Treydte K, Andreu-Hayles L, Dorado-Liñán I, Gutierrez E, Helle G, Leuenberger M, Loader NJ, Rinne-Garmston KT. 2022.** The unknown third-Hydrogen isotopes in tree-ring cellulose across Europe. *Science of The Total Environment* **813**: 152281.
- West AG, Patrickson SJ, Ehleringer JR. 2006.** Water extraction times for plant and soil materials used in stable isotope analysis. *Rapid Communications in Mass Spectrometry: An International Journal Devoted to the Rapid Dissemination of Up-to-the-Minute Research in Mass Spectrometry* **20**(8): 1317-1321.
- West JB, Sobek A, Ehleringer JR. 2008.** A simplified GIS approach to modeling global leaf water isoscapes. *PloS one* **3**(6): e2447.
- White J. 1989.** Stable hydrogen isotope ratios in plants: a review of current theory and some potential applications. Chapter in **Rundel PW, Ehleringer JR, Nagy KA. 1989.** *Stable isotopes in ecological research*. Springer: 142-162.
- Wickham H. 2016.** ggplot2: Elegant Graphics for Data Analysis. *Springer-Verlag New York* Retrieved from <https://ggplot2.tidyverse.org>.
- Wieloch T, Grabner M, Augusti A, Serk H, Ehlers I, Yu J, Schleucher J. 2022.** Metabolism is a major driver of hydrogen isotope fractionation recorded in tree-ring glucose of *Pinus nigra*. *New Phytologist* **234**(2): 449-461.
- Yapp CJ, Epstein S. 1982.** Climatic significance of the hydrogen isotope ratios in tree cellulose. *Nature* **297**(5868): 636-639.

- Zhang Y, Cao K, Goldstein G 2013.** Winter photosynthesis of evergreen broadleaf trees from a montane cloud forest in subtropical China. *Photosynthesis Research for Food, Fuel and the Future*. Springer: 812-817.
- Zhou Y, Grice K, Stuart-Williams H, Hocart CH, Gessler A, Farquhar GD. 2016.** Hydrogen isotopic differences between C₃ and C₄ land plant lipids: consequences of compartmentation in C₄ photosynthetic chemistry and C₃ photorespiration. *Plant, Cell & Environment* **39**(12): 2676-2690.
- Ziegler H 1989.** Hydrogen isotope fractionation in plant tissues. Chapter in **Rundel PW, Ehleringer JR, Nagy KA. 1989.** *Stable Isotopes in Ecological Research*. Springer: 105-123.
- Zweifel R, Sterck F, Braun S, Buchmann N, Eugster W, Gessler A, Häni M, Peters RL, Walthert L, Wilhelm M. 2021.** Why trees grow at night. *New Phytologist* **231**(6): 2174-2185.

Supporting Information

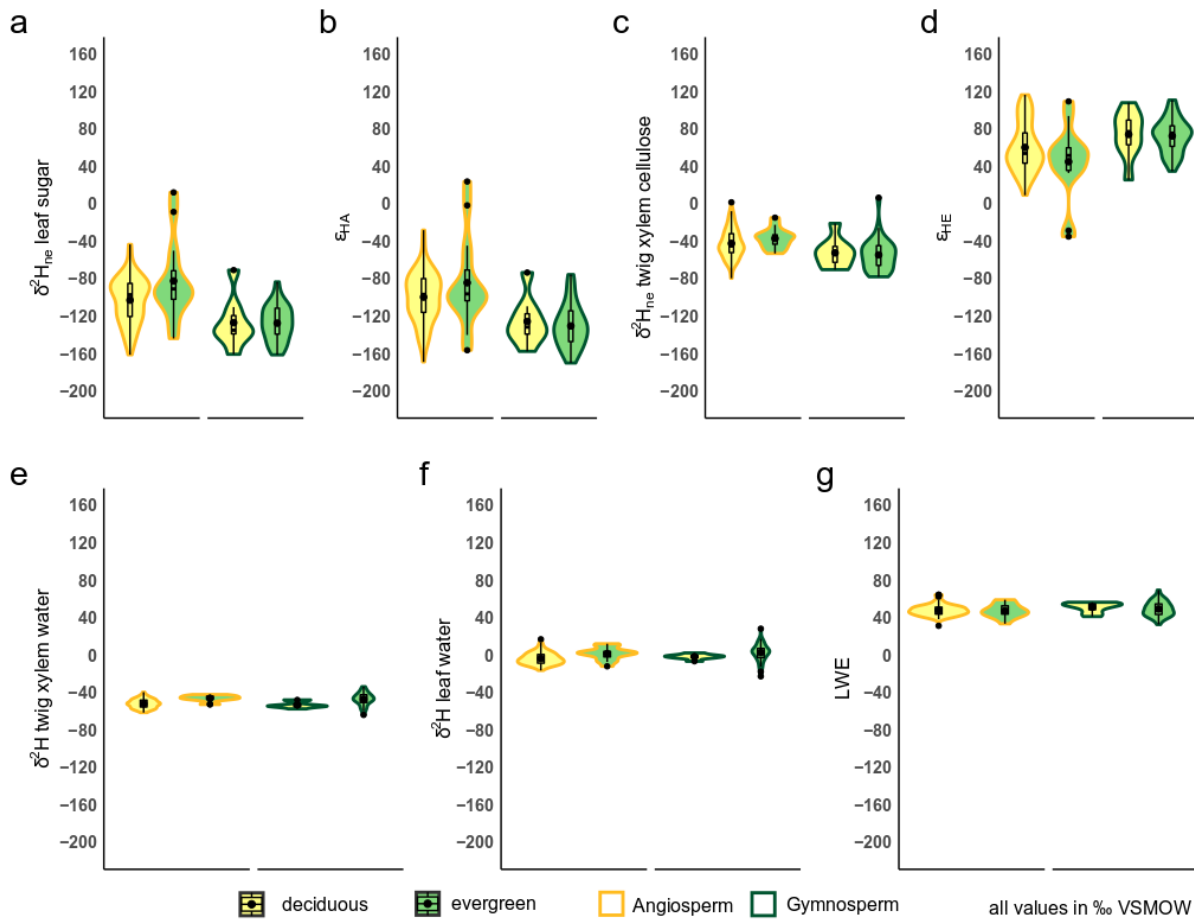


Figure S1: Comparison between a) $\delta^2\text{H}_{\text{ne}}$ of leaf sugar, b) ϵ_{HA} , c) $\delta^2\text{H}_{\text{ne}}$ of twig xylem cellulose, d) ϵ_{HE} , e) $\delta^2\text{H}$ twig xylem water, f) $\delta^2\text{H}$ leaf water, and g) leaf water enrichment between deciduous (light yellow filled) and evergreen (light green filled) angiosperms (dark yellow margin) and gymnosperms (dark green margin). The boxplots within the violin plots are indicating the mean (points) and median (horizontal line) values.

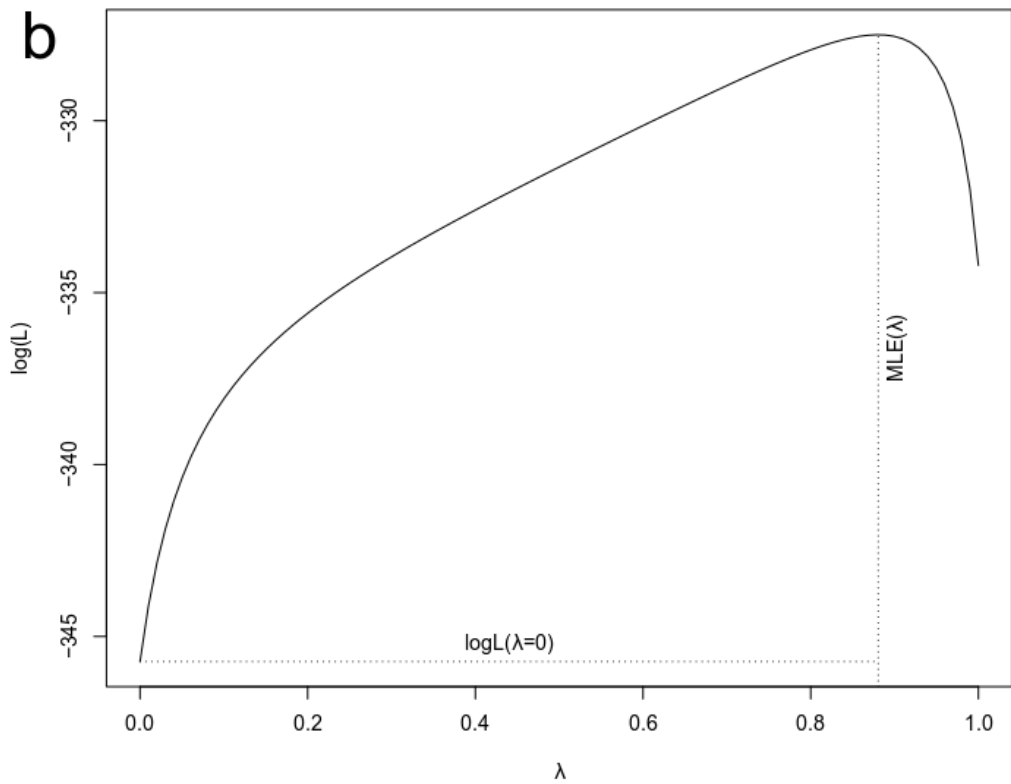
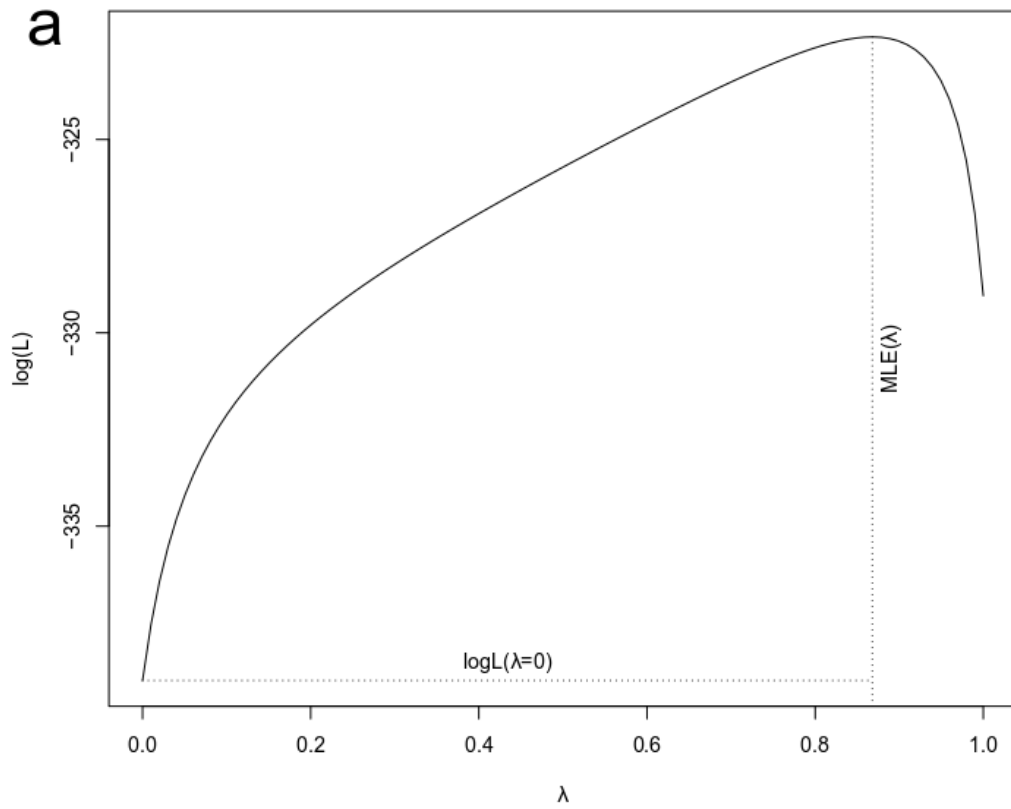


Figure S2: Pagel's λ of a) $\delta^2\text{H}_{\text{ne}}$ leaf sugar and b) ϵ_{HA}

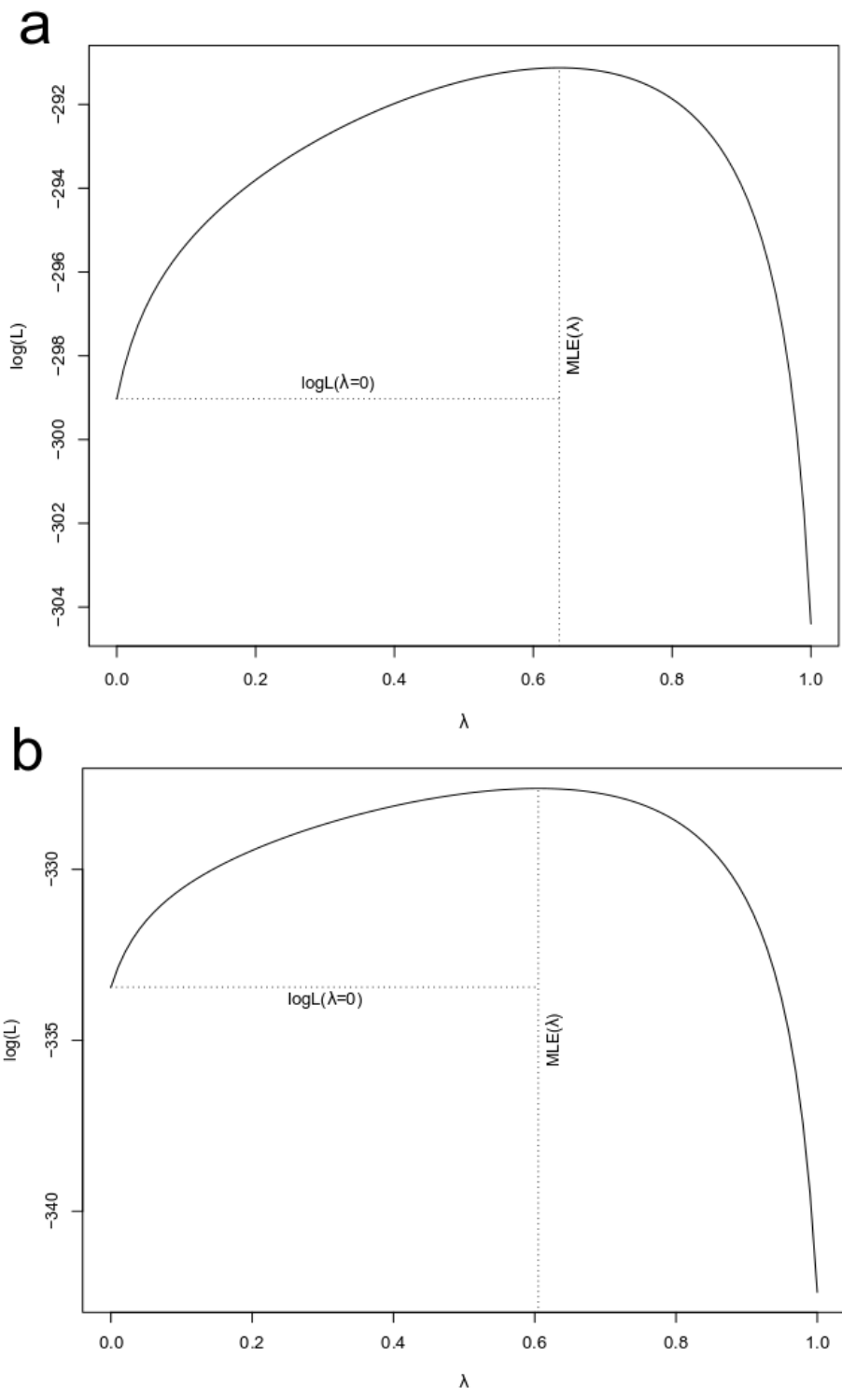


Figure S3: Pagel's λ of a) $\delta^2\text{H}_{\text{nc}}$ twig xylem cellulose and b) ϵ_{HE}

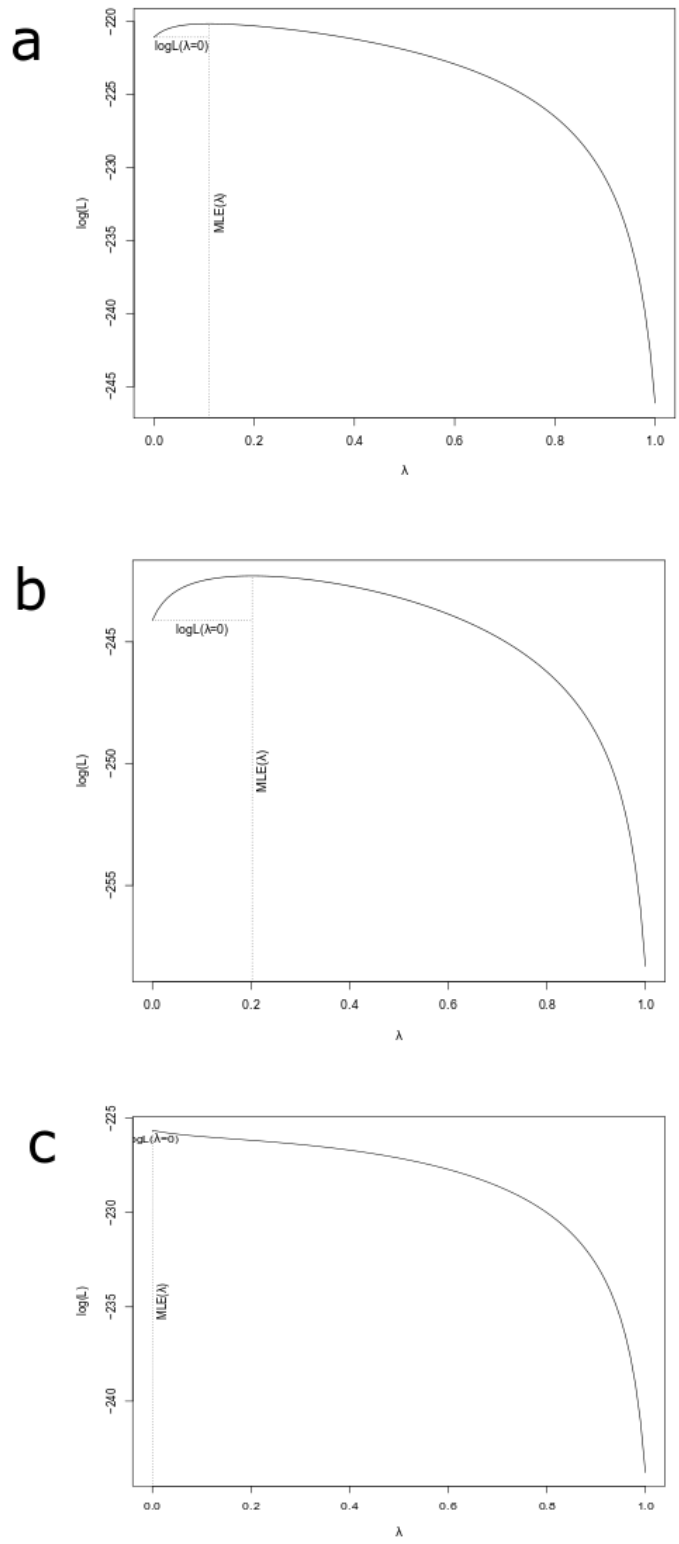


Figure S4: Pagel's λ of a) $\delta^2\text{H}$ twig xylem water, b) $\delta^2\text{H}$ leaf water, and 3) leaf water enrichment

Table S1: List of all sampled trees and their scientific classification, including all measured $\delta^2\text{H}$ and $\delta^2\text{H}_{\text{ne}}$ values, and the ^2H fractionation factors ϵ_{HA} , ϵ_{HE} , as well as the leaf water enrichment LWE. All values are in ‰

Clade	Order	Family	Species	Phenology	$\delta^2\text{H}_{\text{KW}}$	$\delta^2\text{H}_{\text{LW}}$	LWE	$\delta^2\text{H}_{\text{acTxC}}$	$\delta^2\text{H}_{\text{acLS}}$	ϵ_{HA}	ϵ_{HE}
Angiosperm	Aquifoliales	Aquifoliaceae	Ilex aquifolium L.	evergreen	-45.4	-11.6	33.8	-22.0	12.6	24.2	-34.6
Angiosperm	Aquifoliales	Aquifoliaceae	Ilex aquifolium L.	evergreen	-45.6	-5.3	40.4	-14.4	-49.6	-44.3	35.2
Angiosperm	Aquifoliales	Aquifoliaceae	Ilex aquifolium L.	evergreen	-51.9	-7.0	44.9	-36.5	-8.3	-1.3	-28.2
Angiosperm	Buxales	Buxaceae	Buxus sempervirens L.	evergreen	-41.8	2.3	44.1	-41.7	-96.2	-98.5	54.5
Angiosperm	Buxales	Buxaceae	Buxus sempervirens L.	evergreen	-45.9	3.7	49.6	-41.2	-99.4	-103.1	58.2
Angiosperm	Buxales	Buxaceae	Buxus sempervirens L.	evergreen	-44.2	9.8	54.1	-48.8	-90.4	-100.2	41.6
Angiosperm	Fabales	Fabaceae	Gleditsia triacanthos L.	deciduous	-56.2	-4.7	51.5	-45.9	-83.1	-78.4	37.2
Angiosperm	Fabales	Fabaceae	Gleditsia triacanthos L.	deciduous	-47.4	17.2	64.6	-51.4	-151.2	-168.4	99.8
Angiosperm	Fabales	Fabaceae	Gleditsia triacanthos L.	deciduous	-56.9	8.0	64.9	-40.7	-143.0	-151.0	102.3
Angiosperm	Fabales	Fabaceae	Maackia amurensis RUPR. & MAXIM.	deciduous	-55.0	4.2	59.1	-23.6	-132.4	-136.6	108.8
Angiosperm	Fabales	Fabaceae	Styphnolobium japonicum (L.) SCHOTT	deciduous	-58.7	-8.2	50.5	-64.3	-160.8	-152.6	96.5
Angiosperm	Fagales	Betulaceae	Alnus cordata (LOISEL.) DUBY	deciduous	-51.6	-5.8	45.7	-61.6	-151.0	-145.2	89.4
Angiosperm	Fagales	Betulaceae	Alnus cordata (LOISEL.) DUBY	deciduous	-58.8	-6.0	52.8	-54.9	-94.1	-88.1	39.2
Angiosperm	Fagales	Betulaceae	Alnus cordata (LOISEL.) DUBY	deciduous	-50.9	4.0	54.9	-44.6	-89.0	-93.0	44.4
Angiosperm	Fagales	Betulaceae	Alnus incana (L.) MOENCH	deciduous	-51.8	-9.1	42.7	-63.3	-111.0	-101.9	47.7
Angiosperm	Fagales	Betulaceae	Alnus incana (L.) MOENCH	deciduous	-42.9	3.6	46.5	-79.1	-124.2	-127.8	45.1
Angiosperm	Fagales	Betulaceae	Alnus incana (L.) MOENCH	deciduous	-48.6	-0.6	48.0	-61.2	-108.4	-107.8	47.2
Angiosperm	Fagales	Betulaceae	Betula nigra L.	deciduous	-57.0	-8.7	48.4	-66.3	-88.2	-79.5	21.9
Angiosperm	Fagales	Betulaceae	Betula pendula ROTH	deciduous	-43.7	-4.5	39.2	-73.1	-118.7	-114.2	45.6
Angiosperm	Fagales	Betulaceae	Betula pendula ROTH	deciduous	-42.8	2.7	45.4	-59.8	-108.8	-111.5	49.0
Angiosperm	Fagales	Betulaceae	Betula pendula ROTH	deciduous	-50.5	2.3	52.8	-60.5	-70.1	-72.4	9.6
Angiosperm	Fagales	Betulaceae	Betula utilis D.DON	deciduous	-46.3	2.3	48.6	-50.9	-143.1	-145.4	92.2
Angiosperm	Fagales	Betulaceae	Betula utilis D.DON	deciduous	-40.9	11.2	52.1	-61.8	-80.1	-91.3	18.3
Angiosperm	Fagales	Betulaceae	Carpinus betulus L.	deciduous	-44.5	-4.7	39.8	-63.5	-120.9	-116.2	57.4
Angiosperm	Fagales	Betulaceae	Carpinus betulus L.	deciduous	-45.0	6.5	51.5	-31.8	-90.9	-97.4	59.1
Angiosperm	Fagales	Betulaceae	Carpinus betulus L.	deciduous	-39.2	13.6	52.9	-26.5	-96.7	-110.3	70.2
Angiosperm	Fagales	Betulaceae	Ostrya carpinifolia SCOP.	deciduous	-43.5	-0.3	43.2	-55.4	-103.3	-103.0	47.9
Angiosperm	Fagales	Betulaceae	Ostrya carpinifolia SCOP.	deciduous	-46.4	-1.1	45.3	-59.2	-98.6	-97.5	39.4
Angiosperm	Fagales	Betulaceae	Ostrya carpinifolia SCOP.	deciduous	-44.2	3.9	48.1	-61.4	-108.2	-112.1	46.8
Angiosperm	Fagales	Fagaceae	Fagus sylvatica L.	deciduous	-61.0	-9.0	51.9	-51.3	-125.2	-116.2	73.9
Angiosperm	Fagales	Fagaceae	Quercus castaneifolia C.A.MEY.	deciduous	-48.4	-9.7	38.7	-56.3	-101.7	-92.0	45.4
Angiosperm	Fagales	Fagaceae	Quercus cerris L.	deciduous	-51.7	-9.4	42.3	-45.2	-77.0	-67.6	31.8
Angiosperm	Fagales	Fagaceae	Quercus cerris L.	deciduous	-51.1	1.4	52.5	-30.3	-84.5	-85.9	54.2
Angiosperm	Fagales	Fagaceae	Quercus cerris L.	deciduous	-60.0	-6.8	53.2	-52.0	-88.9	-82.1	36.9
Angiosperm	Fagales	Fagaceae	Quercus ilex L.	evergreen	-42.1	4.4	46.5	-33.6	-88.7	-93.1	55.1
Angiosperm	Fagales	Fagaceae	Quercus ilex L.	evergreen	-44.0	4.1	48.1	-48.4	-87.1	-91.2	38.7
Angiosperm	Fagales	Fagaceae	Quercus ilex L.	evergreen	-46.4	2.4	48.8	-29.7	-90.6	-93.0	60.9
Angiosperm	Fagales	Fagaceae	Quercus ilicifolia WANGENH.	deciduous	-57.7	-7.4	50.3	-33.6	-95.3	-87.9	61.7
Angiosperm	Fagales	Fagaceae	Quercus macrolepis KOTSCHY	deciduous	-56.9	-6.4	50.6	-36.0	-85.7	-79.3	49.7
Angiosperm	Fagales	Fagaceae	Quercus marilandica MÜNCHH.	deciduous	-53.9	0.8	54.7	-31.5	-83.5	-84.3	52.0
Angiosperm	Fagales	Fagaceae	Quercus pubescens WILLD.	deciduous	-47.3	-5.6	41.8	-43.5	-111.0	-105.4	67.5
Angiosperm	Fagales	Fagaceae	Quercus pubescens WILLD.	deciduous	-51.2	-0.7	50.4	-33.7	-92.2	-91.5	58.5
Angiosperm	Fagales	Fagaceae	Quercus pubescens WILLD.	deciduous	-51.7	0.7	52.4	-28.9	-137.8	-138.5	108.9
Angiosperm	Fagales	Fagaceae	Quercus robur L.	deciduous	-46.8	1.0	47.8	-38.2	-114.3	-115.3	76.1
Angiosperm	Fagales	Fagaceae	Quercus robur L.	deciduous	-54.0	-6.1	47.9	-22.3	-82.9	-76.8	60.6
Angiosperm	Fagales	Fagaceae	Quercus robur L.	deciduous	-51.7	-0.9	50.8	-41.5	-95.4	-94.5	53.9
Angiosperm	Fagales	Fagaceae	Quercus rubra L.	deciduous	-57.1	-5.5	51.6	-15.8	-125.5	-120.0	109.7
Angiosperm	Fagales	Fagaceae	Quercus suber L.	evergreen	-43.0	-2.3	40.7	-32.4	-65.7	-63.4	33.3
Angiosperm	Fagales	Fagaceae	Quercus suber L.	evergreen	-43.4	0.8	44.2	-52.7	-102.3	-103.1	49.6
Angiosperm	Fagales	Juglandaceae	Carya cordiformis (WANGENH.) K.KOCH	deciduous	-47.8	-6.9	40.9	-57.8	-103.2	-96.3	45.4
Angiosperm	Fagales	Juglandaceae	Carya cordiformis (WANGENH.) K.KOCH	deciduous	-52.2	-10.1	42.0	-42.7	-87.8	-77.7	45.1
Angiosperm	Fagales	Juglandaceae	Carya cordiformis (WANGENH.) K.KOCH	deciduous	-53.5	-7.4	46.0	-43.3	-87.1	-79.7	43.8
Angiosperm	Fagales	Juglandaceae	Juglans nigra L.	deciduous	-49.5	5.1	54.6	-52.3	-84.5	-89.6	32.2
Angiosperm	Fagales	Juglandaceae	Juglans nigra L.	deciduous	-54.7	3.4	58.1	-48.5	-105.7	-109.1	57.2
Angiosperm	Fagales	Juglandaceae	Juglans nigra L.	deciduous	-56.8	1.5	58.3	-34.4	-85.8	-87.3	51.4
Angiosperm	Fagales	Juglandaceae	Juglans regia L.	deciduous	-47.6	-3.7	43.9	-47.3	-120.4	-116.7	73.1
Angiosperm	Fagales	Juglandaceae	Juglans regia L.	deciduous	-47.2	-0.4	46.8	-38.2	-96.6	-96.2	58.4
Angiosperm	Fagales	Juglandaceae	Juglans regia L.	deciduous	-45.9	7.4	53.3	-44.5	-95.9	-103.3	51.4
Angiosperm	Lamiales	Oleaceae	Fraxinus angustifolia VAHL	deciduous	-49.4	-4.4	45.0	-30.3	-71.1	-66.7	40.8
Angiosperm	Lamiales	Oleaceae	Fraxinus excelsior L.	deciduous	-46.9	-15.3	31.6	-11.6	-43.0	-27.7	31.4
Angiosperm	Lamiales	Oleaceae	Fraxinus excelsior L.	deciduous	-47.2	-6.2	41.1	-33.6	-49.6	-43.4	16.0
Angiosperm	Lamiales	Oleaceae	Fraxinus excelsior L.	deciduous	-51.8	1.6	53.4	-24.7	-78.5	-80.1	53.8
Angiosperm	Lamiales	Oleaceae	Fraxinus holotricha WILMOTT EX PALLIS	deciduous	-57.2	-12.1	45.1	-13.1	-75.1	-63.0	62.0
Angiosperm	Lamiales	Oleaceae	Fraxinus holotricha WILMOTT EX PALLIS	deciduous	-53.3	-4.2	49.1	-16.2	-123.0	-118.8	106.8
Angiosperm	Lamiales	Oleaceae	Fraxinus ornus L.	deciduous	-54.7	-12.4	42.2	2.0	-49.1	-36.7	51.1
Angiosperm	Lamiales	Oleaceae	Fraxinus ornus L.	deciduous	-46.6	-4.1	42.6	-10.4	-96.1	-92.0	85.7
Angiosperm	Lamiales	Oleaceae	Fraxinus ornus L.	deciduous	-51.3	-8.3	43.0	-7.5	-68.9	-60.6	61.4

Angiosperm	Magnoliales	Magnoliaceae	Liriodendron chinense (HEMSL.) SARG.	deciduous	-46.3	-2.3	44.0	-46.0	-131.1	-128.8	85.1
Angiosperm	Magnoliales	Magnoliaceae	Liriodendron chinense (HEMSL.) SARG.	deciduous	-50.5	-1.8	48.6	-17.3	-78.3	-76.5	61.0
Angiosperm	Magnoliales	Magnoliaceae	Liriodendron tulipifera L.	deciduous	-49.7	-3.5	46.2	-45.2	-118.4	-114.9	73.2
Angiosperm	Magnoliales	Magnoliaceae	Liriodendron tulipifera L.	deciduous	-49.5	-3.3	46.2	-47.4	-114.1	-110.8	66.7
Angiosperm	Magnoliales	Magnoliaceae	Liriodendron tulipifera L.	deciduous	-51.2	-1.6	49.7	-44.8	-134.0	-132.4	89.2
Angiosperm	Magnoliales	Magnoliaceae	Magnolia grandiflora L.	evergreen	-52.4	1.8	54.2	-43.1	-110.2	-112.0	67.1
Angiosperm	Magnoliales	Magnoliaceae	Magnolia grandiflora L.	evergreen	-48.0	11.4	59.3	-34.1	-128.3	-139.7	94.2
Angiosperm	Magnoliales	Magnoliaceae	Magnolia grandiflora L.	evergreen	-47.0	12.5	59.4	-33.7	-143.5	-156.0	109.8
Angiosperm	Magnoliales	Magnoliaceae	Magnolia kobus DC.	deciduous	-51.7	-10.4	41.3	-32.9	-149.7	-139.3	116.8
Angiosperm	Magnoliales	Magnoliaceae	Magnolia kobus DC.	deciduous	-51.3	-4.0	47.3	-38.7	-76.2	-72.2	37.5
Angiosperm	Magnoliales	Magnoliaceae	Magnolia kobus DC.	deciduous	-55.0	-5.3	49.7	-57.8	-111.7	-106.4	53.9
Angiosperm	Magnoliales	Magnoliaceae	Magnolia tripetala (L.) L.	deciduous	-45.7	-2.9	42.8	-49.0	-74.9	-72.0	25.9
Angiosperm	Magnoliales	Magnoliaceae	Magnolia tripetala (L.) L.	deciduous	-51.0	-6.5	44.5	-30.6	-131.8	-125.3	101.2
Angiosperm	Malvales	Malvaceae	Firmiana simplex (L.) W.WIGHT	deciduous	-53.7	3.4	57.1	-44.6	-85.8	-89.2	41.2
Angiosperm	Malvales	Malvaceae	Tilia americana L.	deciduous	-47.7	-1.1	46.7	-47.1	-75.8	-74.7	28.7
Angiosperm	Malvales	Malvaceae	Tilia cordata MILL.	deciduous	-56.7	-10.4	46.3	-38.1	-82.3	-71.9	44.2
Angiosperm	Malvales	Malvaceae	Tilia cordata MILL.	deciduous	-56.0	-9.2	46.9	-52.6	-84.3	-75.1	31.7
Angiosperm	Malvales	Malvaceae	Tilia cordata MILL.	deciduous	-55.1	-7.4	47.7	-51.4	-84.6	-77.2	33.2
Angiosperm	Rosales	Moraceae	Broussonetia papyrifera (L.) VENT.	deciduous	-50.9	-10.2	40.7	-43.7	-151.2	-141.0	107.5
Angiosperm	Rosales	Moraceae	Broussonetia papyrifera (L.) VENT.	deciduous	-56.8	-16.0	40.8	-40.1	-90.3	-74.3	50.2
Angiosperm	Rosales	Cannabaceae	Celtis occidentalis L.	deciduous	-47.9	-3.9	44.0	-45.9	-110.9	-107.0	65.0
Angiosperm	Rosales	Cannabaceae	Celtis occidentalis L.	deciduous	-48.5	-1.9	46.6	-38.5	-101.9	-100.0	63.4
Angiosperm	Rosales	Moraceae	Maclura pomifera (RAF.) C.K.SCHNEID.	deciduous	-45.2	1.4	46.6	-23.3	-114.1	-115.5	90.8
Angiosperm	Rosales	Moraceae	Maclura pomifera (RAF.) C.K.SCHNEID.	deciduous	-58.1	-8.3	49.8	-10.1	-122.4	-114.1	112.3
Angiosperm	Rosales	Moraceae	Maclura pomifera (RAF.) C.K.SCHNEID.	deciduous	-52.3	-2.2	50.1	-51.7	-138.6	-136.4	86.9
Angiosperm	Rosales	Moraceae	Morus alba L.	deciduous	-53.0	-10.6	42.4	-49.2	-78.5	-67.9	29.3
Angiosperm	Rosales	Moraceae	Morus alba L.	deciduous	-56.5	-12.1	44.4	-48.1	-73.5	-61.4	25.4
Angiosperm	Rosales	Moraceae	Morus alba L.	deciduous	-59.4	-3.3	56.2	-40.4	-64.4	-61.1	24.0
Angiosperm	Rosales	Rosaceae	Prunus avium L.	deciduous	-50.6	-10.7	39.9	-42.7	-94.8	-84.1	52.1
Angiosperm	Rosales	Rosaceae	Prunus avium L.	deciduous	-56.5	-12.3	44.2	-50.5	-88.1	-75.8	37.6
Angiosperm	Rosales	Rosaceae	Prunus avium L.	deciduous	-51.3	-0.2	51.1	-59.0	-92.2	-92.0	33.2
Angiosperm	Sapindales	Sapindaceae	Acer mono MAXIM.	deciduous	-49.4	4.3	53.7	-49.8	-114.7	-119.0	64.9
Angiosperm	Sapindales	Sapindaceae	Acer platanoides L.	deciduous	-58.6	-10.0	48.6	-35.3	-134.0	-124.0	98.7
Angiosperm	Sapindales	Sapindaceae	Acer platanoides L.	deciduous	-56.1	6.6	62.7	-48.0	-127.7	-134.3	79.7
Angiosperm	Sapindales	Sapindaceae	Acer platanoides L.	deciduous	-53.3	11.0	64.3	-29.9	-139.7	-150.7	109.8
Angiosperm	Sapindales	Sapindaceae	Acer rubrum L.	deciduous	-61.0	-11.0	50.1	-30.7	-135.2	-124.2	104.5
Angiosperm	Sapindales	Sapindaceae	Aesculus x carnea HAYNE	deciduous	-56.8	-11.9	44.9	-21.0	-94.1	-82.2	73.1
Angiosperm	Sapindales	Sapindaceae	Aesculus x carnea HAYNE	deciduous	-53.1	-7.7	45.4	-25.3	-116.2	-108.5	90.9
Angiosperm	Sapindales	Sapindaceae	Aesculus x carnea HAYNE	deciduous	-54.7	-7.9	46.8	-25.1	-120.0	-112.1	94.9
Angiosperm	Sapindales	Sapindaceae	Koelreuteria paniculata LAXM.	deciduous	-51.2	-4.7	46.5	-61.4	-89.6	-84.9	28.2
Angiosperm	Sapindales	Rutaceae	Ptelea trifoliata L.	deciduous	-52.7	-8.9	43.8	-58.2	-116.7	-107.8	58.5
Angiosperm	Sapindales	Rutaceae	Ptelea trifoliata L.	deciduous	-54.7	-5.0	49.7	-48.3	-98.2	-93.2	49.9
Angiosperm	Sapindales	Rutaceae	Ptelea trifoliata L.	deciduous	-58.9	-8.4	50.6	-46.3	-120.0	-111.6	73.7
Angiosperm	Saxifragales	Cercidiphyllaceae	Cercidiphyllum japonicum SIEBOLD & ZUCC. EX J.J.HOFFM. & J.H.SCHULT.BIS	deciduous	-47.3	4.8	52.1	-23.0	-86.6	-91.4	63.6
Gymnosperm	Ginkgoales	Ginkgoaceae	Ginkgo biloba L.	deciduous	-47.5	-2.3	45.2	-59.8	-122.0	-119.7	62.2
Gymnosperm	Ginkgoales	Ginkgoaceae	Ginkgo biloba L.	deciduous	-54.2	2.7	56.8	-44.4	-70.4	-73.1	26.0
Gymnosperm	Pinales	Pinaceae	Abies koreana E.H.WILSON	evergreen	-50.9	4.1	55.0	-51.7	-149.5	-153.6	97.8
Gymnosperm	Pinales	Cupressaceae	Callitropsis nootkatensis (D.DON) FARJON & D.K.HARDER	evergreen	-46.9	-1.7	45.2	-69.0	-148.5	-146.8	79.5
Gymnosperm	Pinales	Cupressaceae	Callitropsis nootkatensis (D.DON) FARJON & D.K.HARDER	evergreen	-42.0	5.8	47.8	-74.3	-122.0	-127.8	47.7
Gymnosperm	Pinales	Cupressaceae	Callitropsis nootkatensis (D.DON) FARJON & D.K.HARDER	evergreen	-55.9	1.2	57.1	-60.8	-111.1	-112.3	50.3
Gymnosperm	Pinales	Cupressaceae	Calocedrus decurrens (TORR.) FLORIN	evergreen	-46.4	-2.4	44.0	-47.9	-111.1	-108.7	63.2
Gymnosperm	Pinales	Pinaceae	Cedrus atlantica (ENDL.) G.MANETTI EX CARRIÈRE	evergreen	-50.6	1.3	51.9	-45.7	-136.3	-137.6	90.6
Gymnosperm	Pinales	Cupressaceae	Chamaecyparis lawsoniana (A. MURR.) PARL.	evergreen	-37.3	1.7	39.0	-74.5	-121.9	-123.6	47.4
Gymnosperm	Pinales	Cupressaceae	Chamaecyparis lawsoniana (A. MURR.) PARL.	evergreen	-46.8	5.4	52.2	-53.5	-130.2	-135.6	76.7
Gymnosperm	Pinales	Cupressaceae	Chamaecyparis lawsoniana (A. MURR.) PARL.	evergreen	-46.5	10.1	56.6	-77.5	-151.5	-161.6	74.0
Gymnosperm	Pinales	Cupressaceae	Chamaecyparis obtusa (SIEBOLD & ZUCC.) ENDL.	evergreen	-47.4	5.0	52.4	-40.3	-108.9	-113.9	68.6
Gymnosperm	Pinales	Cupressaceae	Cryptomeria japonica (THUNB. EX L.F.) D.DON	evergreen	-45.9	13.9	59.7	-58.5	-93.7	-107.6	35.2
Gymnosperm	Pinales	Cupressaceae	Cryptomeria japonica (THUNB. EX L.F.) D.DON	evergreen	-41.2	28.5	69.7	-55.4	-112.9	-141.4	57.5
Gymnosperm	Pinales	Cupressaceae	Cunninghamia lanceolata (LAMB.) HOOK.	evergreen	-47.6	-7.8	39.8	-34.0	-83.0	-75.2	49.0

Gymnosperm	Pinales	Pinaceae	Larix kaempferi (LAMB.) CARRIÈRE	deciduous	-47.8	-6.2	41.5	-69.0	-132.9	-126.7	63.9
Gymnosperm	Pinales	Pinaceae	Larix kaempferi (LAMB.) CARRIÈRE	deciduous	-55.0	-1.3	53.7	-55.2	-143.7	-142.4	88.5
Gymnosperm	Pinales	Cupressaceae	Metasequoia glyptostroboides HU & CHENG	deciduous	-53.7	0.8	54.5	-69.9	-136.8	-137.6	66.9
Gymnosperm	Pinales	Pinaceae	Picea likiangensis (FRANCH.) E. PRITZ	evergreen	-44.2	7.5	51.7	-42.4	-120.3	-127.8	77.9
Gymnosperm	Pinales	Pinaceae	Picea likiangensis (FRANCH.) E. PRITZ	evergreen	-47.1	13.9	60.9	-43.3	-115.6	-129.5	72.3
Gymnosperm	Pinales	Pinaceae	Picea abies (L.) H.KARST.	evergreen	-33.4	7.0	40.4	-58.5	-136.8	-143.8	78.3
Gymnosperm	Pinales	Pinaceae	Picea abies (L.) H.KARST.	evergreen	-41.4	2.6	44.0	-49.8	-129.5	-132.1	79.7
Gymnosperm	Pinales	Pinaceae	Picea abies (L.) H.KARST.	evergreen	-42.5	4.6	47.1	-44.3	-120.8	-125.4	76.5
Gymnosperm	Pinales	Pinaceae	Pinus cembra L.	evergreen	-47.8	-4.2	43.6	-46.5	-131.7	-127.5	85.2
Gymnosperm	Pinales	Pinaceae	Pinus nigra J.F.ARNOLD	evergreen	-55.4	-22.3	33.0	6.9	-104.3	-82.0	111.2
Gymnosperm	Pinales	Pinaceae	Pinus nigra J.F.ARNOLD	evergreen	-59.5	-17.3	42.2	-25.3	-106.2	-88.9	80.9
Gymnosperm	Pinales	Pinaceae	Pinus nigra J.F.ARNOLD	evergreen	-63.5	-12.1	51.4	-40.2	-108.4	-96.3	68.2
Gymnosperm	Pinales	Pinaceae	Pinus strobus L.	evergreen	-53.7	-11.7	42.0	-42.6	-136.2	-124.5	93.6
Gymnosperm	Pinales	Pinaceae	Pseudotsuga menziesii (MIRBEL) FRANCO	evergreen	-57.3	-5.1	52.1	-55.2	-151.9	-146.8	96.7
Gymnosperm	Pinales	Cupressaceae	Sequoia sempervirens (D.DON) ENDL.	evergreen	-44.7	3.5	48.3	-65.4	-109.9	-113.4	44.5
Gymnosperm	Pinales	Cupressaceae	Sequoia sempervirens (D.DON) ENDL.	evergreen	-49.4	2.7	52.0	-75.0	-158.7	-161.4	83.7
Gymnosperm	Pinales	Cupressaceae	Sequoiadendron giganteum J.BUCHHOLZ	evergreen	-44.0	15.4	59.4	-62.8	-138.8	-154.2	76.0
Gymnosperm	Pinales	Cupressaceae	Taxodium distichum (L.) RICH.	deciduous	-53.1	-3.1	50.0	-51.9	-160.3	-157.2	108.4
Gymnosperm	Pinales	Cupressaceae	Taxodium distichum (L.) RICH.	deciduous	-54.4	-0.4	54.0	-45.4	-136.3	-135.9	90.9
Gymnosperm	Pinales	Cupressaceae	Taxodium distichum (L.) RICH.	deciduous	-57.1	-0.8	56.3	-20.5	-109.9	-109.1	89.4
Gymnosperm	Pinales	Taxaceae	Taxus baccata L.	evergreen	-37.7	6.1	43.8	-74.3	-142.9	-149.0	68.6
Gymnosperm	Pinales	Taxaceae	Taxus baccata L.	evergreen	-35.7	10.2	46.0	-72.7	-134.5	-144.7	61.8
Gymnosperm	Pinales	Taxaceae	Taxus baccata L.	evergreen	-40.8	17.8	58.6	-65.4	-151.8	-169.6	86.4
Gymnosperm	Pinales	Cupressaceae	Thuja occidentalis L.	evergreen	-41.4	5.6	47.0	-63.7	-126.7	-132.3	63.0
Gymnosperm	Pinales	Cupressaceae	Thuja occidentalis L.	evergreen	-50.3	11.6	61.9	-70.6	-126.2	-137.8	55.6
Gymnosperm	Pinales	Pinaceae	Thuja occidentalis L.	evergreen	-45.8	-2.7	43.1	-53.3	-160.9	-158.2	107.6

Table S2: Temperature data of the two days of sampling

29.08.2019	Temperature [C]	RH [%]
10:00	26.2	59.2
11:00	27.4	53.7
12:00	27.6	55.4
13:00	28.7	51.3
14:00	24.9	60.4
15:00	25.4	60.7
16:00	25.7	60.5
30.08.2019		
10:00	24.2	70.5
11:00	25.3	66
12:00	26.7	59.7
13:00	27.2	55

Table S3: Average $\delta^2\text{H}$ and $\delta^2\text{H}_{\text{ne}}$ values per species including standard deviation (SD), and the 2H fractionation factors ϵ_{HA} , ϵ_{HE} , as well as the leaf water enrichment LWE. All values are in ‰

	n	$\delta^2\text{H}_{\text{ne}}$ leaf sugar [‰]		ϵ_{HA} [‰]		$\delta^2\text{H}_{\text{ne}}$ xylem cellulose [‰]		ϵ_{HE} [‰]		$\delta^2\text{H}$ xylem water [‰]		$\delta^2\text{H}$ leaf water [‰]		Leaf water enrichment [‰]	
		mean	SD	mean	SD	mean	SD	mean	SD	mean	SD	mean	SD	mean	SD
Angiosperms	111	-99.9	28.1	-97.3	30.5	-41.2	15.2	58.7	28.3	-50.8	5.0	-2.6	6.7	48.2	6.1
Gymnosperms	41	-127.0	20.5	-129.1	23.4	-53.7	16.9	73.2	19.6	-47.9	6.7	2.1	9.4	50.0	7.5
Order															
Aquifoliales	3	-15.1	31.7	-7.1	34.7	-24.3	11.2	-9.2	38.6	-47.7	3.7	-8.0	3.3	39.7	5.6
Buxales	3	-95.3	4.6	-100.6	2.3	-43.9	4.3	51.4	8.7	-44.0	2.1	5.3	4.0	49.2	5.0
Fabales	5	-134.1	30.4	-137.4	34.9	-45.2	14.9	88.9	29.3	-54.8	4.4	3.3	10.2	58.1	6.9
Fagales	47	-100.2	18.3	-99.0	18.5	-46.8	14.0	53.3	19.9	-49.4	5.5	-1.2	5.7	48.2	5.0
Ginkgoales	2	-96.2	36.5	-96.4	33.0	-52.1	10.9	44.1	25.6	-50.9	4.7	0.2	3.5	51.0	8.2
Lamiales	9	-72.7	25.3	-65.5	28.6	-16.2	11.4	56.6	27.4	-50.9	3.7	-7.3	5.3	43.7	5.9
Magnoliales	13	-115.6	25.2	-114.3	27.0	-40.0	10.3	75.5	27.2	-49.9	2.6	-1.2	6.5	48.7	5.8
Malvales	5	-82.6	4.0	-77.6	6.7	-46.8	5.8	35.8	6.6	-53.8	3.6	-4.9	5.9	48.9	4.6
Pinales	39	-128.5	18.8	-130.8	22.1	-53.8	17.2	74.7	18.4	-47.7	6.8	2.2	9.6	50.0	7.6
Rosales	13	-101.6	25.3	-94.7	27.0	-41.8	12.7	59.8	31.0	-52.8	4.4	-6.9	5.5	45.9	4.8
Sapindales	12	-117.2	16.2	-112.7	19.9	-39.9	13.7	77.2	24.2	-55.0	3.4	-4.5	7.5	50.6	6.7
Saxifragales	1	-86.6	NA	-91.4	NA	-23.0	NA	63.6	NA	-47.3	NA	4.8	NA	52.1	NA
Family															
Aquifoliaceae	3	-15.1	31.7	-7.1	34.7	-24.3	11.2	-9.2	38.6	-47.7	3.7	-8.0	3.3	39.7	5.6
Betulaceae	18	-105.9	20.6	-106.4	19.6	-57.5	12.8	48.4	21.1	-47.1	5.4	0.5	6.3	47.7	4.6
Buxaceae	3	-95.3	4.6	-100.6	2.3	-43.9	4.3	51.4	8.7	-44.0	2.1	5.3	4.0	49.2	5.0
Cannabaceae	2	-106.4	6.4	-103.5	4.9	-42.2	5.2	64.2	1.1	-48.2	0.4	-2.9	1.4	45.3	1.9
Cercidiphyllaceae	1	-86.6	NA	-91.4	NA	-23.0	NA	63.6	NA	-47.3	NA	4.8	NA	52.1	NA
Fabaceae	5	-134.1	30.4	-137.4	34.9	-45.2	14.9	88.9	29.3	-54.8	4.4	3.3	10.2	58.1	6.9
Fagaceae	20	-96.8	18.0	-94.1	18.2	-37.8	10.8	58.9	21.1	-51.0	5.7	-2.7	4.6	48.3	4.5
Juglandaceae	9	-96.3	11.9	-95.1	13.1	-45.4	7.1	50.9	11.5	-50.6	3.8	-1.2	6.1	49.3	6.8
Magnoliaceae	13	-115.6	25.2	-114.3	27.0	-40.0	10.3	75.5	27.2	-49.9	2.6	-1.2	6.5	48.7	5.8
Malvaceae	5	-82.6	4.0	-77.6	6.7	-46.8	5.8	35.8	6.6	-53.8	3.6	-4.9	5.9	48.9	4.6
Moraceae	8	-104.1	32.1	-96.5	33.9	-38.3	14.4	65.8	37.7	-54.0	4.7	-7.6	5.8	46.4	5.4
Oleaceae	9	-72.7	25.3	-65.5	28.6	-16.2	11.4	56.6	27.4	-50.9	3.7	-7.3	5.3	43.7	5.9
Rosaceae	3	-91.7	3.4	-84.0	8.1	-50.7	8.2	41.0	9.9	-52.8	3.2	-7.7	6.6	45.1	5.7
Rutaceae	3	-111.6	11.8	-104.2	9.7	-50.9	6.4	60.7	12.1	-55.4	3.2	-7.4	2.1	48.0	3.7
Sapindaceae	9	-119.0	17.7	-115.5	22.0	-36.3	13.7	82.7	25.2	-54.9	3.7	-3.5	8.5	51.4	7.4
Cupressaceae	20	-124.9	20.7	-129.7	22.0	-58.5	15.2	66.4	18.6	-47.6	5.3	4.8	8.1	52.3	7.6
Ginkgoaceae	2	-96.2	36.5	-96.4	33.0	-52.1	10.9	44.1	25.6	-50.9	4.7	0.2	3.5	51.0	8.2
Pinaceae	16	-130.3	16.8	-127.7	21.8	-44.8	16.8	85.6	13.4	-49.7	7.6	-2.6	9.7	47.1	7.1
Taxaceae	3	-143.1	8.7	-154.4	13.3	-70.8	4.7	72.3	12.7	-38.1	2.6	11.4	5.9	49.5	8.0
Genus															
Abies	1	-149.5	NA	-153.6	NA	-51.7	NA	97.8	NA	-50.9	NA	4.1	NA	55.0	NA
Acer	5	-130.3	9.7	-130.5	12.6	-38.7	9.5	91.5	18.7	-55.7	4.6	0.2	10.0	55.9	7.2
Aesculus	3	-110.1	14.0	-100.9	16.3	-23.8	2.4	86.3	11.6	-54.9	1.9	-9.2	2.4	45.7	1.0
Alnus	6	-113.0	22.5	-110.6	21.9	-60.8	11.3	52.2	18.5	-50.8	5.2	-2.3	5.5	48.4	4.6
Betula	6	-101.5	27.2	-102.4	26.9	-62.1	7.4	39.4	30.2	-46.9	6.0	0.9	6.9	47.7	5.0
Broussonetia	2	-120.8	43.1	-107.7	47.2	-41.9	2.5	78.9	40.5	-53.9	4.2	-13.1	4.1	40.8	0.1
Buxus	3	-95.3	4.6	-100.6	2.3	-43.9	4.3	51.4	8.7	-44.0	2.1	5.3	4.0	49.2	5.0
Callitropsis	3	-127.2	19.2	-129.0	17.3	-68.0	6.8	59.2	17.7	-48.3	7.1	1.8	3.8	50.0	6.2
Calocedrus	1	-111.1	NA	-108.7	NA	-47.9	NA	63.2	NA	-46.4	NA	-2.4	NA	44.0	NA
Carpinus	3	-102.8	15.9	-108.0	9.6	-40.6	20.0	62.2	7.0	-42.9	3.2	5.2	9.2	48.1	7.2
Carya	3	-92.7	9.1	-84.5	10.2	-47.9	8.6	44.8	0.9	-51.1	2.9	-8.2	1.7	43.0	2.7
Cedrus	1	-136.3	NA	-137.6	NA	-45.7	NA	90.6	NA	-50.6	NA	1.3	NA	51.9	NA
Celtis	2	-106.4	6.4	-103.5	4.9	-42.2	5.2	64.2	1.1	-48.2	0.4	-2.9	1.4	45.3	1.9
Cercidiphyllum	1	-86.6	NA	-91.4	NA	-23.0	NA	63.6	NA	-47.3	NA	4.8	NA	52.1	NA
Chamaecyparis	3	-128.1	17.9	-133.7	20.6	-61.5	17.7	66.7	13.3	-44.5	4.8	5.6	3.5	50.0	7.7
Cryptomeria	1	-103.3	13.6	-124.5	23.9	-57.0	2.2	46.4	15.8	-43.5	3.3	21.2	10.4	64.7	7.0
Cunninghamia	2	-83.0	NA	-75.2	NA	-34.0	NA	49.0	NA	-47.6	NA	-7.8	NA	39.8	NA
Fagus	1	-125.2	NA	-116.2	NA	-51.3	NA	73.9	NA	-61.0	NA	-9.0	NA	51.9	NA
Firmiana	1	-85.8	NA	-89.2	NA	-44.6	NA	41.2	NA	-53.7	NA	3.4	NA	57.1	NA
Fraxinus	9	-72.7	25.3	-65.5	28.6	-16.2	11.4	56.6	27.4	-50.9	3.7	-7.3	5.3	43.7	5.9
Ginkgo	2	-96.2	36.5	-96.4	33.0	-52.1	10.9	44.1	25.6	-50.9	4.7	0.2	3.5	51.0	8.2
Gleditsia	3	-125.8	37.2	-132.6	47.7	-46.0	5.4	79.8	36.9	-53.5	5.3	6.8	11.0	60.3	7.7
Ilex	3	-15.1	31.7	-7.1	34.7	-24.3	11.2	-9.2	38.6	-47.7	3.7	-8.0	3.3	39.7	5.6
Juglans	6	-98.2	13.4	-100.4	11.5	-44.2	6.7	54.0	13.3	-50.3	4.5	2.2	4.0	52.5	5.9
Koeleruteria	1	-89.6	NA	-84.9	NA	-61.4	NA	28.2	NA	-51.2	NA	-4.7	NA	46.5	NA
Larix	2	-138.3	7.6	-134.5	11.1	-62.1	9.8	76.2	17.4	-51.4	5.1	-3.8	3.5	47.6	8.6
Liriodendron	5	-115.2	22.2	-112.7	22.2	-40.1	12.8	75.0	12.0	-49.4	1.9	-2.5	0.9	46.9	2.2

Maackia	1	-132.4	NA	-136.6	NA	-23.6	NA	108.8	NA	-55.0	NA	4.2	NA	59.1	NA
Maclura	3	-125.0	12.5	-122.0	12.5	-28.4	21.3	96.7	13.7	-51.8	6.5	-3.0	4.9	48.8	1.9
Magnolia	8	-115.8	28.3	-115.4	31.0	-40.0	9.4	75.8	34.5	-50.2	3.1	-0.4	8.4	49.8	7.2
Metasequoia	1	-136.8	NA	-137.6	NA	-69.9	NA	66.9	NA	-53.7	NA	0.8	NA	54.5	NA
Morus	3	-72.1	7.1	-63.5	3.8	-45.9	4.8	26.2	2.7	-56.3	3.2	-8.7	4.7	47.7	7.4
Ostrya	3	-103.4	4.8	-104.2	7.4	-58.7	3.0	44.7	4.6	-44.7	1.6	0.8	2.7	45.5	2.4
Picea	5	-124.6	8.5	-131.7	7.2	-47.7	6.7	76.9	2.8	-41.7	5.1	7.1	4.3	48.8	7.9
Pinus	5	-117.4	15.3	-103.8	20.9	-29.5	21.9	87.8	16.0	-56.0	5.9	-13.5	6.8	42.5	6.5
Prunus	3	-91.7	3.4	-84.0	8.1	-50.7	8.2	41.0	9.9	-52.8	3.2	-7.7	6.6	45.1	5.7
Pseudotsuga	1	-151.9	NA	-146.8	NA	-55.2	NA	96.7	NA	-57.3	NA	-5.1	NA	52.1	NA
Ptelea	3	-111.6	11.8	-104.2	9.7	-50.9	6.4	60.7	12.1	-55.4	3.2	-7.4	2.1	48.0	3.7
Quercus	19	-95.3	17.2	-92.9	18.0	-37.1	10.6	58.1	21.3	-50.4	5.4	-2.4	4.5	48.1	4.6
Sequoia	2	-134.3	34.5	-137.4	33.9	-70.2	6.8	64.1	27.7	-47.0	3.3	3.1	0.6	50.2	2.7
Sequoiadendron	1	-138.8	NA	-154.2	NA	-62.8	NA	76.0	NA	-44.0	NA	15.4	NA	59.4	NA
Styphnolobium	1	-160.8	NA	-152.6	NA	-64.3	NA	96.5	NA	-58.7	NA	-8.2	NA	50.5	NA
Taxodium	3	-135.5	25.2	-134.1	24.1	-39.3	16.6	96.2	10.6	-54.9	2.0	-1.4	1.5	53.4	3.2
Taxus	3	-143.1	8.7	-154.4	13.3	-70.8	4.7	72.3	12.7	-38.1	2.6	11.4	5.9	49.5	8.0
Thuja	2	-126.5	0.4	-135.1	3.9	-67.2	4.9	59.3	5.2	-45.8	6.3	8.6	4.3	54.5	10.5
Tilia	4	-81.8	4.1	-74.7	2.2	-47.3	6.6	34.5	6.8	-53.9	4.2	-7.0	4.2	46.9	0.6
Tsuga	1	-160.9	NA	-158.2	NA	-53.3	NA	107.6	NA	-45.8	NA	-2.7	NA	43.1	NA
Species															
Abies koreana	1	-149.5	NA	-153.6	NA	-51.7	NA	97.8	NA	-50.9	NA	4.1	NA	55.0	NA
Acer mono	1	-114.7	NA	-119.0	NA	-49.8	NA	64.9	NA	-49.4	NA	4.3	NA	53.7	NA
Acer platanoides	3	-133.8	6.0	-136.3	13.5	-37.7	9.3	96.1	15.2	-56.0	2.7	2.5	11.1	58.5	8.7
Acer rubrum	1	-135.2	NA	-124.2	NA	-30.7	NA	104.5	NA	-61.0	NA	-11.0	NA	50.1	NA
Aesculus x crenata	3	-110.1	14.0	-100.9	16.3	-23.8	2.4	86.3	11.6	-54.9	1.9	-9.2	2.4	45.7	1.0
Alnus cordata	3	-111.4	34.4	-108.7	31.6	-53.7	8.6	57.7	27.6	-53.8	4.4	-2.6	5.8	51.1	4.8
Alnus incana	3	-114.5	8.5	-112.5	13.6	-67.9	9.8	46.7	1.4	-47.8	4.5	-2.0	6.5	45.7	2.7
Betula nigra	1	-88.2	NA	-79.5	NA	-66.3	NA	21.9	NA	-57.0	NA	-8.7	NA	48.4	NA
Betula pendula	3	-99.2	25.7	-99.4	23.3	-64.5	7.5	34.7	21.8	-45.7	4.2	0.2	4.1	45.8	6.8
Betula utilis	2	-111.6	44.5	-118.4	38.3	-56.4	7.7	55.3	52.3	-43.6	3.8	6.8	6.3	50.3	2.4
Broussonetia papyrifera	2	-120.8	43.1	-107.7	47.2	-41.9	2.5	78.9	40.5	-53.9	4.2	-13.1	4.1	40.8	0.1
Buxus sempervirens	3	-95.3	4.6	-100.6	2.3	-43.9	4.3	51.4	8.7	-44.0	2.1	5.3	4.0	49.2	5.0
Callitropsis nootkatensis	3	-127.2	19.2	-129.0	17.3	-68.0	6.8	59.2	17.7	-48.3	7.1	1.8	3.8	50.0	6.2
Calocedrus decurrens	1	-111.1	NA	-108.7	NA	-47.9	NA	63.2	NA	-46.4	NA	-2.4	NA	44.0	NA
Carpinus betulus	3	-102.8	15.9	-108.0	9.6	-40.6	20.0	62.2	7.0	-42.9	3.2	5.2	9.2	48.1	7.2
Carya cordiformis	3	-92.7	9.1	-84.5	10.2	-47.9	8.6	44.8	0.9	-51.1	2.9	-8.2	1.7	43.0	2.7
Cedrus atlantica	1	-136.3	NA	-137.6	NA	-45.7	NA	90.6	NA	-50.6	NA	1.3	NA	51.9	NA
Celtis occidentalis	2	-106.4	6.4	-103.5	4.9	-42.2	5.2	64.2	1.1	-48.2	0.4	-2.9	1.4	45.3	1.9
Cercidiphyllum japonicum	1	-86.6	NA	-91.4	NA	-23.0	NA	63.6	NA	-47.3	NA	4.8	NA	52.1	NA
Chamaecyparis lawsoniana	3	-134.5	15.3	-140.3	19.5	-68.5	13.1	66.0	16.2	-43.5	5.4	5.7	4.2	49.3	9.2
Chamaecyparis obtusa	1	-108.9	NA	-113.9	NA	-40.3	NA	68.6	NA	-47.4	NA	5.0	NA	52.4	NA
Cryptomeria japonica	2	-103.3	13.6	-124.5	23.9	-57.0	2.2	46.4	15.8	-43.5	3.3	21.2	10.4	64.7	7.0
Cunninghamia lanceolata	1	-83.0	NA	-75.2	NA	-34.0	NA	49.0	NA	-47.6	NA	-7.8	NA	39.8	NA
Fagus sylvatica	1	-125.2	NA	-116.2	NA	-51.3	NA	73.9	NA	-61.0	NA	-9.0	NA	51.9	NA
Firmiana simplex	1	-85.8	NA	-89.2	NA	-44.6	NA	41.2	NA	-53.7	NA	3.4	NA	57.1	NA
Fraxinus angustifolia	1	-71.1	NA	-66.7	NA	-30.3	NA	40.8	NA	-49.4	NA	-4.4	NA	45.0	NA
Fraxinus excelsior	3	-57.0	18.9	-50.4	26.9	-23.3	11.1	33.7	19.0	-48.6	2.7	-6.6	8.4	42.0	10.9
Fraxinus holotricha	2	-99.1	33.9	-90.9	39.5	-14.7	2.2	84.4	31.7	-55.2	2.7	-8.1	5.6	47.1	2.8
Fraxinus ornus	3	-71.4	23.6	-63.1	27.8	-5.3	6.5	66.1	17.8	-50.9	4.0	-8.3	4.2	42.6	0.4
Ginkgo biloba	2	-96.2	36.5	-96.4	33.0	-52.1	10.9	44.1	25.6	-50.9	4.7	0.2	3.5	51.0	8.2
Gleditsia triacanthos	3	-125.8	37.2	-132.6	47.7	-46.0	5.4	79.8	36.9	-53.5	5.3	6.8	11.0	60.3	7.7
Ilex aquifolium	3	-15.1	31.7	-7.1	34.7	-24.3	11.2	-9.2	38.6	-47.7	3.7	-8.0	3.3	39.7	5.6
Juglans nigra	3	-92.0	11.9	-95.3	12.0	-45.1	9.4	46.9	13.1	-53.7	3.7	3.3	1.8	57.0	2.1
Juglans regia	3	-104.3	13.9	-105.4	10.4	-43.3	4.7	61.0	11.1	-46.9	0.9	1.1	5.7	48.0	4.8
Koelreuteria paniculata	1	-89.6	NA	-84.9	NA	-61.4	NA	28.2	NA	-51.2	NA	-4.7	NA	46.5	NA
Larix kaempferi	2	-138.3	7.6	-134.5	11.1	-62.1	9.8	76.2	17.4	-51.4	5.1	-3.8	3.5	47.6	8.6
Liriodendron chinense	2	-104.7	37.3	-102.6	37.0	-31.7	20.3	73.1	17.0	-48.4	2.9	-2.1	0.3	46.3	3.3
Liriodendron tulipifera	3	-122.2	10.5	-119.4	11.5	-45.8	1.4	76.4	11.6	-50.1	1.0	-2.8	1.1	47.4	2.0
Maackia amurensis	1	-132.4	NA	-136.6	NA	-23.6	NA	108.8	NA	-55.0	NA	4.2	NA	59.1	NA
Maclura pomifera	3	-125.0	12.5	-122.0	12.5	-28.4	21.3	96.7	13.7	-51.8	6.5	-3.0	4.9	48.8	1.9
Magnolia grandiflora	3	-127.3	16.7	-135.9	22.2	-37.0	5.3	90.4	21.6	-49.1	2.9	8.6	5.8	57.7	3.0
Magnolia kobus	3	-112.5	36.8	-106.0	33.6	-43.1	13.0	69.4	41.9	-52.6	2.0	-6.5	3.4	46.1	4.3
Magnolia tripetala	2	-103.4	40.2	-98.6	37.7	-39.8	13.0	63.6	53.2	-48.4	3.7	-4.7	2.5	43.6	1.2
Metasequoia glyptostroboides	1	-136.8	NA	-137.6	NA	-69.9	NA	66.9	NA	-53.7	NA	0.8	NA	54.5	NA
Morus alba	3	-72.1	7.1	-63.5	3.8	-45.9	4.8	26.2	2.7	-56.3	3.2	-8.7	4.7	47.7	7.4
Ostrya carpinifolia	3	-103.4	4.8	-104.2	7.4	-58.7	3.0	44.7	4.6	-44.7	1.6	0.8	2.7	45.5	2.4
Picea likiangensis	2	-118.0	3.3	-128.6	1.2	-42.9	0.6	75.1	4.0	-45.6	2.1	10.7	4.5	56.3	6.5
Picea abies	3	-129.0	8.0	-133.8	9.3	-50.9	7.2	78.2	1.6	-39.1	5.0	4.7	2.2	43.8	3.3
Pinus cembra	1	-131.7	NA	-127.5	NA	-46.5	NA	85.2	NA	-47.8	NA	-4.2	NA	43.6	NA
Pinus nigra	3	-106.3	2.1	-89.1	7.2	-19.5	24.1	86.8	22.1	-59.5	4.1	-17.2	5.1	42.2	9.2
Pinus strobus	1	-136.2	NA	-124.5	NA	-42.6	NA	93.6	NA	-53.7	NA	-11.7	NA	42.0	NA
Prunus avium	3	-91.7	3.4	-84.0	8.1	-50.7	8.2	41.0	9.9	-52.8	3.2	-7.7	6.6	45.1	5.7
Pseudotsuga menziesii	1	-151.9	NA	-146.8	NA	-55.2	NA	96.7	NA	-57.3	NA	-5.1	NA	52.1	NA
Ptelea trifoliata	3	-111.6	11.8	-104.2	9.7	-50.9	6.4	60.7	12.1	-55.4	3.2	-7.4	2.1	48.0	3.7
Quercus castaneifolia	1	-101.7	NA	-92.0	NA	-56.3	NA	45.4	NA	-48.4	NA	-9.7	NA	38.7	NA
Quercus cerris	3	-83.5	6.0	-78.5	9.7	-42.5	11.1	41.0	11.7	-54.2	5.0	-4.9	5.6	49.3	6.1
Quercus ilex	3	-88.8	1.8	-92.4	1.1	-37.2	9.9	51.6	11.5	-44.2	2.2	3.6	1.1	47.8	1.2
Quercus ilicifolia	1	-95.3	NA	-87.9	NA	-33.6	NA	61.7	NA	-57.7	NA	-7.4	NA	50.3	NA

<i>Quercus macrolepis</i>	1	-85.7	NA	-79.3	NA	-36.0	NA	49.7	NA	-56.9	NA	-6.4	NA	50.6	NA
<i>Quercus marilandica</i>	1	-83.5	NA	-84.3	NA	-31.5	NA	52.0	NA	-53.9	NA	0.8	NA	54.7	NA
<i>Quercus pubescens</i>	3	-113.7	22.9	-111.8	24.1	-35.4	7.4	78.3	26.9	-50.1	2.4	-1.9	3.3	48.2	5.7
<i>Quercus robur</i>	3	-97.5	15.8	-95.5	19.2	-34.0	10.3	63.5	11.4	-50.8	3.7	-2.0	3.6	48.8	1.7
<i>Quercus rubra</i>	1	-125.5	NA	-120.0	NA	-15.8	NA	109.7	NA	-57.1	NA	-5.5	NA	51.6	NA
<i>Quercus suber</i>	2	-84.0	25.9	-83.2	28.1	-42.6	14.4	41.5	11.5	-43.2	0.3	-0.8	2.2	42.4	2.5
<i>Sequoia sempervirens</i>	2	-134.3	34.5	-137.4	33.9	-70.2	6.8	64.1	27.7	-47.0	3.3	3.1	0.6	50.2	2.7
<i>Sequoiadendron giganteum</i>	1	-138.8	NA	-154.2	NA	-62.8	NA	76.0	NA	-44.0	NA	15.4	NA	59.4	NA
<i>Styphnolobium japonicum</i>	1	-160.8	NA	-152.6	NA	-64.3	NA	96.5	NA	-58.7	NA	-8.2	NA	50.5	NA
<i>Taxodium distichum</i>	3	-135.5	25.2	-134.1	24.1	-39.3	16.6	96.2	10.6	-54.9	2.0	-1.4	1.5	53.4	3.2
<i>Taxus baccata</i>	3	-143.1	8.7	-154.4	13.3	-70.8	4.7	72.3	12.7	-38.1	2.6	11.4	5.9	49.5	8.0
<i>Thuja occidentalis</i>	2	-126.5	0.4	-135.1	3.9	-67.2	4.9	59.3	5.2	-45.8	6.3	8.6	4.3	54.5	10.5
<i>Tilia americana</i>	1	-75.8	NA	-74.7	NA	-47.1	NA	28.7	NA	-47.7	NA	-1.1	NA	46.7	NA
<i>Tilia cordata</i>	3	-83.7	1.3	-74.7	2.7	-47.4	8.0	36.4	6.8	-55.9	0.8	-9.0	1.5	46.9	0.7
<i>Tsuga canadensis</i>	1	-160.9	NA	-158.2	NA	-53.3	NA	107.6	NA	-45.795	NA	-2.7	NA	43.1	NA

Table S4: Results of the ANOVA comparing the measured $\delta^2\text{H}$ and $\delta^2\text{H}_{\text{ne}}$ values as well as the ^2H fractionation factors ϵ_{HA} , ϵ_{HE} , as well as the leaf water enrichment LWE of the different phylogenetic groups, from the order to the family level.

	$\delta^2\text{H}_{\text{ne}}$ LS	ϵ_{HA}	$\delta^2\text{H}_{\text{ne}}$ XC	ϵ_{HE}	$\delta^2\text{H}_{\text{XW}}$	$\delta^2\text{H}_{\text{LW}}$	LWE
Angiosperm	A	A	A	A	A	A	A
Gymnosperm	B	B	B	B	B	B	A
Analysed by Order							
Aquifoliales	A	A	ABC	D	AB	AB	B
Lamiales	B	B	A	ABC	AB	B	B
Malvales	BC	BC	BC	CD	AB	AB	AB
Saxifragales	ABCDE	ABCD	ABC	ABCD	AB	AB	AB
Buxales	BCDE	BCD	ABC	ABCD	AB	AB	AB
Fagales	C	C	BC	BC	AB	AB	B
Rosales	BCDE	BC	BC	ABC	AB	B	B
Magnoliales	CDE	CD	BC	AB	AB	AB	AB
Sapindales	CDE	CD	BC	AB	B	AB	AB
Fabales	DE	D	BC	A	AB	AB	A
Ginkgoales	BCDE	BCD	ABC	ABCD	AB	AB	AB
Pinales	E	D	C	A	A	A	AB

Analysed by Family

Aquifoliaceae	A	A	AB	D	ABC	AB	B
Oleaceae	B	B	A	ABC	BC	B	B
Malvaceae	BC	BC	BC	CD	BC	AB	AB
Cercidiphyllacea	ABCDE	ABCDEF	ABC	ABCD	ABC	AB	AB
Rosaceae	BCDE	BCDE	BC	ABCD	BC	AB	AB
Buxaceae	BCDE	BCDEF	ABC	ABCD	ABC	AB	AB
Juglandaceae	CDE	BCD	BC	BC	BC	AB	AB
Fagaceae	BC	BC	B	BC	BC	AB	AB
Moraceae	BCDE	BCDE	B	ABC	BC	B	AB
Betulaceae	CDE	CDEF	C	C	AB	AB	AB
Cannabaceae	BCDE	BCDEF	ABC	ABC	ABC	AB	AB
Rutaceae	BCDE	BCDEF	BC	ABC	BC	AB	AB
Magnoliaceae	CDE	CDEF	B	ABC	BC	AB	AB
Sapindaceae	CDE	CDEF	AB	AB	C	AB	AB
Fabaceae	DE	DEF	BC	AB	BC	AB	A
Cupressaceae	DE	EF	C	ABC	AB	A	AB
Ginkgoaceae	BCDE	BCDEF	BC	BABCD	ABC	AB	AB
Pinaceae	E	DEF	BC	A	BC	AB	AB
Taxaceae	DE	F	C	ABC	A	A	AB

Analysed by Family: Angiosperms only

Aquifoliaceae	A	A	AB	D	ABC	A	B
Oleaceae	B	B	A	ABC	ABC	A	B
Malvaceae	BC	BC	BC	CD	ABC	A	AB
Cercidiphyllacea	ABCD	ABCD	ABC	ABCD	ABC	A	AB
Rosaceae	BCD	BCD	BC	ABCD	ABC	A	AB
Buxaceae	BCD	BCD	BC	ABCD	AB	A	AB
Juglandaceae	BCD	BCD	BC	ABC	ABC	A	AB
Fagaceae	BC	BC	B	ABC	ABC	A	B
Moraceae	BCD	BCD	B	ABC	BC	A	B
Betulaceae	CD	CD	C	BC	A	A	B
Cannabaceae	BCD	BCD	ABC	ABCD	ABC	A	AB
Rutaceae	BCD	BCD	BC	ABC	ABC	A	AB
Magnoliaceae	CD	CD	B	ABC	ABC	A	AB
Sapindaceae	CD	CD	B	A	C	A	AB
Fabaceae	D	D	BC	AB	ABC	A	A

Analysed by Family: Gymnosperms only

Cupressaceae	A	AB	AB	B	AB	A	A
Ginkgoaceae	A	A	AB	B	AB	A	A
Pinaceae	A	AB	A	A	B	A	A
Taxaceae	A	B	B	AB	A	A	A

Chapter 4

Hydrogen isotope fractionation in plants with C₃, C₄, and CAM CO₂ fixation

Philipp Schuler^{1,2}, Oliver Rehm¹, Valentina Vitali¹, Matthias Saurer¹, Manuela Oettli¹, Lucas Cernusak³, Arthur Gessler^{1,2}, Nina Buchmann², Marco M. Lehmann¹

¹Forest dynamics, Swiss Federal Institute for Forest, Snow and Landscape Research WSL, Birmensdorf, Switzerland

²Department of Environmental Systems Science, ETH Zurich, Zurich, Switzerland

³College of Science and Engineering, James Cook University, Cairns, Australia

This chapter will be submitted in the peer-reviewed journal “New Phytologist”.

Abstract

Measurements of stable isotope ratios in organic compounds are widely used tools for plant ecophysiological studies. However, the complexity of the processes involved in shaping hydrogen isotope values ($\delta^2\text{H}$) in plant carbohydrates has limited its broader application. To investigate the underlying biochemical processes responsible for ^2H fractionation among water, sugars and cellulose in leaves, we studied the three main CO_2 fixation pathways (C_3 , C_4 and CAM) and their response to changes in temperature and vapor pressure deficit (VPD). We show significant differences in autotrophic ^2H fractionation (ϵ_{A}) from water to sugar among the three pathways, as well as in their individual response to changes in air temperature and VPD. Our results suggest that the strong ^2H depleting ϵ_{A} in C_3 plants is likely driven by the photosynthetic H^+ production within the thylakoids, a reaction that is spatially separated in C_4 plants and strongly reduced in CAM plants, leading to the absence of ^2H depletion in the latter two types. However, the heterotrophic ^2H -fractionation (ϵ_{H}) from sugar to cellulose was very similar among the three types of CO_2 fixation, and is likely driven by the plant's metabolism, rather than by isotopic exchange with leaf water. Our study offers new insights into the biochemical drivers of the ^2H fractionation in plant carbohydrates.

Introduction

The hydrogen isotopic composition ($\delta^2\text{H}$) of plant carbohydrates (e.g., sugar, cellulose) has been found to be a proxy for hydrological (Yakir, 1992; Roden *et al.*, 2000), biochemical (Zhou *et al.*, 2018) and physiological processes (Augusti *et al.*, 2006; Lehmann *et al.*, 2022; Wieloch *et al.*, 2022b). For an accurate interpretation of the observed $\delta^2\text{H}$ in the various carbohydrates of plants, such as in ecohydrological studies, it is crucial to understand the underlying biochemical processes behind the ^2H fractionation in plant compounds - from the CO_2 fixation to the formation of cellulose.

The current knowledge on ^2H fractionation processes in the carbohydrate metabolism of plants with C_3 CO_2 fixation indicates an initial ^2H depletion in leaf sugars compared to the leaf water during the light-dependent reactions of CO_2 fixation (Estep & Hoering, 1981; Luo *et al.*, 1991; Schuler *et al.*, 2023). Further along the carbohydrate reaction chain, cellulose becomes ^2H enriched compared to leaf sugars (Cormier *et al.*, 2018; Holloway-Phillips *et al.*, 2022; Lehmann *et al.*, 2022). The autotrophic ^2H fractionation (ϵ_{A}) and the heterotrophic ^2H fractionation (ϵ_{H}) are generally defined as the difference in $\delta^2\text{H}$ between leaf water and leaf sugars, and between sugar and cellulose, respectively (Yakir & DeNiro, 1990; Roden *et al.*, 2000). While the exact mechanism behind the autotrophic ^2H fractionation (ϵ_{A}) is yet to be identified, its amplitude is related to the phylogeny of a plant (Schuler *et al.*, 2023), and might explain a large part of the observed variability of the $\delta^2\text{H}$ in leaf cellulose across different species (Arosio *et al.*, 2020; Holloway-Phillips *et al.*, 2022).

Differences in the strength of $\delta^2\text{H}$ of plant carbohydrates can be found between different CO_2 fixation pathways (Ziegler *et al.*, 1976; Luo & Sternberg, 1991; Schmidt *et al.*, 2003). Leaf bulk sugars and cellulose of plants fixing CO_2 with the C_3 CO_2 fixation pathway show much stronger ^2H depletion compared to leaf water than those of plants with C_4 , and even more compared to plants with CAM CO_2 fixation (Ziegler *et al.*, 1976; Sternberg *et al.*, 1984; Luo & Sternberg, 1991; Schmidt *et al.*, 2003; Schuler *et al.*, 2022). The investigation of these differences in ^2H fractionation among CO_2 fixation types and its response to environmental conditions such as relative air temperature and humidity might enable us to identify, and thus understand, the most important biochemical ^2H fractionation processes that cause $\delta^2\text{H}$ variation in plant carbohydrates within and across the different types of CO_2 fixation.

In C_3 plants, water molecules are split the hydrogen splitting complex of photosystem II (PS II) during the light-dependent reactions of CO_2 fixation in the chloroplasts' thylakoid. This reaction produces protons (H^+), which are used to generate energy and reducing equivalents for the Calvin-

Benson-Bassham cycle (CBB) that occurs in the stroma of the same chloroplasts. The water splitting reaction establishes a high H^+ concentration inside the thylakoid, with a simultaneous low H^+ concentration on the other side of the thylakoid membrane inside the chloroplast stroma (Heldt *et al.*, 1973; Falkner *et al.*, 1976; Heldt, 1980). The water splitting reaction discriminates against 2H , leading to a strongly 2H -depleted pool of reducing equivalents such as NADPH (Luo *et al.*, 1991). New findings showing a strong phylogenetic pattern behind the δ^2H of leaf sugars (Schuler *et al.*, 2023), indicating a relatively simple enzymatic process underlying the 2H fractionation.

In C_4 CO_2 fixation, the water splitting reaction in the thylakoids are the same as in C_3 plants, but are spatially separated from the Calvin-Benson-Bassham cycle (CBB) in the mesophyll and the bundle-sheath (BS) cells, respectively. In the C_4 BS cells, the amount of the hydrogen splitting complex of PS II is strongly reduced, leading to a reduction of 80% of PS II activity (Oswald *et al.*, 1990; Höfer *et al.*, 1992; Meierhoff & Westhoff, 1993). The protons for NADH or NADPH synthesis are mostly derived from malate in the chloroplast stroma of BS cells (Drincovich *et al.*, 2001; Rao & Dixon, 2016), which is synthesized in, and imported from, mesophyll cells. Thus, during the transport among the two cell types, the signal of the strong 2H depletion of PS II is likely not or much less carried into the fresh assimilates.

In CAM CO_2 fixation, initial CO_2 fixation into organic acids takes place over night (Winter & Smith, 2022), and the contribution of PSII to CO_2 fixation is strongly reduced (Niewiadomska *et al.*, 2011). Additionally, in plants with CAM CO_2 fixation, NADH is generated from malic acid as the proton source, a reaction which happens in the cytosol (Drincovich *et al.*, 2001; Chen *et al.*, 2019), and thus an isotopic exchange with the cytosol water may occur. However, plants performing CAM CO_2 fixation are often operating along a whole spectrum between C_3 or C_4 and CAM CO_2 fixation (Winter *et al.*, 2008; Winter, 2019), making it challenging to disentangle the contribution of a certain type of CO_2 fixation to a plant's carbon budget.

Moreover, climatic factors such as air temperature and relative humidity are known to influence isotopic fractionation (Augusti *et al.*, 2006; Farquhar *et al.*, 2007; Cernusak *et al.*, 2016). The three types of CO₂ fixation show different physiological responses to changes in temperature (Yamori *et al.*, 2014; Kumar *et al.*, 2017; dos Santos *et al.*, 2022). For instance, plants with C₃ CO₂ fixation have a lower temperature optimum than plants with C₄ CO₂ fixation (Orsenigo *et al.*, 1997), which might be reflected in different temperature responsiveness in their ²H fractionation, as ²H fractionation is reflecting plant performance (Sanchez-Bragado *et al.*, 2019). In addition, the CO₂ availability, which can be influenced by the stomatal response to changes in VPD (Grossiord *et al.*, 2020), can alter hydrogen isotope fractionation in C₃ plants (Wieloch *et al.*, 2022a). Hence, it is likely that these biochemical and physiological differences in C₃, C₄, and CAM CO₂ fixation contribute to the differences in their δ²H signature.

However, as the type of CO₂ fixation is independent of a plant's secondary metabolism, the biochemical pathways responsible for the ²H fractionation from leaf sugar to cellulose should not be directly affected by the type of CO₂ fixation. Current views on the heterotrophic ²H fractionation assume an isotopic exchange of carbon-bound hydrogen with hydrogen atoms from the surrounding water. This process, which is derived from the analogy with the exchange of carbon-bound oxygen during cellulose synthesis, is believed to be responsible for the observed ²H enrichment during cellulose formation (Yakir & DeNiro, 1990; Augusti *et al.*, 2008; Holloway-Phillips *et al.*, 2022). However, this assumption has not been systematically investigated within and between the three types of CO₂ fixation yet.

The main aim of the study was therefore to determine the autotrophic and heterotrophic ²H fractionation factors in various C₃, C₄, CAM plants growing under different climatic conditions (20 and 30°C air temperature, VPD of 1.2, 1.3 and 2.6 kPa), in order to unravel the processes leading to δ²H variations of plant carbohydrates.

Due to their different optimum temperature, we expect strong but opposite responses in the ^2H fractionation of C_3 and C_4 plants to changes in temperature under a constant VPD. In C_3 plants, we expected the strongest ϵ_A , leading to leaf bulk sugar and cellulose being the most ^2H depleted at 20 °C, as it is closer to their optimum temperature. In contrast in C_4 plants, we expected leaf bulk sugar and cellulose being most ^2H depleted at 30 °C, as C_4 plants are adapted to high temperatures. We expect CAM plants to respond marginally to an increase in temperature, with slightly lower $\delta^2\text{H}$ at 30°C than at 20 °C, as they are adapted to higher temperatures but do not show a strong ^2H depletion in general. A higher VPD is increasing the evaporative ^2H enrichment of leaf water, which is expected to increase the $\delta^2\text{H}$ of the leaf sugar and cellulose in C_3 and C_4 plants, while CAM plants should not be affected, as they perform their gas exchange only during the night, when VPD is constant between the treatments.

To conclude, we hypothesized that:

- 1) The autotrophic ^2H fractionation (ϵ_A) is driven by biochemical reactions during a plant's CO_2 fixation, which differs in plants with different biochemical CO_2 fixation pathways.
- 2) The heterotrophic ^2H fractionation (ϵ_H) is independent of a plant's CO_2 fixation type and not impacted by exchange reactions with leaf water isotopes.
- 3) Temperature and VPD are impacting the autotrophic and heterotrophic ^2H fractionation depending on the physiological response of a certain plant species.

Materials and methods

Growing conditions, and sampling of leaf material

Twenty-six plant species with three different CO₂ fixation pathways were grown between May 2020 and March 2021 in two walk-in climate chambers (Bouygues E&S InTec Schweiz AG, Zurich, Switzerland) under three different controlled climates. The climatic conditions included 20°C with a VPD of 1.2 kPa, 30°C with a VPD of 1.3 kPa, and 30°C with a VPD of 2.6 kPa. The climate chambers were set to 14 hours of daylight with the target conditions, with a photosynthetic active irradiance of 110 μmol m⁻² s⁻¹ was maintained using uniform fluorescent tubes (OSRAM L 36W 777 Fluora, Osram Licht AG, Germany), and 10 hours of nighttime with uniform conditions across all treatments (15 °C with a VPD of 0.7 kPa).

The species selected species covered 11 plant species with C₃ (*Abelmoschus esculentus* (L.) Moench, *Anthurium Linden ex André*, *Begonia maculata* C. DC. ex Huber, *Begonia semperflorens* C. L. Willdenow, *Cyperus alternifolius* Rottb., *Euphorbia pulcherrima* Willd. ex Klotzsch, *Hordeum vulgare* L., *Oryza sativa* L., *Quercus pubescens* Willd., *Salvia hispanica* L., *Zantedeschia aethiopica* (L.) Spreng.), 8 species with C₄ (*Amaranthus caudatus* L., *Amaranthus tricolor* L., *Panicum miliaceum* L., *Pennisetum glaucum* L., *Salsola soda* L., *Setaria italica* (L.) P. Beauv., *Sorghum bicolor* (L.) Moench, *Zea mays* L.), and 7 species with CAM CO₂ fixation pathways (*Curio repens* P. V. Heath, *Delosperma cooperi* (Hook. f.) L.Bolus, *Hylocereus* (A.Berger) Britton & Rose, *Mesembryanthemum cordifolium* L. f., *Phalaenopsis* Blume, *Rhipsalis* (J. S. Muell.) Stearn, *Sedum* L.). Triplicates of seeds or plantlets of all but three species (*H. vulgare*, *O. sativa*, and *Phalaenopsis*) were sown in 3 L pots containing potting soil (Kübelpflanzenerde, RICOTER Erdaufbereitung AG, CH-3270 Aarberg, Switzerland). Due to the small plant size, three times 30 seeds both of *H. vulgare* and *O. sativa* were sown in individual 20 L pots containing the same potting soil, and three *Phalaenopsis* were bought in a plant shop and were continuously grown in

the original 0.5 L pots containing orchid potting mix. The plants with C₃ and C₄ CO₂ fixation pathways were regularly watered to avoid any water limitation, while the plants with CAM CO₂ fixation were watered only once per week to induce drought stress and a high percentage of CAM CO₂ fixation in all species. However, as the $\delta^2\text{H}$ of leaf sugar and leaf cellulose of the two facultative CAM plants *D. cooperi* and *M. cordifolium* were more similar to plants with C₃ CO₂ fixation, we conclude that the reduced watering scheme was not enough to introduce drought stress. The $\delta^2\text{H}$ of the irrigation water was -79.9‰, with a maximum standard deviation of 2 ‰ throughout the experimental period.

After 1-3 months of a specific treatment, depending on the specific growth rate, fully developed leaves of the three replicates per species were sampled. In the case of *H. vulgare* and *O. sativa* (both C₃ grasses), three pools of leaves each consisting of four plants were sampled. The sampling was conducted after 7 hours of light to allow the plants to synthesize sufficient amount of fresh assimilates on the day of harvest and to ensure steady-state leaf water enrichment (Cernusak *et al.*, 2016). The leaf samples were transferred to gas-tight 12 ml glass vials (Exetainer glass vials, Labco, Lampeter, Wales, UK, prod. No. 738W) which were kept on ice until the harvest was complete (i.e., within two hours). Subsequently, the samples were then stored at -20 °C until water extraction.

Extraction of leaf water, sugars, and cellulose

Leaf water of all samples (three replicates per species and climatic condition) was cryogenically extracted (Diao *et al.*, 2022) and stored in glass vials at -20 °C until $\delta^2\text{H}$ measurement. Later, the dry leaf material of each sample was separated into two subsamples. The first subsample was milled (MM400, Retsch, Germany), and the bulk leaf sugar fraction (i.e., “leaf sugar”) was extracted following established protocols for carbon, oxygen and hydrogen isotope analysis (Rinne *et al.*, 2012; Lehmann *et al.*, 2020; Schuler *et al.*, 2023). In brief, the water-soluble content (including sugars, amino acids, etc.) was extracted by mixing the ground leaf material with

deionized water at 85 °C for 30 minutes. The extracted leaf sugar was then separated from the other water-soluble content using ion exchange cartridges (OnGuard II A, H and P, Dionex, Thermo Fisher Scientific, Bremen, Germany). The sugar solutions were frozen, freeze-dried, and the total weight of dried sugar per sample measured. Then, deionized water was added to reach a final concentration of 1 mg per 20 μ l, and the samples were stored at -20 °C until further use.

The second subsample was used for the extraction of leaf holocellulose. 100 mg of leaf material was crushed and packed in F57 fiber filter bags (ANKOM Technology, Macedon NY, U.S.A.). The samples were washed two times for two hours with 5% NaOH at 60 °C. After that, the samples were rinsed three times with boiling deionized water and incubated three times in a mixture of 7% NaClO₂ and 96% acetic acid with a pH of 4-5 at 60 °C for eight hours. After that, the samples were again rinsed three times with boiling deionized water, squeezed using a spatula and dried for at least four hours in the drying oven at 60 °C. In a final step, the purified holocellulose was mixed with deionized water, homogenized with an ultrasonic transducer (UP200St, Hielscher, Germany), and freeze-dried overnight.

$\delta^2\text{H}$ analysis of leaf water

The $\delta^2\text{H}$ values of leaf water samples were measured using a high temperature conversion elemental analyser coupled to a Delta^{plus} XP isotope ratio mass spectrometer (TC/EA-IRMS; Finnigan MAT, Bremen, Germany). The calibration was done using a range of certified waters of different isotope $\delta^2\text{H}$ ratios, resulting in a precision of analyses of 2 ‰.

$\delta^2\text{H}$ analysis of sugar and cellulose using a hot water vapor equilibration method

The $\delta^2\text{H}$ of non-exchangeable hydrogen ($\delta^2\text{H}$) analyses of sugar and cellulose were done according to the previously developed hot water vapor equilibration method (Schuler *et al.*, 2022). Two sets of each sugar sample

were prepared by pipetting 20 μl in pre-weighed 5x9 mm silver foil capsules (Prod. No. SA76981106, Säntis, Switzerland). Both sets were frozen at $-20\text{ }^{\circ}\text{C}$, freeze-dried, and packed into a second silver foil capsule. Similarly, two sets of all cellulose samples were prepared by transferring two replicates of 1 mg per sample into 3.3x5 mm silver foil capsules (Säntis, Switzerland, Prod. No. SA76980506). Both sets of samples were stored in a desiccator at low relative humidity (2-5 %) until $\delta^2\text{H}$ measurement.

The two sets of the samples were then equilibrated with hot water vapour at $130\text{ }^{\circ}\text{C}$ for 2 hours, using one of two isotopically distinct waters for each set ($\delta^2\text{H}$ (Water 1) = -160‰ and $\delta^2\text{H}$ (Water 2) = -428‰). The equilibration apparatus consisted of an electrical heating oven (ED23, Binder, Germany) where an equilibration chamber was inserted (Schuler *et al.*, 2022). After the 2 hours, the excess water was pumped back and discarded. After that, the feeding capillary was switched to a dry nitrogen gas delivering capillary (N25.0, PanGas AG, Dagmersellen, Switzerland, ProdNo. 2220912) for another 2 hours at $130\text{ }^{\circ}\text{C}$ to remove remaining water and water vapor. The samples were then immediately transferred into a Zero Blank Autosampler (N.C. Technologies S.R.L., Milano, Italy), which was installed on a sample port of the TC/EA-IRMS system as described for leaf water analysis. The autosampler was evacuated to 0.001 bar and filled with dry helium gas to avoid reexchange of the exchangeable hydrogen of the samples with the hydrogen of ambient water vapor. Pyrolysis was done in a reactor according to Gehre *et al.* (2004), and carried in a flow of dry helium (150 ml min^{-1}) to the IRMS. Offset corrections of the raw $\delta^2\text{H}$ values were done using polyethylene foil standards (PEF, IAEA-CH-7 polyethylene foil, International Atomic Energy Agency, Vienna, Austria; SD < 0.7‰ within one run).

Calculation of the isotope ratio ($\delta^2\text{H}$)

All isotope ratios (δ) were calculated as given in Eq. 1 (Coplen, 2011):

$$\delta = \frac{R_{\text{Sample}} - R_{\text{Standard}}}{R_{\text{Standard}}}$$

Eq. 1

where $R = {}^2\text{H}/{}^1\text{H}$ is the hydrogen isotope ratio of the sample (R_{Sample}) and the Vienna Standard Mean Ocean Water (VSMOW2; R_{Standard}). To express the resulting δ values in permil (‰), results have been multiplied by 1,000.

The percentage of hydrogen exchanged during the equilibrations (x_e , Eq. 2, from Filot *et al.* (2006)) can be calculated as:

$$x_e = \frac{\delta^2\text{H}_{e1} - \delta^2\text{H}_{e2}}{\alpha_{e-w} \cdot (\delta^2\text{H}_{w1} - \delta^2\text{H}_{w2})}$$

Eq. 2

Then, $\delta^2\text{H}_{ne}$ can then be calculated using x_e , the measured $\delta^2\text{H}$ of one of the two equilibrations, and α_{e-w} , which is the fractionation factor of 1.082 for carbohydrates (Filot *et al.*, 2006; Schuler *et al.*, 2022):

$$\delta^2\text{H}_{ne} = \frac{\delta^2\text{H}_{e1} - x_e \cdot \alpha_{e-w} \cdot \delta^2\text{H}_{w1} - 1000 \cdot x_e \cdot (\alpha_{e-w} - 1)}{1 - x_e}$$

Eq. 3

The calibration was done using three internal sucrose standards for the equilibrations of leaf sugars, three internal cellulose standards for the equilibrations of the leaf cellulose, and were normalized to the international scale with PEF standards, each measured as triplicates. Throughout the manuscript, $\delta^2\text{H}$ has been used instead of $\delta^2\text{H}_{ne}$ to maintain a simple terminology.

Eq. 4 was used to calculate the autotrophic fractionation between leaf water and leaf sugar ϵ_A , and Eq. 5 to calculate the heterotrophic fractionation between leaf sugar and leaf cellulose ϵ_H :

$$\varepsilon_A = \delta^2\text{H}_{\text{leaf sugar}} - \delta^2\text{H}_{\text{leaf water}} \quad \text{Eq. 4}$$

$$\varepsilon_H = \delta^2\text{H}_{\text{leaf cellulose}} - \delta^2\text{H}_{\text{leaf sugar}} \quad \text{Eq. 5}$$

ε_A and ε_H were calculated as in Schuler et al. (2023). More detailed information on the background of the calculations of the $\delta^2\text{H}$ can be found in Schuler *et al.* (2022).

Statistical analyses

Statistical analyses were performed using R version 4.1.2 (R.Core.Team, 2023). Equal variance of the sample amounts among the three types of CO₂ fixation was tested with the Bartlett's test. The p-value of the Bartlett's test for the $\delta^2\text{H}$ of leaf water was 0.8, thus the variance in $\delta^2\text{H}$ of the leaf water is not different among the types of CO₂ fixation. However, the p-values of the Bartlett's tests of leaf sugar and leaf cellulose were < 0.001 , thus the variance in $\delta^2\text{H}$ among leaf sugar and leaf cellulose is different for the three types of CO₂ fixation. Thus, for the analysis within and between the three types of CO₂ fixation and their response to changes in temperature and VPD, Kruskal-Wallis tests followed by Pairwise Wilcoxon Rank Sum Tests as the post hoc analysis, with a p value adjustment using the bonferroni method, were performed. Subsequently, results were displayed by applying Compact Letter Displays (CLD). The within and between CO₂ fixation types as well as the species-specific response to temperature and VPD was tested by using one-way ANOVA followed by tukey post hoc analysis, and results were displayed by applying CLD. Regression analyses were used to determine the general drivers behind the ²H fractionation processes with linear models within the package ggplot2. Due to sample loss, sugar and cellulose of *Amaranthus caudatus* (C₄), and *Phalaenopsis* (CAM) could not be analysed for all climatic conditions. Due to the same reason, *Setaria italica* (C₄) could only be included in the general analysis of the CO₂ fixation pathways. As the $\delta^2\text{H}$ of carbohydrates as well as the ϵ_A of the two facultative CAM species (e.g., performing C₃ CO₂ fixation if the drought stress is not severe enough) indicated a strong contribution of C₃ CO₂ fixation, the comparison between as well as the regression analyses have been conducted with and without these two species.

Results

General patterns of ²H fractionation within and between plants with C₃, C₄, and CAM CO₂ fixation

We observed distinct patterns of $\delta^2\text{H}$ in leaf water, leaf sugar, and leaf cellulose, as well as in the autotrophic and heterotrophic ^2H fractionation factors ϵ_A and ϵ_H , within and between the three CO_2 fixation pathways across all tested species and climatic conditions (Figs. 1, 2, S1, S2, S3, Tables 1, 2).

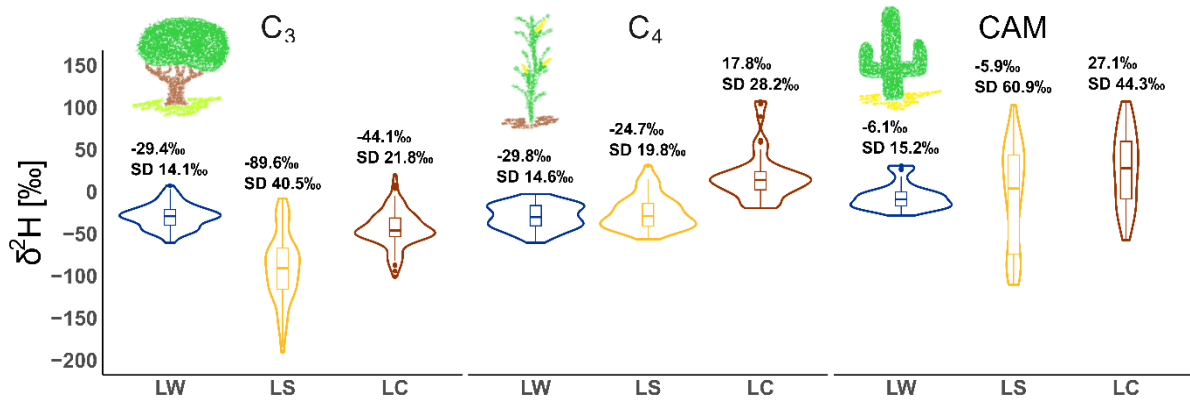


Fig. 1: $\delta^2\text{H}$ of leaf water (LW), leaf sugar (LS), and leaf cellulose (LC) of plants with C_3 , C_4 , and CAM CO_2 fixation, including all measurements of this study. SD = Standard deviation from the mean.

While the $\delta^2\text{H}$ in leaf water across all treatments (Figs. 1, 2, Tables 1, 2) was similar in plants with C_3 and C_4 CO_2 fixation (-29.4‰, SD = 14.1‰, and -29.8‰, SD = 14.6‰, respectively), leaf water of plants with CAM CO_2 fixation was significantly more ^2H enriched (-6.1‰, SD = 15.2‰). With an average $\delta^2\text{H}$ of -89.6‰ (SD = 40.5‰), leaf sugar was significantly more ^2H depleted in plants with C_3 compared to leaf sugar of plants with C_4 (-24.7‰, SD = 19.8‰) or CAM (-5.9‰, SD = 60.9‰) CO_2 fixation. This autotrophic ^2H fractionation (ϵ_A) was lowest in C_3 (-60.2‰, SD = 41.6‰), higher in CAM (0.2‰, SD = 54.4‰), and highest in C_4 plants (5.0‰, SD = 23.2‰). The $\delta^2\text{H}$ of leaf cellulose roughly reflected the pattern observed in leaf sugar, with -44.1‰ in C_3 (SD = 21.8‰), 17.8‰ in C_4 (SD = 28.2‰), and 27.1‰ (SD = 44.3‰) in CAM CO_2 fixation pathways. There was no significant difference in ϵ_H observed among the three types of CO_2 fixation (C_3 = 45.5‰, SD = 30.0‰; C_4 = 42.6‰, SD = 20.5‰; and CAM = 33.0‰, SD = 41.4‰; Table 1).

Table 1: Average $\delta^2\text{H}$, the standard deviation (SD), and the grouping of the results from the Pairwise Wilcoxon Rank Sum Tests by compact letter

display (CLD) of leaf water, leaf sugar, and leaf cellulose, the autotrophic fractionation factor ϵ_A , and the heterotrophic fractionation factor ϵ_H . The CLD are separated into within CO₂ fixation type of the different compounds and fractionation factors (first letter; horizontally comparison), and between CO₂ fixation type within one compound and fractionation factor (second letter; vertically comparison). In the second set of data including CAM*, the facultative CAM species *D. cooperi* and *M. cordifolium* were excluded.

	$\delta^2\text{H}$ Leaf Water			$\delta^2\text{H}$ Leaf Sugar			$\delta^2\text{H}$ Leaf Cellulose			ϵ_A			ϵ_H		
	‰	SD	CLD	‰	SD	CLD	‰	SD	CLD	‰	SD	CLD	‰	SD	CLD
C ₃	-29.4	14.1	b b	-89.6	40.5	e c	-44.1	21.8	c b	-60.2	41.6	d b	45.5	30.0	a a
C ₄	-29.8	14.6	c b	-24.7	19.8	c b	17.8	28.2	b a	5.0	23.2	b a	42.6	20.5	a a
CAM	-6.1	15.2	c a	-5.9	60.9	bc a	27.1	44.3	ab a	0.2	54.4	bc a	33.0	41.4	a a
C ₃	-29.4	14.1	b b	-89.6	40.5	e c	-44.1	21.8	c c	-60.2	41.6	d c	45.5	30.0	a a
C ₄	-29.8	14.6	c b	-24.7	19.8	c b	17.8	28.2	b b	5.0	23.2	b b	42.6	20.5	a a
CAM*	-2.1	15.7	c b	28.0	34.4	ab a	48.5	32.1	a a	30.2	31.6	ab a	20.5	41.1	bc b

Table 2: Average $\delta^2\text{H}$ (‰), the standard deviation (SD), and the grouping of the results from the Pairwise Wilcoxon Rank Sum Tests by compact letter display (CLD; vertical comparison between treatments) of leaf water, leaf sugar, leaf cellulose, the autotrophic fractionation factor ϵ_A , and the heterotrophic fractionation factor ϵ_H among the three CO₂ fixation pathways, in response to the respective growing condition. In the subset CAM*, the facultative CAM species *D. cooperi* and *M. cordifolium* were excluded.

	$\delta^2\text{H}$ Leaf Water			$\delta^2\text{H}$ Leaf Sugar			$\delta^2\text{H}$ Leaf Cellulose			ϵ_{H}						
	%	SD	CLD	%	SD	CLD	%	SD	CLD	%	SD	CLD				
C_3	20 °C, VPD = 1.2 kPa	-31.0	12.6	b	-99.1	47.0	ab	-47.0	23.8	a	-68.1	50.9	a	52.1	34.4	a
	30 °C, VPD = 1.3 kPa	-34.9	13.8	b	-95.5	33.6	b	-49.2	19.6	a	-60.5	33.8	a	46.2	27.3	a
	30 °C, VPD = 2.6 kPa	-22.3	13.2	a	-74.5	36.8	a	-36.1	20.4	a	-52.1	38.4	a	38.4	27.1	a
C_4	20 °C, VPD = 1.2 kPa	-31.5	19.1	a	-26.8	23.2	a	14.2	19.5	a	4.7	28.3	a	41.0	19.3	a
	30 °C, VPD = 1.3 kPa	-33.3	9.3	a	-26.0	14.3	a	11.5	22.2	a	7.2	19.7	a	37.5	19.4	a
	30 °C, VPD = 2.6 kPa	-24.6	13.2	a	-21.4	21.7	a	27.8	38.2	a	3.2	22.1	a	49.2	22.3	a
CAM	20 °C, VPD = 1.2 kPa	-9.0	9.1	b	-22.2	58.3	a	12.7	35.0	a	-13.2	56.0	a	34.9	29.8	a
	30 °C, VPD = 1.3 kPa	-15.5	7.3	b	-2.1	51.6	a	26.0	41.9	a	13.4	46.6	a	28.0	42.3	a
	30 °C, VPD = 2.6 kPa	5.9	17.8	a	4.9	71.0	a	41.1	51.4	a	-0.9	59.5	a	36.2	50.3	a
*CAM	20 °C, VPD = 1.2 kPa	-5.3	8.8	c	14.0	31.1	b	32.4	20.9	a	19.2	37.1	a	18.5	18.8	a
	30 °C, VPD = 1.3 kPa	-13.5	7.2	b	22.8	30.2	ab	43.0	30.0	a	36.4	25.6	a	20.1	42.9	a
	30 °C, VPD = 2.6 kPa	12.7	15.4	a	45.7	36.0	a	68.3	33.6	a	32.9	32.4	a	22.7	54.0	a

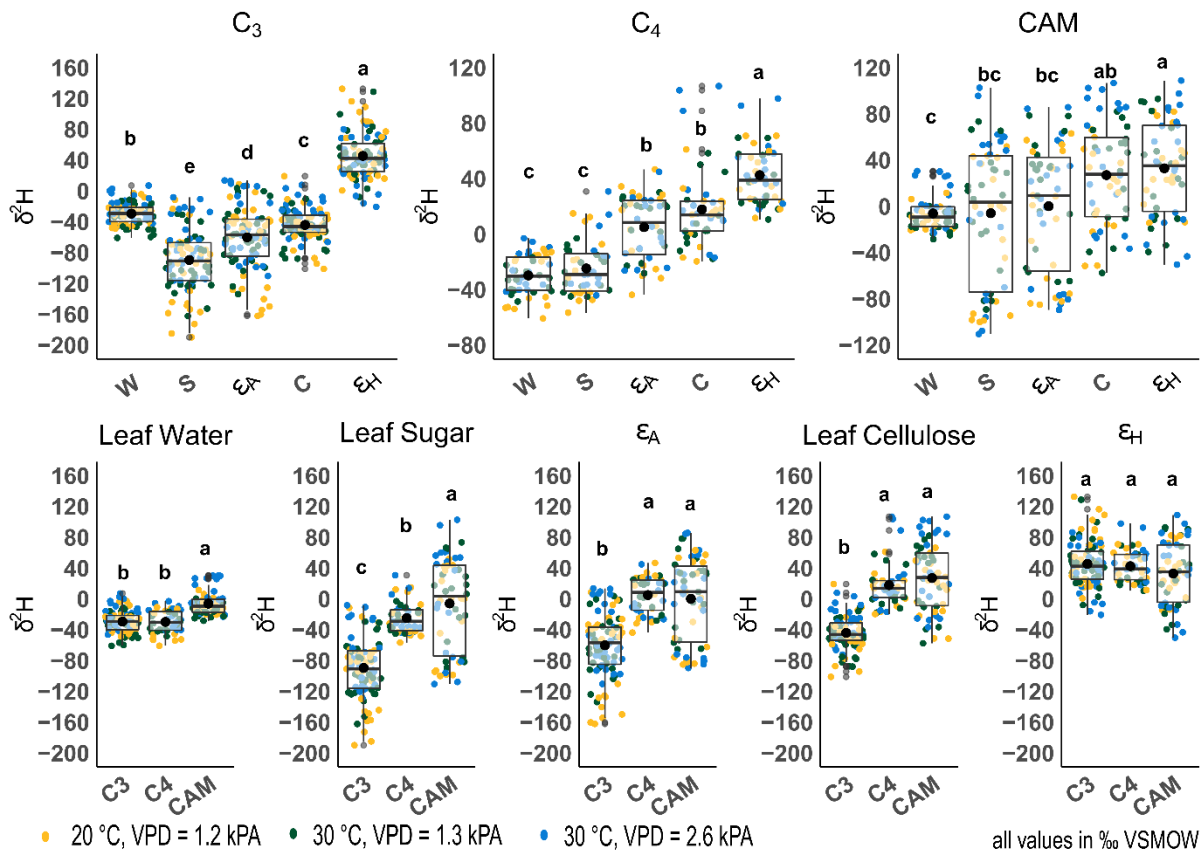


Figure 2: Comparison of the $\delta^2\text{H}$ values and ^2H fractionation factors within (top row) and between (bottom row) the three types of CO_2 fixation pathways and the three climate treatments (yellow points 20°C , $\text{VPD} = 1.2$ kPa; green points 30°C , $\text{VPD} = 1.3$ kPa; blue points 30°C , $\text{VPD} = 2.6$ kPa). Abbreviations: W = Leaf Water, S = Leaf Sugar, ϵ_A = autotrophic ^2H fractionation factor, C = Leaf Cellulose, ϵ_H = heterotrophic ^2H fractionation factor. Letters display the grouping of the results from the Pairwise Wilcoxon Rank Sum Tests by CLD.

If the two facultative CAM species *D. cooperi* and *M. cordifolium* were excluded (Table S1, Fig. S1), the $\delta^2\text{H}$ of the leaf water increased to -2.1‰ (SD 15.7‰), $\delta^2\text{H}$ of leaf sugar to 28‰ (SD = 34.4‰), ϵ_A to 30.2‰ (SD = 31.6‰), the $\delta^2\text{H}$ of leaf cellulose increased to 48.5‰ (SD = 32.1‰), and ϵ_H decreased to 20.5‰ (SD = 41.1‰). In this case, average $\delta^2\text{H}$ of leaf sugar and $\delta^2\text{H}$ of leaf cellulose (Fig. S1) of plants with CAM CO_2 fixation were significantly ^2H enriched compared to the compounds in C_4 CO_2 fixation and ϵ_A was significantly higher. In contrast, ϵ_H of this CAM subset was significantly lower than the ones observed in plants with C_3 and C_4 CO_2 fixation.

Across all tested species, temperature increase from 20 °C to 30°C alone did not lead to significant overall changes in $\delta^2\text{H}$ of leaf water, leaf sugar and leaf cellulose, and ^2H fractionation among the three types of CO_2 fixation (Fig. 3, Table S2). However, the increase in VPD from 1.3 kPa to 2.6 kPa significantly increased the $\delta^2\text{H}$ of leaf water of plants with C_3 and CAM CO_2 fixation, but not in those with C_4 CO_2 fixation. Increasing VPD also lead to higher $\delta^2\text{H}$ values of leaf sugar and leaf cellulose in C_3 plants; however, no change was observed in both of their ^2H fractionation factors. Neither the $\delta^2\text{H}$ of leaf sugar and leaf cellulose nor the ^2H fractionation factors of plants with C_4 and CAM CO_2 fixation showed a general response to changes in temperature and VPD. In summary, the treatments did not significantly change the overall pattern of the $\delta^2\text{H}$ values and ^2H fractionation factors within the three types of CO_2 fixation across all tested species (Fig. S2, S3).

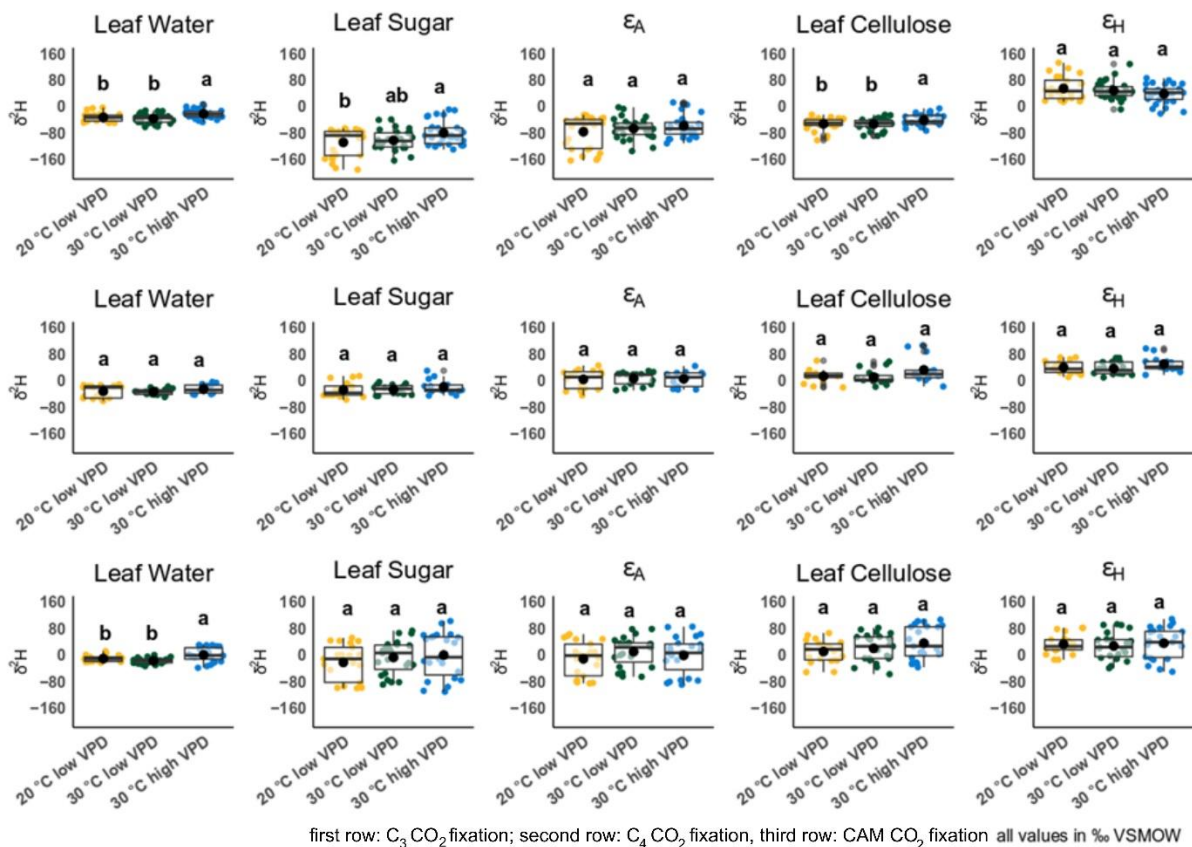


Figure 3: $\delta^2\text{H}$ of leaf water, leaf sugar, ϵ_A (autotrophic ^2H fractionation), leaf cellulose, and ϵ_H (heterotrophic ^2H fractionation) in response to changes of temperature and VPD among the three types of CO_2 fixation. Letters display

the grouping of the results from the Pairwise Wilcoxon Rank Sum Tests by CLD.

Species specific $\delta^2\text{H}$ response to changes in temperature and VPD

Analysing the response to changes in temperature and VPD on a species level revealed a diverse pattern for plants with C_3 , C_4 and CAM CO_2 fixation pathways (Tables 3, 4, 5).

Plants with C_3 CO_2 fixation showed a distinct response in their $\delta^2\text{H}$ of leaf water, leaf sugar, and leaf cellulose as well as fractionation factors to changes in temperature and VPD. The temperature response of the autotrophic ^2H fractionation ϵ_A varied among the species. ϵ_A was more negative at 20 °C for two species (*B. maculata*, *H. vulgare*), and more negative at 30 °C for three species (*A. esculentus*, *O. sativa*, *Q. pubescens*). The heterotrophic ^2H fractionation ϵ_H was significantly more positive at 20 °C in two species (*B. maculata*, *B. semperflorens*), and more positive at 30 °C in one species (*Q. pubescens*). The autotrophic ^2H fractionation ϵ_A was more negative at a VPD of 1.3 kPa for one species (*Z. aethiopica*), and a VPD of 2.6 kPa for two species (*A. esculentus*, *O. sativa*). The heterotrophic ^2H fractionation ϵ_H was more positive at a VPD of 1.3 kPa in two species (*H. vulgare*, *Z. aethiopica*), and a VPD of 2.6 kPa in two species (*O. sativa*, *Q. pubescens*). When ϵ_A decrease (e.g., becoming more negative), ϵ_H usually simultaneously increase (e.g., becoming less positive), as seen for instance in *Quercus pubescens*, the two species of *Begonia*, *Oryza sativa*, *Hordeum vulgare*.

Table 3: Treatment response of the $\delta^2\text{H}$ of leaf water, leaf sugar, and leaf cellulose, the autotrophic ^2H fractionation factor ϵ_A and the heterotrophic ^2H fractionation factor ϵ_H among the species with C_3 CO_2 fixation pathway.

Letters display the grouping of the results from the Pairwise Wilcoxon Rank Sum Tests by CLD, comparing the treatment effect within each species (horizontally).

		20 °C low VPD			30 °C low VPD			30 °C high VPD		
		‰	SD	CLD	‰	SD	CLD	‰	SD	CLD
<i>Q. pubescens</i>	$\delta^2\text{H W}$	-30.0	2.8	b	-42.12	4.0	c	-20.3	1.9	a
	$\delta^2\text{H S}$	-69.3	1.7	a	-118.36	7.5	b	-86.9	10.9	a
	ϵ_A	-39.3	3.0	a	-76.24	5.9	b	-66.6	12.7	b
	$\delta^2\text{H C}$	-48.4	4.2	a	-85.79	3.1	b	-43.1	9.0	a
	ϵ_H	20.9	2.6	c	32.57	4.5	b	43.8	3.9	a
<i>O. sativa</i>	$\delta^2\text{H W}$	-43.2	0.9	ab	-48.83	2.1	b	-42.9	3.2	a
	$\delta^2\text{H S}$	-76.6	8.6	a	-48.83	2.5	b	-116.9	3.1	c
	ϵ_A	-33.4	7.7	a	-53.98	3.9	b	-74.0	5.4	c
	$\delta^2\text{H C}$	-37.4	3.2	a	-54.33	4.3	b	-47.7	3.3	b
	ϵ_H	39.2	8.8	b	48.48	2.8	b	69.1	0.5	a
<i>H. vulgare</i>	$\delta^2\text{H W}$	-28.8	4.8	a	-33.13	0.7	a	-30.3	1.9	a
	$\delta^2\text{H S}$	-173.0	25.0	b	-112.00	13.0	a	-74.8	5.1	a
	ϵ_A	-144.2	29.5	b	-78.87	13.0	a	-44.6	6.9	a
	$\delta^2\text{H C}$	-94.2	7.0	c	-41.08	2.4	a	-59.0	4.9	b
	ϵ_H	78.8	18.9	a	70.92	12.6	a	15.8	8.5	b
<i>S. hispanica</i>	$\delta^2\text{H W}$	-41.8	11.5	b	-27.63	3.3	a	-29.0	0.4	a
	$\delta^2\text{H S}$	-138.3	28.6	a	-27.63	19.1	a	-89.7	4.1	a
	ϵ_A	-96.6	37.6	a	-47.11	18.2	a	-60.6	3.8	a
	$\delta^2\text{H C}$	-58.6	22.6	b	-43.06	10.0	a	-47.8	2.3	a
	ϵ_H	79.7	44.6	a	31.68	9.2	a	41.9	1.8	a
<i>B. semperflorens</i>	$\delta^2\text{H W}$	-26.6	4.4	a	-29.58	1.3	a	-18.7	6.3	a
	$\delta^2\text{H S}$	-161.7	9.9	b	-136.06	15.1	ab	-119.0	8.8	a
	ϵ_A	-135.1	12.8	b	-106.48	16.2	ab	-100.3	9.3	a
	$\delta^2\text{H C}$	-42.3	6.3	a	-54.10	5.5	a	-40.2	13.3	a
	ϵ_H	119.4	12.0	a	81.96	18.4	b	78.8	8.3	b

<i>B. maculata</i>	$\delta^2\text{H W}$	-5.1	2.9	b	-18.20	2.7	c	3.4	3.4	a
	$\delta^2\text{H S}$	-145.1	14.1	b	-18.20	8.9	a	-79.3	15.2	a
	ε_A	-140.1	14.5	b	-88.64	11.6	a	-82.7	12.3	a
	$\delta^2\text{H C}$	-55.1	3.0	b	-48.85	2.1	b	-21.6	8.8	a
	ε_H	90.0	12.6	a	57.99	10.4	b	57.7	13.6	b
<i>Anthurium</i>	$\delta^2\text{H W}$	-32.8	9.7	a	-35.04	2.5	a	-21.8	15.6	a
	$\delta^2\text{H S}$	-71.4	2.5	c	-38.94	1.0	b	-25.9	4.3	a
	ε_A	-27.8	19.3	b	-3.90	3.5	ab	-4.1	12.7	a
	$\delta^2\text{H C}$	-53.8	16.3	b	-21.47	21.8	ab	-14.6	10.4	a
	ε_H	16.4	3.9	a	3.10	15.6	a	11.3	14.0	a
<i>A. esculentus</i>	$\delta^2\text{H W}$	-43.2	1.2	c	-12.54	1.0	a	-18.0	2.0	b
	$\delta^2\text{H S}$	-83.8	9.0	a	-12.54	7.7	a	-110.5	7.3	b
	ε_A	-40.6	8.1	a	-61.15	6.7	b	-92.5	8.8	c
	$\delta^2\text{H C}$	-29.5	5.3	a	-34.99	10.5	a	-63.4	10.6	b
	ε_H	54.3	13.7	a	38.69	4.3	a	47.1	5.2	a
<i>E. pulcherrima</i>	$\delta^2\text{H W}$	-21.7	1.4	a	-29.84	3.7	ab	-33.7	4.6	b
	$\delta^2\text{H S}$	-21.8	9.7	a	-40.61	18.1	a	-32.6	15.3	a
	ε_A	-0.1	8.3	a	-10.76	21.7	a	1.1	15.8	a
	$\delta^2\text{H C}$	-2.1	18.6	a	-17.55	8.3	a	1.2	8.1	a
	ε_H	19.7	21.0	a	23.06	21.5	a	33.8	8.1	a
<i>Z. aethiopica</i>	$\delta^2\text{H W}$	-25.1	1.9	a	-48.85	2.2	b	-22.7	7.3	a
	$\delta^2\text{H S}$	-74.1	8.0	b	-90.42	13.7	b	-14.1	8.2	a
	ε_A	-49.0	7.9	b	-41.57	15.5	b	8.6	3.8	a
	$\delta^2\text{H C}$	-53.3	6.9	b	-51.68	4.9	b	-28.4	1.8	a
	ε_H	20.8	4.8	a	38.74	10.3	a	-14.4	7.2	b
<i>Z. aethiopica</i>	$\delta^2\text{H W}$	-42.6	8.3	b	-59.11	2.1	c	-6.1	4.7	a
	$\delta^2\text{H S}$	-86.6	10.2	ab	-114.59	14.2	b	-63.8	0.5	a
	ε_A	-44.1	17.4	a	-55.48	15.9	a	-57.6	4.2	a
	$\delta^2\text{H C}$	-39.6	3.4	b	-76.41	1.3	c	-27.4	3.3	a
	ε_H	47.0	10.4	a	38.18	14.1	a	36.4	3.8	a

Plant species with C_4 CO_2 fixation showed the least response to changes in temperature and VPD, independent of their C_4 subtype (Figs. 5, S10). *Z. mays* and *A. caudatus*, the latter only analysed for the temperature effect due to sample loss of the high VPD treatment, did not show any significant differences in any of the analysed compounds or ^2H fractionation factors

between the treatments. ϵ_A was more negative in the high VPD treatment in *P. glaucum*, whereas ϵ_H was more positive in *P. glaucum* and *S. bicolor* under high VPD.

Table 4: Treatment response of the $\delta^2\text{H}$ of leaf water, leaf sugar and leaf cellulose, the autotrophic ^2H fractionation factor ϵ_A and the heterotrophic ^2H fractionation factor ϵ_H among the species with C4 CO_2 fixation pathway. Letters display the grouping of the results from the Pairwise Wilcoxon Rank Sum Tests by CLD, comparing the treatment effect (horizontally).

		20 °C low VPD			30 °C low VPD			30 °C high VPD		
		%o	SD	CLD	%o	SD	CLD	%o	SD	CLD
<i>Z. mays</i>	$\delta^2\text{H W}$	-45.4	N.A.	a	-42.09	2.3	a	-38.9	3.6	a
	$\delta^2\text{H S}$	-42.2	N.A.	a	-39.82	3.1	a	-30.0	19.5	a
	ε_A	3.2	N.A.	a	2.26	0.9	a	8.9	15.9	a
	$\delta^2\text{H C}$	-16.9	N.A.	a	-9.01	12.4	a	-7.5	13.2	a
	ε_H	25.3	N.A.	a	30.82	9.3	a	22.5	6.3	a
<i>P. glaucum</i>	$\delta^2\text{H W}$	-50.6	4.0	b	-39.97	1.9	a	-38.8	2.3	a
	$\delta^2\text{H S}$	-17.5	9.6	a	-17.61	2.6	a	-18.9	9.1	a
	ε_A	33.1	11.8	a	22.36	4.1	a	19.9	7.7	a
	$\delta^2\text{H C}$	11.5	9.6	a	6.23	5.6	a	18.9	10.5	a
	ε_H	29.0	4.8	ab	23.84	3.3	b	37.9	2.2	a
<i>S. bicolor</i>	$\delta^2\text{H W}$	-55.5	4.6	b	-40.90	7.7	ab	-30.8	5.2	a
	$\delta^2\text{H S}$	-36.3	15.8	a	-16.88	12.5	a	-36.5	10.7	a
	ε_A	19.2	14.4	a	24.01	5.3	a	-5.8	16.0	a
	$\delta^2\text{H C}$	-4.9	17.2	a	-0.43	7.2	a	10.5	1.3	a
	ε_H	31.3	7.2	ab	16.45	5.3	b	47.0	12.0	a
<i>A. tricolor</i>	$\delta^2\text{H W}$	-18.1	2.3	b	-25.22	2.5	ab	-6.0	3.2	a
	$\delta^2\text{H S}$	-38.1	5.5	a	-39.23	5.2	a	-31.5	4.2	a
	ε_A	-19.9	6.9	a	-14.01	7.7	a	-25.5	1.1	a
	$\delta^2\text{H C}$	17.4	5.6	a	1.26	12.9	a	23.3	8.5	a
	ε_H	55.4	10.2	ab	40.49	17.7	b	54.8	11.0	a
<i>S. soda</i>	$\delta^2\text{H W}$	-14.6	1.8	a	-31.34	1.6	b	-13.7	1.2	a
	$\delta^2\text{H S}$	12.2	2.8	a	-10.20	2.3	b	17.0	12.6	a
	ε_A	26.8	4.3	a	21.14	3.5	a	30.6	12.7	a
	$\delta^2\text{H C}$	39.3	19.4	b	51.13	6.8	b	99.8	9.6	a
	ε_H	27.2	21.6	b	61.32	6.9	ab	82.8	21.6	a
<i>A. caudatus</i>	$\delta^2\text{H W}$	-13.9	3.6	a	-18.01	1.8	a	N.A.	N.A.	N.A.
	$\delta^2\text{H S}$	-49.0	7.1	a	-42.64	3.2	a	N.A.	N.A.	N.A.
	ε_A	-35.2	7.4	a	-24.63	5.0	a	N.A.	N.A.	N.A.
	$\delta^2\text{H C}$	18.2	4.4	a	13.53	15.7	a	N.A.	N.A.	N.A.
	ε_H	67.3	6.3	a	56.18	18.9	a	N.A.	N.A.	N.A.
<i>S. italica</i>	$\delta^2\text{H W}$	N.A.	N.A.	N.A.	N.A.	N.A.	N.A.	-26.3	4.6	N.A.
	$\delta^2\text{H S}$	N.A.	N.A.	N.A.	N.A.	N.A.	N.A.	-36.3	0.7	N.A.
	ε_A	N.A.	N.A.	N.A.	N.A.	N.A.	N.A.	-10.0	3.9	N.A.
	$\delta^2\text{H C}$	N.A.	N.A.	N.A.	N.A.	N.A.	N.A.	4.1	16.9	N.A. ¹³³
	ε_H	N.A.	N.A.	N.A.	N.A.	N.A.	N.A.	40.4	16.2	N.A.

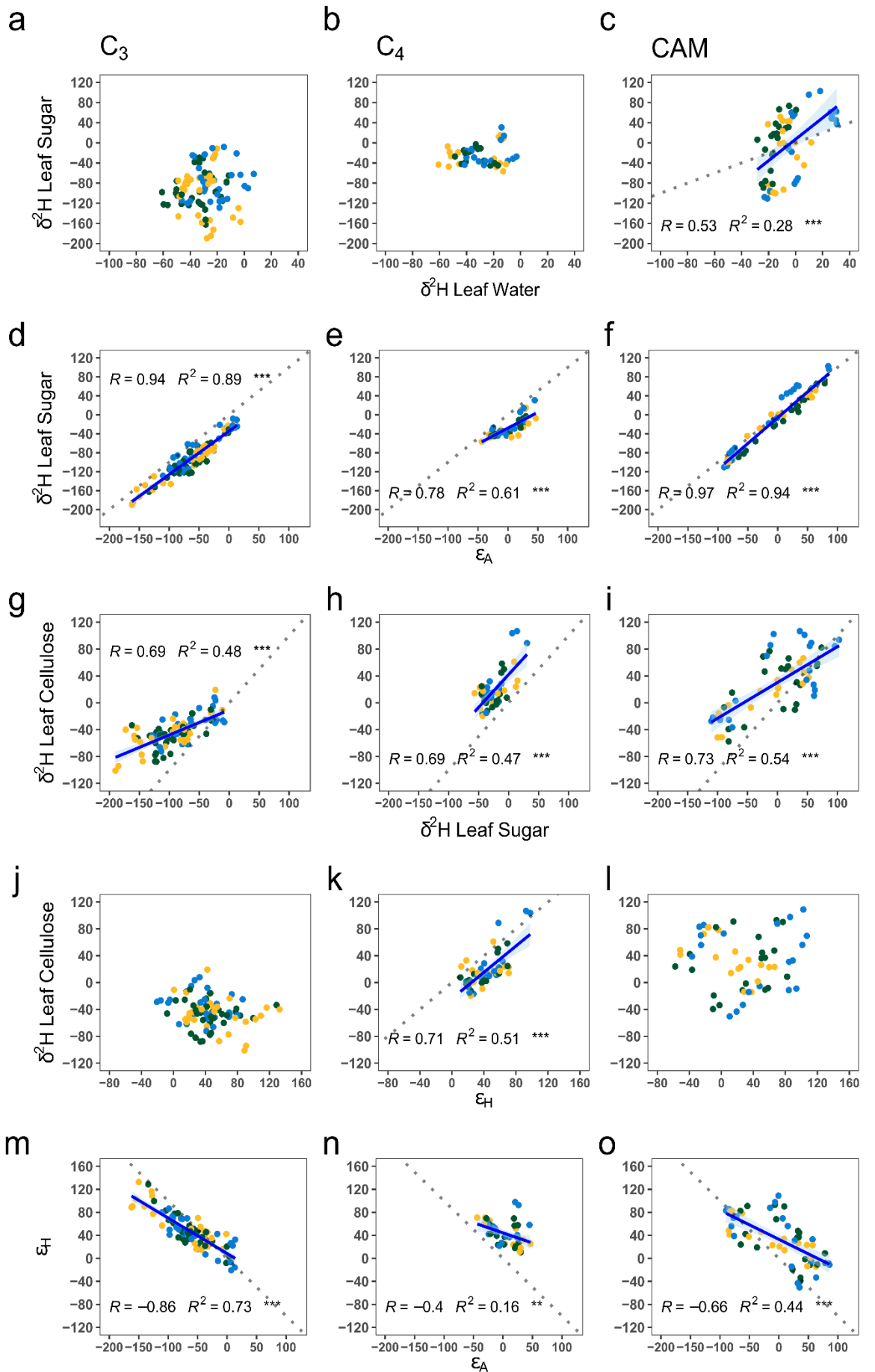
Plant species with CAM CO₂ fixation showed a distinct response in their isotopic composition to the treatments (Table 5, Figs. 6, S11). ϵ_A was more negative at 20 °C than at 30 °C in three species (*Hyleroocereus*, *M. cordifolium*, *Sedum*), and at 30 °C than at 20 °C in one species (*Rhipsalis*). ϵ_H was more positive at 20 °C than at 30 °C in one species (*Hyleroocereus*), and higher at 30 °C than at 20 °C in one species (*C. repens*). The autotrophic fractionation ϵ_A was more negative at a VPD of 2.6 kPA in one species (*D. cooperi*). The heterotrophic fractionation factor ϵ_H did not significantly respond to changes in VPD.

Table 5: Treatment response of the $\delta^2\text{H}$ of leaf water, leaf sugar and leaf cellulose, the autotrophic ^2H fractionation factor ϵ_A and the heterotrophic ^2H fractionation factor ϵ_H among the species with CAM CO₂ fixation. Letters display the grouping of the results from the Pairwise Wilcoxon Rank Sum Tests by CLD, comparing the treatment effect (horizontally).

		20 °C low VPD			30 °C low VPD			30 °C high VPD		
		%	SD	CLD	%	SD	CLD	%	SD	CLD
<i>D. cooperi</i>	$\delta^2\text{H W}$	-19.3	0.5	a	-23.73	1.3	b	-21.0	2.0	ab
	$\delta^2\text{H S}$	-91.6	8.4	ab	-82.22	6.7	a	-104.7	7.7	b
	ϵ_A	-72.4	8.8	ab	-58.49	6.2	a	-83.8	6.3	b
	$\delta^2\text{H C}$	-13.8	9.3	a	-10.30	27.4	a	-25.0	2.7	a
	ϵ_H	77.8	5.0	a	71.92	25.9	a	79.7	8.3	a
<i>M. cordifolium</i>	$\delta^2\text{H W}$	-13.4	4.0	b	-17.72	1.0	b	0.5	1.2	a
	$\delta^2\text{H S}$	-97.2	3.8	b	-68.56	18.4	a	-75.6	5.6	ab
	ϵ_A	-83.7	1.4	b	-50.84	19.5	a	-76.1	4.4	ab
	$\delta^2\text{H C}$	-39.8	20.0	a	-47.06	14.9	a	-19.6	20.4	a
	ϵ_H	57.4	21.6	a	21.50	3.5	a	55.9	17.1	a
<i>Rhipsalis</i>	$\delta^2\text{H W}$	-8.9	2.8	b	-8.65	4.2	b	27.6	2.3	a
	$\delta^2\text{H S}$	46.0	5.1	a	23.40	11.8	b	57.2	7.6	a
	ϵ_A	54.9	7.6	a	32.05	7.7	b	29.6	7.0	b
	$\delta^2\text{H C}$	37.3	8.5	a	-7.38	4.4	b	21.2	12.0	a
	ϵ_H	-8.7	9.0	a	-30.79	10.4	a	-35.9	19.2	a
<i>Hylocereus</i>	$\delta^2\text{H W}$	-11.5	8.1	b	-5.53	6.3	ab	14.0	5.9	a
	$\delta^2\text{H S}$	34.4	10.1	c	68.45	4.3	b	99.2	5.0	a
	ϵ_A	46.0	12.2	b	73.98	7.7	a	85.1	0.9	a
	$\delta^2\text{H C}$	58.7	8.4	a	65.12	14.9	a	89.0	6.6	a
	ϵ_H	24.2	1.8	a	-3.33	10.5	b	-10.1	1.6	b
<i>Sedum</i>	$\delta^2\text{H W}$	-3.0	12.7	b	-15.99	2.0	b	29.1	1.9	a
	$\delta^2\text{H S}$	-0.4	1.5	c	16.54	2.6	b	45.3	8.3	a
	ϵ_A	2.5	11.5	b	32.53	1.1	a	16.2	10.2	ab
	$\delta^2\text{H C}$	23.2	10.9	c	56.91	8.3	b	97.5	11.5	a
	ϵ_H	23.7	9.9	a	40.37	6.3	a	52.2	19.6	a
<i>C. repens</i>	$\delta^2\text{H W}$	2.4	3.4	a	-18.95	3.1	b	-4.6	1.5	a
	$\delta^2\text{H S}$	-24.2	23.0	a	-19.63	5.5	a	-12.0	5.7	a
	ϵ_A	-26.5	26.1	a	-0.68	8.6	a	-7.4	7.1	a
	$\delta^2\text{H C}$	10.6	15.3	b	64.15	15.7	a	86.1	16.2	a
	ϵ_H	34.8	13.0	b	83.78	13.7	a	98.1	10.5	a
<i>Phalaenopsis</i>	$\delta^2\text{H W}$	N.A.	N.A.	N.A.	-18.48	8.6	b	-2.0	1.1	a
	$\delta^2\text{H S}$	N.A.	N.A.	N.A.	25.44	16.8	b	56.5	3.5	a
	ϵ_A	N.A.	N.A.	N.A.	43.93	9.0	a	58.5	4.2	a
	$\delta^2\text{H C}$	N.A.	N.A.	N.A.	36.03	13.2	a	54.7	31.7	a
	ϵ_H	N.A.	N.A.	N.A.	10.59	30.0	a	-1.8	33.2	a

Drivers of the observed $\delta^2\text{H}$ values and ^2H fractionation factors

The linear regression analysis revealed correlations of various strength between the $\delta^2\text{H}$ of the different compounds and ^2H fractionation factors in the three types of CO_2 fixation (Fig. 4, S4-S9). $\delta^2\text{H}$ of leaf water did not significantly correlate with $\delta^2\text{H}$ of leaf sugar in C_3 and C_4 CO_2 fixation, but explained 28% of the variation in CAM plants. ε_{A} was highly correlated with $\delta^2\text{H}$ of leaf sugar, explaining 94% of the variation in plants with CAM, 89% in plants with C_3 , and 61% in plants with C_4 CO_2 fixation. About half of the variation in $\delta^2\text{H}$ of leaf cellulose was explained by the $\delta^2\text{H}$ of leaf sugar (i.e., 48% for C_3 , 47% for C_4 , and 54% for CAM plants). ε_{H} only correlated with $\delta^2\text{H}$ of leaf cellulose of the plants with C_4 CO_2 fixation, explaining 51% of the observed variation. In all three types of CO_2 fixation, ε_{H} was negatively correlated with ε_{A} , with the latter explaining 16% of ε_{H} in C_4 , 44% of ε_{H} in CAM, and 73% of ε_{H} in C_3 CO_2 fixation. These patterns largely remained after separating the three types of CO_2 fixation by the three treatments (Fig. S4, S5, S6).



● 20 °C, VPD = 1.2 kPa ● 30 °C, VPD = 1.3 kPa ● 30 °C, VPD = 2.6 kPa all values in ‰ VSMOW

Figure 4: Regression analysis within and between the three types of CO₂ fixation showing R, the correlations; R², the proportion of variance that can be explained, and asterisks indicating significant differences (*, P ≤ 0.05; **, P ≤ 0.01; ***, P ≤ 0.001) : First column C₃ CO₂ fixation, second column C₄ CO₂ fixation, third column CAM CO₂ fixation. a, b, c: δ²H leaf sugar / δ²H leaf water; d, e, f: δ²H leaf sugar / ε_A; g, h, i: δ²H leaf cellulose / δ²H leaf sugar; j, k, l: δ²H leaf cellulose / ε_H, m, n, o: ε_A / ε_H. The blue line indicates the linear model, and the dashed grey line the 1:1 line. VSMOW, Vienna Standard Mean Ocean Water

Discussion

This study on the biochemical drivers of autotrophic and heterotrophic ²H fractionation among C₃, C₄ and CAM CO₂ fixation of terrestrial plants helps to facilitate a better understanding of the causes of δ²H variations in leaf carbohydrates.

The biochemical drivers of autotrophic ²H fractionation among C₃, C₄ and CAM CO₂ fixation

By measuring the δ²H values of leaf water and bulk sugar, we were able to determine for the first time the autotrophic ²H-fractionation factor between leaf water and leaf sugars (ε_A) for plants of different CO₂ fixation pathways (Figs 1, S1, Tables 1-5). We found that ε_A caused a strong photosynthetic ²H depletion of on average -60.2‰ from leaf water to leaf sugar in plants with C₃ CO₂ fixation (Table 1). In contrast, we observed an autotrophic ²H enrichment of 5.0‰ in plants with C₄ CO₂ fixation and no autotrophic ²H fractionation in CAM plants (Table 1). However, after excluding the two facultative CAM species (*D. cooperi* and *M. cordifolium*) from the analysis, ε_A in CAM plants resulted in a ²H enrichment of 30.2‰ from leaf water to leaf sugar (Table 1). It is not clear whether the higher δ²H values of CAM plant leaf water is due to more ²H enriched soil water caused by reduced irrigation, possibly leading to more evaporatively enriched soil water, or due to differences in leaf water enrichment. The moderate correlation

between leaf water $\delta^2\text{H}$ and leaf sugar $\delta^2\text{H}$ in CAM plants (Fig. 4), is likely due to the contribution of C_3 CO_2 fixation to the total CO_2 fixation in some species, as leaf water $\delta^2\text{H}$ did not affect ^2H fractionation (Fig. S8).

The correlation between the $\delta^2\text{H}$ of the different compounds and the two ^2H fractionation factors of C_3 , C_4 and CAM CO_2 fixation (Fig. 4), point to distinct physiological and anatomical aspects that influence the hydrogen isotope composition of plant carbohydrates. While $\delta^2\text{H}$ of leaf sugars and ϵ_A are highly correlated in C_3 and CAM plants ($R = 0.94$ and 0.97 , respectively), this correlation is reduced in C_4 plants ($R = 0.78$). A strong correlation between $\delta^2\text{H}$ of leaf sugars and ϵ_A indicates an isotopic fractionation in equilibrium (Schuler *et al.* 2023). As there is no reason to assume that the C_4 plants were not in isotopic and biochemical equilibrium, this pattern was likely caused by different $\delta^2\text{H}$ values in water of bundle sheet (BS) cells compared to whole leaf water, as water in the BS cells is isotopically closer to source water taken up by the plant and therefore less isotopically enriched than water in mesophyll (M) cells (Smith *et al.*, 1991; Zhou *et al.*, 2016). Thus, ϵ_A might not be correctly calculated in C_4 plants when using the bulk leaf water $\delta^2\text{H}$.

A closer examination of the biochemical reactions among the three types of CO_2 fixation (Figs. 5, 6, 7) illustrates the biochemical and anatomical background that might be responsible for these observed patterns.

In C_3 CO_2 fixation (Fig. 5), the photosynthetic H^+ generation via the splitting of H_2O in the chloroplast's thylakoids results in a strongly ^2H depleted NADPH pool (Luo *et al.*, 1991), a reaction that might even decrease the $\delta^2\text{H}$ of the water inside the chloroplast stroma during photosynthetically active periods (Schuler *et al.*, 2023). This strongly ^2H depleted hydrogen pool is imprinted to the fresh assimilates which are synthesized during the Calvin Benson Bassham (CBB) Cycle, leading to the observed negative values of ϵ_A (Table 3). In addition, the strength of the autotrophic ^2H fractionation in C_3 CO_2 fixation is species-specific (Table 3) and reflects a plant's phylogeny (Schuler *et al.*, 2023).

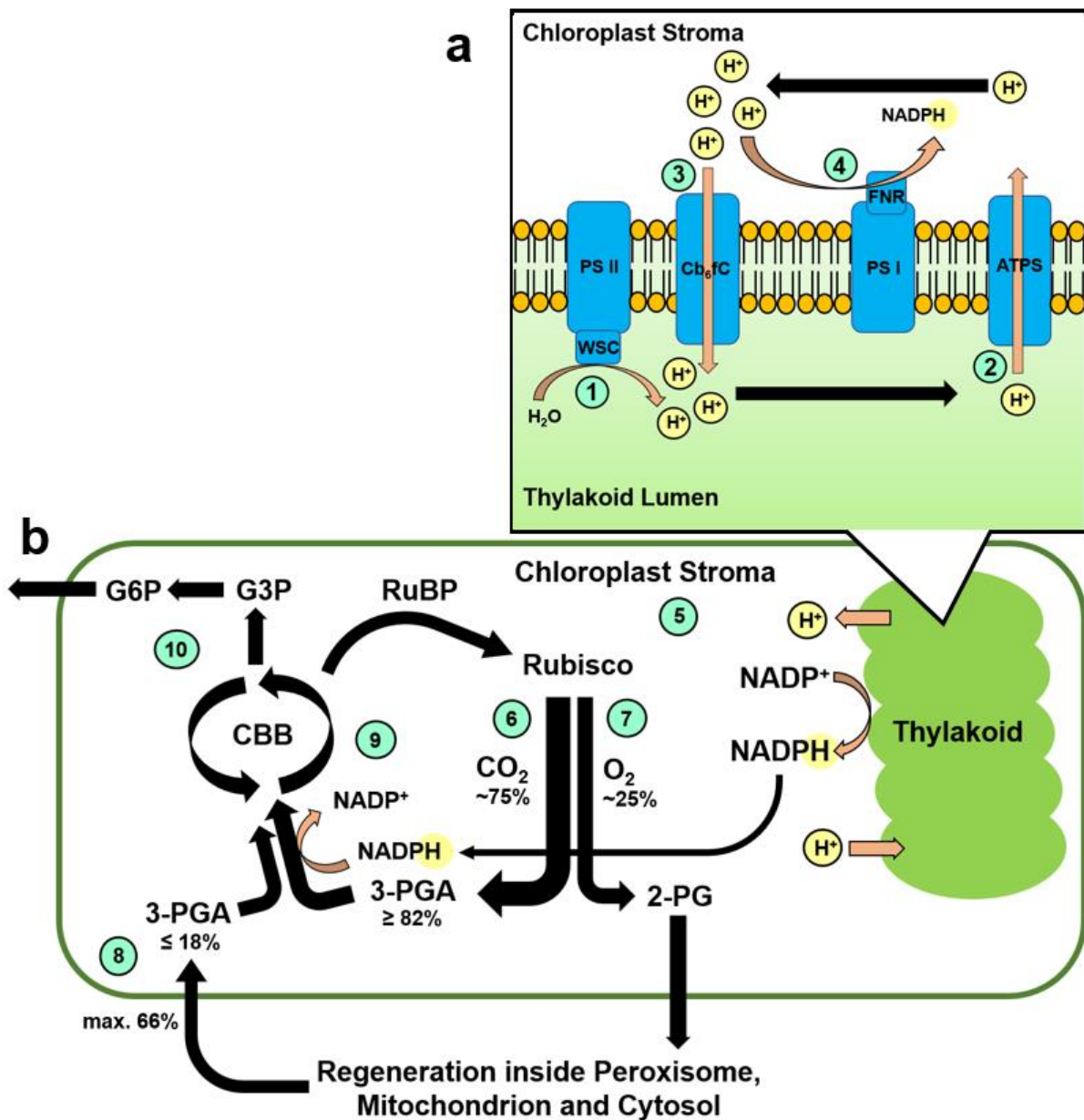


Figure 5: Simplified scheme of C₃ CO₂ fixation (modified from Schuler *et al.* (2023)): Light depending reactions (a) according to Allen *et al.* (2011), light independent reactions (b) according to Busch (2020). Proton fluxes are indicated by arrows, orange arrows indicate reactions directly involving hydrogen. Light-dependent reactions (a, 1-4): (1) Initial proton production by the split of the water molecules by the water-splitting complex (WSC) of PS II (Ferreira *et al.*, 2004). (2) The proton pump of the ATP synthase (ATPS, Seelert *et al.* (2000)), which pumps protons from the thylakoid lumen into the chloroplast stroma. The $\delta^2\text{H}$ value of the proton pool in the chloroplast stroma can be potentially influenced by a selective H⁺ transport by the ATPS,

or 3) the proton transfer back into the thylakoid lumen by the cytochrome b_6/f complex (Cb_6fC , Cramer *et al.* (2011)). (4) The NADPH synthesis by the ferredoxin-NADP⁺ reductase (FNR, Nelson and Ben-Shem (2005)), which is connected to photosystem I (PS I), is using protons from the pool of the chloroplast stroma, which derives from the light-dependent reactions of the thylakoid. During the light-independent reactions (b, 5-10), the δ^2H value of the 5) proton pool in the chloroplast stroma is incorporated during the CO₂ assimilation process and probably further altered by other ²H fractionation processes. 6) About 75% of RuBisCO binds CO₂ to 3-PGA, and 7) about 25% of RuBisCO binds oxygen in a process called photorespiration (Busch, 2020) and needs to be regenerated as 2-phosphoglycolate (2-PG) to 8) 3-PGA (Bauwe, 2018). At least 82% of the 3-PGA pool comes from direct CO₂ fixation and maximum 18% from photorespiration (Busch, 2020). Further exchanges in biochemical reactions involving hydrogen occur during 9) the Calvin-Benson-Bassham (CBB) cycle, and 10) the synthesis of glucose-6-phosphate (G6P) out of glyceraldehyde-3-phosphate (G3P).

In contrast, water splitting during the light-dependent reactions of C₄ CO₂ fixation (Fig. 6) takes place in the chloroplasts of M cells (Sage & Monson, 1998), and is not functional in BS cells (Meierhoff & Westhoff, 1993), where carbohydrate synthesis takes place. To generate the required NADPH in the BS cell chloroplast, H⁺ is imported from M cells via the malate-pyruvate shuttle in the NADP-Me subtype (Fig. 6a), and via the import of aspartic acid in the NAD-Me subtype (Fig. 6b). Due to this spatial separation of the two reactions, the strong ²H depletion during PS II is not or only partially imprinted in the fresh assimilates (Figs. 1, 2, Table 1, Zhou *et al.*, 2016). Photorespiration can be excluded as a major driver of the observed relative ²H enrichment compared to C₃ plants (Zhou *et al.*, 2018), as it is limited to a minimum in plants with C₄ CO₂ fixation (Bauwe, 2011). We therefore speculate that the ϵ_A observed here in C₄ plants (Table 4) may be caused by NADPH generation in the NADP-Me subtype at the end of the malate-pyruvate shuttle in the BS chloroplast (Fig. 6a step 3), respectively by NADH

generation in the BS mitochondria during the decarboxylation of oxaloacetic acid (Fig. 6b step 3) in the NAD-Me subtype.

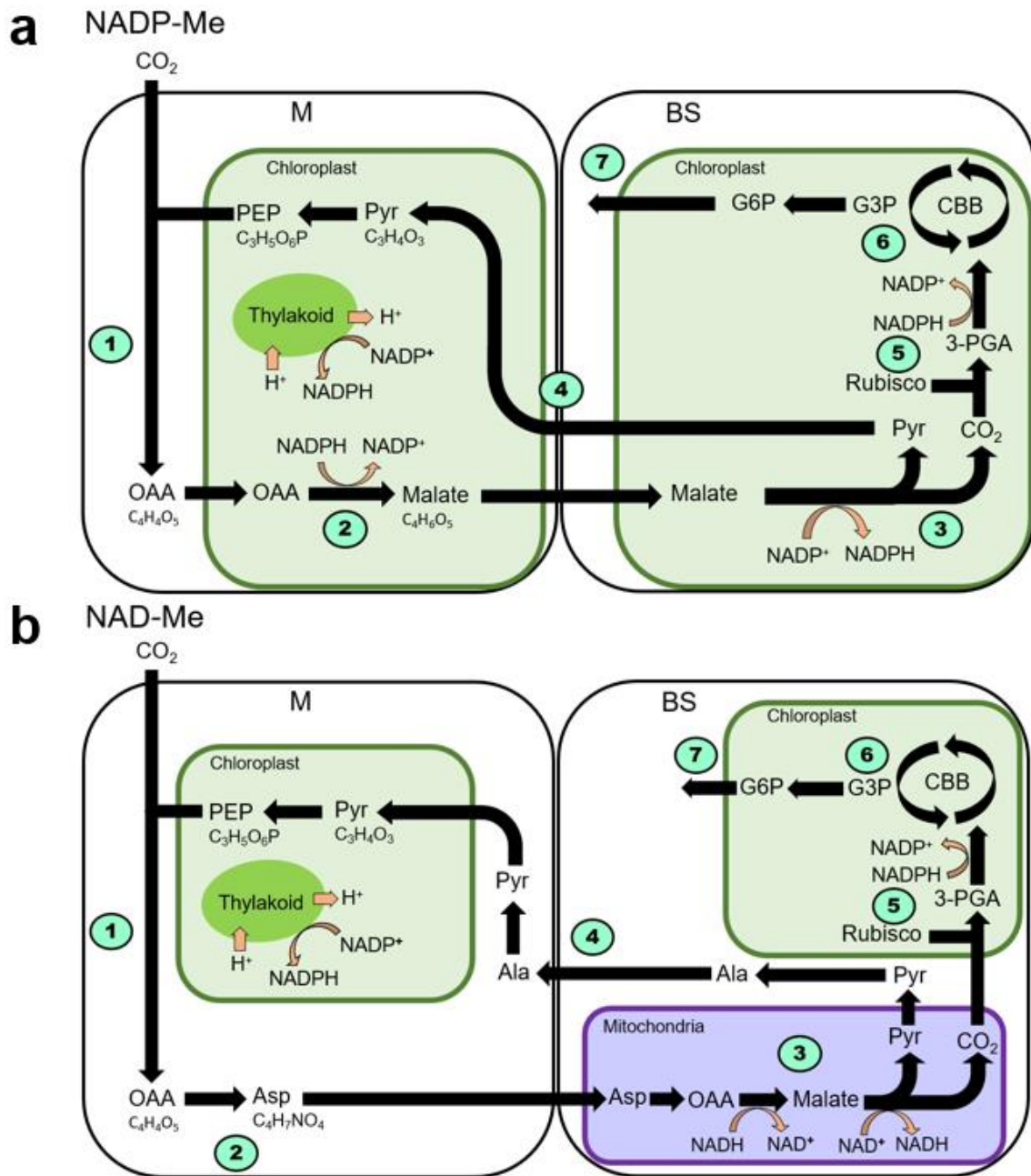


Figure 6: Simplified scheme of C_4 CO_2 fixation according to Ludwig (2016) and Rao and Dixon (2016) . **a)** shows the reactions involving hydrogen within the NADP-Me subtype, while **b)** shows the reactions within the NAD-Me subtype. In the NADP-Me subtype **a)**, **1)** CO_2 is initially bound to phosphoenolpyruvate (PEP) by the enzyme phosphoenolpyruvate carboxylase (PEPC) in the mesophyll (M) cells cytosol, forming oxaloacetate

(OAA). OAA is transferred into the M cells chloroplasts, **2**) where it receives two more hydrogen atoms from NADPH, which was formed during the light-dependent reactions around the M cells thylakoids, forming malate. The malate is transported into the chloroplasts of the bundle sheet (BS) cells and acts as a proton carrier. **3**) There, malate is decarboxylated by NADP-Me, producing CO₂ and pyruvate, as well as two NADPH from NADP⁺ using the carried protons. The pyruvate is transported back into the M cells chloroplasts **4**), where it is used to regenerate the PEP pool. The CO₂ release from malate in combination with the absence of the O₂ production by the light-dependent reactions is creating a high CO₂ and low O₂ environment in the chloroplasts of the BS cells. Thus, **5**) photorespiration is minimized given that O₂ uptake is strongly reduced by RUBISCO, which increases CO₂ uptake efficiency. As during the C₃ CO₂ fixation, the **6**) final carbohydrate synthesis takes place in the CBB cycle, and **7**) carbohydrates are further allocated within the cell and eventually the leaf tissue. The **b**) NAD-Me subtype differs from the former as **2**) aspartic acid (Asp) is formed out of the OAA in the M cells cytosol, which is eventually transported into the BS cells mitochondria, where **3**) it is decarboxylated to produce the CO₂ which is transferred to the BS cells chloroplasts.

In CAM CO₂ fixation (Fig. 7), water splitting during the light-dependent reactions is strongly reduced (Niewiadomska *et al.*, 2011). As in C₄ NAD-Me subtype CO₂ fixation, the organic acid sequence of oxaloacetate, malate, and malic acid acts as the main proton source for the light-independent reactions in CAM plants (Winter, K & Smith, JAC, 1996). Unlike in C₄ CO₂ fixation, the synthesis of these organic acids takes place in the same cells as the final CO₂ fixation, but is separated in time during the night (Winter, K & Smith, J, 1996). During the day, NADH is produced by the decarboxylation of malate into CO₂ and pyruvate, and while pyruvate is transferred to the pool of storage carbohydrates, NADH and CO₂ are transferred to the chloroplasts for CO₂ assimilation (Winter, K & Smith, JAC, 1996). As photorespiration is also strongly reduced in CAM plants, it can be speculated that organic acid cycle reactions are responsible for the

observed ^2H enrichment (Fig. 1, Table 5). In facultative CAM plants, PS II activity remains high in the absence of sufficient drought and light stress, allowing C_3 -type CO_2 fixation. Consequently, a high percentage of H^+ for CO_2 fixation comes from NADPH produced during PS II, resulting in C_3 -type ϵ_A and hence $\delta^2\text{H}$ of sugar and cellulose, as observed in *D. cooperi* and *M. cordifolium* (Table 5). This obscured the ^2H enriching ϵ_A from leaf water to leaf sugar in CAM plants, which was only seen after excluding these two species from the analysis (Tables 1, 2).

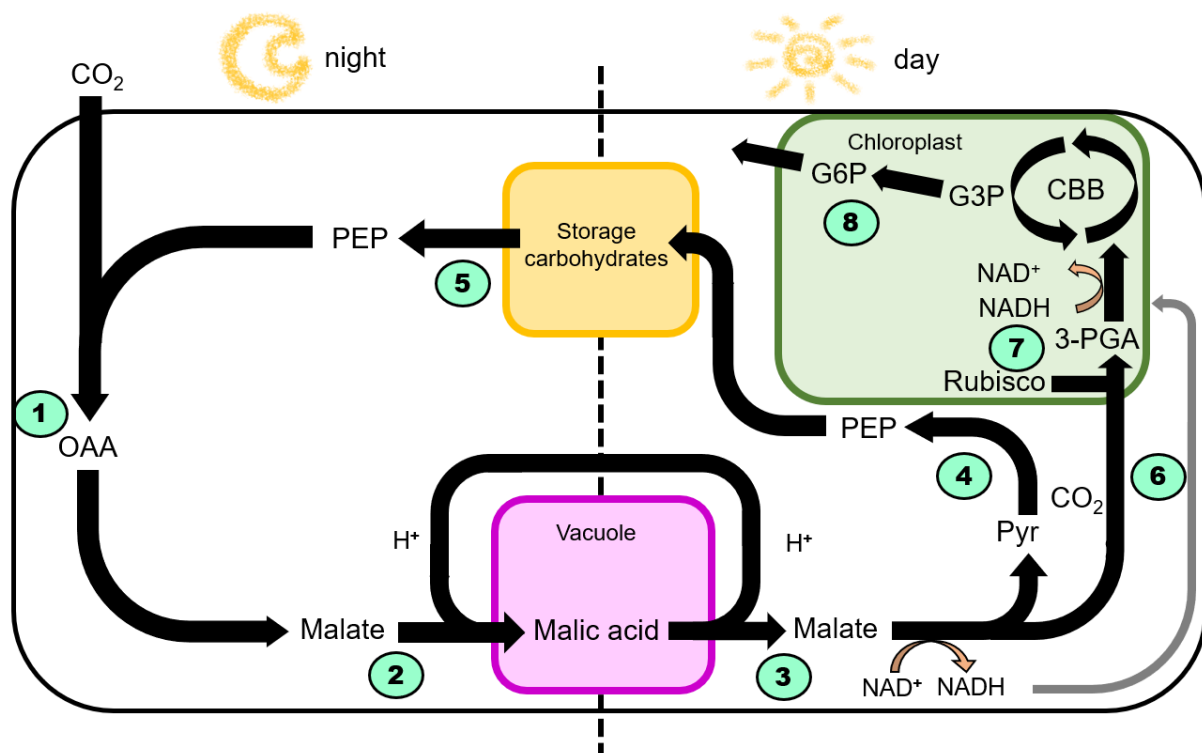


Figure 7: Simplified scheme of CAM CO_2 fixation, including only the steps crucial for hydrogen isotopes, modified from Schiller and Bräutigam (2021) and Winter and Smith (2022). The chemical reactions in CAM CO_2 fixation are temporally separated, with the primary CO_2 fixation (steps 1, 2, and 5) occurring during the night, and the carbohydrate synthesis (steps 3, 4, 6, 7, and 8) during the day (Winter, K & Smith, J, 1996; Winter, K & Smith, JAC, 1996). During the night, 1) CO_2 is taken up via the stomata and used to carboxylate PEP by PEPC, forming OAA as a H^+ carrier. Subsequently, 2) malate is formed out of OAA, which is eventually being stored as malic acid in the cell's vacuole. During the day, 3) malic acid is exported out of the

vacuole, transformed into malate and decarboxylated in the cytoplasm, releasing CO₂ and generating H⁺ for regenerating NADH, which is 6) transferred into the chloroplasts, where 7) the high CO₂ concentration inhibits photorespiration, and the NADH from the decarboxylation of the organic acid carrier is consumed for the CBB cycle. Eventually, 8) the fresh assimilates are exported out of the chloroplast and redistributed within the leaf.

Patterns and drivers of the heterotrophic ²H fractionation ϵ_H

The $\delta^{2\text{H}}$ of leaf sugar explains roughly 50% of the observed $\delta^{2\text{H}}$ in leaf cellulose of C₃, C₄ and CAM plants (Fig. 4), which has been observed by Holloway-Phillips *et al.* (2022), indicating a common mechanism for the heterotrophic ²H fractionation in all three types of CO₂ fixation. In contrast, $\delta^{2\text{H}}$ of leaf cellulose does only significantly correlate with ϵ_H in plants with C₄ CO₂ fixation. This could be explained by a different timing of the cellulose synthesis in C₄ compared with C₃ and CAM plants. Leaves of monocotyledones, which are the majority of the C₄ plants in this study, show a distinct diel growth pattern, growing mainly during the day (Poire *et al.*, 2010), while the leaves of dicots continue to grow during the night (Kronenberg *et al.*, 2021). This assumption is also supported by the steeper slope of the linear regression between $\delta^{2\text{H}}$ of the leaf cellulose and $\delta^{2\text{H}}$ of the leaf sugar in C₄ species (Fig. S10), which is close to the 1:1 line. Thus, the observed pattern might be caused by an imbalanced composition regarding monocotyledon and dicotyledon plant species among the three types of CO₂ fixation, rather than by the type of CO₂ fixation itself.

We observed significantly negative correlations between ϵ_A and ϵ_H in all three types of CO₂ fixation (R = -0.86, R² = 0.73, p = *** in C₃; R = -0.4, R² = 0.16, p = ** in C₄; and R = 0.66, R² = 0.44, p = *** in CAM CO₂ fixation; Fig. 4). An explanation for this strong negative correlation might be that, in C₃ plants, both the autotrophic ²H depletion and the heterotrophic ²H enrichment of

the sugar pool are affected by the metabolic activity of a plant. In this case, the more metabolically active a plant is, the stronger will be the ^2H depleting ϵ_A as well as the ^2H enriching ϵ_H . The strongly reduced explanatory power in C_4 plants might be due to the earlier discussed relative ^2H depletion of the water inside the BS cells (Zhou *et al.*, 2018), a strongly reduced transfer of the autotrophic ^2H depletion by PS II caused by the NADPH/NADH transfer between the M and BS cells, or the different timing of cellulose synthesis in monocotyledon plant species (Poire *et al.*, 2010). In this case, the reduced relationship between ϵ_A and ϵ_H in plants with CAM CO_2 fixation compared to plants with C_3 CO_2 fixation might be caused by the generally slower metabolic rate of these plants, causing a reduced ϵ_H , which was observed in species with strong CAM CO_2 fixation (Fig. S1).

For certain growing conditions, there were significant but inconsistent correlations between $\delta^2\text{H}$ of leaf cellulose and leaf water (Fig. S7). However, there were distinct patterns when examining the relationship between ϵ_H and $\delta^2\text{H}$ of leaf water in different types of CO_2 fixation (Fig. S8). In C_3 plants, ϵ_H did not correlate with $\delta^2\text{H}$ of leaf water. In C_4 plants, there was a positive correlation, while in CAM plants under high temperature, there was a negative correlation between ϵ_H and $\delta^2\text{H}$ of leaf water. These findings are surprising because the biochemical reactions responsible for ^2H fractionation during cellulose synthesis should not fundamentally differ among the three types of CO_2 fixation.

A possible impact on the various measured fractionation factor could be based on variations of the plants carbohydrate metabolism. For instance, the timing and reactions involving leaf transitory starch dynamics varies in plants with C_3 , C_4 , and CAM CO_2 fixation (Weise *et al.*, 2011). One possible explanation for the negative correlation between ϵ_H and $\delta^2\text{H}$ of leaf water in CAM plants is a gradual contribution of C_3 and CAM CO_2 fixation among different species. Notably, excluding the two facultative CAM species (Fig. S1, Table S1) resulted in lower ϵ_H values, suggesting that autotrophic ^2H fractionation could be influenced by a plant's metabolic rate. CAM plants

are known to have lower growth rates and metabolic activity than plants with C₃ and C₄ CO₂ fixation (Lüttge 2004).

Compound specific ²H response to changes in temperature and VPD is highly species specific

Comparing the temperature and VPD responses of C₃, C₄ and CAM plants across all species (Table 2), we found no general temperature and only minor VPD effects on $\delta^2\text{H}$ of leaf water, leaf sugar and leaf cellulose in C₃ and CAM plants (Fig. 3). However, we observed various significant species-specific responses of $\delta^2\text{H}$ of leaf water, leaf sugar and leaf cellulose, as well as their ε_A and ε_H , to changes in temperature and VPD (Tables 3, 4, 5). We suggest that the observed lack of general responses is caused by the generally high variability of $\delta^2\text{H}$, which masks temperature and VPD effects that can be seen at the species level.

In C₃ plants (Fig. 3), the observed species-specific changes might result from various processes, such as an up- or down-regulation of their photosynthetic activity (i.e. the light-dependent reactions), transpiration rate, increased rate of photorespiration or increased respiration rate caused by a higher metabolic activity (Sanchez-Bragado *et al.*, 2019; Holloway-Phillips *et al.*, 2022). This can depend on a plant's physiological response to changes in climatic conditions (Bolstad *et al.*, 2003), their species specific climate adaption (Cavieres *et al.*, 2000; Loveys *et al.*, 2002), but also to the amount of photosynthetic active radiation, water, and nutrient availability. Plants with C₄ CO₂ fixation pathways showed a much more limited response to changes in both temperature and VPD (Fig. 4). This might be due to the lower overall autotrophic ²H fractionation in C₄ compared to C₃ and CAM CO₂ fixation (Fig. 1). An interesting outlier among the tested C₄ plants was *Salsola soda*, a species already known to switch from C₃ to C₄ CO₂ fixation after its seedling stage (Lauterbach *et al.*, 2017). The increase in $\delta^2\text{H}$ of the leaf cellulose and ε_H observed here with increasing temperature and VPD are comparable to what was observed in some species with CAM CO₂ fixation

(Fig. 5). *S. soda* is a succulent annual halophyte that is native to the Mediterranean Basin. Thus, the species is clearly strongly adapted to water limitation, and one can speculate that it might perform some level of CAM CO₂ fixation in response to harsher climatic conditions. Similarly, we assume that the observed variation in some of the CAM plants was triggered by an up-regulation of CAM with a simultaneous down regulation of C₃ CO₂ fixation in response to higher temperature and VPD.

Conclusions

We demonstrated that the different biochemical reactions involved in C₃, C₄ and CAM CO₂ fixation are the principal drivers of their autotrophic ²H fractionation as well as their response to changes in climatic conditions. While ε_H is probably based on the same reactions among all plants, it is likely shaped by processes such as a plant's metabolic activity, and the diel timing of its growth. The diversity of the processes involved in ²H fractionation in plant carbohydrates might make it less straightforward to implement δ²H analysis in a broad range of studies. However, it might become a tool for various plant ecophysiological investigations, such as studies on facultative CAM or plant internal CO₂ dynamics.

Acknowledgements

Our work was supported by the SNF Ambizione project "TreeCarbo" (No. 179978, granted to MML).

References

- Allen JF, de Paula WB, Puthiyaveetil S, Nield J. 2011.** A structural phylogenetic map for chloroplast photosynthesis. *Trends in Plant Science* **16**(12): 645-655.
- Arosio T, Ziehmer-Wenz M, Nicolussi K, Schlüchter C, Leuenberger M. 2020.** Larch Cellulose Shows Significantly Depleted Hydrogen Isotope Values With Respect to Evergreen Conifers in Contrast to Oxygen and Carbon Isotopes. *Frontiers in Earth Science* **8**(579).

- Augusti A, Betson TR, Schleucher J. 2006.** Hydrogen exchange during cellulose synthesis distinguishes climatic and biochemical isotope fractionations in tree rings. *New Phytologist* **172**(3): 490-499.
- Augusti A, Betson TR, Schleucher J. 2008.** Deriving correlated climate and physiological signals from deuterium isotopomers in tree rings. *Chemical Geology* **252**(1-2): 1-8.
- Bauwe H. 2011.** Photorespiration: The Bridge to C₄ Photosynthesis. Chapter in **Raghavendra AS, Sage RF 2011.** *C₄ photosynthesis and related CO₂ concentrating mechanisms*. Springer: 81-108
- Bauwe H. 2018.** Photorespiration—Damage Repair Pathway of the Calvin-Benson Cycle. *Annual Plant Reviews* **50**: 293-342.
- Bolstad PV, Reich P, Lee T. 2003.** Rapid temperature acclimation of leaf respiration rates in *Quercus alba* and *Quercus rubra*. *Tree Physiology* **23**(14): 969-976.
- Busch FA. 2020.** Photorespiration in the context of Rubisco biochemistry, CO₂ diffusion and metabolism. *The Plant Journal* **101**(4): 919-939.
- Cavieres LA, Rada F, Azócar A, García-Núñez C, Cabrera HM. 2000.** Gas exchange and low temperature resistance in two tropical high mountain tree species from the Venezuelan Andes. *Acta Oecologica* **21**(3): 203-211.
- Cernusak LA, Barbour MM, Arndt SK, Cheesman AW, English NB, Feild TS, Helliker BR, Holloway-Phillips MM, Holtum JAM, Kahmen A, et al. 2016.** Stable isotopes in leaf water of terrestrial plants. *Plant, Cell & Environment* **39**(5): 1087-1102.
- Chen Q, Wang B, Ding H, Zhang J, Li S. 2019.** The role of NADP-malic enzyme in plants under stress. *Plant Science* **281**: 206-212.
- Coplen TB. 2011.** Guidelines and recommended terms for expression of stable-isotope-ratio and gas-ratio measurement results. *Rapid Communications in Mass Spectrometry* **25**(17): 2538-2560.

- Cormier M-A, Werner RA, Sauer PE, Gröcke DR, Leuenberger MC, Wieloch T, Schleucher J, Kahmen A. 2018.** ^2H -fractionations during the biosynthesis of carbohydrates and lipids imprint a metabolic signal on the $\delta^2\text{H}$ values of plant organic compounds. *New Phytologist* **218**(2): 479-491.
- Cramer WA, Hasan SS, Yamashita E. 2011.** The Q cycle of cytochrome bc complexes: a structure perspective. *Biochimica et Biophysica Acta (BBA)-Bioenergetics* **1807**(7): 788-802.
- Diao H, Schuler P, Goldsmith GR, Siegwolf RT, Saurer M, Lehmann MM. 2022.** On uncertainties in plant water isotopic composition following extraction by cryogenic vacuum distillation. *Hydrology and Earth System Sciences Discussions*: 1-17.
- dos Santos TB, Ribas AF, de Souza SGH, Budzinski IGF, Domingues DS. 2022.** Physiological responses to drought, salinity, and heat stress in plants: a review. *Stresses* **2**(1): 113-135.
- Drincovich MaF, Casati P, Andreo CS. 2001.** NADP-malic enzyme from plants: a ubiquitous enzyme involved in different metabolic pathways. *FEBS letters* **490**(1-2): 1-6.
- Estep MF, Hoering TC. 1981.** Stable Hydrogen Isotope Fractionations during Autotrophic and Mixotrophic Growth of Microalgae. *Plant Physiology* **67**(3): 474-477.
- Falkner G, Horner F, Werdan K, Heldt HW. 1976.** pH changes in the cytoplasm of the blue-green alga *Anacystis nidulans* caused by light-dependent proton flux into the thylakoid space. *Plant Physiology* **58**(6): 717-718.
- Farquhar GD, Cernusak LA, Barnes B. 2007.** Heavy water fractionation during transpiration. *Plant Physiology* **143**(1): 11-18.

- Ferreira KN, Iverson TM, Maghlaoui K, Barber J, Iwata S. 2004.** Architecture of the photosynthetic oxygen-evolving center. *Science* **303**(5665): 1831-1838.
- Filot MS, Leuenberger M, Pazdur A, Boettger T. 2006.** Rapid online equilibration method to determine the D/H ratios of non-exchangeable hydrogen in cellulose. *Rapid Communications in Mass Spectrometry* **20**(22): 3337-3344.
- Gehre M, Geilmann H, Richter J, Werner R, Brand W. 2004.** Continuous flow $^2\text{H}/^1\text{H}$ and $^{18}\text{O}/^{16}\text{O}$ analysis of water samples with dual inlet precision. *Rapid Communications in Mass Spectrometry* **18**(22): 2650-2660.
- Grossiord C, Buckley TN, Cernusak LA, Novick KA, Poulter B, Siegwolf RT, Sperry JS, McDowell NG. 2020.** Plant responses to rising vapor pressure deficit. *New Phytologist* **226**(6): 1550-1566.
- Heldt H 1980.** [57] Measurement of metabolite movement across the envelope and of the pH in the stroma and the thylakoid space in intact chloroplasts. *Methods in Enzymology*: Elsevier, 604-613.
- Heldt HW, Werdan K, Milovancev M, Geller G. 1973.** Alkalization of the chloroplast stroma caused by light-dependent proton flux into the thylakoid space. *Biochimica et Biophysica Acta (BBA)-Bioenergetics* **314**(2): 224-241.
- Höfer MU, Santore UJ, Westhoff P. 1992.** Differential accumulation of the 10-, 16- and 23-kDa peripheral components of the water-splitting complex of photosystem II in mesophyll and bundle-sheath chloroplasts of the dicotyledonous C_4 plant *Flaveria trinervia* (Spreng.) C. Mohr. *Planta* **186**(2): 304-312.
- Holloway-Phillips M, Baan J, Nelson DB, Lehmann MM, Tcherkez G, Kahmen A. 2022.** Species variation in the hydrogen isotope composition of leaf cellulose is mostly driven by isotopic variation in leaf sucrose. *Plant, Cell & Environment* **45**(9): 2636-2651.

- Kronenberg L, Yates S, Ghiasi S, Roth L, Friedli M, Ruckle ME, Werner RA, Tschurr F, Binggeli M, Buchmann N. 2021.** Rethinking temperature effects on leaf growth, gene expression and metabolism: Diel variation matters. *Plant, Cell & Environment* **44**(7): 2262-2276.
- Kumar V, Sharma A, Soni JK, Pawar N. 2017.** Physiological response of C₃, C₄ and CAM plants in changeable climate. *The Pharma Innovation* **6**(9, Part B): 70.
- Lauterbach M, Billakurthi K, Kadereit G, Ludwig M, Westhoff P, Gowik U. 2017.** C₃ cotyledons are followed by C₄ leaves: intra-individual transcriptome analysis of *Salsola soda* (Chenopodiaceae). *Journal of Experimental Botany* **68**(2): 161-176.
- Lehmann MM, Egli M, Brinkmann N, Werner RA, Saurer M, Kahmen A. 2020.** Improving the extraction and purification of leaf and phloem sugars for oxygen isotope analyses. *Rapid Communications in Mass Spectrometry* **34**(19): e8854.
- Lehmann MM, Schuler P, Cormier M-A, Allen ST, Leuenberger M, Voelker S. 2022.** The Stable Hydrogen Isotopic Signature: From Source Water to Tree Rings. Chapter in **Siegwolf RT, Brooks JR, Roden J, Saurer M. 2022.** *Stable Isotopes in Tree Rings: Inferring Physiological, Climatic and Environmental Responses*. Springer: 331-359
- Loveys B, Scheurwater I, Pons T, Fitter A, Atkin O. 2002.** Growth temperature influences the underlying components of relative growth rate: an investigation using inherently fast-and slow-growing plant species. *Plant, Cell & Environment* **25**(8): 975-988.
- Ludwig M. 2016.** The roles of organic acids in C₄ photosynthesis. *Frontiers in Plant Science* **7**: 647.
- Luo Y-H, Steinberg L, Suda S, Kumazawa S, Mitsui A. 1991.** Extremely low D/H ratios of photoproduced hydrogen by cyanobacteria. *Plant and Cell Physiology* **32**(6): 897-900.

- Luo Y-H, Sternberg L. 1991.** Deuterium heterogeneity in starch and cellulose nitrate of CAM and C₃ plants. *Phytochemistry* **30**(4): 1095-1098.
- Lüttge U. 2004.** Ecophysiology of Crassulacean Acid Metabolism (CAM). *Annals of Botany* **93**(6): 629-652
- Meierhoff K, Westhoff P. 1993.** Differential biogenesis of photosystem II in mesophyll and bundle-sheath cells of monocotyledonous NADP-malic enzyme-type C₄ plants: the non-stoichiometric abundance of the subunits of photosystem II in the bundle-sheath chloroplasts and the translational activity of the plastome-encoded genes. *Planta* **191**(1): 23-33.
- Nelson N, Ben-Shem A. 2005.** The structure of photosystem I and evolution of photosynthesis. *Bioessays* **27**(9): 914-922.
- Niewiadomska E, Bilger W, Gruca M, Mulisch M, Miszalski Z, Krupinska K. 2011.** CAM-related changes in chloroplastic metabolism of *Mesembryanthemum crystallinum* L. *Planta* **233**(2): 275-285.
- Orsenigo M, Patrignani G, Rascio N. 1997.** Ecophysiology of C₃, C₄ and CAM plants. Chapter in **Pessaraki M. 1997.** *Handbook of Photosynthesis*: 1-25.
- Oswald A, Streubel M, Ljungberg U, Hermans J, Eskins K, Westhoff P. 1990.** Differential biogenesis of photosystem-II in mesophyll and bundle-sheath cells of 'malic'enzyme NADP⁺-type C₄ plants: A comparative protein and RNA analysis. *European Journal of Biochemistry* **190**(1): 185-194.
- Poire R, Wiese-Klinkenberg A, Parent B, Mielewczik M, Schurr U, Tardieu F, Walter A. 2010.** Diel time-courses of leaf growth in monocot and dicot species: endogenous rhythms and temperature effects. *Journal of Experimental Botany* **61**(6): 1751-1759.

- R.Core.Team** 2023. R: A language and environment for statistical computing. *R Foundation for Statistical Computing, Vienna, Austria.*
- Rao X, Dixon RA.** 2016. The differences between NAD-ME and NADP-ME subtypes of C₄ photosynthesis: more than decarboxylating enzymes. *Frontiers in Plant Science* 7: 1525.
- Rinne KT, Saurer M, Streit K, Siegwolf RT.** 2012. Evaluation of a liquid chromatography method for compound-specific $\delta^{13}\text{C}$ analysis of plant carbohydrates in alkaline media. *Rapid Communications in Mass Spectrometry* 26(18): 2173-2185.
- Roden JS, Lin G, Ehleringer JR.** 2000. A mechanistic model for interpretation of hydrogen and oxygen isotope ratios in tree-ring cellulose. *Geochimica et Cosmochimica Acta* 64(1): 21-35.
- Sage RF, Monson RK.** 1998. *C₄ plant biology*: Elsevier.
- Sanchez-Bragado R, Serret MD, Marimon RM, Bort J, Araus JL.** 2019. The Hydrogen Isotope Composition $\delta^2\text{H}$ Reflects Plant Performance. *Plant Physiology* 180(2): 793-812.
- Schiller K, Bräutigam A.** 2021. Engineering of crassulacean acid metabolism. *Annual Review of Plant Biology* 72: 77-103.
- Schmidt H-L, Werner RA, Eisenreich W.** 2003. Systematics of ^2H patterns in natural compounds and its importance for the elucidation of biosynthetic pathways. *Phytochemistry Reviews* 2(1): 61-85.
- Schuler P, Cormier MA, Werner RA, Buchmann N, Gessler A, Vitali V, Saurer M, Lehmann MM.** 2022. A high temperature water vapor equilibration method to determine non-exchangeable hydrogen isotope ratios of sugar, starch, and cellulose. *Plant, Cell & Environment* 45(1): 12-22.
- Schuler P, Vitali V, Saurer M, Gessler A, Buchmann N, Marco M L.** 2023. Hydrogen isotope fractionation in carbohydrates of leaves and xylem

- tissues follows distinct phylogenetic patterns: a common garden experiment with 73 tree and shrub species. *New Phytologist* **239**(2): 547-561.
- Seelert H, Poetsch A, Dencher NA, Engel A, Stahlberg H, Müller DJ. 2000.** Proton-powered turbine of a plant motor. *Nature* **405**(6785): 418-419.
- Smith BN, Ziegler H, Lipp J. 1991.** Isotopic evidence for mesophyll reduction in *Zea mays*, an NADP-Malic enzyme plant. *Naturwissenschaften* **78**(8): 358-359.
- Sternberg L, DeNiro MJ. 1983.** Isotopic composition of cellulose from C₃, C₄, and CAM plants growing near one another. *Science* **220**(4600): 947-949.
- Sternberg L, Deniro MJ, Ajie H. 1984.** Stable hydrogen isotope ratios of saponifiable lipids and cellulose nitrate from CAM, C₃ and C₄ plants. *Phytochemistry* **23**(11): 2475-2477.
- Weise SE, van Wijk KJ, Sharkey TD. 2011.** The role of transitory starch in C₃, CAM, and C₄ metabolism and opportunities for engineering leaf starch accumulation. *Journal of Experimental Botany* **62**(9): 3109-3118.
- Wieloch T, Augusti A, Schleucher J. 2022a.** Anaplerotic flux into the Calvin-Benson cycle: hydrogen isotope evidence for in vivo occurrence in C₃ metabolism. *New Phytologist* **234**(2): 405-411.
- Wieloch T, Grabner M, Augusti A, Serk H, Ehlers I, Yu J, Schleucher J. 2022b.** Metabolism is a major driver of hydrogen isotope fractionation recorded in tree-ring glucose of *Pinus nigra*. *New Phytologist* **234**(2): 449-461.
- Winter K. 2019.** Ecophysiology of constitutive and facultative CAM photosynthesis. *Journal of Experimental Botany* **70**(22): 6495-6508.
- Winter K, Garcia M, Holtum JA. 2008.** On the nature of facultative and constitutive CAM: environmental and developmental control of CAM

- expression during early growth of *Clusia*, *Kalanchoë*, and *Opuntia*. *Journal of Experimental Botany* **59**(7): 1829-1840.
- Winter K, Smith J. 1996.** An introduction to crassulacean acid metabolism. Biochemical principles and ecological diversity. Chapter in **Winter K, Smith JAC. 1996.** *Crassulacean Acid Metabolism: Biochemistry, Ecophysiology and Evolution*: Springer: 1-13.
- Winter K, Smith JAC. 1996.** Crassulacean acid metabolism: current status and perspectives. Chapter in **Winter K, Smith JAC. 1996.** *Crassulacean Acid Metabolism: Biochemistry, Ecophysiology and Evolution*: Springer: 389-426.
- Winter K, Smith JAC. 2022.** CAM photosynthesis: the acid test. *New Phytologist* **233**(2): 599-609.
- Yakir D. 1992.** Variations in the natural abundance of oxygen-18 and deuterium in plant carbohydrates. *Plant, Cell & Environment* **15**(9): 1005-1020.
- Yakir D, DeNiro MJ. 1990.** Oxygen and hydrogen isotope fractionation during cellulose metabolism in *Lemna gibba* L. *Plant Physiology* **93**(1): 325-332.
- Yamori W, Hikosaka K, Way DA. 2014.** Temperature response of photosynthesis in C₃, C₄, and CAM plants: temperature acclimation and temperature adaptation. *Photosynthesis Research* **119**(1): 101-117.
- Zhou Y, Grice K, Stuart-Williams H, Hocart CH, Gessler A, Farquhar GD. 2016.** Hydrogen isotopic differences between C₃ and C₄ land plant lipids: consequences of compartmentation in C₄ photosynthetic chemistry and C₃ photorespiration. *Plant, Cell & Environment* **39**(12): 2676-2690.
- Zhou Y, Zhang B, Stuart-Williams H, Grice K, Hocart CH, Gessler A, Kayler ZE, Farquhar GD. 2018.** On the contributions of photorespiration and

compartmentation to the contrasting intramolecular ^2H profiles of C_3 and C_4 plant sugars. *Phytochemistry* **145**: 197-206.

Ziegler H, Osmond C, Stichler W, Trimborn P. 1976. Hydrogen isotope discrimination in higher plants: correlations with photosynthetic pathway and environment. *Planta* **128**(1): 85-92.

Supporting Information

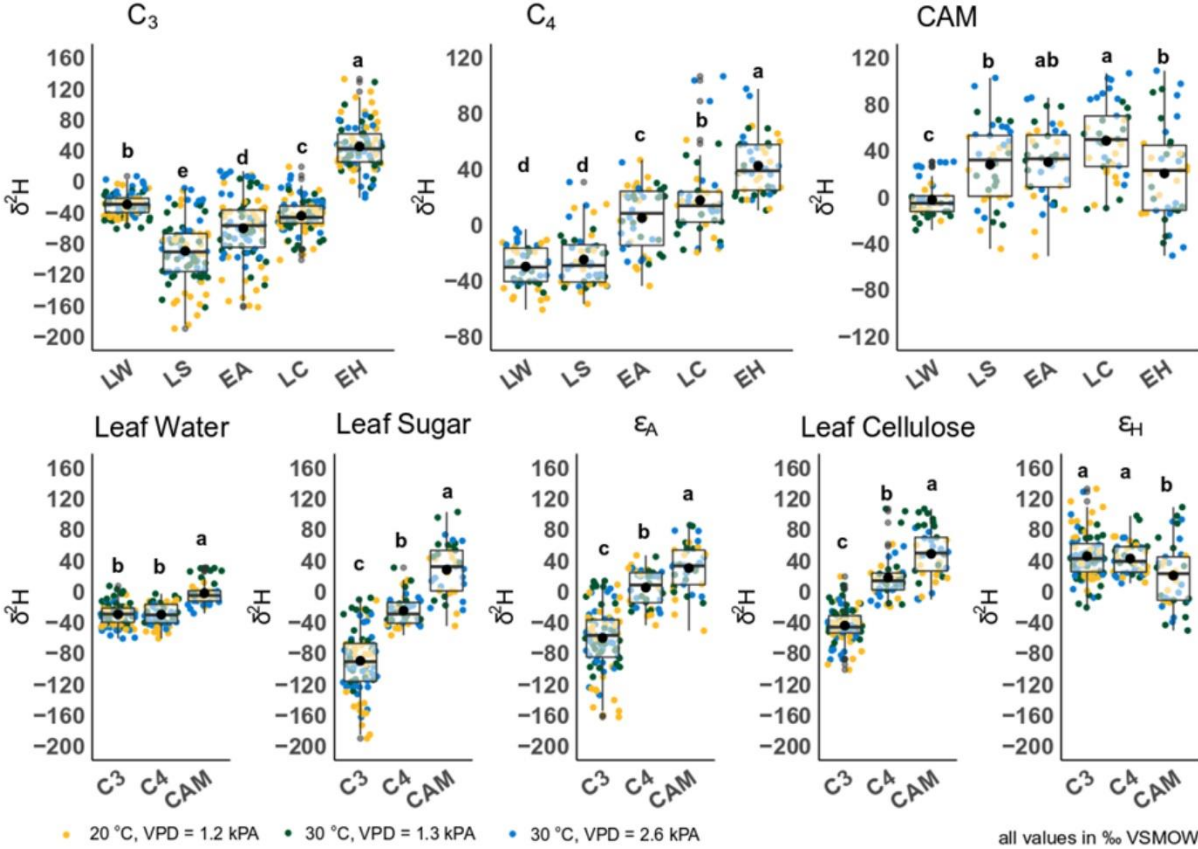


Figure S1: Comparison of the $\delta^2\text{H}$ values and ^2H fractionation factors within (top row) and between (bottom row) the three types of CO_2 fixation pathways and the three climate treatments (yellow points 20°C , $\text{VPD} = 1.2 \text{ kPa}$; green points 30°C , $\text{VPD} = 1.3 \text{ kPa}$; blue points 30°C , $\text{VPD} = 2.6 \text{ kPa}$). Abbreviations: LW = Leaf Water, LS = Leaf Sugar, ϵ_A and EA = autotrophic ^2H fractionation, LC = Leaf Cellulose, ϵ_H and EH = heterotrophic ^2H fractionation. Facultative CAM species *D. cooperi* and *M. cordifolium* removed from analys

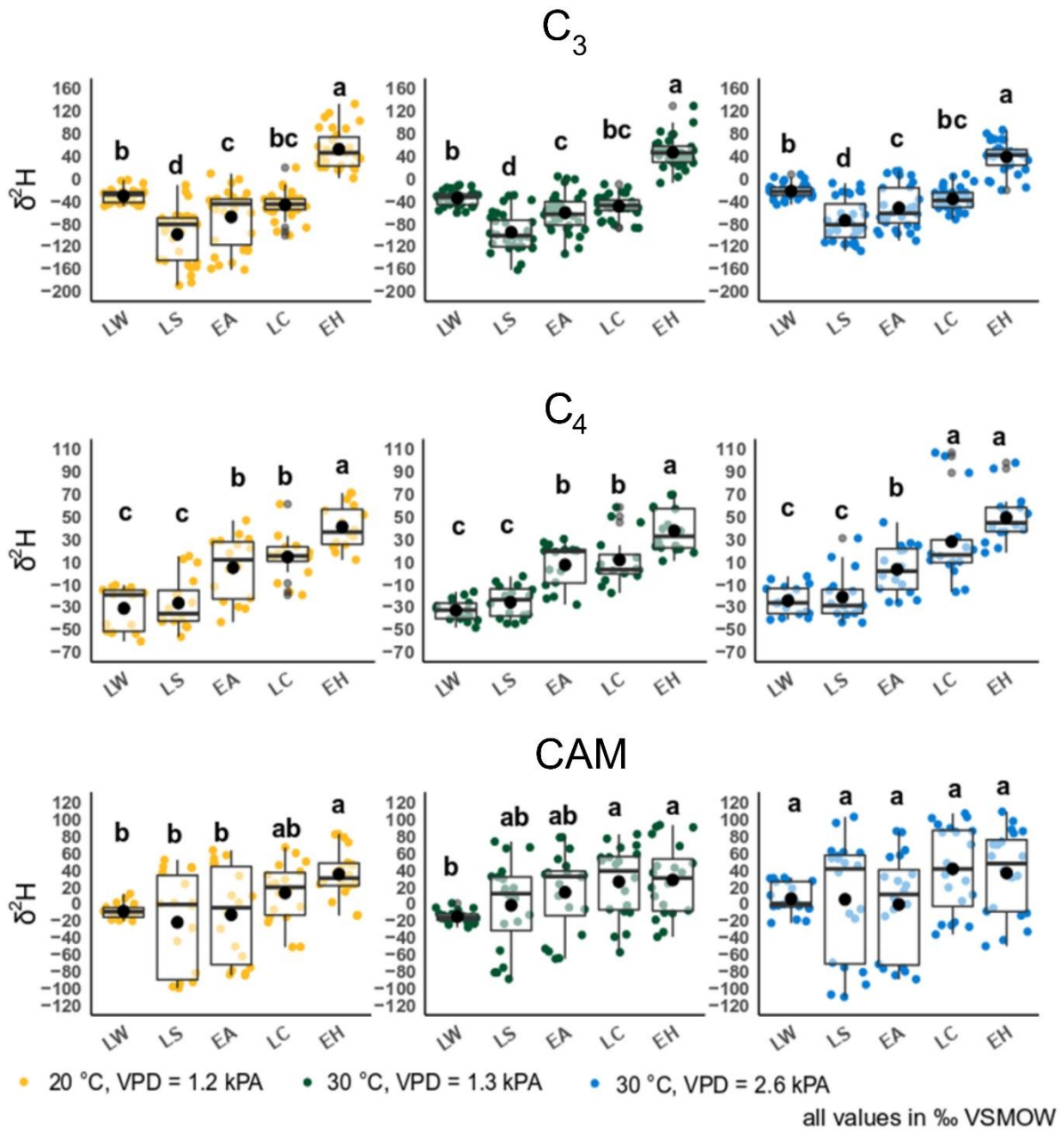


Figure S2: Combined $\delta^2\text{H}$ values of all tested plant species within a CO_2 fixation pathway (i.e., C_3 , C_4 , CAM) of leaf water (LW), leaf sugar (LS), ϵ_A (EA), leaf cellulose (LC) and ϵ_H (EH) in response to changes in temperature and VPD.

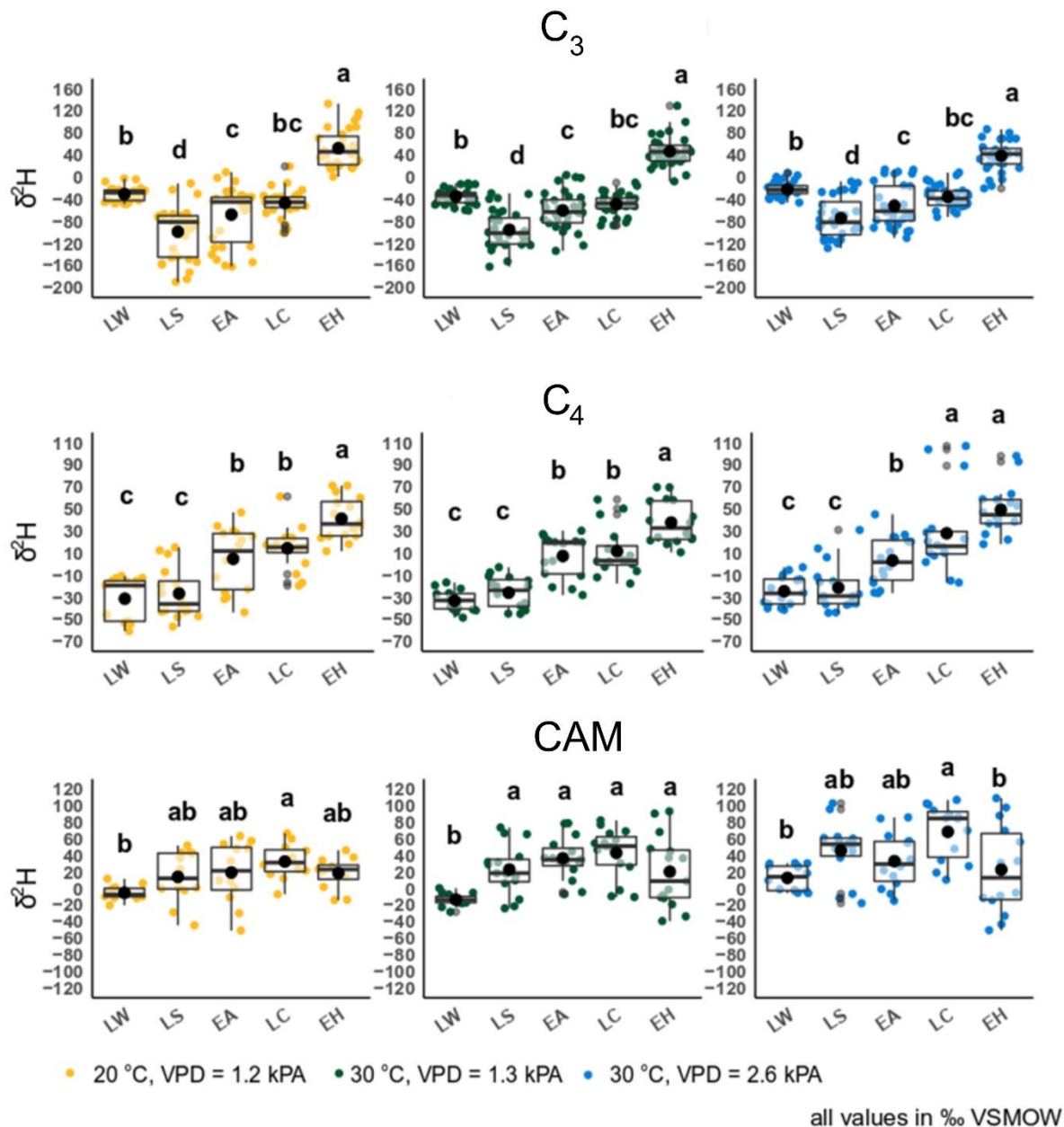


Figure S3: Combined $\delta^2\text{H}$ values of all tested plant species within a CO₂ fixation pathway (i.e., C₃, C₄, CAM) of leaf water (LW), leaf sugar (LS), ϵ_A (EA), leaf cellulose (LC) and ϵ_H (EH) in response to changes in temperature and VPD. The two facultative CAM species *D. cooperi* and *M. cordifolium* removed from analysis

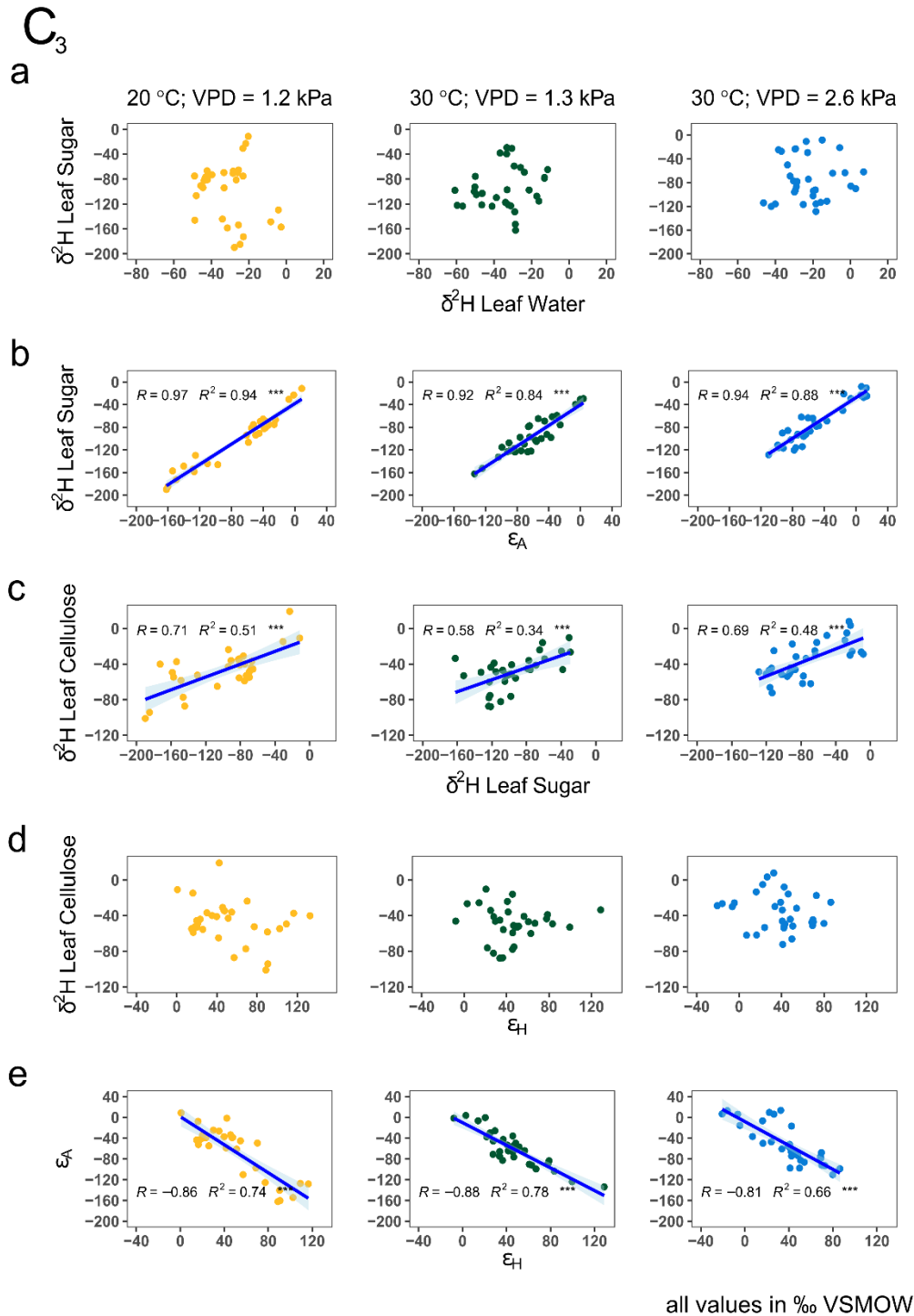


Figure S4: Regression analysis showing the effect of changing temperature and VPD on C₃ CO₂ fixation: a) $\delta^2\text{H}$ leaf sugar / $\delta^2\text{H}$ leaf water; b) $\delta^2\text{H}$ leaf sugar / ϵ_A ; c) $\delta^2\text{H}$ leaf cellulose / $\delta^2\text{H}$ leaf sugar; d) $\delta^2\text{H}$ leaf cellulose / ϵ_H ; e) ϵ_A / ϵ_H . The blue line represents the linear regression. Asterisks indicating significant differences (*, $P \leq 0.05$; **, $P \leq 0.01$; ***, $P \leq 0.001$).

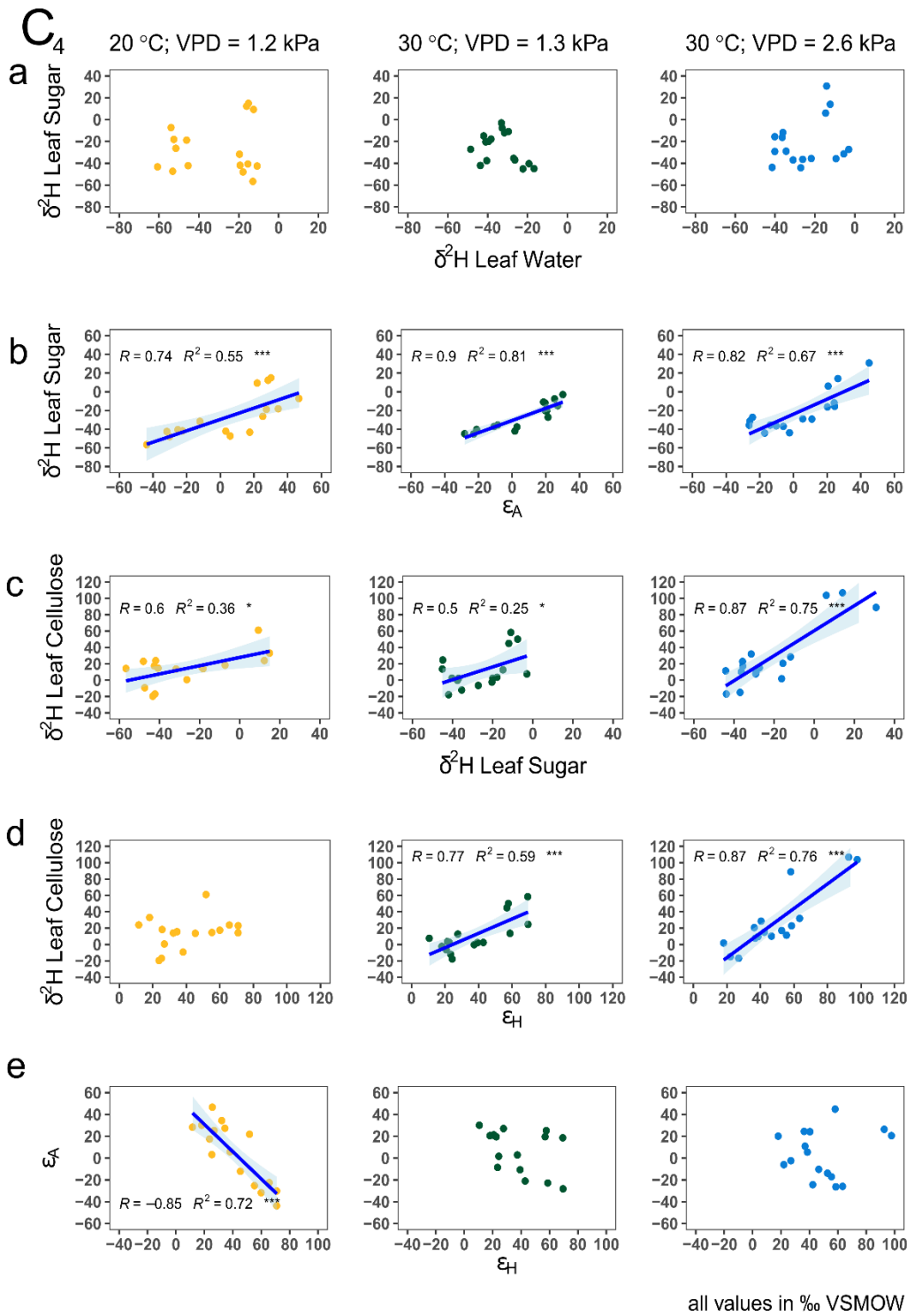


Figure S5: Regression analysis showing the effect of changing temperature and VPD on C_4 CO_2 fixation: a) δ^2H leaf sugar / δ^2H leaf water; b) δ^2H leaf sugar / ϵ_A ; c) δ^2H leaf cellulose / δ^2H leaf sugar; d) δ^2H leaf cellulose / ϵ_H ; e) ϵ_A / ϵ_H . The blue line represents the linear regression. Asterisks indicating significant differences (*, P ≤ 0.05; **, P ≤ 0.01; ***, P ≤ 0.001).

CAM

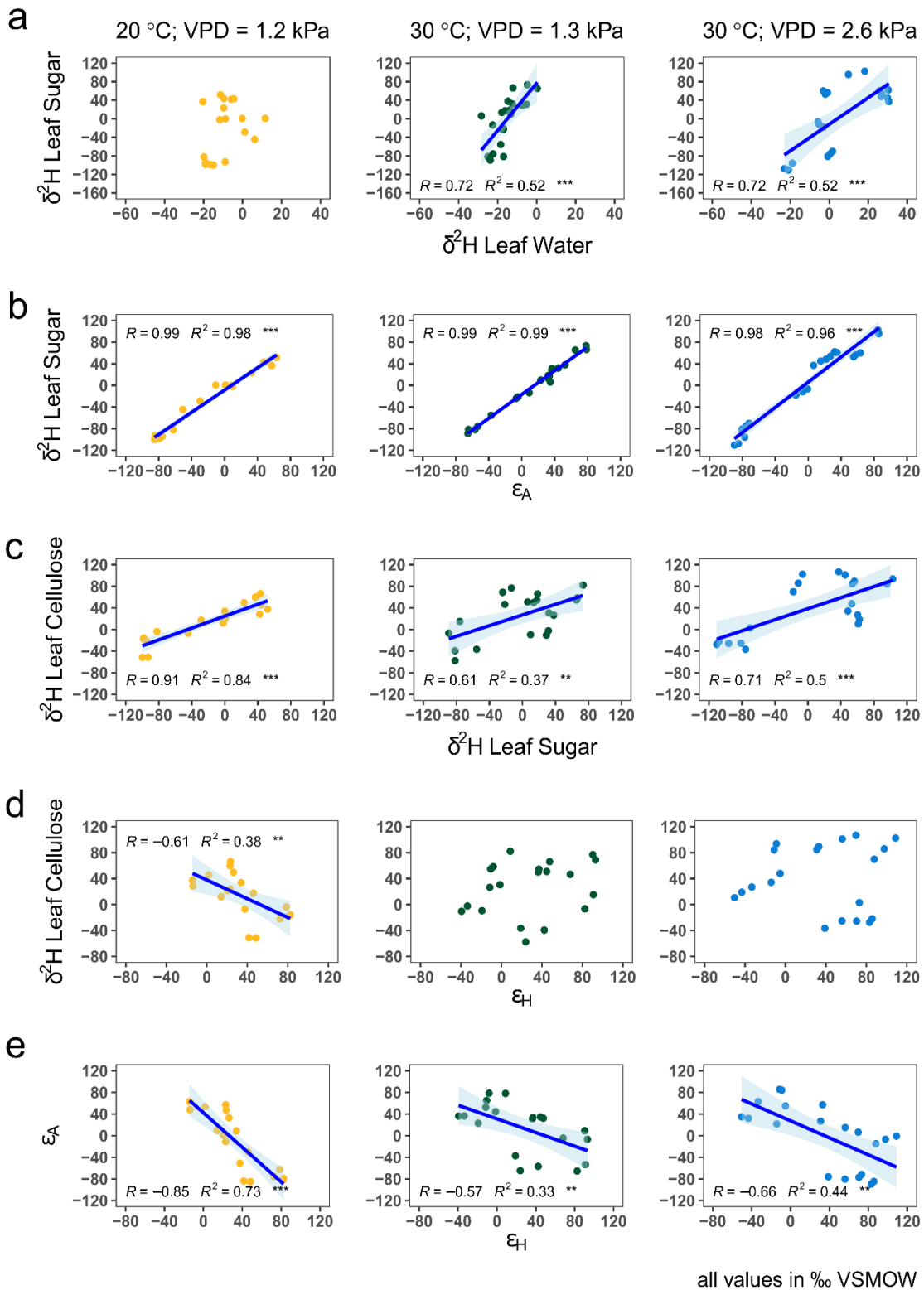


Figure S6: Regression analysis showing the effect of changing temperature and VPD on CAM CO₂ fixation: a) $\delta^2\text{H}$ leaf sugar / $\delta^2\text{H}$ leaf water; b) $\delta^2\text{H}$ leaf

sugar / ϵ_A ; c) $\delta^2\text{H}$ leaf cellulose / $\delta^2\text{H}$ leaf sugar; d) $\delta^2\text{H}$ leaf cellulose / ϵ_H ; e) ϵ_A / ϵ_H . The blue line represents the linear regression. Asterisks indicating significant differences (*, $P \leq 0.05$; **, $P \leq 0.01$; ***, $P \leq 0.001$).

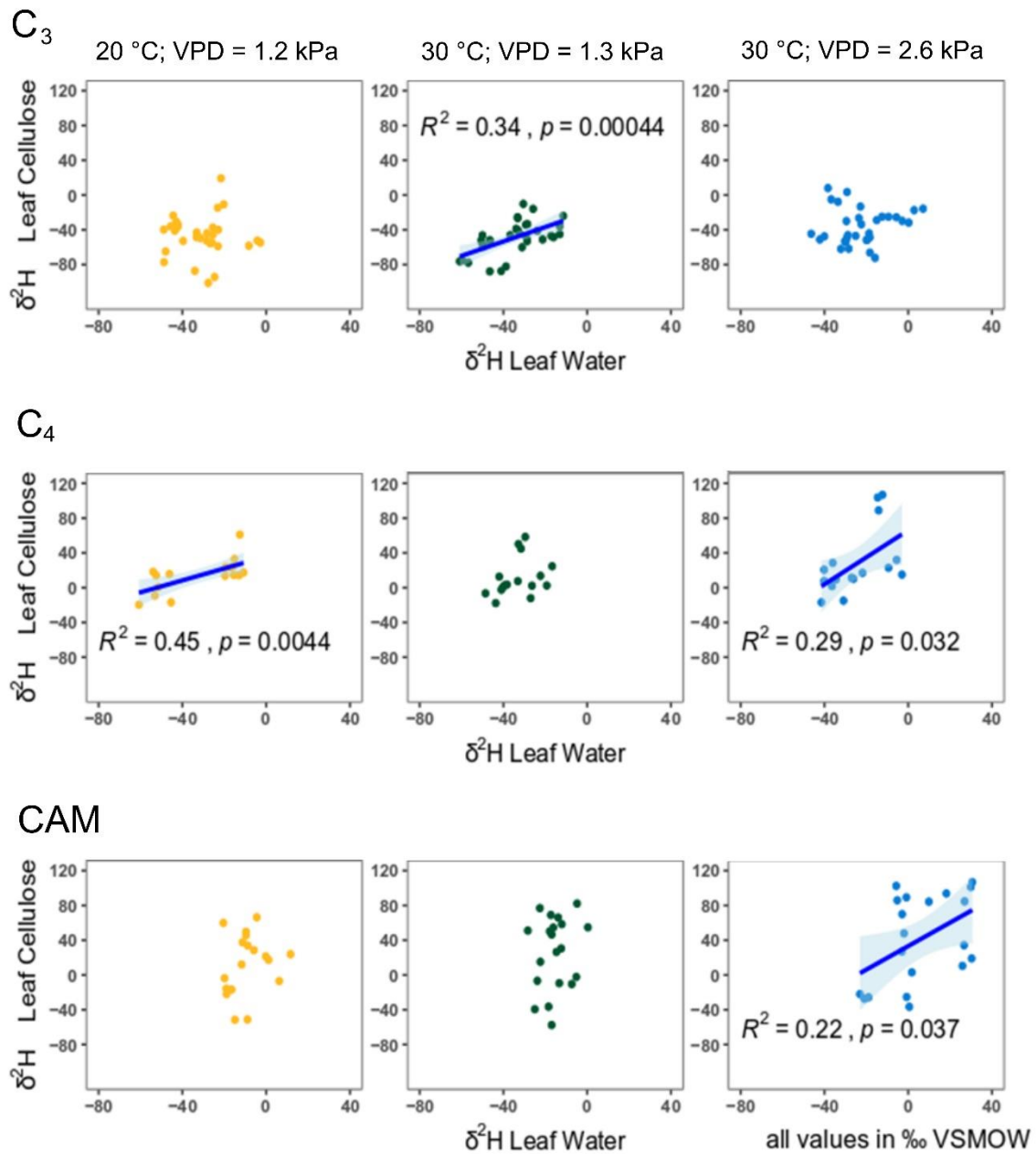


Figure S7: Correlation between $\delta^2\text{H}$ of leaf cellulose and leaf water between the three treatments and the three types of CO_2 fixation. The blue line represents the linear regression.

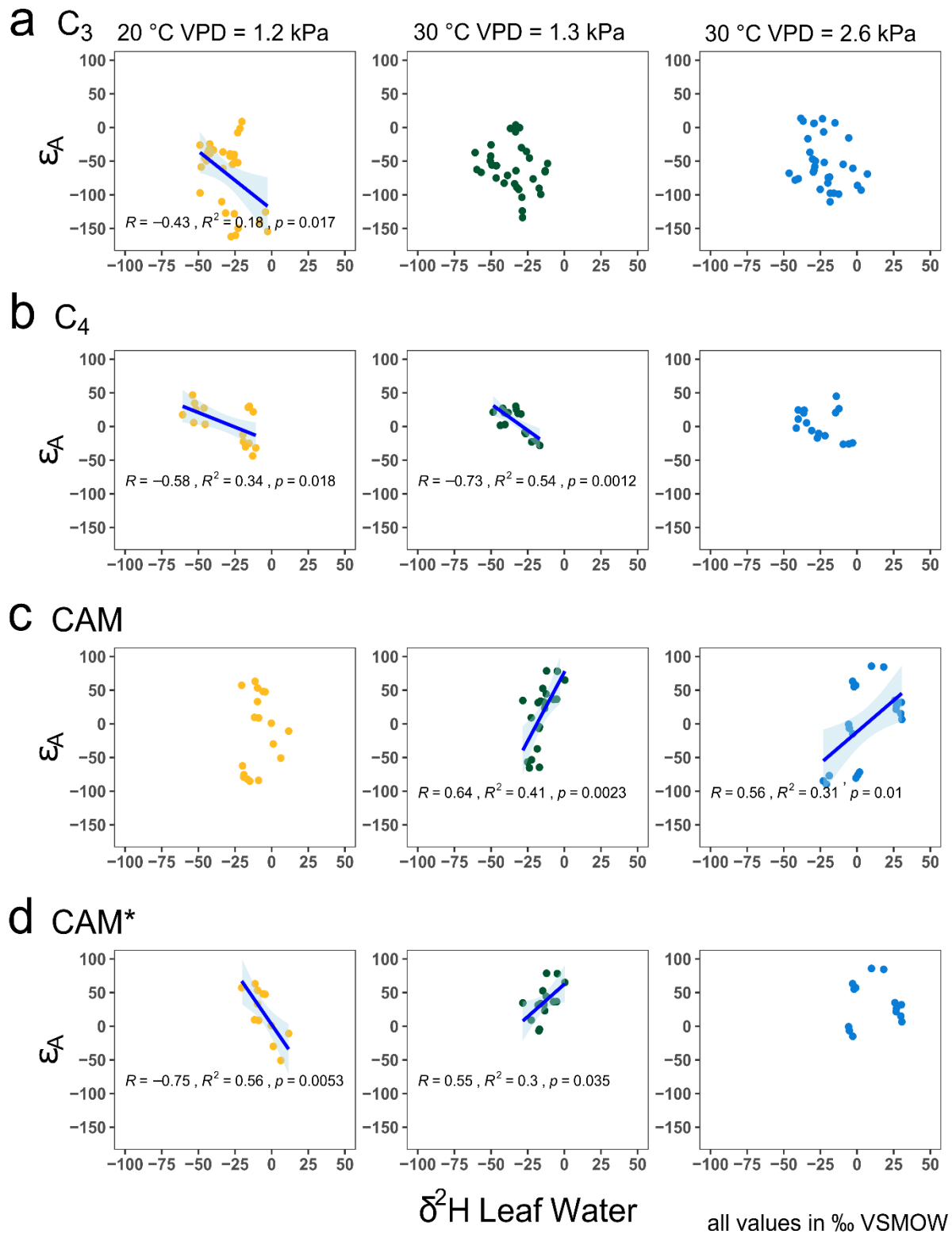


Figure S8: Correlation between ϵ_A and δ^2H of leaf water of a) C_3 , b) C_4 , c) CAM plants, as well as d) CAM plants excluding the two facultative CAM species *D. cooperi* and *M. cordifolium* (CAM*), separated by growing condition.

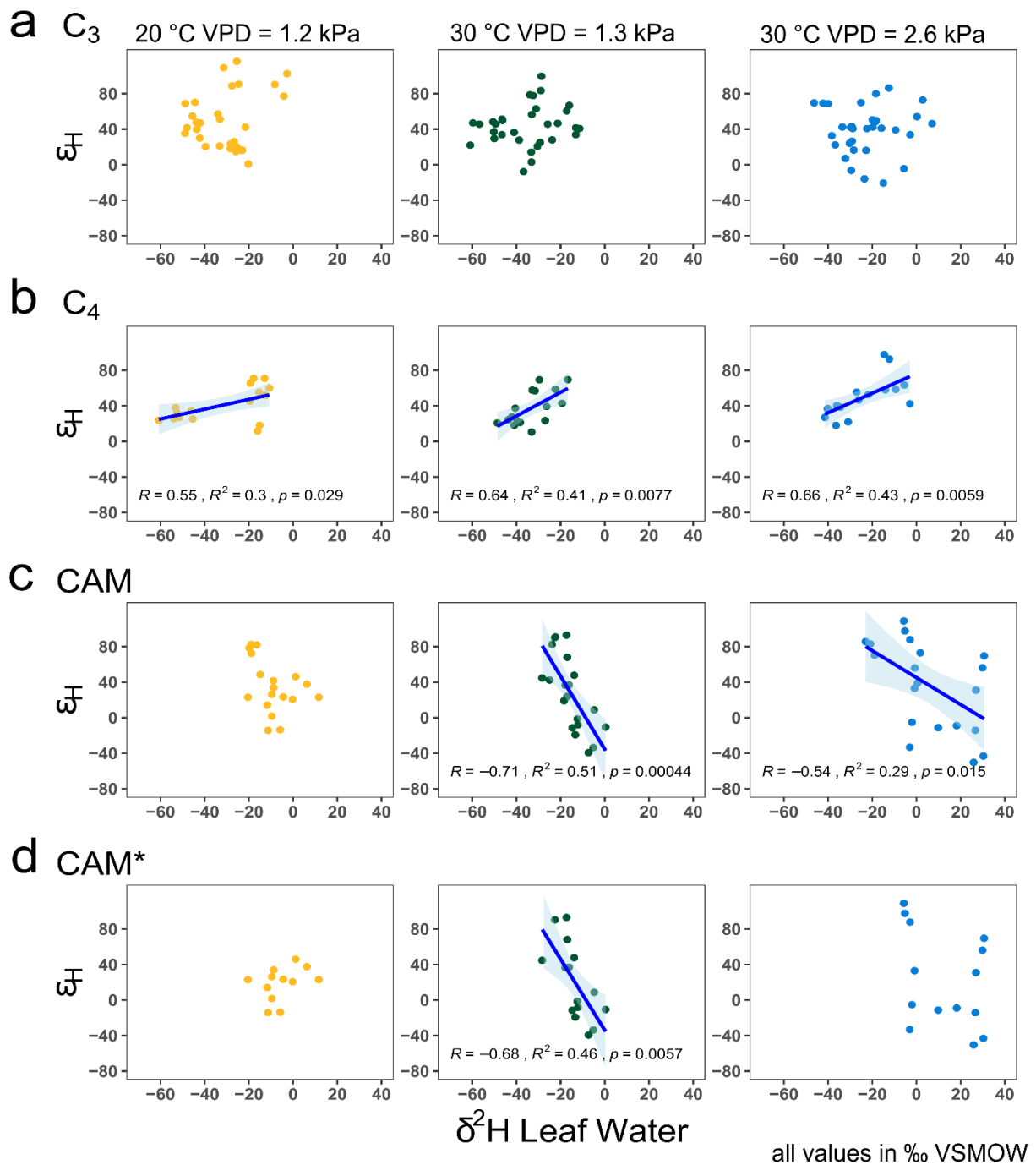


Figure S9: Correlation between ϵ_H and $\delta^2\text{H}$ of leaf water of a) C_3 , b) C_4 , c) CAM plants, as well as d) CAM plants excluding the two facultative CAM species *D. cooperi* and *M. cordifolium* (CAM*), separated by growing condition.

Chapter 5

Hot and Hungry: High temperatures induced carbohydrate depletion in leaves - insights from triple isotope fractionations

Philipp Schuler^{1,2}, Margaux Didion-Gency³, Valentina Vitali¹, Haoyu Diao¹, Matthias Saurer¹, Manuela Oettli¹, Nina Buchmann^{1,2}, Arthur Gessler^{1,2}, Marco M. Lehmann¹

¹Forest dynamics, Swiss Federal Institute for Forest, Snow and Landscape Research WSL, Birmensdorf, Switzerland

²Department of Environmental Systems Science, ETH Zurich, Zurich, Switzerland

³Plant Ecology Research Laboratory - PERL, Ecole Polytechnique Fédérale de Lausanne

This chapter will be submitted in the peer-reviewed journal “Nature Plants”.

Abstract

Accurate predictions and reconstructions of vegetation responses to global warming and unprecedented temperature extremes require a precise understanding of fundamental plant physiological processes and how these are imprinted on the plants' stable isotope compositions. Here we studied the temperature response (T_{air} ; 10°C to 40°C, in 5°C steps, each step for five days) of photosynthetic traits, gas-exchange, non-structural carbohydrate (NSC) concentrations, as well as the carbon, oxygen and hydrogen isotopic composition of water and sugars in leaves of well-watered C_3 trees, forbs and grasses as well as one C_4 grass, while maintaining a constant vapor pressure deficit. Increasing air temperature led to a depletion of leaf NSC, triggered by an increasing respiration rate relative to gross photosynthesis, resulting in a unique fingerprint in the leaf sugar triple isotope pattern. Our findings suggest that in a hotter world, plants that cannot acclimate their metabolic rate to higher temperatures are at risk of leaf carbohydrate depletion, and that such a carbon imbalance might be identified by using stable isotope analysis. This may eventually translate into a reduced growth rate, making them more vulnerable to other stressors, and eventually to carbohydrate starvation.

Main

CO₂ fixation, the key process that provides the carbohydrates needed for plant growth and productivity, is strongly dependent on various environmental factors, of which temperature is one of the important (Regehr & Bazzaz, 1976). The rate of CO₂ fixation can increase with increasing temperature up to a certain threshold, after which it starts to decrease due to a number of factors, including damage to the photosynthetic machinery and impairment of enzyme functioning (Medlyn *et al.*, 2002), and a reduction in CO₂ uptake due to stomatal closure (Schulze *et al.*, 1973). The optimum temperature for CO₂ fixation varies between plant species, typically ranging from 20-30°C, but can be stable up to 46°C in heat adapted and acclimated plant species (Downton *et al.*, 1984).

Post-photosynthetic metabolism is essential for plant growth and survival, providing energy and building blocks for growth, as well as compounds that contribute to plant defence and acclimation to the environment. Metabolic rates increase with temperature (Criddle *et al.*, 1994), for instance due to increased enzyme activity (Raison, 1973). This can lead to a decrease in energy efficiency if maintenance costs become too high, thus, thereby reducing the plant's ability to produce a surplus of carbohydrates for growth and storage (McMichael & Burke, 1994).

As high temperatures can lead to changes in both CO₂ fixation and respiration rates, the internal carbohydrate dynamics of plants are temperature dependent (Adams *et al.*, 2013; Rehschuh *et al.*, 2022). In addition, plants may allocate more carbon to heat-shock proteins and other protective mechanisms at higher temperatures (Al-Whaibi, 2011), which may reduce the availability of carbon for growth and reproduction.

Assessing the effects of rising temperatures on plant metabolism can be challenging because temperature changes are often associated with concomitant changes in vapor pressure deficit (VPD, Grossiord *et al.* (2020)), which can impact plant physiology and biochemistry in complex ways (Jansen *et al.*, 2014; Schönbeck *et al.*, 2022). For instance, high VPD

can lead to stomatal closure and reduced carbon uptake (Tinoco-Ojanguren & Pearcy, 1993), which can affect CO₂ fixation and ultimately plant growth (Kawamitsu *et al.*, 1987). In summary, the effects of temperature increase on plant metabolism, including CO₂ fixation, metabolism and carbohydrate dynamics, are complex and multifaceted. Therefore, separating the effects of temperature and VPD on plant physiology is critical for predicting the impacts of climate change on plant growth and productivity, and for developing effective mitigation and adaptation strategies for agricultural and natural ecosystems.

The fractionation of ²H, ¹⁸O and ¹³C during carbohydrate synthesis and metabolism is influenced by various processes. These processes include the CO₂ concentration (Cernusak *et al.*, 2013), temperature (Sternberg & Ellsworth, 2011), and enzymatic reactions (Schuler *et al.* 2023). However, there is still a lack of comprehensive studies that connect the temperature response of plant physiological processes, carbohydrate metabolism, and the fractionation processes of ²H, ¹⁸O and ¹³C. Thus, in this study we are using the triple isotope approach to both investigate the temperature response of plant internal carbon dynamics and the response of ²H, ¹⁸O, and ¹³C isotope fractionation in relation to the change in carbon dynamics.

To isolate the effects of rising temperature under a constant VPD on plant metabolism, we conducted a climate chamber experiment where we grew six C₃ (including two trees, *Quercus pubescens* WILLD. and *Phytolacca dioica* L.; two grasses, *Hordeum vulgare* L. and *Oryza sativa* L.; and two forbs, *Salvia hispanica* L. and *Solanum cheesmaniae* (RILEY) FOSBURG) and one C₄ (*Sorghum bicolor* (L.) MOENCH) plant species in a climate chamber (Fig. 1). The C₄ plant was selected because, in a previous experiment (Chapter 4 of this thesis), C₄ plants, unlike C₃ plants, did not show a temperature response in their δ²H of leaf sugar and leaf cellulose. This selection includes one temperate and one subtropical tree species and five agriculturally important crops from different geographical backgrounds and climatic zones. To reduce the pool of old NSC in the plants between each temperature cycle, we kept the plants in the dark at 20 °C for 48 hours. This

depletion of old NSC was used to assure that the stable isotope signals (^2H , ^{18}O and ^{13}C) reflected the physiological conditions of the plants at that temperature. We exposed the plants to a constant temperature for five days, starting at 10 °C and subsequently increasing to 40°C in 5°C steps (Fig. 1a). This allowed the plants (Smith & Freeman, 2006) to adjust short-term acclimate photosynthetic processes and respiration (Dewar *et al.*, 1999) to each of the tested temperatures. After four days, we sampled leaves for non-structural carbohydrates (NSC) and stable isotope analyses (Fig. 1b), and we conducted gas exchange and fluorescence measurements on the fifth day (Fig. 1c).

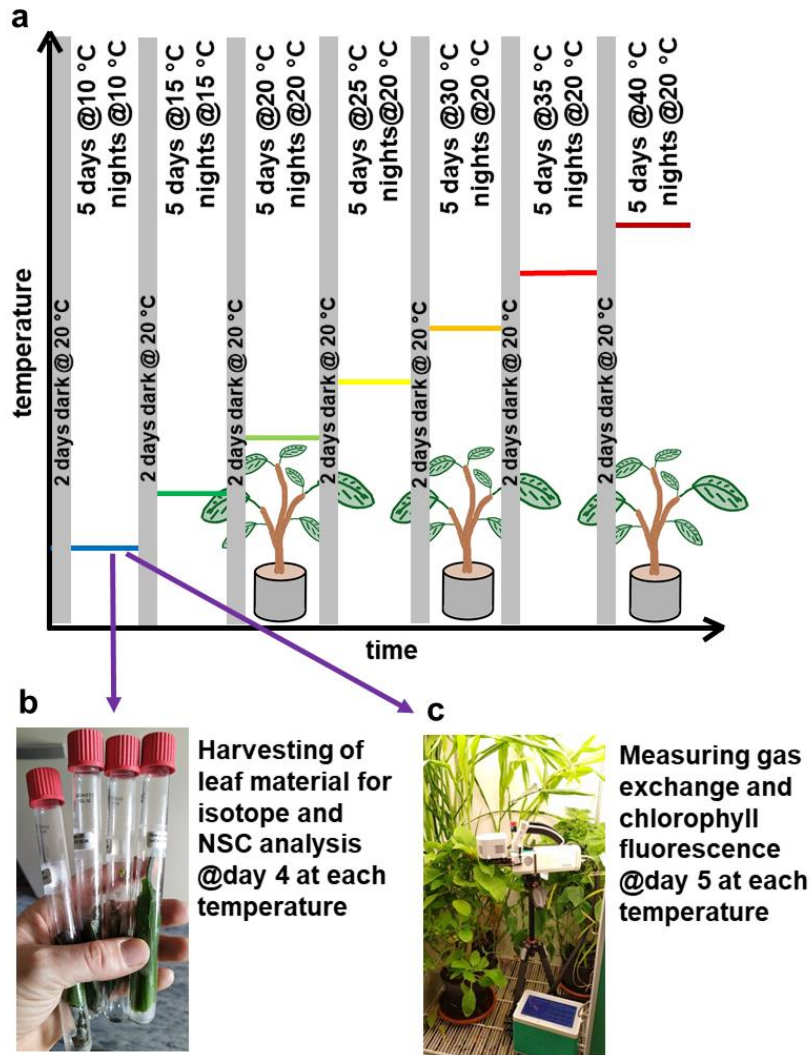


Figure 1: Graphical summary of the experimental design. **a)** The plants were growing in a climate chamber, where the temperature during the 18 daytime hours increased every week by 5 °C from 10 to 40 °C with a constant VPD. When the daytime temperature was set to 10 and 15 °C, nighttime temperature remained unchanged to avoid chilling damage. When the daytime temperature settings were 20 to 40 °C, nighttime temperature was set to 20 °C to standardize biochemical processes and enable the regeneration of the photosynthetic apparatus. **b)** On the fourth day, leaf samples were collected to measure the NSC content and the isotopic composition of the leaf water and leaf sugar in the early afternoon. **c)** On the fifth day, gas exchange and chlorophyll fluorescence measurements were performed to study the plant physiological response to the increasing temperature.

With this study, we show that air temperatures above 30 °C alone can drive C₃ plants into leaf-level carbohydrate depletion, caused by a lack in ability to downregulate respiration rates and a strong reduction of the assimilation rates. This was imprinted in an increasing $\delta^2\text{H}$ and a decreasing $\delta^{13}\text{C}$ of the leaf sugar. The C₄ plant maintained low respiration and high assimilation rates even at high temperatures above 35 °C, and thus no leaf sugar temperature response of $\delta^2\text{H}$ and $\delta^{13}\text{C}$ was observed. In conclusion, the better understanding of the plant internal carbohydrate dynamics in response to highly elevated daytime temperature will help to improve our understanding of plant response to changing climates.

Results

Temperature response of the leaf gas exchange and the functioning of PSII

The measured physiological traits responded strongly to the temperature treatment and reached a maximum, or a minimum in the case of C_i and non-photochemical quenching (NPQ), except for R_{dark} , within the tested temperature range from 10 to 40 °C (modelled values of Table 1 derived from analysis in Fig. 2, 3). While most of the plants had their modelled maximum net assimilation rate ($A_{\text{net max}}$) below 30°C (25.1-29.2 °C), the maximum net assimilation rate was modelled to be at 37.2 °C in *S. hispanica* and 32.1 °C in *S. bicolor*, respectively. While C₄ plants, like *S. bicolor*, have in general a higher temperature optimum than C₃ plants (Orsenigo *et al.*, 1997), we observed the highest optimum temperature ($A_{\text{net max}}$) in the C₃ plant *S. hispanica*. A_{gross} reached a maximum at lower temperatures than the electron transport (ETR) in *P. dioica* and *H. vulgare*. Comparing NPQ and maximum quantum efficiency of photosystem II (Fv/Fm) with A_{gross} shows a more similar temperature response of NPQ with A_{gross} .

Table 1: Air temperature in °C of: the maximum net assimilation rate ($A_{\text{net max}}$), the maximum gross photosynthesis rate ($A_{\text{gross max}}$), the maximum electron transport rate of PSII (ETR_{max}), the minimum fraction of dark respiration contributing to gross photosynthesis ($\%R_{\text{dark}}$ of A_{gross}), the maximum fraction of the total non-structural carbohydrate (NSC) pool consisted of starch, the minimum non-photochemical quenching (NPQ), the maximum quantum efficiency of photosystem II (F_v/F_m), the maximum quantum yield of photosystem II (Φ_{PSII}), and the minimum intracellular CO_2 concentration (c_i), calculated with the polynomial equations derived from each temperature response for different plant species (Figs. 2, 3).

	$A_{\text{net max}}$ °C	$A_{\text{gross max}}$ °C	ETR_{max} °C	min. $\%R_{\text{dark}}$ of A_{gross} °C	max. $\%Starch$ of total NSC °C	NPQ_{min} °C	$F_v/F_m \text{ max}$ °C	$\Phi_{\text{PSII max}}$ °C	$c_i \text{ min}$ °C
<i>P. dioica</i>	25.1	26.1	27.7	18.6	16.7	25.9	25.1	25.9	N.S.
<i>Q. pubescens</i>	25.3	28	26.9	18.5	11.5	28.3	21.7	25.1	23.5
<i>S. cheesmaniae</i>	25.3	31.8	27.9	18.9	21.5	26.2	24.3	26.1	24.6
<i>S. hispanica</i>	37.2	52.2	37.7	15.3	16.4	38.8	22.6	30.8	17.8
<i>O. sativa</i>	29.2	38.1	29.3	21.1	7.8	23.2	10.6	29.5	24.8
<i>H. vulgare</i>	26	28.3	29.8	18.6	15.1	29.1	19.7	25.4	21.1
<i>S. bicolor</i>	32.1	34	32.8	25.3	11.9	30.6	24.7	28.9	25.1

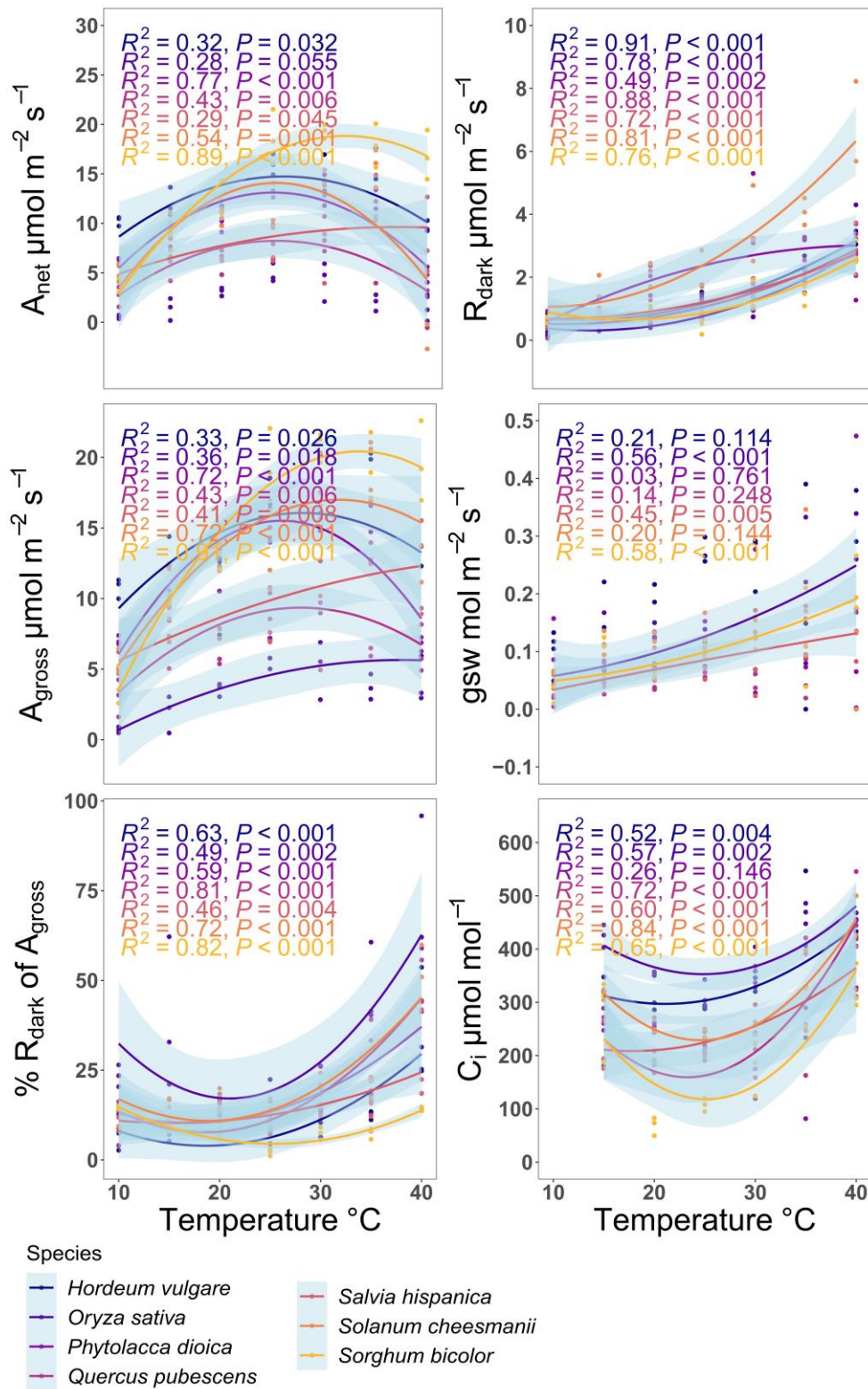


Figure 2: Temperature response of the net assimilation rate A_{net} , the dark respiration rates R_{dark} , the gross photosynthesis (A_{gross} , i.e., $A_{\text{net}} + R_{\text{dark}}$), the stomatal conductance (g_s), the percent proportion R_{dark} contributes to A_{gross} , and the intracellular CO_2 concentration (c_i). Species are indicated by colours,

quadratic model depicting the relationship are shown only for species showing a significant response ($p \leq 0.05$), and the light blue shading denotes the 95% confidence level interval for predictions of the quadratic fit.

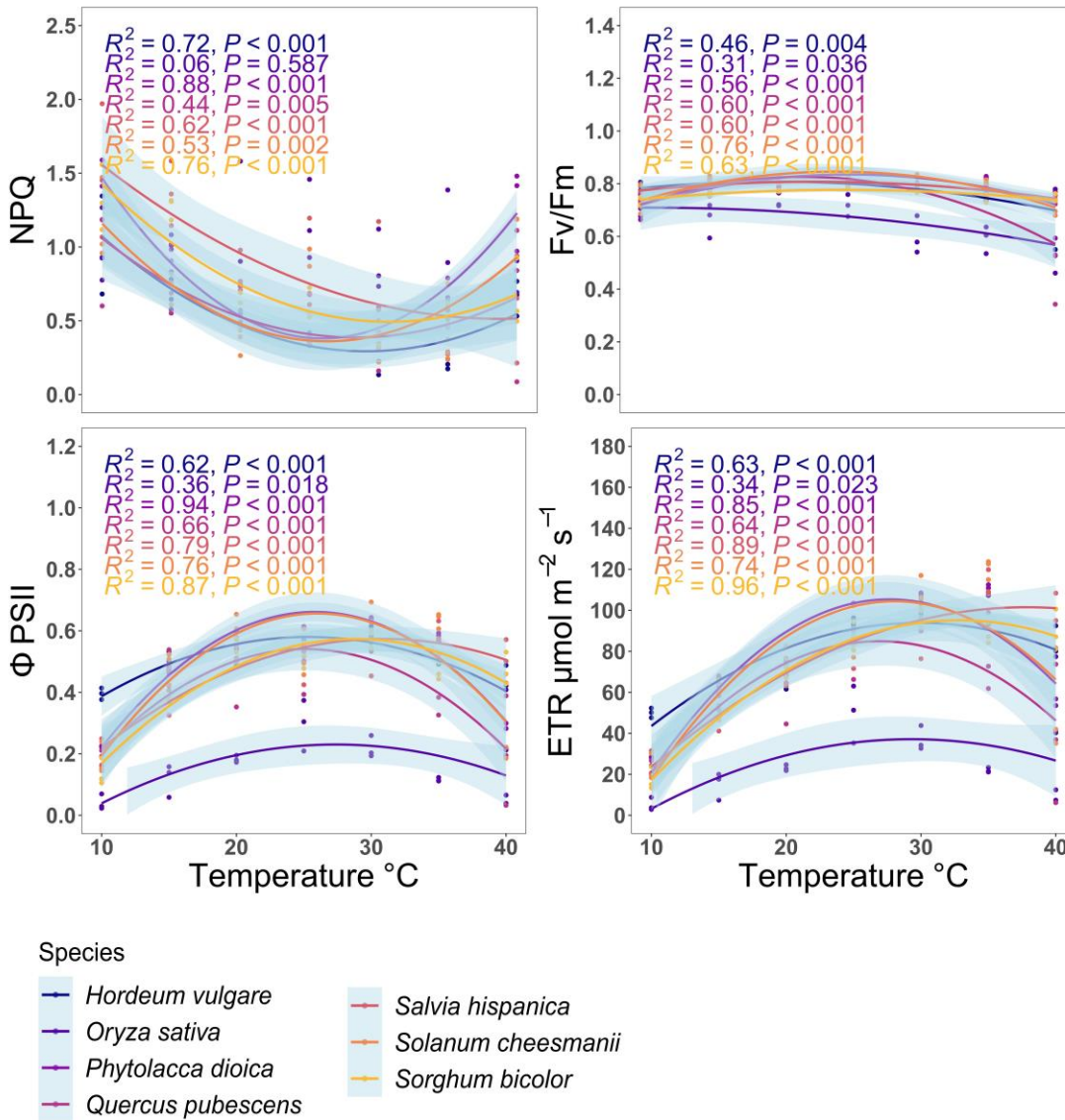


Figure 3: Temperature response of non-photochemical quenching (NPK), the maximum quantum efficiency of photosystem II (Fv/Fm), the quantum yield of PSII (Φ PSII), and the electron transport rate (ETR). Species are indicated by colours, quadratic model depicting the relationship are shown only for species showing a significant response ($p \leq 0.05$), and the light blue shading denotes the 95% confidence level interval for predictions of the quadratic fit.

Changes in non-structural carbohydrate concentration in response to rising temperatures

The general temperature response of the total NSC was similar within all species beside *H. vulgare* and *S. cheesmaniae* (Fig. 3), with a continuous reduction in total NSC concentration (in mg 100 mg⁻¹). While sugar concentration increased with increasing temperature in four out of the seven species, starch concentration decreased in all species at temperatures above 25 °C (Fig. 4).

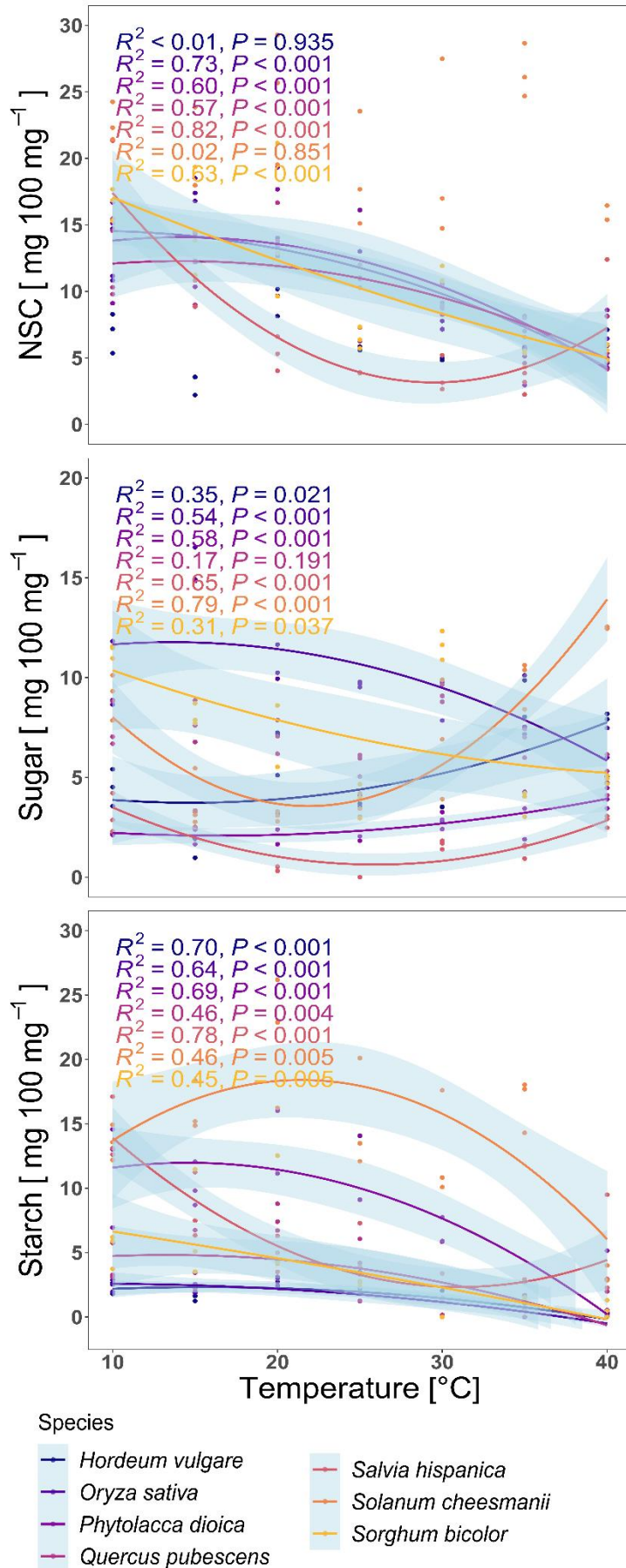


Figure 4: Temperature response of the plant internal non-structural carbohydrates (NSC). Top: total NSC in $\text{mg } 100\text{mg}^{-1}$ dry weight; middle: total sugar in $\text{mg } 100\text{mg}^{-1}$ dry weight; bottom: starch in $\text{mg } 100\text{mg}^{-1}$ dry weight. Species are indicated by colours, quadratic model depicting the relationship are shown only for species showing a significant response ($p \leq 0.05$), and the light blue shading denotes the 95% confidence level interval for predictions of the quadratic fit.

We were able to identify two groups depending on their NSC storage strategy (Fig. S1): One group, including *Q. pubescens*, *S. hispanica* and *S. cheesmaniae*, stored more than 75% of the total leaf NSC as starch. The NSC pool of the other group, containing *H. vulgare*, *O. sativa*, *S. bicolor* and *P. dioica*, always contained less than 50% starch.

The triple isotope response to rising temperature

The three measured isotopes (^{13}C , ^{18}O , and ^2H) showed distinct responses to the increasing temperature (Fig. 5), where isotope values of the temperature response are normalized to the average species-specific value for each species ($\Delta^{13}\text{C}$, $\Delta^{18}\text{O}$, and $\Delta^2\text{H}$). $\Delta^{13}\text{C}$ of the leaf sugar and $\Delta^{18}\text{O}$ of the leaf water and leaf sugar decreased with increasing temperature. While it cannot be completely ruled out, the trend in $\Delta^{13}\text{C}$ in leaf sugar was likely not directly driven by changes in the ^{13}C composition of the atmosphere (Figure S1, S3). The trend in $\Delta^{18}\text{O}$ in leaf sugar was mainly caused by changes in $\Delta^{18}\text{O}$ of the leaf water, but with an additional change in ϵ_{OA} (Fig. 5). In contrary, the temperature effect on $\Delta^2\text{H}$ of leaf water was very small, while the temperature effect in $\Delta^2\text{H}$ of leaf sugar was leading to a significant enriching of ^2H with higher temperature, which was caused by the biological ^2H fractionation ϵ_{HA} .

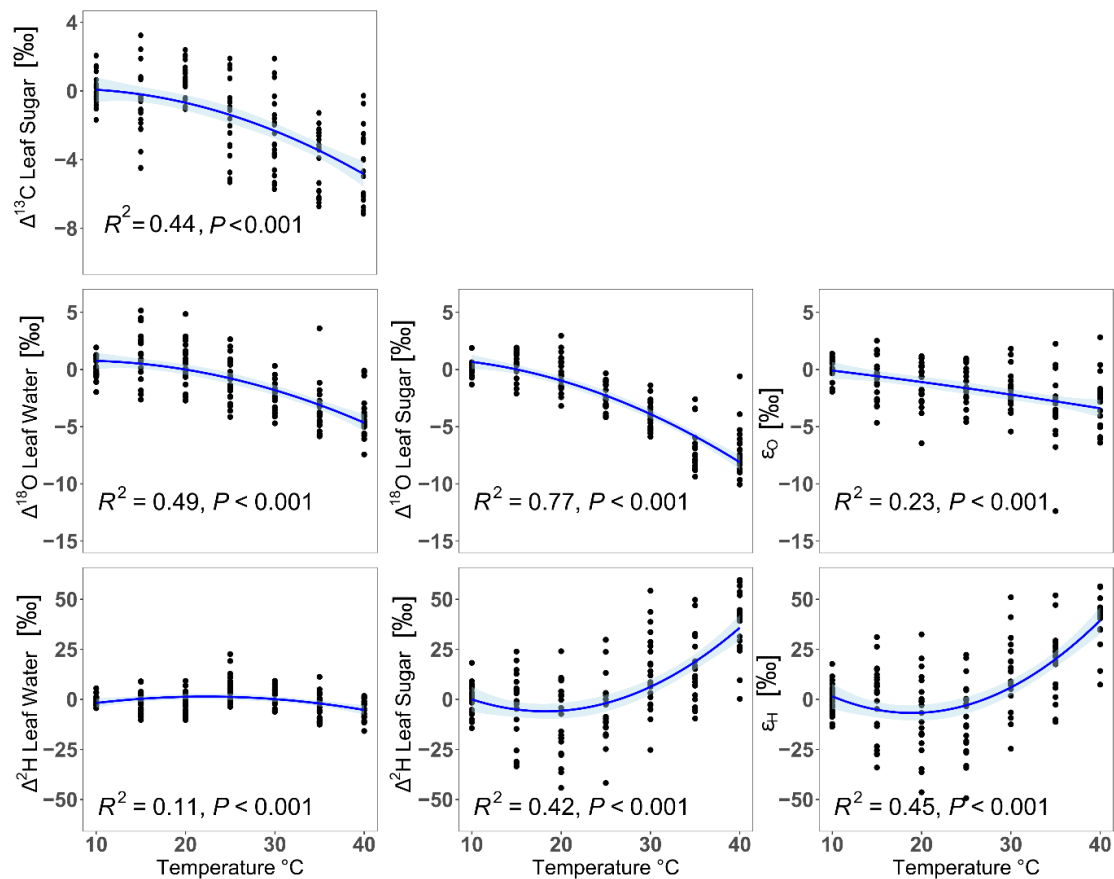


Figure 5: The isotope response to rising temperature of $\Delta^{13}\text{C}$ in leaf sugar, and of $\Delta^{18}\text{O}$ and $\Delta^2\text{H}$ in leaf water and leaf sugar, and the apparent ^{18}O and ^2H fractionation between leaf water and leaf sugar. Values are given as Δ ; e.g. normalized to average δ values measured at $10\text{ }^\circ\text{C}$ individually for each species. The blue line represents the quadratic model depicting the relationship between temperature and Δ values and fractionation factors of the three isotopes in leaf water and leaf sugar, and the light blue shading denotes the 95% confidence level interval for predictions of the quadratic fit.

Drivers underlying the temperature-induced changes in the apparent ^{13}C , ^{18}O , and ^2H fractionation

The main drivers of the δ values of each isotope (Fig. 6) could be derived from the principal component analysis (PCA, Fig. S2). The main driver of the $\delta^{13}\text{C}$ in leaf sugar was R_{dark} , the main driver of the $\delta^{18}\text{O}$ in leaf sugar was the $\delta^{18}\text{O}$ in leaf water, and the main driver of the $\delta^2\text{H}$ in leaf sugar was the percentage R_{dark} contributes to A_{gross} .

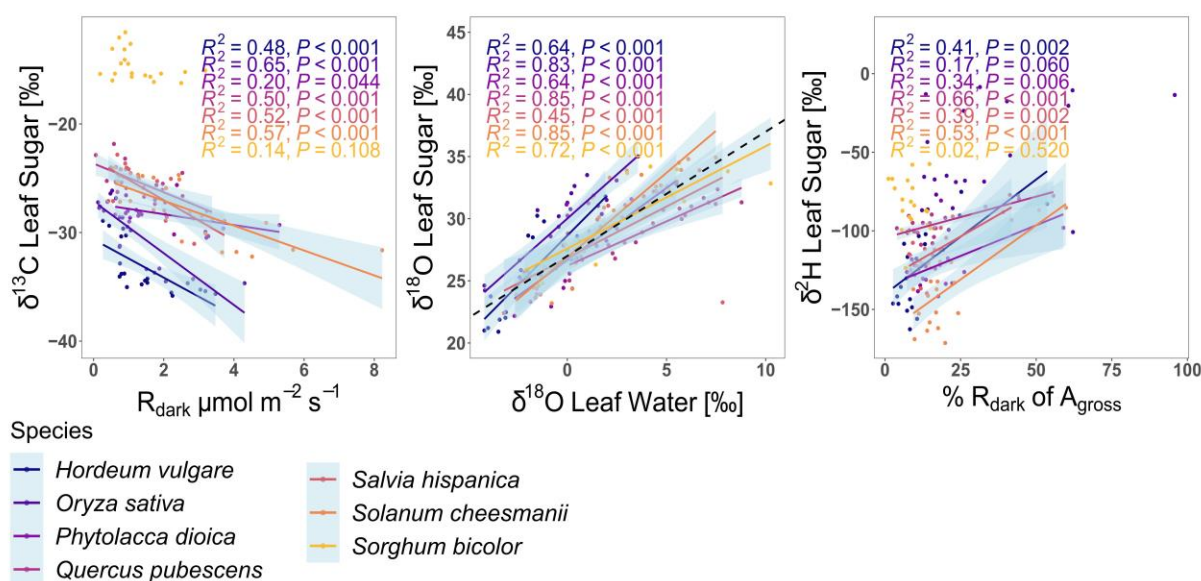


Figure 6: Main drivers of changes in the ^{13}C , ^{18}O , and ^2H isotope composition of leaf sugars are: for $\delta^{13}\text{C}$ in leaf sugar the respiration rate (R_{dark}), for $\delta^{18}\text{O}$ in leaf sugar the $\delta^{18}\text{O}$ of the leaf water, for $\delta^2\text{H}$ in leaf sugar and the percent R_{dark} contributes to gross photosynthesis ($\% R_{\text{dark}}$ of A_{gross}). Species are indicated by colours, linear regressions are shown only for species showing a significant response ($p \leq 0.05$), and the light blue shading denotes the 95% confidence level interval for predictions of the linear fit.

The $\delta^{13}\text{C}$ of leaf sugar on the species level (Fig. 7) was highly significantly negatively related to temperature in all species, negatively related to the percentage R_{dark} contributes to A_{gross} in all C_3 plants, positively related to the percentage starch contributes to the total leaf NSC pool in six of the seven species, and negatively related to C_i in 4 of the seven species.

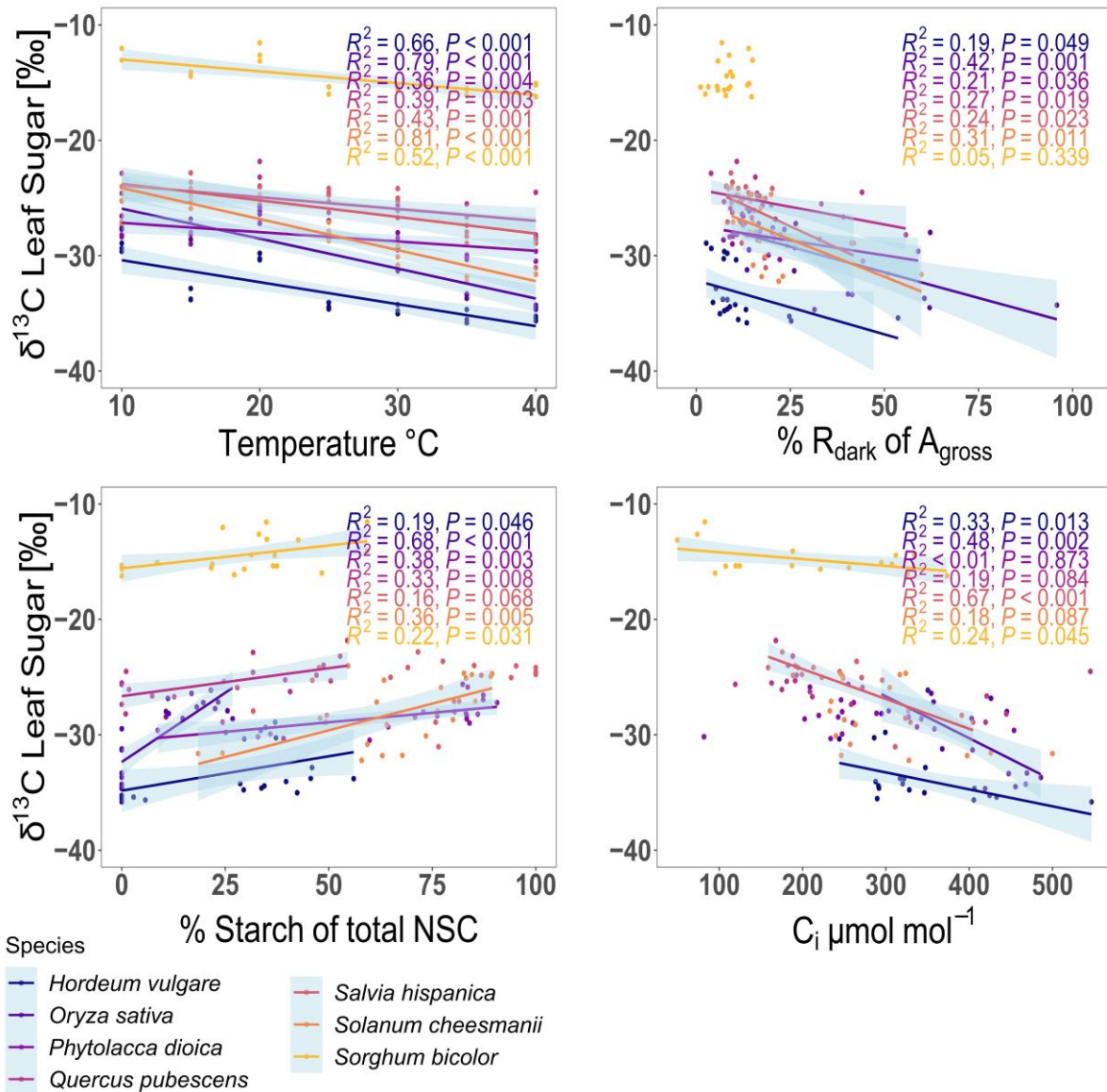


Figure 7: Linear regression analysis of the response of $\delta^{13}\text{C}$ in leaf sugars to increasing air temperature (Temperature °C), the percentage R_{dark} contributes to A_{gross} (% R_{dark} of A_{gross}), the percentage starch contributes to the total content of non-structural carbohydrates (NSC; % Starch of total NSC), and to the intracellular CO_2 concentration (c_i). Species are indicated by colours, linear

regressions are shown only for species showing a significant response ($p \leq 0.05$), and the light blue shading denotes the 95% confidence level interval for predictions of the linear fit.

The $\delta^{18}\text{O}$ of leaf sugar and leaf water on the species level (Fig. 8) was strongly negatively correlated to temperature in all species. ϵ_{OA} was negatively related to temperature in all species beside *Q. pubescens*, and $\delta^{18}\text{O}$ of leaf water was negatively related to the stomatal conductance (g_s) in three of seven species.

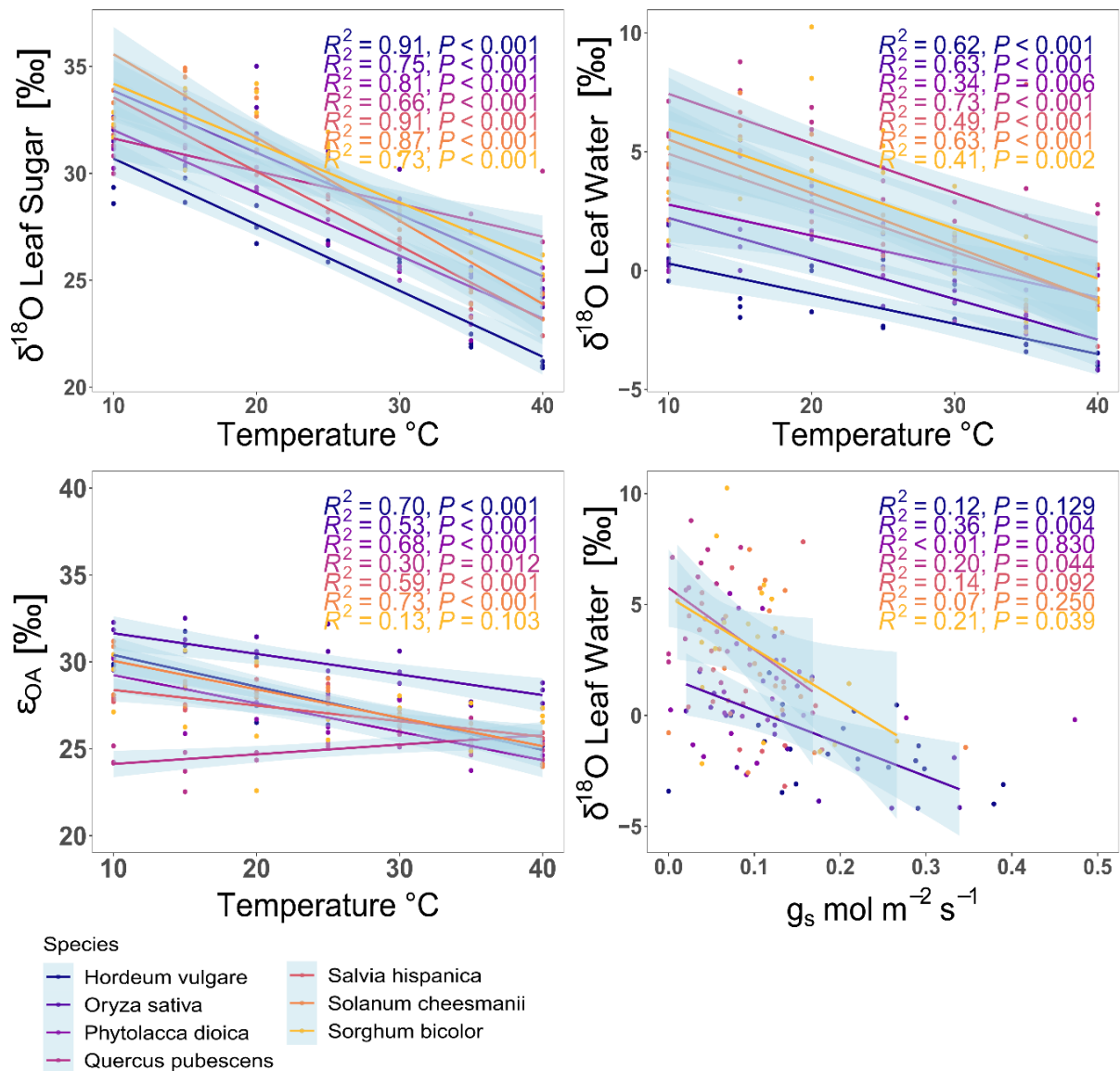


Figure 8: The response of $\delta^{18}\text{O}$ in leaf sugar and leaf water to increasing air temperature, the response of ϵ_{OA} to rising air temperature, and the relation of $\delta^{18}\text{O}$ in leaf water to stomatal conductance (g_s). Species are indicated by colours, linear regressions are shown only for species showing a significant

response ($p \leq 0.05$), and the light blue shading denotes the 95% confidence level interval for predictions of the linear fit.

The $\delta^2\text{H}$ of leaf sugar (Fig. 9) showed a strong response of temperature, with the lowest values around 2 to 25°C for all species, but with species-specific increases at lower and higher temperatures. The $\delta^2\text{H}$ of leaf sugar was negatively related to the percentage starch contributed to the total leaf NSC concentration, but was not related to the electron transport rate of PSII (ETR).

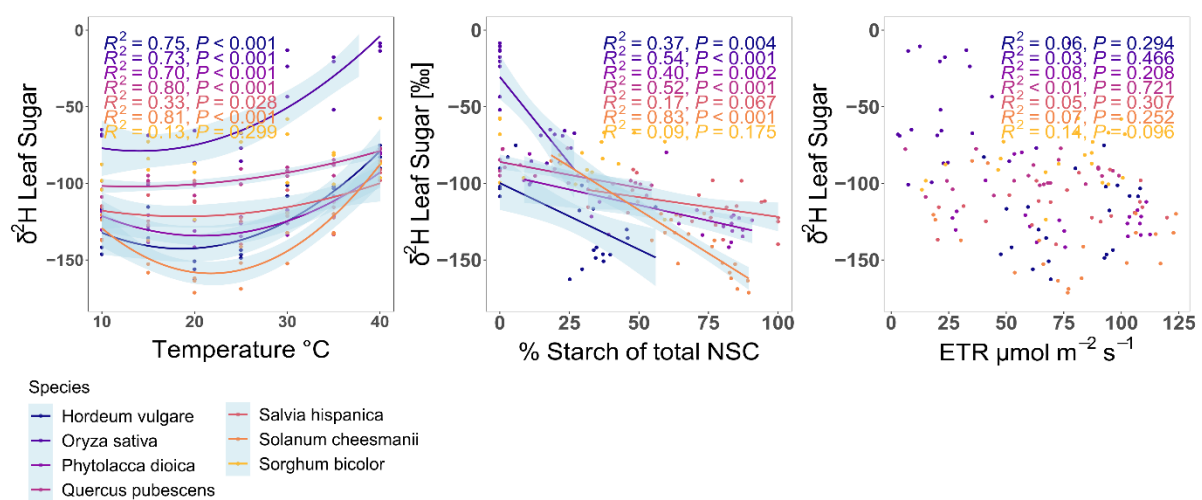


Figure 9: The response of $\delta^2\text{H}$ in leaf sugar to increasing air temperature, the percent proportion starch contributes to the total NSC content (% Starch of total NSC), and to the electron transport rate (ETR). Species are indicated by colours, quadratic fit (left panel) and linear regressions (center and right panel) are shown only for species showing a significant response ($p \leq 0.05$), and the light blue shading denotes the 95% confidence level interval for predictions of the quadratic (left panel) and linear fit (center and right panel).

The species-specific responses of ϵ_{CA} , ϵ_{OA} , and ϵ_{HA} as well as the average for plants with C_3 CO_2 fixation are listed in Table 2.

Table 2: Temperature response of the apparent ^{13}C fractionation between CO_2 and leaf sugar ϵ_{CA} , the apparent ^{18}O fractionation between leaf water and leaf sugar ϵ_{OA} , and the apparent ^2H fractionation between leaf water and leaf sugar ϵ_{HA} , calculated by using the temperature response formula derived from Fig. 3.

Temperature Response of ϵ_{CA} and ϵ_{CA} in ‰					
Species	Formula	10 °C	20 °C	30 °C	40 °C
<i>H. vulgare</i>	-0.19x-22.1	-24.0	-25.9	-27.8	-29.7
<i>O. sativa</i>	-0.26x-16.9	-19.5	-22.1	-24.7	-27.3
C_3 <i>P. dioica</i>	-0.0807x-19.9	-20.7	-21.5	-22.3	-23.1
<i>Q. pubescens</i>	-0.102x-16.5	-17.5	-18.5	-19.6	-20.6
<i>S. hispanica</i>	-0.144x-15.9	-17.3	-18.8	-20.2	-21.7
<i>S. cheesmaniae</i>	-0.269x-15	-17.7	-20.4	-23.1	-25.8
C_4 <i>S. bicolor</i>	-0.113x-5.3	-6.4	-7.5	-8.7	-9.8
mean C_3	-0.1743x-17.7	-19.5	-21.2	-22.9	-24.7
SD C_3	N.A.	5.5	5.7	6.1	6.5
Temperature Response of ϵ_{OA} and ϵ_{OA} in ‰					
Species	Formula	10 °C	20 °C	30 °C	40 °C
<i>H. vulgare</i>	-0.182x+32.2	30.4	28.6	26.7	24.9
<i>O. sativa</i>	-0.119x+32.8	31.6	30.4	29.2	28.0
C_3 <i>P. dioica</i>	-0.163x+30.9	29.3	27.6	26.0	24.4
<i>Q. pubescens</i>	0.0554x+23.6	24.2	24.7	25.3	25.8
<i>S. hispanica</i>	-0.141x+30	28.6	27.2	25.8	24.4
<i>S. cheesmaniae</i>	-0.164x+31.7	30.1	28.4	26.8	25.1
C_4 <i>S. bicolor</i>	-0.0682x+29.9	29.2	28.5	27.9	27.2
mean C_3	-0.119x+30.2	29.0	27.8	26.6	25.4
SD C_3	N.A.	2.4	1.7	1.4	1.4
Temperature Response of ϵ_{HA} and ϵ_{HA} in ‰					
Species	Formula	10 °C	20 °C	30 °C	40 °C
<i>H. vulgare</i>	0.168x ² -6.88x-35.1	-87.1	-105.5	-90.3	-41.5
<i>O. sativa</i>	0.131x ² -4.15x-6.24	-34.6	-36.8	-12.8	37.4
C_3 <i>P. dioica</i>	0.132x ² -5.47x-49.9	-91.4	-106.5	-95.2	-57.5
<i>Q. pubescens</i>	0.0438x ² -1.1x-63.3	-69.9	-67.8	-56.9	-37.2
<i>S. hispanica</i>	0.0522x ² -1.76x-75.6	-88.0	-89.9	-81.4	-62.5
<i>S. cheesmaniae</i>	0.235x ² -10.2x-22.5	-101	-132.5	-117	-54.5
C_4 <i>S. bicolor</i>	N.S.	N.A.	N.A.	N.A.	N.A.
mean C_3	0.127x ² -4.93x-42.11	-78.7	-89.8	-75.6	-36.0
SD C_3	N.A.	23.8	33.6	36.4	37.2

Discussion

In recent years, it became clear that drought-induced tree mortality is strongly caused by hydraulic failure (Rowland *et al.*, 2015; Kono *et al.*, 2019). However, the impact of rising temperatures on leaf carbohydrate dynamics observed in this study (Fig. 4) suggests that increased temperatures alone might cause carbohydrate depletion at the leaf level. This may make plants more vulnerable to further stressors that reduce CO₂ fixation and structural integrity, such as drought and rising VPD. Net assimilation rates decreased at temperatures above 30 °C, caused by reduced photosystem II functionality as indicated by increasing NPQ and decreasing ETR and Φ_{PSII} . The concomitant increase in respiration rate required plants to invest most to all of their newly assimilated carbohydrates in metabolic functioning and survival, leading to a sharp reduction in carbohydrate reserves on the leaf level (Fig. 4) (Scafaro *et al.*, 2021). However, the response of respiration to high temperatures is impacted by several factors (Scafaro *et al.*, 2021) and how these processes are imprinted in the apparent fractionation of ¹³C, ¹⁸O, and ²H in leaf sugar can further inform us on the leaf functioning under high temperature.

Growing under moderate temperatures up to 30 °C, the here investigated plant species were able to store carbohydrates in their leaves. This is attributed to the photosynthetic CO₂ fixation, which produces more carbohydrates than the leaf currently allocates for respiration. The $\delta^{13}\text{C}$ of the assimilated sugars are driven by processes such as the ¹³C fractionation during diffusion of CO₂ through air inside the stomatal pore, and the discrimination against ¹³CO₂ by Rubisco (Farquhar *et al.*, 1982a; Farquhar *et al.*, 1982b). However, under an exposition to high temperatures > 30°C, A_{net} of the tested C₃ species strongly decreased (Fig. 2), while the leaf respiration rate increased. Due to this shift, the leaf carbohydrate pools started to decrease (Fig. 4). We speculate that under high temperatures, leaves were not able to invest into the build-up of starch reserves. Instead, they may have used an increasing proportion of the assimilated carbon to maintain

metabolic functionality. This response may indicate an imbalance between CO₂ fixation and NSC consumption, which might have caused the dieback of one *S. cheesmaniae* and about 75% of the *H. vulgare* at 40°C. Due to the increasing respiration rate, a higher portion of the leaf internal CO₂ originates from internal respiratory processes, including photorespiration, which is ¹³C depleted (Tcherkez *et al.*, 2011), which is leading to a mismatch between the measured $\delta^{13}\text{C}$ of the leaf sugar and the $\delta^{13}\text{C}$ of the modeled leaf biomass (Fig. S5). Since the model predicts changes of $\delta^{13}\text{C}$ mainly due to differences in the ratio of CO₂ inside and outside the leaf, it does not differentiate between different sources of the CO₂, e.g. between CO₂ deriving from the atmosphere vs. CO₂ deriving directly from internal respiration. Thus, assimilates which are formed during phases of high respiratory activity at high temperatures became more depleted in ¹³C. Since the exchange of air in the climate chamber was high (Fig. S1), the ¹³C depletion is unlikely to derive from an accumulation of ¹³C depleted CO₂ inside the chamber. Interestingly, as we observed this process in the absence of soil drought and under low VPD, a combination with reduced soil water availability and an increased VPD might further alter this response (Zhao *et al.*, 2013; Jansen *et al.*, 2014). Our findings may indicate further mechanisms that need to be taken into account when interpreting calculations of water-use efficiency or reconstructions of past climatic conditions by using $\delta^{13}\text{C}$ values of carbohydrates, including cellulose. However, these findings might only be of importance when a strong temperature increase is happening in the absence of soil drought and under a high relative humidity.

Our results on $\delta^{18}\text{O}$ aligns with previous studies (Yakir & DeNiro, 1990; Roden *et al.*, 2000; Zech *et al.*, 2014), showing the $\delta^{18}\text{O}$ of carbohydrates is mainly driven by $\delta^{18}\text{O}$ of leaf water (Fig. 6). However, we could also demonstrate that the $\delta^{18}\text{O}$ of leaf sugar is also dependent on temperature (Fig. 8), as the autotrophic ¹⁸O fractionation between leaf water and leaf sugar (ϵ_{OA}) is temperature dependent (Figs. 5, 8). We observed a negative linear ϵ_{OA} -temperature relation with a stronger photosynthetic ¹⁸O

enrichment at lower temperatures for all except *Q. pubescens* (Table 2, Fig. 8). A similar temperature response has previously been demonstrated for cellulose in wheat seedlings under light exclusion (Sternberg & Ellsworth, 2011). Our findings demonstrate that for a correct understanding and interpretation of $\delta^{18}\text{O}$ in plant organic matter, the temperature dependence of the photosynthetically ^{18}O fractionation needs to be taken into account.

Unlike the processes that are shaping the $\delta^{13}\text{C}$ and $\delta^{18}\text{O}$ of new assimilates, the biochemical processes responsible for the leaf sugar $\delta^2\text{H}$ are more complex (Table 2; Figs. 5, 6, 9). While CO_2 fixation is producing sugar highly depleted in ^2H (Zhang *et al.*, 2002), an increasing respiration rate is increasing the $\delta^2\text{H}$ of the remaining leaf sugar (Holloway-Phillips *et al.*, 2022). The most likely explanation for this process would be a preferential usage of sugar containing lighter ^1H instead of ^2H for respiration, leading the remaining sugar pool to become relative ^2H enriched. For instance, an equilibrium tritium isotope effects has been observed between glucose and the human brain hexokinase (Lewis & Schramm, 2003), the first enzyme involved in glycolysis.

The temperature response of leaf sugar $\delta^2\text{H}$ with changes of more than 50‰ from 10 to 40°C is much stronger compared to that of $\delta^{13}\text{C}$ and $\delta^{18}\text{O}$, where the changes are typically in a range below 10‰, making the $\delta^2\text{H}$ of carbohydrates a more sensitive tool to investigate a leaf's carbon dynamics. However, the results of this study on the temperature response of leaf functioning and leaf carbohydrate dynamics, and its translation into the isotopic composition of carbohydrates (Fig. 4) enable now to differentiate between processes based on the triple isotope approach. For instance, the ^2H enrichment in tree-ring cellulose after defoliation indicates a remobilisation of stored carbohydrates (Vitali *et al.*, 2023).

As the observed temperature response of A_{net} and R_{dark} are both non-linear and asynchronous processes (Fig. 2a; Scafaro *et al.* (2021), the resulting temperature response of the apparent ^2H fractionation can be best described with a species-specific 2nd order polynomial equation (Figs. 2c, 3d, Table 2).

The ^2H enrichment due to higher respiration rates on the leaf level also indicate that a prolonged respiration is leading to a ^2H enrichment of the remaining substrate. This could explain why storage carbohydrates are ^2H enriched in heterotrophic tissues (Lehmann *et al.*, 2021), without the need for a speculated isotopic exchange between stored carbohydrates and surrounding water. However, further systematic studies on respiratory ^2H fractionation are needed to investigate these processes.

These findings point out that further research is needed to investigate the long term response of plants to temperatures above 30 °C, as most of the studies are conducted at temperatures below 30 °C (Dewar *et al.*, 1999; Atkin & Tjoelker, 2003). If plants cannot adjust their respiration rates to high temperatures, they might ultimately face carbon starvation if the imbalance between assimilation and respiration rates persists for too long. Additional studies to investigate the here observed leaf-level temperature-induced carbohydrate depletion on a whole plant-level could contribute to the understanding the high temperature response of plants. For instance of distribution limits of deciduous species at the high temperature edges of their range, as plant species that are unable to down-regulate their respiration rate during periods of reduced or halted CO_2 fixation, such as the leafless period in deciduous species, will inevitably face carbohydrate starvation.

Methods

Experimental design and plant growing conditions

To isolate the effects of rising temperature under a constant VPD on leaf physiology, metabolism, and the corresponding triple isotope fractionation, we established a specific experimental and sampling design (Fig. 1). We selected six C₃ and one C₄ plant species, with different biochemical and anatomical features as well as temperature adaptations. For the C₃ species, we selected two trees, *Quercus pubescens* WILLD. and *Phytolacca dioica* L.; two grasses, *Hordeum vulgare* L. and *Oryza sativa* L.; and two forbs, *Salvia hispanica* L. and *Solanum cheesmaniae* (RILEY) FOSBURG. For the C₄ plant, we selected the grass *Sorghum bicolor* (L.) MOENCH. With this species selection, we aimed to make the results of this study relevant to a broad field of plant sciences, including plant ecophysiology, forestry and forest ecology, as well as agriculture. Starting in November 2021, we grew replicates of plants (three replicates for *Quercus pubescens*, *Phytolacca dioica*, *Solanum cheesmaniae*, *Sorghum bicolor*, ~50 replicates for *Hordeum vulgare* and *Oryza sativa*) for 2 to 3 months in a climate chamber (Plant Growth Chamber PGR15, Controlled Environments Limited (CONVIRON), Winnipeg, Manitoba, Canada) at the Swiss Federal Institute for Forest, Snow, And Landscapae Research WSL, at a temperature of 25 °C, a VPD of 1 kPa, and with a photosynthetic active radiation (PAR) of 800 μmol of photons m⁻² s⁻¹. After the initial growth period, the actual treatment period of seven weeks started. To reduce the pool of old leaf NSC between each temperature cycle, plants were kept in the dark at 20 °C for 48 hours. This depletion of old NSC was used to obtain an unadulterated stable isotope (²H, ¹⁸O and ¹³C) signal, reflecting the plant physiological conditions at the respective temperature, and thus to avoid autocorrelation. During the start of each week, we exposed the plants for five days to 18 hours of a constant daytime temperature, starting at 10 °C and subsequently increasing to 40°C in 5°C steps every week (Fig. 1a). This allowed the plants to acclimate to each of the studied temperatures. The nighttime temperature for the daytime 10,

15, and 20 °C treatments was the same as the daytime temperature and a VPD of 1 kPa to avoid chilling damage. Nighttime temperatures for 25, 30, 35, and 40 °C were all set to 20°C and a VPD of 1 kPa to enable the plants to recover their photosynthetic machinery overnight. After four days of treatment, we sampled leaves for non-structural carbohydrates (NSC) and stable isotope analysis (Fig. 1b) in the early afternoon. After five days, we conducted gas exchange and fluorescence measurements (Fig. 1c). The separation of leaf sampling and gas exchange measurements was done to avoid any influence of introduced unstable conditions during gas exchange measurements, such as uptake of ^{13}C depleted CO_2 from human respiration (Fig. S2). At 40 °C, one of the three replicates of *S. cheesmaniae* and about two third of the *H. vulgare* plants died.

Measurement of CO_2 and $\delta^{13}\text{CO}_2$

CO_2 concentration and $\delta^{13}\text{CO}_2$ in the climate chamber were measured continuously over the study period by a CO_2 isotope ratio infrared spectrometer (IRIS; Delta Ray, Thermo Fisher Scientific Inc., Bremen, Germany). The instrument was calibrated for both concentration dependency of the isotope ratio measurements and the span of the isotope ratio and concentration measurements using two reference gas with known isotope ratios ($\delta^{13}\text{C}$ of -9 ‰ and -25.5 ‰, VPDB), and two reference gases with known CO_2 concentrations (362.1 and 1154 $\mu\text{mol mol}^{-1}$).

Plant physiological measurements

After 5 days exposure to each temperature, one leaf per plant was dark adapted by gently folding aluminium foil around it for at least 20 minutes. After that, dark respiration (R_{dark}) and dark-adapted fluorescence were measured using a Li-6800 (LI-COR Biosciences, Lincoln, NE, USA) at the same condition (CO_2 , RH, and temperature) as present in the climate chamber but without light. After that, photosynthetic active radiation (PAR) of the LI-6800 was set to the value of the climate chamber (CO_2 , RH, and temperature still the same as in the climate chamber) and a light-adapted leaf of the same

plant in close proximity was fixed into the measuring chamber. The leaf and the chamber were allowed to equilibrate for 15 to 20 minutes until A_{net} reached a plateau before the measurements of A_{net} , stomatal conductance (g_s) and CO_2 concentration in the leaf intercellular air space (C_i), as well as light-adapted fluorescence. Gross photosynthesis (A_{gross}) was calculated as the difference between A_{net} and R_{dark} , and with this, the percentage R_{dark} contributes to A_{gross} ($\%R_{\text{dark}}$ of A_{gross}) could be calculated. With the dark- and light-adapted fluorescence measurements, the LI-6800 automatically calculated the non-photochemical quenching (NPQ), the photosynthetic efficiency of photosystem II (F_v/F_m), the quantum yield of photosystem II (ΦPSII), and the electron transport rate of photosystem II (ETR).

Sampling of plant material

For each temperature step, three samples each consist of several light-exposed leaves were collected from each plant in the early afternoon using scissors. Leaf material was sampled in excess to make sure there was enough plant material and water (> 2 mL of water for all samples) to avoid methodological bias during water extraction (Diao *et al.*, 2022). The fully developed leaves were immediately transferred into individual gas-tight 12 ml glass vials (Prod. No. 738W, Exetainer, Labco, Lampeter, UK, stored on dry ice, and transferred in a $-20\text{ }^\circ\text{C}$ freezer until further use.

Extraction of leaf water and sugars

Leaf water was cryogenically extracted using a hot water bath at $80\text{ }^\circ\text{C}$ and a vacuum (< 0.02 mbar) for 2 h (West *et al.*, 2006; Diao *et al.*, 2022), then stored in glass vials at $-20\text{ }^\circ\text{C}$ until isotope analysis. After the water extraction, the dried leaf material was ground (MM400, Retsch, Haan, Germany), and the bulk leaf sugar fraction was then extracted from 100 mg of leaf powder following established protocols (Rinne *et al.*, 2012; Lehmann *et al.*, 2020). First, the ground leaf material was mixed with deionized water in a 2 ml reaction vial and the water-soluble content was extracted at $85\text{ }^\circ\text{C}$ for 30 minutes. Leaf sugars were then purified from the water-soluble

content using ion exchange cartridges (OnGuard II A, H and P, Dionex, Thermo Fisher Scientific, Bremen, Germany). Finally, leaf sugar material was acquired by freeze-drying the purified sugar solutions.

$\delta^2\text{H}$ and $\delta^{18}\text{O}$ analyses of leaf water ($\delta^2\text{H}_{\text{LW}}$ and $\delta^{18}\text{O}_{\text{LW}}$)

The $\delta^2\text{H}$ and $\delta^{18}\text{O}$ of water samples was measured with a high temperature conversion elemental analyser coupled to a DeltaPlus XP isotope ratio mass spectrometer (TC/EA-IRMS; Finnigan MAT, Bremen, Germany). Calibration was done using a range of certified waters of different isotope $\delta^2\text{H}$ and $\delta^{18}\text{O}$ ratios, respectively, resulting in a precision of analysis of 2%. All the obtained values can be found in Table S1.

$\delta^2\text{H}$ analyses of sugars and cellulose using a hot water vapor equilibration method

The here used procedure originates mainly from the description in Schuler et al. 2023. $\delta^2\text{H}$ of sugars were analysed according to the previously developed hot water vapor equilibration method (Schuler *et al.*, 2022). Dry sugar samples were dissolved in water, with a target concentration of 1 mg sugar per 20 μL water. The reason for this relatively high target was to reduce sample volume and increase its viscosity, thereby reducing the risk of losing sample material while processing. Two identical sets of each sugar sample, with 1 mg sample material each, were prepared by pipetting 20 μL sugar solution into pre-weighed 5 \times 9 mm silver foil capsules (Prod. No. SA76981106, Säntis, Switzerland). Sugar samples for $\delta^{13}\text{C}$ and $\delta^{18}\text{O}$ measurements were prepared by transferring 20 μL sugar solution of the same solution into pre-weighed 3.3 \times 5 mm silver foil capsules (Prod. No. SA76980506, Säntis). All samples were then frozen at -20°C , freeze-dried with a condenser temperature of -50°C , and the duplicates for $\delta^2\text{H}$ measurements were packed into a second 5 \times 9 mm silver foil capsule. Sugar samples were stored in a desiccator at low relative humidity (2-5%) until $\delta^2\text{H}$, $\delta^{13}\text{C}$ and $\delta^{18}\text{O}$ measurements.

For the $\delta^2\text{H}$ measurements, the sets of duplicates were then equilibrated with hot water vapour by evaporating two isotopically distinct waters ($\delta^2\text{H}$ water 1 = -160‰ and $\delta^2\text{H}$ water 2 = -428‰) at 130°C (Schuler *et al.*, 2022). After 2 h, the samples were dried with dry nitrogen gas (N25.0, Prod. No. 2220912, PanGas AG, Dagmersellen, Switzerland) for 2 h at 130°C. After that, they were immediately transferred into a Zero Blank Autosampler (N.C. Technologies S.r.l., Milano, Italy), which was installed on a sample port of a high-temperature elemental analyser system. The latter was coupled via a ConFlo III referencing interface to a Delta^{plus} XP IRMS (TC/EA-IRMS, Finnigan MAT, Bremen, Germany). The autosampler was evacuated to 0.01 mbar and filled with dry helium gas. The samples were pyrolysed in a reactor according to Gehre *et al.* (2004), and carried in a flow of dry helium (150 ml min⁻¹) to the IRMS. Raw $\delta^2\text{H}$ values were offset corrected using polyethylene foil standards (IAEA-CH-7 polyethylene foil, International Atomic Energy Agency, Vienna, Austria; SD < 0.7‰ within one run).

$\delta^{13}\text{C}$ and $\delta^{18}\text{O}$ measurements were done according to established protocols (Weigt *et al.*, 2015; Lehmann *et al.*, 2020).

Calculation of the non-exchangeable hydrogen isotope ratio ($\delta^2\text{H}_{\text{ne}}$), ϵ_{HA} and ϵ_{HE}

The here used procedure originates mainly from the description in Schuler *et al.* 2023. All isotope ratios (δ) were calculated as given in Eq. 1 (Coplen, 2011):

$$\delta = \frac{R_{\text{Sample}} - R_{\text{Standard}}}{R_{\text{Standard}}}$$

Eq. 1

where $R = ^2\text{H}/^1\text{H}$ of the sample (R_{sample}) and of Vienna Standard Mean Ocean Water (VSMOW2; R_{standard}) as the standard defining the international isotope scale. To express the resulting δ in permil (‰), results were multiplied by 1,000.

According to Filot et al. (2006), the %-proportion of exchanged hydrogen during the equilibrations (x_e , Eq. 2) can be calculated as:

$$x_e = \frac{\delta^2H_{e1} - \delta^2H_{e2}}{\alpha_{e-w} \cdot (\delta^2H_{w1} - \delta^2H_{w2})} \quad \text{Eq. 2}$$

where δ^2H_{e1} and δ^2H_{e2} are the measured δ^2H values of the two equilibrated subsamples, δ^2H_{w1} and δ^2H_{w2} are the δ^2H values of the two waters used, and α_{e-w} is the fractionation factor of 1.082, which is the same for sugars and cellulose (Filot *et al.*, 2006; Schuler *et al.*, 2022). Typical x_e values for pure sugars are between 0.32 and 0.36 (Schuler *et al.*, 2022).

δ^2H_{ne} can then be calculated with Eq. 3 using one of the two equilibrations (equilibration one in this example, δ^2H_{e1} and δ^2H_{w1}):

$$\delta^2H_{ne} = \frac{\delta^2H_{e1} - x_e \cdot \alpha_{e-w} \cdot \delta^2H_{w1} - 1000 \cdot x_e \cdot (\alpha_{e-w} - 1)}{1 - x_e} \quad \text{Eq. 3}$$

Three sucrose samples for the equilibrations of leaf sugars and three cellulose samples for the equilibrations of the twig xylem cellulose, each measured in triplicates, were used as internal reference material to calibrate the results. For the sake of simplicity, δ^2H has been used throughout the manuscript instead of δ^2H_{ne} .

The apparent autotrophic fractionation factors between precursor and product ($^{13}C = \epsilon_{CA}$, $^{18}O = \epsilon_{OA}$, and $^2H = \epsilon_{HA}$) were calculated with Eq. 4, Eq. 5, and Eq. 6, respectively:

$$\epsilon_{CA} = \delta^{13}C_{\text{leaf sugar}} - \delta^{13}C_{\text{CO}_2} \quad \text{Eq. 4}$$

$$\epsilon_{OA} = \delta^{18}O_{\text{leaf sugar}} - \delta^{18}O_{\text{leaf water}} \quad \text{Eq. 5}$$

$$\epsilon_{HA} = \delta^2H_{\text{leaf sugar}} - \delta^2H_{\text{leaf water}} \quad \text{Eq. 6}$$

As in Schuler et al. (2023), the two biological fractionation factors ϵ_A and ϵ_H were expressed as the actual difference between the $\delta^{13}\text{C}$, $\delta^{18}\text{O}$, and $\delta^2\text{H}$ of leaf sugars and the $\delta^{13}\text{C}$ of the atmospheric CO_2 in the climate chamber as well as the $\delta^{18}\text{O}$ and $\delta^2\text{H}$ of leaf water. All the obtained values can be found in Table S1.

Leaf-level non-structural carbohydrates analysis

The sampled leaf material was dried during the cryogenic water extraction at 80 °C until a stable weight was attained. Then, leaves were ground in fine powder and measurement of the non-structural carbohydrate (NSC) concentration was done following previous established protocols (Hoch *et al.*, 2002; Schönbeck *et al.*, 2018). Ten to twelve mg of finely ground leaf material were heated in 2 mL distilled water for 30 min. An aliquot of 200 μL was treated with invertase from baker's yeast (*S. cerevisiae*, Sigma-Aldrich Chemie GmbH, Germany) for an hour to degrade sucrose and convert fructose into glucose. The sugar concentration was determined at 340 nm in a 96-well plate spectrophotometer (Thermo Fisher Scientific Multiskan GO, Finland) after an enzymatic conversion to gluconate-6-phosphate of about 35 min, using glucose Assay Reagent (Sigma-Aldrich Chemie GmbH, Germany) and Isomerase from baker's yeast (*S. cerevisiae*, Sigma-Aldrich Chemie GmbH, Germany). The total amount of NSC was measured by taking an aliquot of 500 μL of the extract (including starch and sugar) and treated for 15 h at 49 °C with Amyloglucosidase from *Aspergillus niger* (Sigma-Aldrich Chemie GmbH, Germany) to digest starch into glucose. Total glucose (corresponding to total NSC concentration) was determined using a spectrophotometer, as explained above. The starch concentration was calculated as the total NSC subtracted by the sugar concentration. Standard solutions, including pure starch, glucose, fructose, sucrose, and standard plant powder (Orchard leaves; Leco, USA), were used as references for the comparison and reproducibility of the results between runs. All the obtained values can be found in Table S3.

Statistical analyses

Statistical analyses were performed using R version 4.1.2 (R.Core.Team, 2023). Linear and polynomial models, implemented in the R package *ggplot2* (Wickham, 2016), were used to determine the leaf physiological temperature response, the general temperature response, and specific drivers underlying the ^{13}C , ^{18}O , and ^2H fractionation processes. PCA analysis were done with the R packages *ggbiplot* and *factoextra*. The final assembly of the graphs was done using the R package *patchwork* (Pedersen, 2022).

References

- Adams HD, Germino MJ, Breshears DD, Barron-Gafford GA, Guardiola-Claramonte M, Zou CB, Huxman TE. 2013.** Nonstructural leaf carbohydrate dynamics of *Pinus edulis* during drought-induced tree mortality reveal role for carbon metabolism in mortality mechanism. *New Phytologist* **197**(4): 1142-1151.
- Al-Wahaibi MH. 2011.** Plant heat-shock proteins: a mini review. *Journal of King Saud University-Science* **23**(2): 139-150.
- Atkin OK, Tjoelker MG. 2003.** Thermal acclimation and the dynamic response of plant respiration to temperature. *Trends in Plant Science* **8**(7): 343-351.
- Cernusak LA, Barbour MM, Arndt SK, Cheesman AW, English NB, Feild TS, Helliker BR, Holloway-Phillips MM, Holtum JAM, Kahmen A, et al. 2016.** Stable isotopes in leaf water of terrestrial plants. *Plant, Cell & Environment* **39**(5): 1087-1102.
- Cernusak LA, Tcherkez G, Keitel C, Cornwell WK, Santiago LS, Knohl A, Barbour MM, Williams DG, Reich PB, Ellsworth DS. 2009.** Why are non-photosynthetic tissues generally ^{13}C enriched compared with leaves in C_3 plants? Review and synthesis of current hypotheses. *Functional Plant Biology* **36**(3): 199-213.

- Cernusak LA, Ubierna N, Winter K, Holtum JA, Marshall JD, Farquhar GD. 2013.** Environmental and physiological determinants of carbon isotope discrimination in terrestrial plants. *New Phytologist* **200**(4): 950-965.
- Coplen TB. 2011.** Guidelines and recommended terms for expression of stable-isotope-ratio and gas-ratio measurement results. *Rapid Communications in Mass Spectrometry* **25**(17): 2538-2560.
- Craig H, Gordon LI. 1965.** Deuterium and oxygen 18 variations in the ocean and the marine atmosphere. *Conference on Stable Isotopes in Oceanographic Studies and Paleotemperatures: Consiglio nazionale delle ricerche, Laboratorio de geologia nucleare, Pisa*
- Criddle R, Hopkin M, McArthur E, Hansen L. 1994.** Plant distribution and the temperature coefficient of metabolism. *Plant, Cell & Environment* **17**(3): 233-243.
- Dewar RC, Medlyn BE, Mcmurtrie RE. 1999.** Acclimation of the respiration/photosynthesis ratio to temperature: insights from a model. *Global Change Biology* **5**(5): 615-622.
- Diao H, Schuler P, Goldsmith GR, Siegwolf RT, Saurer M, Lehmann MM. 2022.** On uncertainties in plant water isotopic composition following extraction by cryogenic vacuum distillation. *Hydrology and Earth System Sciences Discussions*: 1-17.
- Downton WJS, Berry JA, Seemann JR. 1984.** Tolerance of photosynthesis to high temperature in desert plants. *Plant Physiology* **74**(4): 786-790.
- Farquhar GD, Ball M, von Caemmerer S, Roksandic Z. 1982a.** Effect of salinity and humidity on $\delta^{13}\text{C}$ value of halophytes-Evidence for diffusional isotope fractionation determined by the ratio of intercellular/atmospheric partial pressure of CO_2 under different environmental conditions. *Oecologia* **52**(1):121-124.

- Farquhar GD, Cernusak LA, Barnes B. 2007.** Heavy Water Fractionation during Transpiration. *Plant Physiology* **143**(1): 11-18.
- Farquhar GD, O'Leary MH, Berry JA. 1982b.** On the relationship between carbon isotope discrimination and the intercellular carbon dioxide concentration in leaves. *Functional Plant Biology* **9**(2): 121-137.
- Filot MS, Leuenberger M, Pazdur A, Boettger T. 2006.** Rapid online equilibration method to determine the D/H ratios of non-exchangeable hydrogen in cellulose. *Rapid Communications in Mass Spectrometry* **20**(22): 3337-3344.
- Gehre M, Geilmann H, Richter J, Werner R, Brand W. 2004.** Continuous flow $^2\text{H}/^1\text{H}$ and $^{18}\text{O}/^{16}\text{O}$ analysis of water samples with dual inlet precision. *Rapid Communications in Mass Spectrometry* **18**(22): 2650-2660.
- Grossiord C, Buckley TN, Cernusak LA, Novick KA, Poulter B, Siegwolf RT, Sperry JS, McDowell NG. 2020.** Plant responses to rising vapor pressure deficit. *New Phytologist* **226**(6): 1550-1566.
- Hoch G, Popp M, Körner C. 2002.** Altitudinal increase of mobile carbon pools in *Pinus cembra* suggests sink limitation of growth at the Swiss treeline. *Oikos* **98**(3): 361-374.
- Holloway-Phillips M, Baan J, Nelson DB, Lehmann MM, Tcherkez G, Kahmen A. 2022.** Species variation in the hydrogen isotope composition of leaf cellulose is mostly driven by isotopic variation in leaf sucrose. *Plant, Cell & Environment* **45**(9): 2636-2651.
- Jansen K, Du B, Kayler Z, Siegwolf R, Ensminger I, Rennenberg H, Kammerer B, Jaeger C, Schaub M, Kreuzwieser J. 2014.** Douglas-fir seedlings exhibit metabolic responses to increased temperature and atmospheric drought. *PloS one* **9**(12): e114165.
- Kawamitsu Y, Agata W, Miura S. 1987.** Effects of Vapour Pressure Difference on CO_2 Assimilation Rate, Leaf Conductance and Water Use

Efficiency in Grass Species. *Journal of the Faculty of Agriculture, Kyushu University* 31(1/2): 1-10

Kono Y, Ishida A, Saiki S-T, Yoshimura K, Dannoura M, Yazaki K, Kimura F, Yoshimura J, Aikawa S-i. 2019. Initial hydraulic failure followed by late-stage carbon starvation leads to drought-induced death in the tree *Trema orientalis*. *Communications Biology* 2(1): 8.

Lehmann MM, Egli M, Brinkmann N, Werner RA, Saurer M, Kahmen A. 2020. Improving the extraction and purification of leaf and phloem sugars for oxygen isotope analyses. *Rapid Communications in Mass Spectrometry* 34(19): e8854.

Lehmann MM, Vitali V, Schuler P, Leuenberger M, Saurer M. 2021. More than climate: Hydrogen isotope ratios in tree rings as novel plant physiological indicator for stress conditions. *Dendrochronologia* 65: 125788.

Lewis BE, Schramm VL. 2003. Binding equilibrium isotope effects for glucose at the catalytic domain of human brain hexokinase. *Journal of the American Chemical Society* 125(16): 4785-4798.

McMichael B, Burke J. 1994. Metabolic activity of cotton roots in response to temperature. *Environmental and Experimental Botany* 34(2): 201-206.

Medlyn B, Dreyer E, Ellsworth D, Forstreuter M, Harley P, Kirschbaum M, Le Roux X, Montpied P, Strassemeier J, Walcroft A. 2002. Temperature response of parameters of a biochemically based model of photosynthesis. II. A review of experimental data. *Plant, Cell & Environment* 25(9): 1167-1179.

Orsenigo M, Patrignani G, Rascio N. 1997. Ecophysiology of C₃, C₄ and CAM plants. Chapter in **Pessaraki M. 1997.** *Handbook of Photosynthesis*. Marcel Dekker, Inc.: 1-25.

Pedersen T. 2022. patchwork: The Composer of Plots.

- R.Core.Team** 2023. R: A language and environment for statistical computing. *R Foundation for Statistical Computing, Vienna, Austria.*
- Raison JK.** 1973. The influence of temperature-induced phase changes on the kinetics of respiratory and other membrane-associated enzyme systems. *Journal of Bioenergetics and Biomembranes.* 4: 285-309.
- Regehr DL, Bazzaz F.** 1976. Low temperature photosynthesis in successional winter annuals. *Ecology* 57(6): 1297-1303.
- Rehseh R, Rehseh S, Gast A, Jakob AL, Lehmann MM, Saurer M, Gessler A, Ruehr NK.** 2022. Tree allocation dynamics beyond heat and hot drought stress reveal changes in carbon storage, belowground translocation and growth. *New Phytologist* 233(2): 687-704.
- Rinne KT, Saurer M, Streit K, Siegwolf RT.** 2012. Evaluation of a liquid chromatography method for compound-specific $\delta^{13}\text{C}$ analysis of plant carbohydrates in alkaline media. *Rapid Communications in Mass Spectrometry* 26(18): 2173-2185.
- Roden JS, Lin G, Ehleringer JR.** 2000. A mechanistic model for interpretation of hydrogen and oxygen isotope ratios in tree-ring cellulose. *Geochimica et Cosmochimica Acta* 64(1): 21-35.
- Rowland L, da Costa AC, Galbraith DR, Oliveira RS, Binks OJ, Oliveira AA, Pullen A, Doughty CE, Metcalfe D, Vasconcelos SS.** 2015. Death from drought in tropical forests is triggered by hydraulics not carbon starvation. *Nature* 528(7580): 119-122.
- Scafaro AP, Fan Y, Posch BC, Garcia A, Coast O, Atkin OK.** 2021. Responses of leaf respiration to heatwaves. *Plant, Cell & Environment* 44(7): 2090-2101.
- Schönbeck L, Gessler A, Hoch G, McDowell NG, Rigling A, Schaub M, Li MH.** 2018. Homeostatic levels of nonstructural carbohydrates after 13 yr of drought and irrigation in *Pinus sylvestris*. *New Phytologist* 219(4): 1314-1324.

- Schönbeck LC, Schuler P, Lehmann MM, Mas E, Mekarni L, Pivovarov AL, Turberg P, Grossiord C. 2022.** Increasing temperature and vapour pressure deficit lead to hydraulic damages in the absence of soil drought. *Plant, Cell & Environment* **45**(11): 3275-3289.
- Schuler P, Cormier MA, Werner RA, Buchmann N, Gessler A, Vitali V, Saurer M, Lehmann MM. 2022.** A high temperature water vapor equilibration method to determine non-exchangeable hydrogen isotope ratios of sugar, starch, and cellulose. *Plant, Cell & Environment* **45**(1): 12-22.
- Schulze E-D, Lange O, Kappen L, Buschbom U, Evenari M. 1973.** Stomatal responses to changes in temperature at increasing water stress. *Planta* **110**: 29-42.
- Slot M, Nardwattanawong T, Hernández GG, Bueno A, Riederer M, Winter K. 2021.** Large differences in leaf cuticle conductance and its temperature response among 24 tropical tree species from across a rainfall gradient. *New Phytologist* **232**(4): 1618-1631.
- Smith FA, Freeman KH. 2006.** Influence of physiology and climate on δD of leaf wax n-alkanes from C_3 and C_4 grasses. *Geochimica et Cosmochimica Acta* **70**(5): 1172-1187.
- Sternberg L, Ellsworth PFV. 2011.** Divergent biochemical fractionation, not convergent temperature, explains cellulose oxygen isotope enrichment across latitudes. *PloS one* **6**(11): e28040.
- Tcherkez G, Mahé A, Hodges M. 2011.** $^{12}C/^{13}C$ fractionations in plant primary metabolism. *Trends in Plant Science* **16**(9): 499-506.
- Tinoco-Ojanguren C, Pearcy RW. 1993.** Stomatal dynamics and its importance to carbon gain in two rainforest *Piper* species: I. VPD effects on the transient stomatal response to lightflecks. *Oecologia* **94**: 388-394.

- Vitali V, Peters RL, Lehmann MM, Leuenberger M, Treydte K, Büntgen U, Schuler P, Saurer M. 2023.** Tree-ring isotopes from the Swiss Alps reveal non-climatic fingerprints of cyclic insect population outbreaks over the past 700 years. *Tree Physiology* **43**(5): 706-721.
- Weigt RB, Bräunlich S, Zimmermann L, Saurer M, Grams TE, Dietrich HP, Siegwolf RT, Nikolova PS. 2015.** Comparison of $\delta^{18}\text{O}$ and $\delta^{13}\text{C}$ values between tree-ring whole wood and cellulose in five species growing under two different site conditions. *Rapid Communications in Mass Spectrometry* **29**(23): 2233-2244.
- West AG, Patrickson SJ, Ehleringer JR. 2006.** Water extraction times for plant and soil materials used in stable isotope analysis. *Rapid Communications in Mass Spectrometry: An International Journal Devoted to the Rapid Dissemination of Up-to-the-Minute Research in Mass Spectrometry* **20**(8): 1317-1321.
- Wickham H. 2016.** ggplot2: Elegant Graphics for Data Analysis. Springer-Verlag New York Retrieved from <https://ggplot2.tidyverse.org>.
- Yakir D, DeNiro MJ. 1990.** Oxygen and hydrogen isotope fractionation during cellulose metabolism in *Lemna gibba* L. *Plant Physiology* **93**(1): 325-332.
- Zech M, Mayr C, Tuthorn M, Leiber-Sauheitl K, Glaser B. 2014.** Oxygen isotope ratios ($^{18}\text{O}/^{16}\text{O}$) of hemicellulose-derived sugar biomarkers in plants, soils and sediments as paleoclimate proxy I: Insight from a climate chamber experiment. *Geochimica et Cosmochimica Acta* **126**: 614-623.
- Zhang B-L, Billault I, Li X, Mabon F, Remaud G, Martin ML. 2002.** Hydrogen isotopic profile in the characterization of sugars. Influence of the metabolic pathway. *Journal of Agricultural and Food Chemistry* **50**(6): 1574-1580.

Zhao J, Hartmann H, Trumbore S, Ziegler W, Zhang Y. 2013. High temperature causes negative whole-plant carbon balance under mild drought. *New Phytologist* **200**(2): 330-339.

Supporting Information

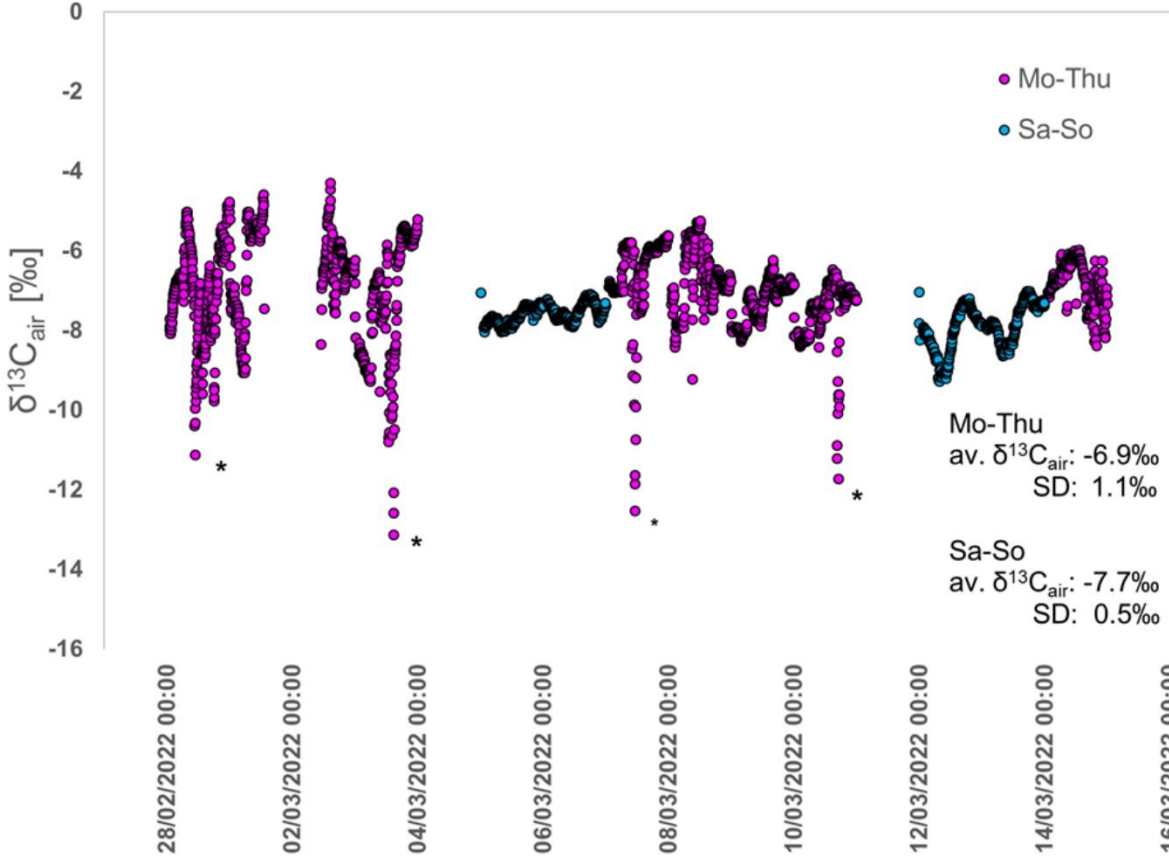


Figure 21: $\delta^{13}\text{C}$ of air CO_2 inside the climate chamber measured between 28.02.2022 and 14.03.2022, when the air temperature treatments were 10, 15, and 20 °C. Short-term drops (<30 min.), where are indicated by *, are caused by human respiration and occurred during visits to the climate chamber. The rapid recovery to previous $\delta^{13}\text{C}$ after the dips indicates a high rate of gas exchange between climate chamber and the surrounding atmosphere. Pink circles: $\delta^{13}\text{C}$ of air CO_2 from Monday to Thursday where CO_2 fixation occurred; light blue circles from Saturday to Sunday, where the climate chamber was constantly dark at 20 °C and thus only respiration occurred. Fridays are excluded since the isotopic variation during measurements will not influence the results as the sampling was performed on Thursdays.

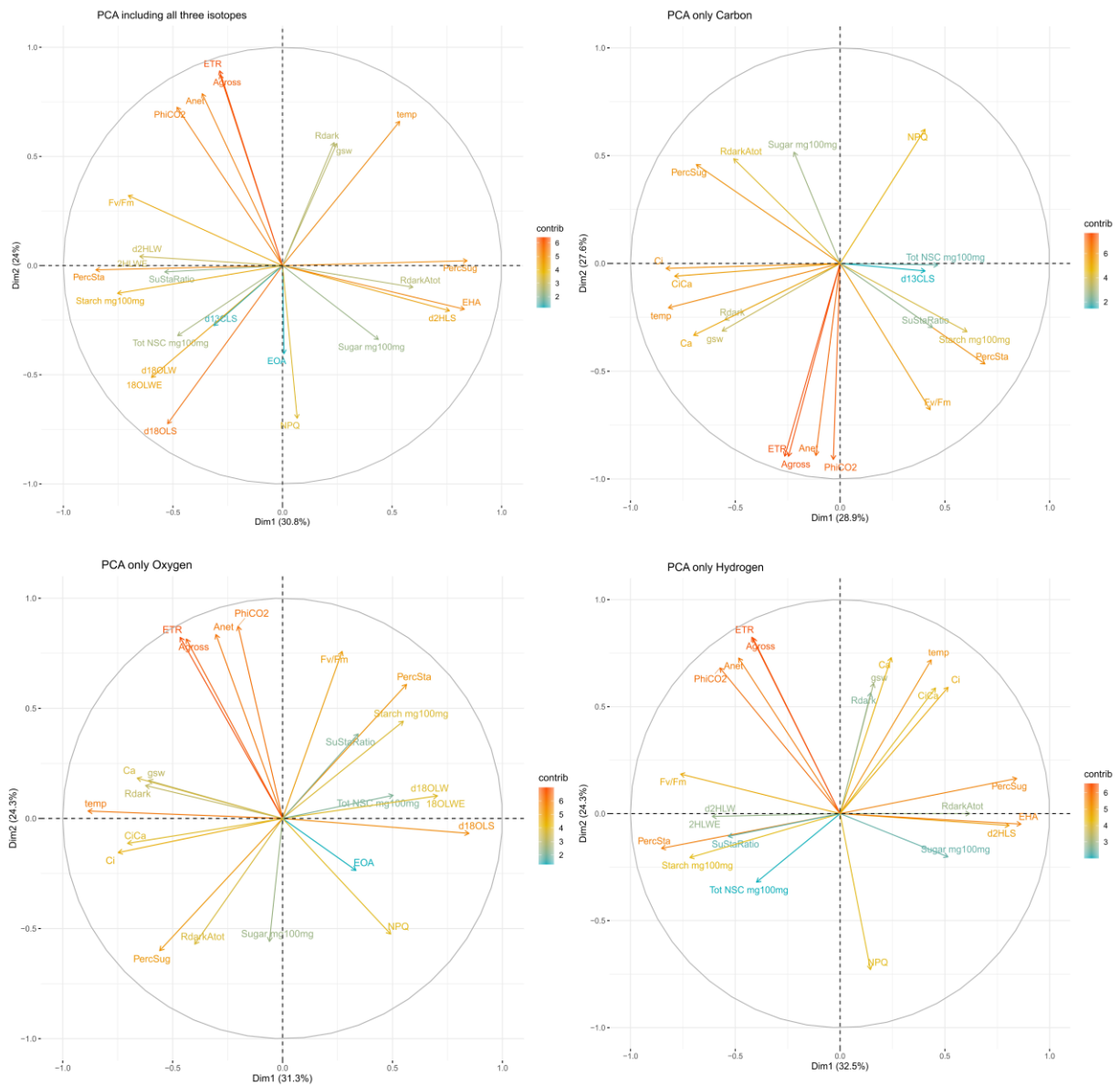


Figure S2: Principal Component Analysis (PCA) showing the patterns between the all the measured variables including: top left) ^{13}C , ^{18}O , and ^2H ; top right) only ^{13}C ; bottom left) only ^{18}O ; bottom right) only ^2H .

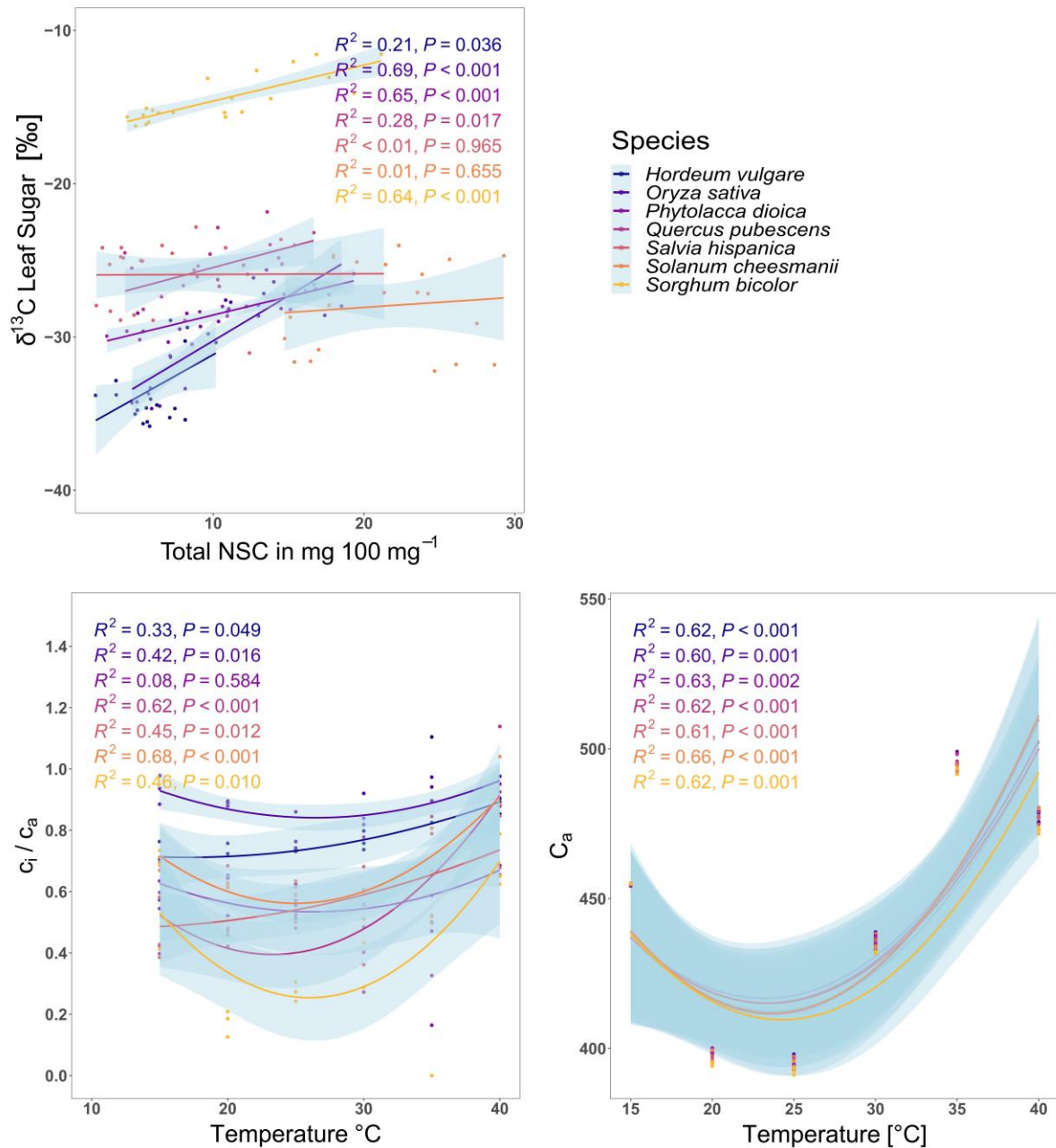


Figure S3: $\delta^{13}\text{C}$ of leaf sugar in response to the total leaf NSC concentration in $\text{mg } 100 \text{ mg}^{-1}$ leaf biomass, the temperature response of the $c_i:c_a$ ratio, and the temperature response of c_a . Species are indicated by colours, the linear and quadratic model depicting the relationships are shown only for species showing a significant response ($p \leq 0.05$), and the light blue shading denotes the 95% confidence level interval for predictions of the linear and quadratic fit, respectively.

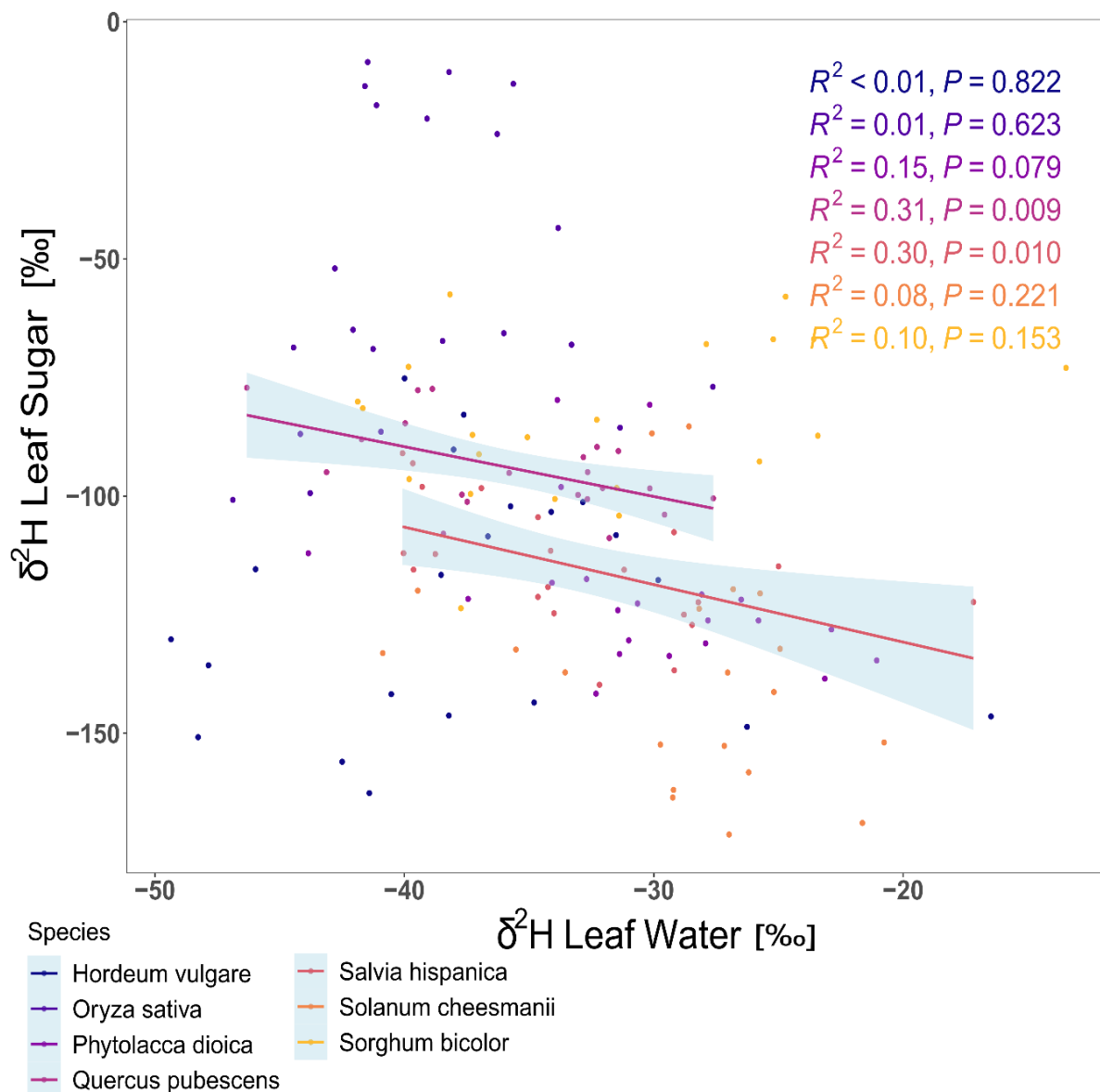


Figure S4: Relation of the $\delta^2\text{H}$ of the leaf sugar with the $\delta^2\text{H}$ of the leaf water. Species are indicated by colours, linear models depicting the relationship are shown only for species showing a significant response ($p \leq 0.05$), and the light blue shading denotes the 95% confidence level interval for predictions of the linear fit.

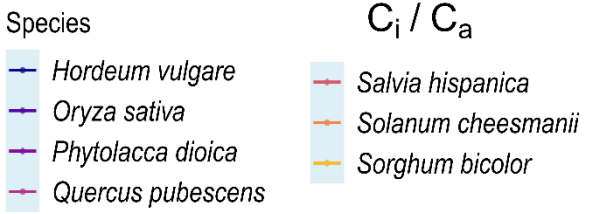
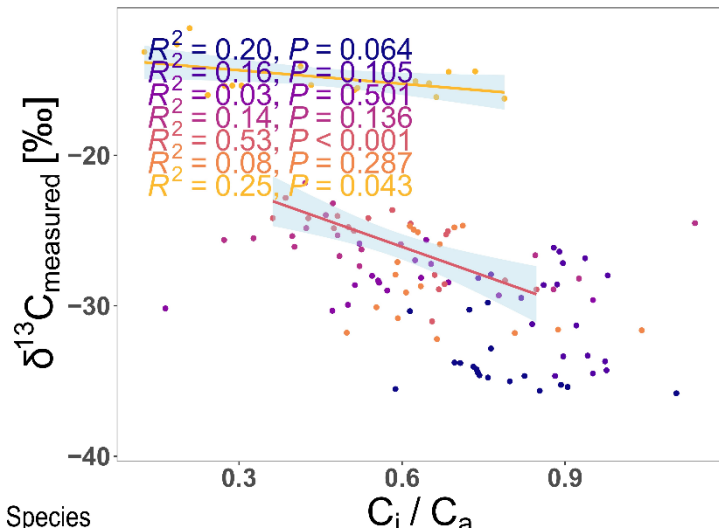
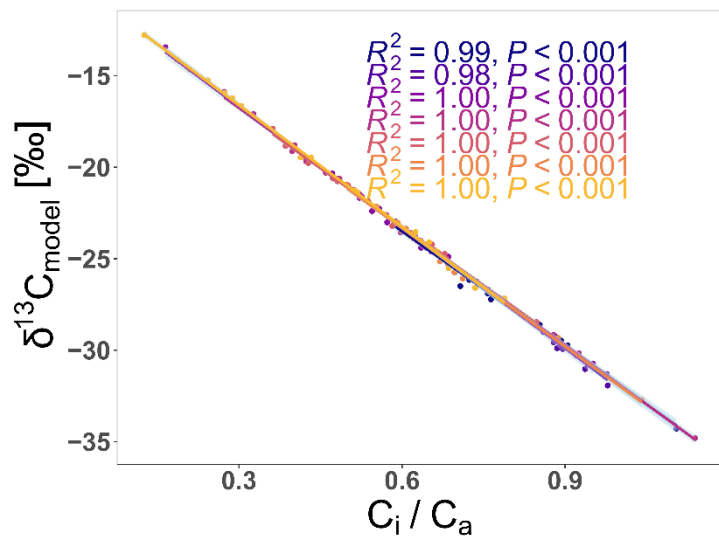
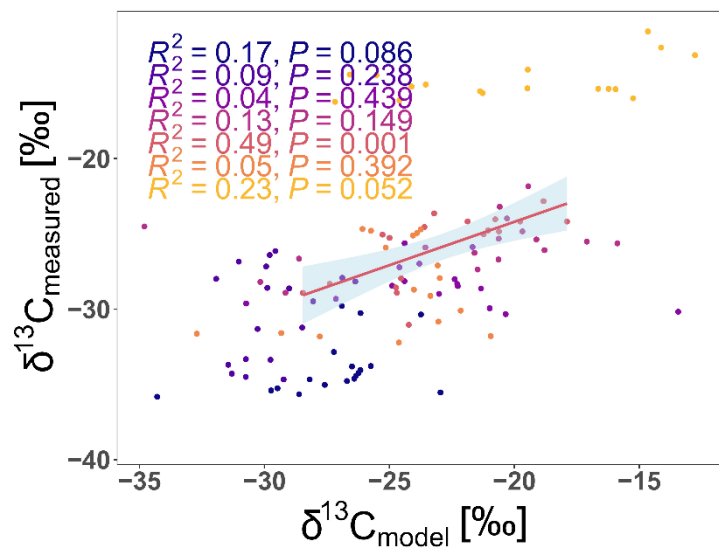


Figure S5: Linear regressions analysis of: top panel) the measured $\delta^{13}\text{C}$ of the leaf sugar against the modelled $\delta^{13}\text{C}$ values according to the Farquhar model, middle panel) the $\delta^{13}\text{C}$ according to the Farquhar model against the ratio of C_i over C_a , bottom panel) the measured $\delta^{13}\text{C}$ of the leaf sugar against the ratio of C_i over C_a . Species are indicated by colours, linear models depicting the relationship are shown only for species showing a significant response ($p \leq 0.05$), and the light blue shading denotes the 95% confidence level interval for predictions of the linear fit.

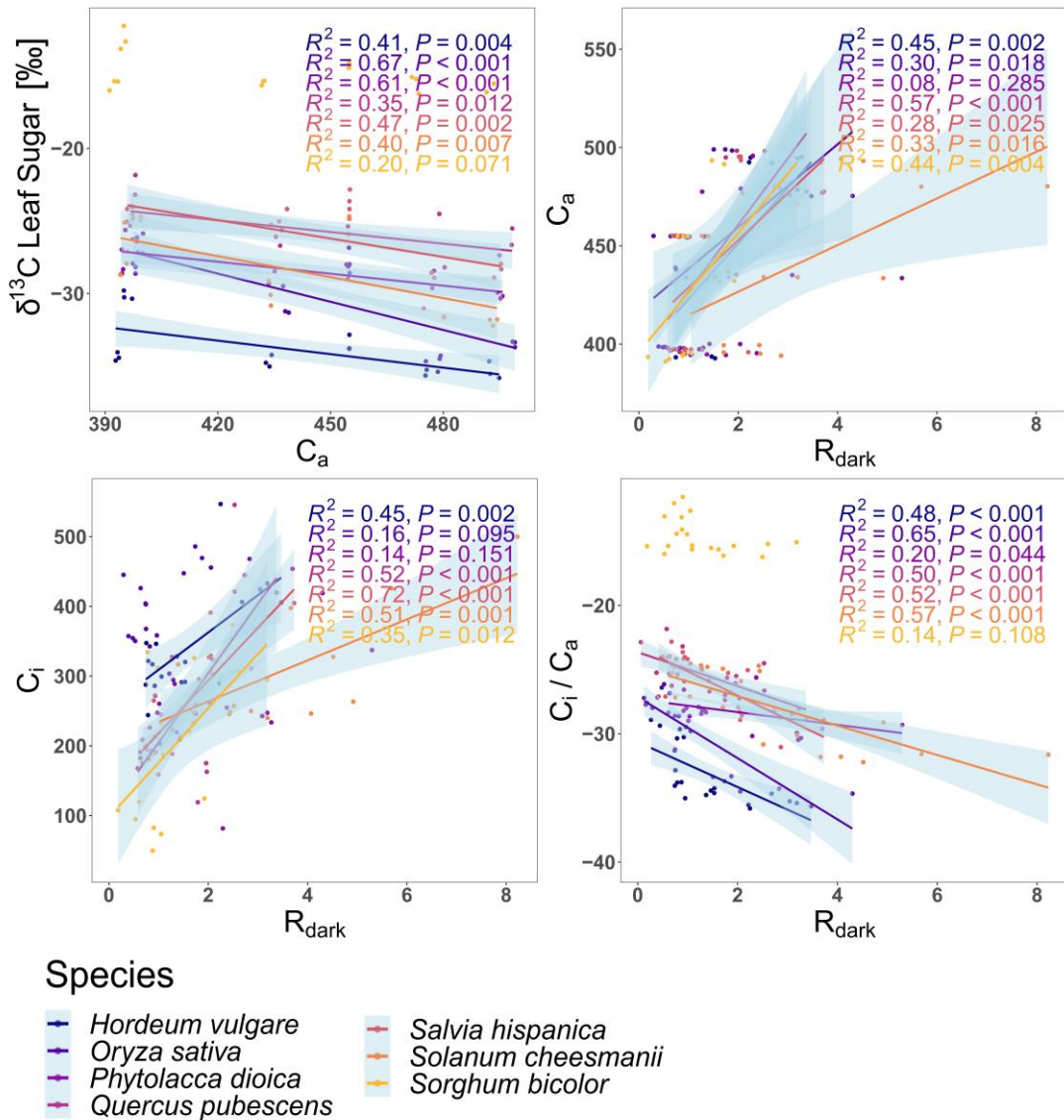


Figure S6: Linear regressions analysis of: top left panel) the measured $\delta^{13}\text{C}$ of the leaf sugar against the ambient CO_2 concentration in the climate chamber (c_a); top right panel) the leaf internal CO_2 concentration (c_i) against the dark respiration rate (R_{dark}); middle left panel) the measured $\delta^{13}\text{C}$ of the leaf sugar against the leaf internal CO_2 concentration (c_i); middle right panel) the leaf internal CO_2 concentration (c_i) against the dark respiration rate (R_{dark}); bottom panel) the ratio of C_i over C_a against the dark respiration rate (R_{dark}). Species are indicated by colours, linear models depicting the relationship are shown only for species showing a significant response ($p \leq 0.05$), and the light blue shading denotes the 95% confidence level interval for predictions of the linear fit.

Table S1: Temperature response of $\delta^{18}\text{O}$, $\delta^2\text{H}$ and $\delta^{13}\text{C}$ of irrigation water ($\delta^{18}\text{O}_{\text{IW}}$, $\delta^2\text{H}_{\text{IW}}$), leaf water ($\delta^{18}\text{O}_{\text{LW}}$, $\delta^2\text{H}_{\text{LW}}$), leaf sugar ($\delta^{18}\text{O}_{\text{LS}}$, $\delta^2\text{H}_{\text{LS}}$, $\delta^{13}\text{C}_{\text{LS}}$) and CO_2 of the air ($\delta^{13}\text{C}_{\text{Air}}$), as well as the biological fractionation factors between precursors (e.g. leaf water for ^{18}O and ^2H and CO_2 for ^{13}C) and leaf sugar (ϵ_{OA} , ϵ_{HA} and ϵ_{CA}) of the seven tested species.

Species	temp [°C]	$\delta^{18}\text{O}_{\text{IW}}$ [‰]	$\delta^{18}\text{O}_{\text{LW}}$ [‰]	$^{18}\text{O}_{\text{LWE}}$ [‰]	$\delta^{18}\text{O}_{\text{LS}}$ [‰]	ϵ_{OA} [‰]	$\delta^2\text{H}_{\text{IW}}$ [‰]	$\delta^2\text{H}_{\text{LW}}$ [‰]	$^2\text{H}_{\text{LWE}}$ [‰]	$\delta^2\text{H}_{\text{LS}}$ [‰]	ϵ_{HA} [‰]	$\delta^{13}\text{C}_{\text{Air}}$ [‰]	$\delta^{13}\text{C}_{\text{LS}}$ [‰]	ϵ_{CA} [‰]
<i>Hordeum vulgare</i>	10	-11.2	-0.4	10.8	29.3	29.8	-74.1	-40.5	33.6	-141.8	-101.2	-6.9	-29.4	-22.5
<i>Hordeum vulgare</i>	10	-11.2	0.5	11.7	28.6	28.1	-74.1	-38.2	35.9	-146.3	-108.0	-6.9	-28.9	-22.0
<i>Hordeum vulgare</i>	10	-11.2	1.9	13.2	31.8	29.9	-74.1	-38.5	35.6	-116.6	-78.1	-6.9	-29.6	-22.7
<i>Hordeum vulgare</i>	15	-11.2	-1.2	10.1	29.8	31.0	-74.1	-46.0	28.1	-115.4	-69.5	-6.9	-33.8	-26.9
<i>Hordeum vulgare</i>	15	-11.2	-1.5	9.7	30.2	31.8	-74.1	-49.4	24.8	-130.2	-80.8	-6.9	-33.8	-26.9
<i>Hordeum vulgare</i>	15	-11.2	-2.0	9.3	28.6	30.6	-74.1	-47.8	26.3	-135.7	-87.8	-6.9	-32.8	-25.9
<i>Hordeum vulgare</i>	20	-11.2	-1.7	9.5	28.5	30.2	-74.1	-48.3	25.8	-150.8	-102.6	-6.9	-30.3	-23.4
<i>Hordeum vulgare</i>	20	-11.2	0.2	11.4	26.7	26.5	-74.1	-41.4	32.7	-162.6	-121.2	-6.9	-29.8	-22.9
<i>Hordeum vulgare</i>	20	-11.2	0.0	11.2	27.5	27.5	-74.1	-42.5	31.6	-156.0	-113.5	-6.9	-30.4	-23.5
<i>Hordeum vulgare</i>	25	-11.2	0.5	11.7	26.8	26.4	-74.1	-16.5	57.6	-146.5	-130.0	-6.9	-34.1	-27.2
<i>Hordeum vulgare</i>	25	-11.2	-2.3	8.9	25.9	28.2	-74.1	-26.3	47.8	-148.7	-122.4	-6.9	-34.4	-27.5
<i>Hordeum vulgare</i>	25	-11.2	-2.4	8.8	26.7	29.1	-74.1	-34.8	39.3	-143.5	-108.7	-6.9	-34.6	-27.7
<i>Hordeum vulgare</i>	30	-11.2	-0.6	10.7	26.0	26.6	-74.1	-29.8	44.3	-117.7	-87.9	-6.9	-34.2	-27.3
<i>Hordeum vulgare</i>	30	-11.2	-1.4	9.9	25.5	26.8	-74.1	-31.5	42.6	-108.2	-76.7	-6.9	-35.0	-28.1
<i>Hordeum vulgare</i>	30	-11.2	-2.0	9.2	25.8	27.9	-74.1	-32.8	41.3	-101.3	-68.4	-6.9	-34.8	-27.9
<i>Hordeum vulgare</i>	35	-11.2	-3.1	8.1	22.0	25.1	-74.1	-36.6	37.5	-108.5	-71.8	-6.9	-34.7	-27.8
<i>Hordeum vulgare</i>	35	-11.2	-3.4	7.8	21.9	25.3	-74.1	-35.7	38.4	-102.1	-66.4	-6.9	-35.8	-28.9
<i>Hordeum vulgare</i>	35	-11.2	-3.1	8.1	22.5	25.6	-74.1	-34.1	40.0	-103.3	-69.2	-6.9	-35.5	-28.6
<i>Hordeum vulgare</i>	40	-11.2	-4.0	7.2	21.2	25.2	-74.1	-38.0	36.1	-90.2	-52.2	-6.9	-35.3	-28.4
<i>Hordeum vulgare</i>	40	-11.2	-4.2	7.1	21.0	25.2	-74.1	-40.0	34.1	-75.2	-35.2	-6.9	-35.7	-28.8
<i>Hordeum vulgare</i>	40	-11.2	-3.5	7.8	20.9	24.4	-74.1	-37.6	36.5	-82.9	-45.2	-6.9	-35.4	-28.5
<i>Oryza sativa</i>	10	-11.2	0.2	11.4	32.0	31.8	-74.1	-41.3	32.9	-69.0	-27.7	-6.9	-27.7	-20.8
<i>Oryza sativa</i>	10	-11.2	0.4	11.6	32.6	32.3	-74.1	-42.1	32.1	-64.9	-22.9	-6.9	-27.6	-20.7
<i>Oryza sativa</i>	10	-11.2	2.0	13.2	31.5	29.5	-74.1	-33.3	40.8	-68.1	-34.8	-6.9	-27.2	-20.3
<i>Oryza sativa</i>	15	-11.2	1.7	13.0	30.4	28.6	-74.1	-43.8	30.3	-99.4	-55.6	-6.9	-26.8	-19.9
<i>Oryza sativa</i>	15	-11.2	0.0	11.2	31.3	31.3	-74.1	-46.9	27.2	-100.8	-53.9	-6.9	-28.0	-21.1
<i>Oryza sativa</i>	15	-11.2	1.0	12.2	33.5	32.5	-74.1	-44.4	29.7	-68.7	-24.2	-6.9	-28.6	-21.7
<i>Oryza sativa</i>	20	-11.2	2.5	13.7	33.1	30.6	-74.1	-40.9	33.2	-86.4	-45.5	-6.9	-26.1	-19.2
<i>Oryza sativa</i>	20	-11.2	3.6	14.8	35.0	31.4	-74.1	-36.0	38.1	-65.7	-29.6	-6.9	-27.2	-20.3
<i>Oryza sativa</i>	20	-11.2	1.3	12.6	31.9	30.5	-74.1	-44.2	29.9	-86.9	-42.7	-6.9	-26.4	-19.5
<i>Oryza sativa</i>	25	-11.2	1.6	12.8	31.0	29.5	-74.1	-27.6	46.5	-77.0	-49.3	-6.9	-27.9	-21.0
<i>Oryza sativa</i>	25	-11.2	-1.5	9.7	30.7	32.2	-74.1	-38.5	35.6	-67.3	-28.8	-6.9	-28.6	-21.7
<i>Oryza sativa</i>	25	-11.2	0.2	11.4	30.8	30.6	-74.1	-31.4	42.8	-85.6	-54.2	-6.9	-28.2	-21.3
<i>Oryza sativa</i>	30	-11.2	-0.4	10.8	30.2	30.6	-74.1	-36.3	37.8	-23.7	12.6	-6.9	-31.3	-24.4
<i>Oryza sativa</i>	30	-11.2	0.0	11.3	28.8	28.8	-74.1	-33.8	40.3	-43.5	-9.6	-6.9	-29.5	-22.6
<i>Oryza sativa</i>	30	-11.2	-0.8	10.4	28.6	29.4	-74.1	-35.6	38.5	-13.1	22.6	-6.9	-31.2	-24.3
<i>Oryza sativa</i>	35	-11.2	-1.9	9.3	25.6	27.5	-74.1	-39.1	35.0	-20.4	18.7	-6.9	-33.7	-26.8
<i>Oryza sativa</i>	35	-11.2	-2.4	8.8	25.3	27.7	-74.1	-41.1	33.0	-17.6	23.5	-6.9	-33.3	-26.4
<i>Oryza sativa</i>	35	-11.2	-2.3	8.9	25.2	27.5	-74.1	-42.8	31.3	-52.0	-9.2	-6.9	-33.4	-26.5
<i>Oryza sativa</i>	40	-11.2	-4.2	7.1	24.2	28.4	-74.1	-41.5	32.6	-8.5	33.0	-6.9	-34.7	-27.8
<i>Oryza sativa</i>	40	-11.2	-4.2	7.1	24.6	28.8	-74.1	-41.6	32.5	-13.6	28.0	-6.9	-34.3	-27.4
<i>Oryza sativa</i>	40	-11.2	-3.9	7.4	23.7	27.6	-74.1	-38.2	35.9	-10.6	27.6	-6.9	-34.5	-27.6

<i>Phytolacca dioica</i>	10	-11.2	1.1	12.3	31.2	30.2	-74.1	-31.0	43.1	-130.4	-99.4	-6.9	-26.6	-19.7
<i>Phytolacca dioica</i>	10	-11.2	0.0	11.2	31.1	31.2	-74.1	-34.1	40.0	-118.3	-84.2	-6.9	-28.4	-21.5
<i>Phytolacca dioica</i>	10	-11.2	0.0	11.2	30.2	30.2	-74.1	-30.7	43.5	-122.6	-92.0	-6.9	-28.2	-21.3
<i>Phytolacca dioica</i>	15	-11.2	4.8	16.1	32.2	27.3	-74.1	-23.1	51.0	-138.5	-115.3	-6.9	-28.1	-21.2
<i>Phytolacca dioica</i>	15	-11.2	5.5	16.7	32.8	27.3	-74.1	-22.9	51.2	-128.1	-105.2	-6.9	-28.0	-21.1
<i>Phytolacca dioica</i>	15	-11.2	4.8	16.1	30.7	25.9	-74.1	-28.1	46.0	-120.7	-92.7	-6.9	-29.0	-22.1
<i>Phytolacca dioica</i>	20	-11.2	1.7	12.9	29.3	27.7	-74.1	-31.4	42.7	-124.1	-92.6	-6.9	-27.2	-20.3
<i>Phytolacca dioica</i>	20	-11.2	3.2	14.5	31.6	28.3	-74.1	-27.9	46.2	-131.1	-103.1	-6.9	-25.9	-19.0
<i>Phytolacca dioica</i>	20	-11.2	2.5	13.7	29.2	26.7	-74.1	-32.3	41.8	-141.7	-109.3	-6.9	-25.6	-18.7
<i>Phytolacca dioica</i>	25	-11.2	-0.2	11.0	27.8	28.0	-74.1	-25.8	48.3	-126.2	-100.4	-6.9	-28.6	-21.7
<i>Phytolacca dioica</i>	25	-11.2	0.7	12.0	26.7	25.9	-74.1	-26.5	47.6	-121.8	-95.3	-6.9	-28.3	-21.4
<i>Phytolacca dioica</i>	25	-11.2	2.0	13.2	28.2	26.3	-74.1	-21.1	53.0	-134.6	-113.6	-6.9	-27.0	-20.1
<i>Phytolacca dioica</i>	30	-11.2	-2.2	9.1	25.7	27.8	-74.1	-32.7	41.4	-117.5	-84.8	-6.9	-28.5	-21.6
<i>Phytolacca dioica</i>	30	-11.2	-0.1	11.1	25.0	25.1	-74.1	-27.8	46.3	-126.2	-98.4	-6.9	-29.3	-22.4
<i>Phytolacca dioica</i>	30	-11.2	-1.3	9.9	25.4	26.7	-74.1	-29.4	44.7	-133.7	-104.3	-6.9	-28.0	-21.1
<i>Phytolacca dioica</i>	35	-11.2	-0.8	10.4	22.9	23.7	-74.1	-31.4	42.7	-133.3	-101.9	-6.9	-30.3	-23.4
<i>Phytolacca dioica</i>	35	-11.2	-2.7	8.6	22.2	24.8	-74.1	-43.8	30.3	-112.1	-68.2	-6.9	-29.9	-23.0
<i>Phytolacca dioica</i>	35	-11.2	-1.9	9.4	23.3	25.2	-74.1	-37.4	36.7	-121.7	-84.2	-6.9	-30.2	-23.3
<i>Phytolacca dioica</i>	40	-11.2	0.1	11.3	25.6	25.5	-74.1	-30.2	43.9	-80.7	-50.6	-6.9	-28.4	-21.5
<i>Phytolacca dioica</i>	40	-11.2	-0.2	11.0	24.4	24.6	-74.1	-33.7	40.4	-98.1	-64.4	-6.9	-29.6	-22.7
<i>Phytolacca dioica</i>	40	-11.2	0.2	11.5	24.4	24.1	-74.1	-33.9	40.2	-79.8	-45.9	-6.9	-30.5	-23.6
<i>Quercus pubescens</i>	10	-11.2	7.1	18.4	31.3	24.2	-74.1	-30.2	44.0	-98.4	-68.2	-6.9	-22.9	-16.0
<i>Quercus pubescens</i>	10	-11.2	5.8	17.0	30.0	24.2	-74.1	-29.6	44.5	-103.9	-74.4	-6.9	-24.6	-17.7
<i>Quercus pubescens</i>	10	-11.2	5.7	16.9	30.8	25.2	-74.1	-31.8	42.3	-108.8	-77.1	-6.9	-25.2	-18.3
<i>Quercus pubescens</i>	15	-11.2	7.5	18.7	31.2	23.7	-74.1	-33.0	41.1	-99.8	-66.7	-6.9	-25.4	-18.5
<i>Quercus pubescens</i>	15	-11.2	8.8	20.0	31.3	22.5	-74.1	-32.1	42.1	-98.3	-66.2	-6.9	-24.8	-17.9
<i>Quercus pubescens</i>	15	-11.2	7.6	18.8	32.4	24.8	-74.1	-32.7	41.5	-95.0	-62.3	-6.9	-25.9	-19.0
<i>Quercus pubescens</i>	20	-11.2	6.2	17.5	31.0	24.7	-74.1	-37.5	36.6	-101.2	-63.7	-6.9	-21.8	-14.9
<i>Quercus pubescens</i>	20	-11.2	5.9	17.2	30.3	24.3	-74.1	-37.7	36.4	-99.7	-62.0	-6.9	-24.0	-17.1
<i>Quercus pubescens</i>	20	-11.2	6.9	18.1	31.7	24.8	-74.1	-38.4	35.7	-108.0	-69.5	-6.9	-23.2	-16.3
<i>Quercus pubescens</i>	25	-11.2	3.0	14.2			-74.1	-31.4	42.7	-90.5	-59.1	-6.9		
<i>Quercus pubescens</i>	25	-11.2	3.8	15.0	28.9	25.1	-74.1	-27.6	46.5	-100.5	-72.9	-6.9	-26.3	-19.4
<i>Quercus pubescens</i>	25	-11.2	4.3	15.6	29.6	25.3	-74.1	-32.7	41.4	-100.6	-68.0	-6.9	-25.3	-18.4
<i>Quercus pubescens</i>	30	-11.2	2.1	13.3	27.9	25.8	-74.1	-32.8	41.3	-91.8	-59.0	-6.9	-25.6	-18.7
<i>Quercus pubescens</i>	30	-11.2	2.9	14.1	28.1	25.2	-74.1	-32.3	41.8	-89.6	-57.4	-6.9	-26.1	-19.2
<i>Quercus pubescens</i>	30	-11.2	1.5	12.7	27.8	26.3	-74.1	-35.8	38.3	-95.1	-59.3	-6.9	-26.7	-19.8
<i>Quercus pubescens</i>	35	-11.2	3.5	14.7	28.1	24.6	-74.1	-40.0	34.1	-84.6	-44.7	-6.9	-25.5	-18.6
<i>Quercus pubescens</i>	35	-11.2	0.5	11.8	27.3	26.8	-74.1	-43.1	31.0	-95.0	-51.8	-6.9	-27.4	-20.5
<i>Quercus pubescens</i>	35	-11.2	2.3	13.5	27.2	24.9	-74.1	-41.7	32.4	-88.0	-46.3	-6.9	-26.6	-19.7
<i>Quercus pubescens</i>	40	-11.2	2.8	14.0	30.1	27.3	-74.1	-38.9	35.2	-77.4	-38.5	-6.9	-24.5	-17.6
<i>Quercus pubescens</i>	40	-11.2	2.4	13.6	26.8	24.4	-74.1	-39.5	34.7	-77.7	-38.2	-6.9	-28.2	-21.3
<i>Quercus pubescens</i>	40	-11.2	0.1	11.3	25.0	24.9	-74.1	-46.3	27.8	-77.2	-30.8	-6.9	-28.9	-22.0
<i>Salvia hispanica</i>	10	-11.2	3.9	15.1	31.8	27.9	-74.1	-31.2	42.9	-115.5	-84.3	-6.9	-27.1	-20.2
<i>Salvia hispanica</i>	10	-11.2	4.5	15.7	32.2	27.7	-74.1	-25.0	49.1	-114.8	-89.8	-6.9	-24.0	-17.1
<i>Salvia hispanica</i>	10	-11.2	4.4	15.6	32.2	27.8	-74.1	-29.2	44.9	-136.7	-107.5	-6.9	-27.1	-20.2
<i>Salvia hispanica</i>	15	-11.2	5.0	16.3	32.6	27.5	-74.1	-34.0	40.1	-124.7	-90.7	-6.9	-24.2	-17.3
<i>Salvia hispanica</i>	15	-11.2	5.5	16.8	33.0	27.4	-74.1	-29.2	44.9	-107.6	-78.4	-6.9	-22.8	-15.9
<i>Salvia hispanica</i>	15	-11.2	6.7	17.9	33.9	27.2	-74.1	-28.5	45.6	-127.2	-98.7	-6.9	-23.6	-16.7
<i>Salvia hispanica</i>	20	-11.2	2.9	14.1	31.1	28.2	-74.1	-34.1	40.0	-111.5	-77.4	-6.9	-24.0	-17.1
<i>Salvia hispanica</i>	20	-11.2	2.1	13.3	31.0	29.0	-74.1	-36.9	37.2	-98.3	-61.4	-6.9	-24.8	-17.9
<i>Salvia hispanica</i>	20	-11.2	1.5	12.7	29.9	28.4	-74.1	-38.8	35.4	-112.2	-73.5	-6.9	-25.0	-18.1
<i>Salvia hispanica</i>	25	-11.2	0.1	11.3	28.8	28.7	-74.1	-32.2	41.9	-139.8	-107.6	-6.9	-24.5	-17.6
<i>Salvia hispanica</i>	25	-11.2	1.1	12.3	29.0	27.9	-74.1	-28.8	45.3	-125.0	-96.2	-6.9	-24.2	-17.3
<i>Salvia hispanica</i>	25	-11.2	0.6	11.9	28.2	27.6	-74.1	-28.2	45.9	-122.4	-94.2	-6.9	-24.8	-17.9
<i>Salvia hispanica</i>	30	-11.2	0.7	11.9	27.0	26.3	-74.1	-34.6	39.5	-121.3	-86.6	-6.9	-25.0	-18.1
<i>Salvia hispanica</i>	30	-11.2	0.4	11.6	26.7	26.4	-74.1	-34.6	39.5	-104.4	-69.8	-6.9	-24.2	-17.3
<i>Salvia hispanica</i>	30	-11.2	0.4	11.7	26.5	26.0	-74.1	-34.2	39.9	-119.2	-84.9	-6.9	-25.3	-18.4
<i>Salvia hispanica</i>	35	-11.2	7.8	19.1	23.3	15.4	-74.1	-17.2	56.9	-122.3	-105.1	-6.9	-28.9	-22.0
<i>Salvia hispanica</i>	35	-11.2	-1.6	9.6	23.6	25.3	-74.1	-39.6	34.5	-115.5	-75.9	-6.9	-27.9	-21.0
<i>Salvia hispanica</i>	35	-11.2	-1.5	9.7	23.9	25.5	-74.1	-40.0	34.1	-112.0	-72.0	-6.9	-28.3	-21.4
<i>Salvia hispanica</i>	40	-11.2	-1.4	9.9	23.9	25.3	-74.1	-39.7	34.5	-93.1	-53.4	-6.9	-28.9	-22.0
<i>Salvia hispanica</i>	40	-11.2	-3.2	8.0	22.4	25.6	-74.1	-39.3	34.8	-98.1	-58.8	-6.9	-31.0	-24.1
<i>Salvia hispanica</i>	40	-11.2	-1.5	9.7	24.4	25.9	-74.1	-40.1	34.0	-91.0	-50.9	-6.9	-28.6	-21.7

<i>Solanum cheesmanii</i>	10	-11.2	2.1	13.4	33.3	31.2	-74.1	-33.6	40.6	-137.2	-103.6	-6.9	-24.0	-17.1
<i>Solanum cheesmanii</i>	10	-11.2	4.5	15.7	32.6	28.1	-74.1	-25.7	48.4	-120.5	-94.8	-6.9	-25.3	-18.4
<i>Solanum cheesmanii</i>	10	-11.2	3.0	14.2	33.9	30.9	-74.1	-28.2	45.9	-123.7	-95.6	-6.9	-27.2	-20.3
<i>Solanum cheesmanii</i>	15	-11.2	7.5	18.7	34.9	27.4	-74.1	-26.2	47.9	-158.2	-132.0	-6.9	-24.7	-17.8
<i>Solanum cheesmanii</i>	15	-11.2	5.6	16.9	34.5	28.9	-74.1	-27.2	46.9	-152.7	-125.5	-6.9	-24.8	-17.9
<i>Solanum cheesmanii</i>	15	-11.2	6.1	17.3	34.8	28.7	-74.1	-27.0	47.1	-137.2	-110.2	-6.9	-25.9	-19.0
<i>Solanum cheesmanii</i>	20	-11.2	5.7	17.0	33.9	28.2	-74.1	-27.0	47.1	-171.4	-144.4	-6.9	-24.7	-17.8
<i>Solanum cheesmanii</i>	20	-11.2	4.7	15.9	32.7	28.0	-74.1	-29.2	44.9	-163.6	-134.3	-6.9	-24.9	-18.0
<i>Solanum cheesmanii</i>	20	-11.2	3.7	15.0	33.5	29.8	-74.1	-29.2	44.9	-161.9	-132.7	-6.9	-25.1	-18.2
<i>Solanum cheesmanii</i>	25	-11.2	1.9	13.1	30.9	29.0	-74.1	-25.2	48.9	-141.3	-116.1	-6.9	-27.9	-21.0
<i>Solanum cheesmanii</i>	25	-11.2	2.3	13.6	30.7	28.3	-74.1	-21.6	52.5	-168.9	-147.3	-6.9	-27.1	-20.2
<i>Solanum cheesmanii</i>	25	-11.2	1.6	12.8	30.1	28.5	-74.1	-20.8	53.3	-151.9	-131.2	-6.9	-28.7	-21.8
<i>Solanum cheesmanii</i>	30	-11.2	1.3	12.6	28.6	27.3	-74.1	-26.8	47.3	-119.6	-92.8	-6.9	-30.1	-23.2
<i>Solanum cheesmanii</i>	30	-11.2	0.8	12.1	27.4	26.5	-74.1	-29.7	44.4	-152.4	-122.6	-6.9	-29.1	-22.2
<i>Solanum cheesmanii</i>	30	-11.2	1.2	12.5	28.3	27.0	-74.1	-24.9	49.2	-132.2	-107.2	-6.9	-30.8	-23.9
<i>Solanum cheesmanii</i>	35	-11.2	-1.4	9.8	24.6	26.1	-74.1	-35.5	38.6	-132.4	-96.8	-6.9	-31.8	-24.9
<i>Solanum cheesmanii</i>	35	-11.2	-1.7	9.6	24.4	26.1	-74.1	-39.5	34.6	-119.9	-80.5	-6.9	-32.2	-25.3
<i>Solanum cheesmanii</i>	35	-11.2	-2.6	8.7	23.9	26.5	-74.1	-40.9	33.2	-133.1	-92.2	-6.9	-31.8	-24.9
<i>Solanum cheesmanii</i>	40	-11.2	0.2	11.5	24.4	24.1	-74.1	-28.6	45.5	-85.3	-56.7	-6.9	-31.6	-24.7
<i>Solanum cheesmanii</i>	40	-11.2	-0.8	10.4	23.2	24.0	-74.1	-30.1	44.0	-86.8	-56.7	-6.9	-31.6	-24.7
<i>Sorghum bicolor</i>	10	-11.2	5.2	16.4	32.3	27.1	-74.1	-31.5	42.6	-98.3	-66.8	-6.9	-13.1	-6.2
<i>Sorghum bicolor</i>	10	-11.2	1.3	12.5	31.7	30.4	-74.1	-35.1	39.0	-87.6	-52.5	-6.9	-12.0	-5.1
<i>Sorghum bicolor</i>	10	-11.2	3.3	14.5	32.9	29.6	-74.1	-31.4	42.7	-104.1	-72.7	-6.9	-11.6	-4.7
<i>Sorghum bicolor</i>	15	-11.2	5.5	16.8	34.0	28.5	-74.1	-32.3	41.8	-83.9	-51.6	-6.9	-14.5	-7.6
<i>Sorghum bicolor</i>	15	-11.2	3.9	15.2	30.2	26.2	-74.1	-37.0	37.1	-91.2	-54.2	-6.9	-14.4	-7.5
<i>Sorghum bicolor</i>	15	-11.2	3.0	14.3	33.7	30.7	-74.1	-39.8	34.3	-72.8	-32.9	-6.9	-14.1	-7.2
<i>Sorghum bicolor</i>	20	-11.2	10.2	21.5	32.8	22.6	-74.1	-23.4	50.7	-87.3	-63.8	-6.9	-13.1	-6.2
<i>Sorghum bicolor</i>	20	-11.2	8.1	19.3	33.8	25.7	-74.1	-25.8	48.3	-92.7	-66.9	-6.9	-12.6	-5.7
<i>Sorghum bicolor</i>	20	-11.2	4.2	15.4	34.2	30.0	-74.1	-37.7	36.4	-123.6	-85.9	-6.9	-11.6	-4.7
<i>Sorghum bicolor</i>	25	-11.2	4.1	15.4	31.2	27.1	-74.1	-23.6	50.5	-66.9	-43.3	-6.9	-15.4	-8.5
<i>Sorghum bicolor</i>	25	-11.2	5.3	16.5	31.9	26.7	-74.1	-25.2	48.9	-66.9	-41.7	-6.9	-16.0	-9.1
<i>Sorghum bicolor</i>	25	-11.2	5.9	17.1	31.4	25.5	-74.1	-13.5	60.6	-73.0	-59.5	-6.9	-15.4	-8.5
<i>Sorghum bicolor</i>	30	-11.2	3.6	14.8	30.9	27.3	-74.1	-24.7	49.4	-58.0	-33.2	-6.9	-15.4	-8.5
<i>Sorghum bicolor</i>	30	-11.2	1.6	12.8	28.5	26.9	-74.1	-27.9	46.2	-67.9	-40.0	-6.9	-15.6	-8.7
<i>Sorghum bicolor</i>	30	-11.2	-0.1	11.1	27.9	28.0	-74.1	-37.3	36.8	-99.5	-62.2	-6.9	-15.3	-8.4
<i>Sorghum bicolor</i>	35	-11.2	-1.2	10.0	24.8	26.0	-74.1	-41.7	32.4	-81.5	-39.8	-6.9	-15.5	-8.6
<i>Sorghum bicolor</i>	35	-11.2	-2.2	9.1	25.5	27.6	-74.1	-41.9	32.2	-80.1	-38.2	-6.9	-15.6	-8.7
<i>Sorghum bicolor</i>	35	-11.2	1.4	12.7	26.3	24.9	-74.1	-34.0	40.1	-100.6	-66.6	-6.9	-16.1	-9.2
<i>Sorghum bicolor</i>	40	-11.2	-1.6	9.6	25.3	26.9	-74.1	-37.3	36.8	-87.1	-49.8	-6.9	-15.2	-8.3
<i>Sorghum bicolor</i>	40	-11.2	-1.2	10.1	26.2	27.4	-74.1	-38.2	35.9	-57.5	-19.3	-6.9	-16.2	-9.3
<i>Sorghum bicolor</i>	40	-11.2	-1.3	9.9	25.2	26.5	-74.1	-39.8	34.3	-96.4	-56.6	-6.9	-15.1	-8.2

Table S2: Temperature response of net assimilation (A_{net}), dark respiration (R_{dark}), gross photosynthesis (A_{gross}), percentage R_{dark} contributes to A_{gross} , stomatal conductance to water vapor (gsw), intercellular CO_2 (C_i), and the ambient to leaf CO_2 ratio of the seven tested species.

Species	temp [°C]	A_{net} [$\mu\text{mol m}^{-2} \text{s}^{-1}$]	R_{dark} [$\mu\text{mol m}^{-2} \text{s}^{-1}$]	A_{gross} [$\mu\text{mol m}^{-2} \text{s}^{-1}$]	$R_{\text{dark}}/A_{\text{tot}}$ [%]	gsw [$\text{mol m}^{-2} \text{s}^{-1}$]	C_i [$\mu\text{mol mol}^{-1}$]	CiCa
<i>Hordeum vulgare</i>	10	10.6	0.4	11.0	4.0	0.105	N.A.	N.A.
<i>Hordeum vulgare</i>	10	9.7	0.3	10.0	2.7	0.133	N.A.	N.A.
<i>Hordeum vulgare</i>	10	10.5	0.8	11.3	7.5	0.117	N.A.	N.A.
<i>Hordeum vulgare</i>	15	8.8	0.8	9.6	8.3	0.112	322	0.71
<i>Hordeum vulgare</i>	15	11.5	0.9	12.4	7.1	0.142	317	0.70
<i>Hordeum vulgare</i>	15	13.6	0.8	14.4	5.2	0.221	347	0.76
<i>Hordeum vulgare</i>	20	11.7	0.9	12.6	7.3	0.186	286	0.72
<i>Hordeum vulgare</i>	20	11.8	1.1	12.8	8.3	0.216	299	0.76
<i>Hordeum vulgare</i>	20	6.6	0.8	7.4	10.6	0.073	244	0.61
<i>Hordeum vulgare</i>	25	15.9	0.7	16.7	4.4	0.266	288	0.73
<i>Hordeum vulgare</i>	25	14.9	1.5	16.4	8.9	0.256	291	0.74
<i>Hordeum vulgare</i>	25	17.0	1.5	18.5	8.3	0.298	292	0.74
<i>Hordeum vulgare</i>	30	13.3	1.5	14.8	10.4	0.204	320	0.74
<i>Hordeum vulgare</i>	30	14.1	1.0	15.1	6.3	0.291	346	0.80
<i>Hordeum vulgare</i>	30	17.0	1.4	18.3	7.5	0.288	328	0.76
<i>Hordeum vulgare</i>	35	17.6	2.7	20.3	13.2	0.390	406	0.83
<i>Hordeum vulgare</i>	35	14.5	2.2	16.7	13.4	0.000	547	1.10
<i>Hordeum vulgare</i>	35	17.6	2.2	19.9	11.2	0.148	290	0.59
<i>Hordeum vulgare</i>	40	9.3	3.0	12.3	24.7	0.379	424	0.89
<i>Hordeum vulgare</i>	40	10.3	3.5	13.8	25.2	0.291	406	0.85
<i>Hordeum vulgare</i>	40	2.8	3.2	5.9	53.6	0.132	433	0.90
<i>Oryza sativa</i>	10	0.5	0.2	0.7	23.4	0.020	N.A.	N.A.
<i>Oryza sativa</i>	10	0.7	0.2	0.9	20.4	0.049	N.A.	N.A.
<i>Oryza sativa</i>	10	0.4	0.1	0.5	26.4	0.036	N.A.	N.A.
<i>Oryza sativa</i>	15	2.4	0.6	3.0	21.1	0.167	426	0.94
<i>Oryza sativa</i>	15	0.2	0.3	0.5	62.2	0.067	445	0.98
<i>Oryza sativa</i>	15	1.5	0.7	2.3	32.8	0.053	403	0.89
<i>Oryza sativa</i>	20	3.2	0.5	3.7	14.1	0.125	350	0.88
<i>Oryza sativa</i>	20	2.7	0.4	3.0	13.0	0.123	357	0.90
<i>Oryza sativa</i>	20	3.4	0.5	3.9	12.2	0.150	354	0.89
<i>Oryza sativa</i>	25	6.0	1.2	7.2	16.9	0.110	303	0.76
<i>Oryza sativa</i>	25	4.2	0.8	5.0	16.4	0.138	343	0.86
<i>Oryza sativa</i>	25	4.5	1.3	5.8	22.4	0.074	295	0.74
<i>Oryza sativa</i>	30	2.1	0.7	2.8	26.0	0.124	404	0.92
<i>Oryza sativa</i>	30	5.9	1.0	6.9	14.0	0.134	358	0.82
<i>Oryza sativa</i>	30	4.8	0.7	5.5	13.5	0.124	368	0.84
<i>Oryza sativa</i>	35	1.1	1.7	2.9	60.6	0.333	486	0.97
<i>Oryza sativa</i>	35	2.8	1.9	4.6	40.3	0.220	469	0.94
<i>Oryza sativa</i>	35	2.1	1.5	3.6	41.4	0.080	447	0.90
<i>Oryza sativa</i>	40	9.4	4.3	13.7	31.4	0.339	419	0.88
<i>Oryza sativa</i>	40	0.1	2.8	3.0	95.8	0.260	468	0.98
<i>Oryza sativa</i>	40	1.3	2.1	3.3	62.0	0.175	456	0.95

<i>Phytolacca dioica</i>	10	6.5	0.9	7.4	12.5	0.064	N.A.	N.A.
<i>Phytolacca dioica</i>	10	6.3	0.6	6.9	8.9	0.086	N.A.	N.A.
<i>Phytolacca dioica</i>	10	5.9	0.9	6.8	13.5	0.157	N.A.	N.A.
<i>Phytolacca dioica</i>	15	10.8	1.3	12.2	10.9	0.109	289	0.64
<i>Phytolacca dioica</i>	15	8.9	1.0	9.9	9.8	0.071	247	0.54
<i>Phytolacca dioica</i>	15	9.6	1.0	10.6	9.6	0.082	260	0.57
<i>Phytolacca dioica</i>	20	10.2	2.0	12.3	16.6	0.126	261	0.65
<i>Phytolacca dioica</i>	20	9.1	1.4	10.5	13.5	0.079	209	0.52
<i>Phytolacca dioica</i>	20	11.1	2.4	13.5	17.6	0.134	255	0.64
<i>Phytolacca dioica</i>	25	13.3	1.0	14.3	7.3	0.116	202	0.51
<i>Phytolacca dioica</i>	25	12.6	1.4	14.0	9.8	0.121	219	0.56
<i>Phytolacca dioica</i>	25	13.3	1.8	15.0	11.6	0.152	246	0.62
<i>Phytolacca dioica</i>	30	11.8	3.1	14.9	20.8	0.103	243	0.56
<i>Phytolacca dioica</i>	30	14.9	5.3	20.2	26.2	0.277	337	0.78
<i>Phytolacca dioica</i>	30	12.8	3.2	16.1	20.1	0.028	N.A.	N.A.
<i>Phytolacca dioica</i>	35	11.5	3.3	14.7	22.2	0.073	234	0.47
<i>Phytolacca dioica</i>	35	13.4	3.2	16.6	19.2	0.091	247	0.50
<i>Phytolacca dioica</i>	35	10.3	2.3	12.6	18.2	0.041	82	0.16
<i>Phytolacca dioica</i>	40	5.6	1.3	6.9	18.5	0.065	327	0.69
<i>Phytolacca dioica</i>	40	2.6	3.7	6.3	59.0	0.473	454	0.95
<i>Phytolacca dioica</i>	40	4.0	3.2	7.3	44.3	0.002	N.A.	N.A.
<i>Quercus pubescens</i>	10	1.6	0.1	1.6	3.9	0.004	N.A.	N.A.
<i>Quercus pubescens</i>	10	3.6	0.7	4.2	16.2	0.024	N.A.	N.A.
<i>Quercus pubescens</i>	10	2.8	0.4	3.2	11.9	0.020	N.A.	N.A.
<i>Quercus pubescens</i>	15	7.6	0.8	8.4	9.5	0.046	181	0.40
<i>Quercus pubescens</i>	15	4.2	0.8	5.0	16.8	0.026	193	0.42
<i>Quercus pubescens</i>	15	9.2	0.9	10.2	9.1	0.084	272	0.60
<i>Quercus pubescens</i>	20	4.8	0.6	5.4	10.8	0.034	168	0.42
<i>Quercus pubescens</i>	20	7.3	0.6	7.9	8.0	0.056	183	0.46
<i>Quercus pubescens</i>	20	4.8	0.9	5.7	15.7	0.038	188	0.47
<i>Quercus pubescens</i>	25	9.6	0.8	10.4	7.9	0.095	226	0.57
<i>Quercus pubescens</i>	25	6.4	0.7	7.1	9.6	0.056	209	0.53
<i>Quercus pubescens</i>	25	7.9	0.6	8.6	7.4	0.064	191	0.48
<i>Quercus pubescens</i>	30	7.2	1.8	9.0	19.9	0.037	119	0.27
<i>Quercus pubescens</i>	30	10.7	2.0	12.7	15.5	0.068	175	0.40
<i>Quercus pubescens</i>	30	8.3	1.4	9.7	14.8	0.061	212	0.48
<i>Quercus pubescens</i>	35	4.0	2.0	5.9	33.3	0.019	163	0.33
<i>Quercus pubescens</i>	35	12.2	1.7	14.0	12.5	0.087	258	0.52
<i>Quercus pubescens</i>	35	4.0	2.5	6.5	39.1	0.095	421	0.85
<i>Quercus pubescens</i>	40	3.2	2.5	5.7	44.1	0.000	545	1.14
<i>Quercus pubescens</i>	40	-0.6	2.7	4.9	55.7	0.000	445	0.93
<i>Quercus pubescens</i>	40	4.8	3.4	8.2	41.3	0.168	420	0.88
<i>Salvia hispanica</i>	10	4.6	0.4	5.0	8.3	0.036	N.A.	N.A.
<i>Salvia hispanica</i>	10	5.7	0.5	6.2	8.0	0.024	N.A.	N.A.
<i>Salvia hispanica</i>	10	4.1	0.6	4.7	11.8	0.043	N.A.	N.A.
<i>Salvia hispanica</i>	15	6.1	0.8	6.9	11.2	0.039	194	0.43
<i>Salvia hispanica</i>	15	6.7	0.7	7.3	9.2	0.039	176	0.39
<i>Salvia hispanica</i>	15	8.5	0.9	9.4	9.6	0.074	265	0.58
<i>Salvia hispanica</i>	20	6.2	0.9	7.2	13.2	0.050	191	0.48
<i>Salvia hispanica</i>	20	6.6	1.3	7.8	16.2	0.052	189	0.47
<i>Salvia hispanica</i>	20	9.8	2.2	12.0	18.4	0.134	271	0.68
<i>Salvia hispanica</i>	25	6.6	1.1	7.6	13.9	0.072	245	0.62
<i>Salvia hispanica</i>	25	9.9	0.9	10.8	8.5	0.090	213	0.54
<i>Salvia hispanica</i>	25	6.2	0.7	6.9	10.7	0.052	199	0.50
<i>Salvia hispanica</i>	30	8.9	1.3	10.2	12.6	0.069	223	0.51
<i>Salvia hispanica</i>	30	3.9	1.0	4.9	20.2	0.023	159	0.36
<i>Salvia hispanica</i>	30	13.8	1.8	15.7	11.6	0.171	296	0.68
<i>Salvia hispanica</i>	35	14.9	2.1	16.9	12.1	0.157	330	0.67
<i>Salvia hispanica</i>	35	10.7	2.0	12.8	15.8	0.109	327	0.66
<i>Salvia hispanica</i>	35	10.4	2.0	12.5	16.4	0.179	391	0.79
<i>Salvia hispanica</i>	40	5.2	3.7	8.9	41.8	0.136	405	0.85
<i>Salvia hispanica</i>	40	12.7	2.9	15.5	18.5	0.135	311	0.66
<i>Salvia hispanica</i>	40	7.2	2.1	9.3	22.4	0.083	323	0.68

<i>Solanum cheesmanii</i>	10	5.8	0.6	6.4	9.4	0.065	N.A.	N.A.
<i>Solanum cheesmanii</i>	10	4.1	0.7	4.8	14.4	0.066	N.A.	N.A.
<i>Solanum cheesmanii</i>	10	4.2	0.8	5.0	15.2	0.059	N.A.	N.A.
<i>Solanum cheesmanii</i>	15	7.3	1.3	8.6	14.8	0.094	324	0.71
<i>Solanum cheesmanii</i>	15	11.1	1.4	12.5	11.2	0.136	317	0.70
<i>Solanum cheesmanii</i>	15	10.0	2.1	12.1	17.1	0.112	305	0.67
<i>Solanum cheesmanii</i>	20	9.7	2.4	12.2	19.9	0.107	245	0.61
<i>Solanum cheesmanii</i>	20	10.5	1.7	12.2	14.0	0.117	248	0.62
<i>Solanum cheesmanii</i>	20	11.5	2.4	13.9	17.6	0.132	249	0.63
<i>Solanum cheesmanii</i>	25	10.3	1.7	12.0	14.2	0.106	233	0.59
<i>Solanum cheesmanii</i>	25	9.6	1.0	10.7	9.8	0.100	234	0.59
<i>Solanum cheesmanii</i>	25	14.1	2.9	16.9	16.9	0.167	250	0.63
<i>Solanum cheesmanii</i>	30	14.3	3.2	17.5	18.2	0.124	240	0.55
<i>Solanum cheesmanii</i>	30	15.4	4.9	20.3	24.2	0.154	263	0.61
<i>Solanum cheesmanii</i>	30	14.1	2.5	16.6	15.1	0.134	257	0.59
<i>Solanum cheesmanii</i>	35	17.4	3.7	21.1	17.4	0.346	398	0.81
<i>Solanum cheesmanii</i>	35	16.1	4.5	20.6	21.9	0.170	328	0.66
<i>Solanum cheesmanii</i>	35	13.6	4.1	17.7	23.0	0.092	246	0.50
<i>Solanum cheesmanii</i>	40	-2.7	8.2	10.9	75.3	0.132	500	1.04
<i>Solanum cheesmanii</i>	40	-0.2	5.7	5.9	96.3	0.000	426	0.89
<i>Sorghum bicolor</i>	10	3.0	0.5	3.6	15.0	0.010	N.A.	N.A.
<i>Sorghum bicolor</i>	10	4.5	0.7	5.2	13.9	0.039	N.A.	N.A.
<i>Sorghum bicolor</i>	10	2.6	N.A.	2.6	N.A.	0.039	N.A.	N.A.
<i>Sorghum bicolor</i>	15	9.2	1.0	10.2	9.7	0.108	312	0.69
<i>Sorghum bicolor</i>	15	8.8	0.8	9.6	8.1	0.125	334	0.73
<i>Sorghum bicolor</i>	15	8.9	0.9	9.8	9.1	0.054	188	0.41
<i>Sorghum bicolor</i>	20	14.3	0.9	15.2	5.8	0.068	50	0.13
<i>Sorghum bicolor</i>	20	11.0	1.1	12.1	8.7	0.056	73	0.19
<i>Sorghum bicolor</i>	20	12.3	0.9	13.2	6.8	0.065	83	0.21
<i>Sorghum bicolor</i>	25	16.1	0.2	16.3	1.1	0.093	108	0.27
<i>Sorghum bicolor</i>	25	21.5	0.5	22.1	2.4	0.120	95	0.24
<i>Sorghum bicolor</i>	25	18.3	0.6	18.9	3.2	0.111	119	0.30
<i>Sorghum bicolor</i>	30	19.4	1.9	21.3	9.0	0.104	124	0.29
<i>Sorghum bicolor</i>	30	20.0	1.6	21.6	7.5	0.160	221	0.51
<i>Sorghum bicolor</i>	30	18.6	1.1	19.6	5.6	0.126	187	0.43
<i>Sorghum bicolor</i>	35	15.7	1.5	17.1	8.6	0.111	256	0.52
<i>Sorghum bicolor</i>	35	17.8	1.1	18.9	5.7	0.039	N.A.	0.00
<i>Sorghum bicolor</i>	35	20.1	1.7	21.8	7.9	0.210	326	0.66
<i>Sorghum bicolor</i>	40	16.6	2.6	19.2	13.6	0.176	307	0.65
<i>Sorghum bicolor</i>	40	14.5	2.5	17.0	14.7	0.266	373	0.79
<i>Sorghum bicolor</i>	40	19.4	3.2	22.6	14.1	0.194	295	0.62

Table S3: Temperature response of the amount of non-structural carbohydrates (NSC), sugar, starch, per 100 mg leaf dry mass, the contribution in % of sugar and starch to the total leaf NSC, and the ratio of leaf sugar to leaf starch of the seven tested species.

Species	temp [°C]	NSC [mg per 100mg]	Sugar [mg per 100mg]	Starch [mg per 100mg]	Sugar [% of total NSC]	Starch [% of total NSC]	Sugar:Starch Ratio
<i>Hordeum vulgare</i>	10	8.29	5.41	2.88	65	35	0.53
<i>Hordeum vulgare</i>	10	7.17	4.52	2.66	63	37	0.59
<i>Hordeum vulgare</i>	10	5.36	3.56	1.80	66	34	0.51
<i>Hordeum vulgare</i>	15	2.21	0.97	1.24	44	56	1.27
<i>Hordeum vulgare</i>	15	3.57	1.94	1.63	54	46	0.84
<i>Hordeum vulgare</i>	15	3.56	1.92	1.63	54	46	0.85
<i>Hordeum vulgare</i>	20	8.14	5.11	3.03	63	37	0.59
<i>Hordeum vulgare</i>	20	9.67	7.24	2.43	75	25	0.34
<i>Hordeum vulgare</i>	20	10.18	7.17	3.01	70	30	0.42
<i>Hordeum vulgare</i>	25	5.85	3.53	2.32	60	40	0.66
<i>Hordeum vulgare</i>	25	6.27	4.11	2.16	66	34	0.53
<i>Hordeum vulgare</i>	25	5.57	3.69	1.88	66	34	0.51
<i>Hordeum vulgare</i>	30	4.94	3.53	1.41	71	29	0.40
<i>Hordeum vulgare</i>	30	4.83	2.78	2.04	58	42	0.74
<i>Hordeum vulgare</i>	30	4.97	3.51	1.46	71	29	0.42
<i>Hordeum vulgare</i>	35	7.46	9.86	0.00	100	0	N.A.
<i>Hordeum vulgare</i>	35	5.79	8.03	0.00	100	0	N.A.
<i>Hordeum vulgare</i>	35	5.63	7.51	0.00	100	0	N.A.
<i>Hordeum vulgare</i>	40	7.12	8.18	0.00	100	0	N.A.
<i>Hordeum vulgare</i>	40	5.35	5.05	0.31	94	6	0.06
<i>Hordeum vulgare</i>	40	8.15	7.91	0.23	97	3	0.03
<i>Oryza sativa</i>	10	11.16	8.65	2.52	77	23	0.29
<i>Oryza sativa</i>	10	10.83	8.87	1.96	82	18	0.22
<i>Oryza sativa</i>	10	14.72	11.82	2.90	80	20	0.25
<i>Oryza sativa</i>	15	16.79	14.92	1.87	89	11	0.13
<i>Oryza sativa</i>	15	18.51	16.53	1.98	89	11	0.12
<i>Oryza sativa</i>	15	17.40	14.84	2.56	85	15	0.17
<i>Oryza sativa</i>	20	12.67	9.94	2.73	78	22	0.27
<i>Oryza sativa</i>	20	13.36	10.24	3.11	77	23	0.30
<i>Oryza sativa</i>	20	14.02	11.66	2.36	83	17	0.20
<i>Oryza sativa</i>	25	13.00	9.68	3.32	74	26	0.34
<i>Oryza sativa</i>	25	13.00	9.52	3.48	73	27	0.37
<i>Oryza sativa</i>	25	11.03	9.78	1.25	89	11	0.13
<i>Oryza sativa</i>	30	7.17	9.07	0.00	100	0	N.A.
<i>Oryza sativa</i>	30	7.78	9.76	0.00	100	0	N.A.
<i>Oryza sativa</i>	30	7.15	7.85	0.00	100	0	N.A.
<i>Oryza sativa</i>	35	5.71	7.16	0.00	100	0	N.A.
<i>Oryza sativa</i>	35	5.83	7.54	0.00	100	0	N.A.
<i>Oryza sativa</i>	35	8.14	10.11	0.00	100	0	N.A.
<i>Oryza sativa</i>	40	5.92	7.47	0.00	100	0	N.A.
<i>Oryza sativa</i>	40	4.63	6.00	0.00	100	0	N.A.
<i>Oryza sativa</i>	40	6.45	4.72	0.00	73	0	N.A.
<i>Phytolacca dioica</i>	10	16.68	2.12	14.57	13	87	6.89
<i>Phytolacca dioica</i>	10	9.11	2.17	6.94	24	76	3.20
<i>Phytolacca dioica</i>	10	15.12	2.12	13.01	14	86	6.14
<i>Phytolacca dioica</i>	15	14.50	2.44	12.06	17	83	4.94
<i>Phytolacca dioica</i>	15	12.20	2.39	9.81	20	80	4.10
<i>Phytolacca dioica</i>	15	10.35	1.66	8.70	16	84	5.25
<i>Phytolacca dioica</i>	20	17.68	1.65	16.02	9	91	9.68
<i>Phytolacca dioica</i>	20	19.32	3.18	16.15	16	84	5.08
<i>Phytolacca dioica</i>	20	13.53	2.39	11.15	18	82	4.67
<i>Phytolacca dioica</i>	25	10.94	1.82	9.11	17	83	5.00
<i>Phytolacca dioica</i>	25	10.95	1.83	9.12	17	83	4.99
<i>Phytolacca dioica</i>	25	16.12	2.05	14.07	13	87	6.87
<i>Phytolacca dioica</i>	30	8.25	2.41	5.85	29	71	2.43
<i>Phytolacca dioica</i>	30	9.16	3.26	5.89	36	64	1.81
<i>Phytolacca dioica</i>	30	10.62	2.88	7.74	27	73	2.68
<i>Phytolacca dioica</i>	35	7.02	4.28	2.74	61	39	0.64
<i>Phytolacca dioica</i>	35	2.96	1.90	1.06	64	36	0.56
<i>Phytolacca dioica</i>	35	5.13	3.44	1.69	67	33	0.49
<i>Phytolacca dioica</i>	40	5.00	4.47	0.53	89	11	0.12
<i>Phytolacca dioica</i>	40	4.28	3.91	0.37	91	9	0.10
<i>Phytolacca dioica</i>	40	8.60	3.45	5.15	40	60	1.49

<i>Quercus pubescens</i>	10	10.31	7.04	3.27	68	32	0.46
<i>Quercus pubescens</i>	10	9.79	6.69	3.11	68	32	0.46
<i>Quercus pubescens</i>	10	14.56	8.81	5.75	61	39	0.65
<i>Quercus pubescens</i>	15	9.00	6.78	2.22	75	25	0.33
<i>Quercus pubescens</i>	15	14.34	7.60	6.74	53	47	0.89
<i>Quercus pubescens</i>	15	12.29	8.86	3.43	72	28	0.39
<i>Quercus pubescens</i>	20	13.59	6.18	7.40	46	54	1.20
<i>Quercus pubescens</i>	20	13.77	7.06	6.71	51	49	0.95
<i>Quercus pubescens</i>	20	16.66	7.87	8.79	47	53	1.12
<i>Quercus pubescens</i>	25	6.27	5.03	1.24	80	20	0.25
<i>Quercus pubescens</i>	25	10.30	6.11	4.19	59	41	0.69
<i>Quercus pubescens</i>	25	12.02	5.95	6.06	50	50	1.02
<i>Quercus pubescens</i>	30	8.74	9.65	0.00	100	0	N.A.
<i>Quercus pubescens</i>	30	8.94	8.79	0.16	98	2	0.02
<i>Quercus pubescens</i>	30	10.40	9.08	1.32	87	13	0.15
<i>Quercus pubescens</i>	35	4.61	5.99	0.00	100	0	0.00
<i>Quercus pubescens</i>	35	6.57	7.01	0.00	100	0	0.00
<i>Quercus pubescens</i>	35	8.02	7.43	0.59	93	7	0.08
<i>Quercus pubescens</i>	40	4.15	4.11	0.04	99	1	0.01
<i>Quercus pubescens</i>	40	5.37	5.31	0.05	99	1	0.01
<i>Quercus pubescens</i>	40	8.12	6.15	1.98	76	24	0.32
<i>Salvia hispanica</i>	10	15.47	2.86	12.61	19	81	4.41
<i>Salvia hispanica</i>	10	15.39	2.29	13.11	15	85	5.72
<i>Salvia hispanica</i>	10	21.33	4.21	17.11	20	80	4.06
<i>Salvia hispanica</i>	15	10.83	3.35	7.48	31	69	2.24
<i>Salvia hispanica</i>	15	8.86	2.52	6.34	28	72	2.51
<i>Salvia hispanica</i>	15	14.49	3.25	11.24	22	78	3.46
<i>Salvia hispanica</i>	20	6.61	0.31	6.30	5	95	20.07
<i>Salvia hispanica</i>	20	4.04	0.53	3.51	13	87	6.61
<i>Salvia hispanica</i>	20	5.31	0.32	5.00	6	94	15.82
<i>Salvia hispanica</i>	25	7.29	0.00	7.29	0	100	20.00
<i>Salvia hispanica</i>	25	3.91	0.00	3.91	0	100	20.00
<i>Salvia hispanica</i>	25	3.87	0.00	3.87	0	100	20.00
<i>Salvia hispanica</i>	30	5.20	1.83	3.38	35	65	1.85
<i>Salvia hispanica</i>	30	2.66	1.39	1.27	52	48	0.91
<i>Salvia hispanica</i>	30	3.14	1.70	1.45	54	46	0.85
<i>Salvia hispanica</i>	35	3.86	0.93	2.93	24	76	3.14
<i>Salvia hispanica</i>	35	2.25	1.54	0.72	68	32	0.46
<i>Salvia hispanica</i>	35	3.19	1.61	1.58	50	50	0.98
<i>Salvia hispanica</i>	40	6.02	3.06	2.96	51	49	0.97
<i>Salvia hispanica</i>	40	12.41	2.91	9.49	23	77	3.26
<i>Salvia hispanica</i>	40	4.75	2.47	2.28	52	48	0.92
<i>Solanum cheesmanii</i>	10	22.31	10.12	12.19	45	55	1.21
<i>Solanum cheesmanii</i>	10	21.43	7.85	13.57	37	63	1.73
<i>Solanum cheesmanii</i>	10	24.25	9.32	14.93	38	62	1.60
<i>Solanum cheesmanii</i>	15	17.98	3.12	14.86	17	83	4.77
<i>Solanum cheesmanii</i>	15	17.97	2.77	15.20	15	85	5.48
<i>Solanum cheesmanii</i>	15	23.85	5.46	18.39	23	77	3.37
<i>Solanum cheesmanii</i>	20	29.27	3.09	26.19	11	89	8.48
<i>Solanum cheesmanii</i>	20	25.67	2.80	22.87	11	89	8.18
<i>Solanum cheesmanii</i>	20	19.52	3.29	16.23	17	83	4.93
<i>Solanum cheesmanii</i>	25	17.68	4.19	13.49	24	76	3.22
<i>Solanum cheesmanii</i>	25	23.54	3.44	20.11	15	85	5.85
<i>Solanum cheesmanii</i>	25	15.11	3.02	12.09	20	80	4.00
<i>Solanum cheesmanii</i>	30	14.74	3.91	10.83	27	73	2.77
<i>Solanum cheesmanii</i>	30	27.49	9.89	17.60	36	64	1.78
<i>Solanum cheesmanii</i>	30	16.99	6.91	10.09	41	59	1.46
<i>Solanum cheesmanii</i>	35	28.65	10.62	18.03	37	63	1.70
<i>Solanum cheesmanii</i>	35	24.68	10.38	14.30	42	58	1.38
<i>Solanum cheesmanii</i>	35	26.10	8.41	17.69	32	68	2.10
<i>Solanum cheesmanii</i>	40	15.39	12.55	2.84	82	18	0.23
<i>Solanum cheesmanii</i>	40	16.46	12.45	4.00	76	24	0.32

<i>Sorghum bicolor</i>	10	17.68	11.49	6.20	65	35	0.54
<i>Sorghum bicolor</i>	10	15.31	11.57	3.74	76	24	0.32
<i>Sorghum bicolor</i>	10	16.85	10.96	5.88	65	35	0.54
<i>Sorghum bicolor</i>	15	13.82	8.71	5.11	63	37	0.59
<i>Sorghum bicolor</i>	15	11.24	7.71	3.52	69	31	0.46
<i>Sorghum bicolor</i>	15	19.35	7.88	11.47	41	59	1.46
<i>Sorghum bicolor</i>	20	9.63	5.53	4.11	57	43	0.74
<i>Sorghum bicolor</i>	20	12.87	8.60	4.26	67	33	0.50
<i>Sorghum bicolor</i>	20	21.14	8.61	12.53	41	59	1.45
<i>Sorghum bicolor</i>	25	6.37	3.98	2.39	63	37	0.60
<i>Sorghum bicolor</i>	25	5.73	2.96	2.77	52	48	0.94
<i>Sorghum bicolor</i>	25	7.34	4.66	2.68	63	37	0.58
<i>Sorghum bicolor</i>	30	10.76	10.89	0.00	100	0	N.A.
<i>Sorghum bicolor</i>	30	10.82	11.64	0.00	100	0	N.A.
<i>Sorghum bicolor</i>	30	11.92	12.33	0.00	100	0	N.A.
<i>Sorghum bicolor</i>	35	5.36	4.20	1.16	78	22	0.28
<i>Sorghum bicolor</i>	35	4.30	3.03	1.27	70	30	0.42
<i>Sorghum bicolor</i>	35	5.55	4.04	1.51	73	27	0.37
<i>Sorghum bicolor</i>	40	5.99	4.68	1.31	78	22	0.28
<i>Sorghum bicolor</i>	40	4.86	4.93	0.00	100	0	N.A.
<i>Sorghum bicolor</i>	40	5.58	5.10	0.48	91	9	0.09

Table S4: Temperature response of the chlorophyll fluorescence measurements, the ratio between cell internal and ambient CO₂ concentration, e.g. the ratio of minimum to maximum fluorescence (FvFm), Photosystem II efficiency (PhiPSII), electron transport rate (ETR), quantum yield calculated from CO₂ assimilation (PhiCO₂), and the non-photochemical quenching (NPQ) of the seven tested species.

Species	temp [°C]	CiCa	FvFm	PhiPS2	ETR [μmol s ⁻¹]	PhiCO ₂ [μmol μmol ⁻¹]	NPQ
<i>Hordeum vulgare</i>	10	N.A.	0.79	0.41	52.3	0.044	0.68
<i>Hordeum vulgare</i>	10	N.A.	0.81	0.38	47.6	0.039	1.35
<i>Hordeum vulgare</i>	10	N.A.	0.77	0.40	50.1	0.045	0.92
<i>Hordeum vulgare</i>	15	0.71	0.79	0.47	59.4	0.038	1.01
<i>Hordeum vulgare</i>	15	0.70	0.79	0.51	64.0	0.049	0.78
<i>Hordeum vulgare</i>	15	0.76	0.80	0.53	67.3	0.057	0.65
<i>Hordeum vulgare</i>	20	0.72	0.81	0.54	68.4	0.050	0.49
<i>Hordeum vulgare</i>	20	0.76	0.80	0.55	69.3	0.051	0.55
<i>Hordeum vulgare</i>	20	0.61	0.81	0.49	61.6	0.029	0.49
<i>Hordeum vulgare</i>	25	0.73	0.81	0.55	93.5	0.049	0.42
<i>Hordeum vulgare</i>	25	0.74	0.78	0.55	92.7	0.049	0.38
<i>Hordeum vulgare</i>	25	0.74	0.80	0.57	96.3	0.055	0.33
<i>Hordeum vulgare</i>	30	0.74	0.80	0.56	94.8	0.044	0.34
<i>Hordeum vulgare</i>	30	0.80	0.78	0.61	103.6	0.045	0.13
<i>Hordeum vulgare</i>	30	0.76	0.79	0.58	98.3	0.054	0.23
<i>Hordeum vulgare</i>	35	0.83	0.76	0.57	107.2	0.054	0.21
<i>Hordeum vulgare</i>	35	1.10	0.73	0.49	93.2	0.044	0.27
<i>Hordeum vulgare</i>	35	0.59	0.76	0.57	108.2	0.052	0.17
<i>Hordeum vulgare</i>	40	0.89	0.76	0.42	80.0	0.032	0.77
<i>Hordeum vulgare</i>	40	0.85	0.77	0.49	92.5	0.036	0.53
<i>Hordeum vulgare</i>	40	0.90	0.55	0.21	40.3	0.016	0.68
<i>Oryza sativa</i>	10	N.A.	0.71	0.03	3.7	0.003	0.78
<i>Oryza sativa</i>	10	N.A.	0.68	0.07	8.8	0.004	1.27
<i>Oryza sativa</i>	10	N.A.	0.76	0.02	2.9	0.002	0.93
<i>Oryza sativa</i>	15	0.94	0.72	0.14	17.6	0.012	0.83
<i>Oryza sativa</i>	15	0.98	0.59	0.06	7.4	0.002	0.58
<i>Oryza sativa</i>	15	0.89	0.68	0.16	20.0	0.009	1.08
<i>Oryza sativa</i>	20	0.88	0.72	0.20	24.7	0.015	0.77
<i>Oryza sativa</i>	20	0.90	0.72	0.17	21.8	0.012	0.90
<i>Oryza sativa</i>	20	0.89	0.76	0.18	22.7	0.016	1.58
<i>Oryza sativa</i>	25	0.76	0.76	0.37	63.0	0.021	1.46
<i>Oryza sativa</i>	25	0.86	0.68	0.21	35.3	0.015	1.11
<i>Oryza sativa</i>	25	0.74	0.72	0.30	51.3	0.017	0.93
<i>Oryza sativa</i>	30	0.92	0.68	0.20	34.2	0.008	1.12
<i>Oryza sativa</i>	30	0.82	0.54	0.26	43.8	0.020	0.73
<i>Oryza sativa</i>	30	0.84	0.58	0.19	32.6	0.016	0.80
<i>Oryza sativa</i>	35	0.97	0.53	0.11	21.2	0.008	1.39
<i>Oryza sativa</i>	35	0.94	0.64	0.12	23.4	0.012	0.66
<i>Oryza sativa</i>	35	0.90	0.60	0.11	21.4	0.010	0.89
<i>Oryza sativa</i>	40	0.88	0.78	0.41	77.4	0.036	0.69
<i>Oryza sativa</i>	40	0.98	0.46	0.04	7.4	0.008	0.93
<i>Oryza sativa</i>	40	0.95	0.53	0.07	12.4	0.009	0.91

<i>Phytolacca dioica</i>	10	N.A.	0.76	0.22	28.0	0.029	1.59
<i>Phytolacca dioica</i>	10	N.A.	0.76	0.23	28.5	0.027	1.41
<i>Phytolacca dioica</i>	10	N.A.	0.66	0.21	26.6	0.027	1.18
<i>Phytolacca dioica</i>	15	0.64	0.78	0.50	63.2	0.048	0.98
<i>Phytolacca dioica</i>	15	0.54	0.77	0.48	60.2	0.039	1.02
<i>Phytolacca dioica</i>	15	0.57	0.79	0.46	58.3	0.042	0.91
<i>Phytolacca dioica</i>	20	0.65	0.81	0.58	73.0	0.049	0.57
<i>Phytolacca dioica</i>	20	0.52	0.83	0.59	75.2	0.042	0.74
<i>Phytolacca dioica</i>	20	0.64	0.79	0.60	75.6	0.053	0.48
<i>Phytolacca dioica</i>	25	0.51	0.82	0.61	102.6	0.042	0.33
<i>Phytolacca dioica</i>	25	0.56	0.83	0.61	103.5	0.041	0.34
<i>Phytolacca dioica</i>	25	0.62	0.82	0.61	102.8	0.045	0.38
<i>Phytolacca dioica</i>	30	0.56	0.83	0.63	107.0	0.044	0.42
<i>Phytolacca dioica</i>	30	0.78	0.82	0.64	108.1	0.060	0.32
<i>Phytolacca dioica</i>	30	N.A.	0.83	0.64	108.5	0.048	0.50
<i>Phytolacca dioica</i>	35	0.47	0.82	0.59	112.4	0.039	0.65
<i>Phytolacca dioica</i>	35	0.50	0.82	0.58	110.8	0.044	0.57
<i>Phytolacca dioica</i>	35	0.16	0.83	0.57	108.6	0.033	0.79
<i>Phytolacca dioica</i>	40	0.69	0.76	0.28	53.5	0.018	1.42
<i>Phytolacca dioica</i>	40	0.95	0.59	0.22	41.0	0.017	0.97
<i>Phytolacca dioica</i>	40	N.A.	0.74	0.30	56.8	0.019	1.48
<i>Quercus pubescens</i>	10	N.A.	0.77	0.19	24.2	0.006	1.47
<i>Quercus pubescens</i>	10	N.A.	0.74	0.21	26.7	0.017	1.19
<i>Quercus pubescens</i>	10	N.A.	0.73	0.12	15.0	0.012	0.60
<i>Quercus pubescens</i>	15	0.40	0.79	0.54	68.1	0.033	0.69
<i>Quercus pubescens</i>	15	0.42	0.75	0.42	53.4	0.020	0.76
<i>Quercus pubescens</i>	15	0.60	0.78	0.47	59.7	0.040	0.55
<i>Quercus pubescens</i>	20	0.42	0.80	0.51	64.6	0.021	0.73
<i>Quercus pubescens</i>	20	0.46	0.80	0.55	69.2	0.031	0.47
<i>Quercus pubescens</i>	20	0.47	0.79	0.35	44.6	0.023	0.46
<i>Quercus pubescens</i>	25	0.57	0.80	0.53	90.0	0.031	0.40
<i>Quercus pubescens</i>	25	0.53	0.80	0.50	84.5	0.021	0.68
<i>Quercus pubescens</i>	25	0.48	0.81	0.39	66.3	0.025	0.35
<i>Quercus pubescens</i>	30	0.27	0.80	0.57	96.3	0.027	0.59
<i>Quercus pubescens</i>	30	0.40	0.78	0.53	90.0	0.038	0.16
<i>Quercus pubescens</i>	30	0.48	0.80	0.54	91.6	0.029	0.31
<i>Quercus pubescens</i>	35	0.33	0.75	0.38	72.7	0.016	0.59
<i>Quercus pubescens</i>	35	0.52	0.75	0.52	98.9	0.037	0.29
<i>Quercus pubescens</i>	35	0.85	0.75	0.33	61.8	0.017	0.45
<i>Quercus pubescens</i>	40	1.14	0.34	0.19	36.9	0.015	0.09
<i>Quercus pubescens</i>	40	0.93	0.53	0.03	6.2	0.006	1.11
<i>Quercus pubescens</i>	40	0.88	0.72	0.39	73.7	0.022	0.84

<i>Salvia hispanica</i>	10	N.A.	0.77	0.16	20.7	0.020	1.97
<i>Salvia hispanica</i>	10	N.A.	0.72	0.25	31.5	0.025	1.07
<i>Salvia hispanica</i>	10	N.A.	0.80	0.16	20.2	0.019	1.45
<i>Salvia hispanica</i>	15	0.43	0.82	0.33	41.1	0.027	1.58
<i>Salvia hispanica</i>	15	0.39	0.82	0.41	51.3	0.029	1.36
<i>Salvia hispanica</i>	15	0.58	0.81	0.48	61.1	0.037	1.14
<i>Salvia hispanica</i>	20	0.48	0.81	0.51	64.1	0.028	0.77
<i>Salvia hispanica</i>	20	0.47	0.80	0.50	63.1	0.031	0.98
<i>Salvia hispanica</i>	20	0.68	0.79	0.55	69.3	0.047	0.71
<i>Salvia hispanica</i>	25	0.62	0.79	0.42	71.6	0.023	1.20
<i>Salvia hispanica</i>	25	0.54	0.80	0.54	91.0	0.032	0.61
<i>Salvia hispanica</i>	25	0.50	0.80	0.52	87.2	0.021	0.69
<i>Salvia hispanica</i>	30	0.51	0.80	0.57	95.6	0.030	0.57
<i>Salvia hispanica</i>	30	0.36	0.78	0.45	76.4	0.015	1.17
<i>Salvia hispanica</i>	30	0.68	0.80	0.63	105.7	0.046	0.33
<i>Salvia hispanica</i>	35	0.67	0.79	0.63	119.8	0.045	0.27
<i>Salvia hispanica</i>	35	0.66	0.80	0.58	109.1	0.034	0.51
<i>Salvia hispanica</i>	35	0.79	0.76	0.57	108.1	0.033	0.24
<i>Salvia hispanica</i>	40	0.85	0.73	0.43	81.6	0.023	0.94
<i>Salvia hispanica</i>	40	0.66	0.74	0.57	108.4	0.041	0.21
<i>Salvia hispanica</i>	40	0.68	0.75	0.50	95.0	0.025	0.65
<i>Solanum cheesmanii</i>	10	N.A.	0.79	0.24	30.2	0.025	1.47
<i>Solanum cheesmanii</i>	10	N.A.	0.69	0.15	18.3	0.019	1.02
<i>Solanum cheesmanii</i>	10	N.A.	0.71	0.15	19.2	0.020	0.96
<i>Solanum cheesmanii</i>	15	0.71	0.82	0.42	53.7	0.034	0.82
<i>Solanum cheesmanii</i>	15	0.70	0.83	0.52	66.1	0.049	0.75
<i>Solanum cheesmanii</i>	15	0.67	0.81	0.51	64.3	0.048	0.61
<i>Solanum cheesmanii</i>	20	0.61	0.81	0.61	76.7	0.048	0.39
<i>Solanum cheesmanii</i>	20	0.62	0.83	0.57	72.5	0.048	0.44
<i>Solanum cheesmanii</i>	20	0.63	0.82	0.65	82.7	0.055	0.26
<i>Solanum cheesmanii</i>	25	0.59	0.84	0.49	83.4	0.036	0.87
<i>Solanum cheesmanii</i>	25	0.59	0.82	0.46	77.1	0.032	0.99
<i>Solanum cheesmanii</i>	25	0.63	0.83	0.61	102.3	0.050	0.38
<i>Solanum cheesmanii</i>	30	0.55	0.83	0.63	106.2	0.052	0.31
<i>Solanum cheesmanii</i>	30	0.61	0.82	0.69	117.0	0.060	0.22
<i>Solanum cheesmanii</i>	30	0.59	0.84	0.63	106.3	0.049	0.32
<i>Solanum cheesmanii</i>	35	0.81	0.80	0.65	122.6	0.056	0.29
<i>Solanum cheesmanii</i>	35	0.66	0.81	0.65	123.7	0.054	0.24
<i>Solanum cheesmanii</i>	35	0.50	0.81	0.61	114.9	0.047	0.37
<i>Solanum cheesmanii</i>	40	1.04	0.68	0.19	35.1	0.015	1.19
<i>Solanum cheesmanii</i>	40	0.89	0.70	0.22	42.0	0.014	1.19

<i>Sorghum bicolor</i>	10	N.A.	0.75	0.12	15.0	0.014	1.56
<i>Sorghum bicolor</i>	10	N.A.	0.72	0.19	23.6	0.021	1.30
<i>Sorghum bicolor</i>	10	N.A.	0.75	0.11	13.4	0.009	1.12
<i>Sorghum bicolor</i>	15	0.69	0.76	0.38	47.6	0.040	1.31
<i>Sorghum bicolor</i>	15	0.73	0.76	0.37	46.5	0.038	1.18
<i>Sorghum bicolor</i>	15	0.41	0.77	0.39	48.8	0.039	1.31
<i>Sorghum bicolor</i>	20	0.13	0.77	0.58	72.8	0.060	0.47
<i>Sorghum bicolor</i>	20	0.19	0.77	0.53	67.1	0.048	0.69
<i>Sorghum bicolor</i>	20	0.21	0.77	0.53	67.2	0.052	0.62
<i>Sorghum bicolor</i>	25	0.27	0.78	0.48	80.6	0.048	0.72
<i>Sorghum bicolor</i>	25	0.24	0.79	0.56	94.4	0.065	0.52
<i>Sorghum bicolor</i>	25	0.30	0.78	0.52	87.5	0.056	0.56
<i>Sorghum bicolor</i>	30	0.29	0.77	0.59	99.9	0.063	0.41
<i>Sorghum bicolor</i>	30	0.51	0.77	0.60	101.5	0.064	0.34
<i>Sorghum bicolor</i>	30	0.43	0.77	0.54	91.8	0.058	0.45
<i>Sorghum bicolor</i>	35	0.52	0.75	0.44	84.1	0.045	0.75
<i>Sorghum bicolor</i>	35	0.00	0.73	0.46	87.1	0.050	0.48
<i>Sorghum bicolor</i>	35	0.66	0.76	0.50	94.3	0.057	0.62
<i>Sorghum bicolor</i>	40	0.65	0.73	0.46	87.1	0.051	0.57
<i>Sorghum bicolor</i>	40	0.79	0.76	0.43	81.2	0.045	0.93
<i>Sorghum bicolor</i>	40	0.62	0.74	0.53	100.6	0.060	0.50

Chapter 6

General discussion

Measuring the stable isotope composition of plant carbohydrates can provide information about plant functioning or allow us to reconstruct past climatic conditions. However, this requires detailed knowledge of the isotopic fractionation processes involved. While the biological fractionation processes of ^{13}C and ^{18}O isotopes are relatively well understood, the processes responsible for biological ^2H fractionation remained elusive.

In my thesis, I first implemented a high-throughput method to measure the $\delta^2\text{H}$ of a large number of carbohydrate samples. I have then investigated various biochemical and physiological processes in the carbohydrate metabolism of plants at the leaf and twig level. My aim was to include a large number of plant species from various functional groups to test them under different climatic conditions in order to uncover the biological drivers behind the ^2H fractionation.

With this approach I was able to investigate how the ^2H fractionation reflects the phylogenetic relationship between tree and shrub species in leaves and twigs and what we can learn from this, how the different biochemical pathways of plants with C_3 , C_4 and CAM CO_2 fixation affects the ^2H fractionation at the leaf level, and how this fractionation interacts with changes in temperature and VPD. Finally, I investigated how a strong temperature increase affects the leaf-level carbon balance of plants, and how this is reflected in the fractionation of ^2H , ^{13}C and ^{18}O isotopes.

In the following sections, I will discuss the findings of my work, put them into context and discuss what we still need to study to fully understand ^2H fractionation at the whole plant level.

The ^2H fractionation during CO_2 fixation ϵ_{HA} is driven by enzymatic reactions, reflects the phylogeny of trees and shrubs, and varies between different types of CO_2 fixation

Photosynthetic ^2H fractionation has long been considered to be a stable process, consistent within a type of CO_2 fixation (Luo *et al.*, 1991; Roden *et al.*, 2000), and only altered by the amount of exchange with hydrogen from the surrounding water (Sternberg, 1989; Luo & Sternberg, 1992; Augusti *et al.*, 2006; Holloway-Phillips *et al.*, 2022). However, in recent years it has become increasingly clear that ^2H fractionation is influenced by plant performance (Sanchez-Bragado *et al.*, 2019) and metabolism (Wieloch *et al.*, 2022), and varies between different plant species (Holloway-Phillips *et al.*, 2022) and types of CO_2 fixation (Zhang *et al.*, 2002).

In Chapter 3, we used a phylogenetic analysis to show that the photosynthetic ^2H fractionation between leaf water and leaf sugar, as well as the $\delta^2\text{H}$ of leaf sugar, strongly reflect the phylogenetic relationships among tree and shrub species. We concluded that this photosynthetic ^2H fractionation in C_3 plants is likely driven by a relatively simple enzymatic reaction during the light-dependent reactions of CO_2 fixation, leading to the species-specific ^2H depletion in sugars of C_3 plants (Holloway-Phillips *et al.*, 2022). This finding was further supported by Chapter 4, where we compared the differences in ^2H fractionation in plants with C_3 , C_4 and CAM CO_2 fixation. The light-dependent reactions of C_3 CO_2 fixation take place in the same cells as the final CO_2 fixation, whereas this process is spatially separated in C_4 and largely absent in CAM plants. Since the sugars of C_3 plants were highly depleted in ^2H in contrast to C_4 and CAM species, the ^2H depleting reaction most likely takes place during the light-dependent reactions.

The species-specific response to temperature changes observed in Chapter 4 could not be reproduced in the same way in Chapter 5. We suggest that the species-specific pattern in ^2H fractionation in response to changes in

temperature and VPD observed in Chapter 4 may be caused by the lower light availability (with a photosynthetic active radiation of 110 $\mu\text{mol photons m}^{-2} \text{s}^{-1}$ in chapter 4 vs. 800 $\mu\text{mol photons m}^{-2} \text{s}^{-1}$ in chapter 5). This could lead to species-specific changes in the balance between photosynthesis and respiration, depending on the ability of a plant species to assimilate under low light conditions (Niinemets *et al.*, 1999; Niinemets, 2007). Therefore, some species may have responded by increasing respiration relative to photosynthesis more than others, resulting in respiratory ^2H enrichment of leaf sugar and cellulose. On the other hand, plants that are better adapted to fix CO_2 under low light conditions may have benefited from the temperature increase with higher photosynthesis compared to respiration and thus have more ^2H -depleted sugars at 30 °C.

The post-photosynthetic ^2H fractionation in carbohydrates

In the standard model for calculating $\delta^2\text{H}$ in plant carbohydrates, exchange reactions between the hydrogen of the carbohydrates and the hydrogen of the surrounding water is a central concept behind heterotrophic ^2H enrichment (Yakir & DeNiro, 1990; Roden *et al.*, 2000). However, we did not find any evidence for a link between the heterotrophic ^2H fractionation between sugar and cellulose in Chapter 3 and 4. Instead, the main factor influencing the $\delta^2\text{H}$ of cellulose is the $\delta^2\text{H}$ of sugar, including strong evidence for a respiratory ^2H enrichment in Chapter 5, as already indicated by the results of previous studies (Holloway-Phillips *et al.*, 2022). The post-photosynthetic respiratory ^2H enrichment could be caused by a preferential use of sugar with the lighter ^1H isotope during glycolysis, similar to the known tritium isotope equilibrium effects between glucose and human brain hexokinase (Lewis & Schramm, 2003).

Outlook

In order to develop a new model for ^2H fractionation in plant carbohydrates, further experiments and sampling campaigns addressing specific questions

are needed. For instance, the respiratory ^2H enrichment needs to be further investigated, such as in heterotrophic tissues in combination with studies on the nature of the ^2H fractionation during cellulose synthesis. In addition, a better understanding of carbohydrate fluxes and their dynamics over the seasons at the whole plant level is crucial to correctly model and interpret $\delta^2\text{H}$ values in plant carbohydrates such as NSC storage pools in xylem and root tissues or tree-ring cellulose.

References

- Augusti A, Betson TR, Schleucher J. 2006.** Hydrogen exchange during cellulose synthesis distinguishes climatic and biochemical isotope fractionations in tree rings. *New Phytologist* **172**(3): 490-499.
- Holloway-Phillips M, Baan J, Nelson DB, Lehmann MM, Tcherkez G, Kahmen A. 2022.** Species variation in the hydrogen isotope composition of leaf cellulose is mostly driven by isotopic variation in leaf sucrose. *Plant, Cell & Environment* **45**(9): 2636-2651.
- Lewis BE, Schramm VL. 2003.** Binding equilibrium isotope effects for glucose at the catalytic domain of human brain hexokinase. *Journal of the American Chemical Society* **125**(16): 4785-4798.
- Luo Y-H, Steinberg L, Suda S, Kumazawa S, Mitsui A. 1991.** Extremely low D/H ratios of photoproduced hydrogen by cyanobacteria. *Plant and Cell Physiology* **32**(6): 897-900.
- Luo Y-H, Sternberg LdSL. 1992.** Hydrogen and oxygen isotopic fractionation during heterotrophic cellulose synthesis. *Journal of Experimental Botany* **43**(1): 47-50.
- Niinemets U. 2007.** Photosynthesis and resource distribution through plant canopies. *Plant, Cell & Environment* **30**(9): 1052-1071.
- Niinemets Ü, Oja V, Kull O. 1999.** Shape of leaf photosynthetic electron transport versus temperature response curve is not constant along

- canopy light gradients in temperate deciduous trees. *Plant, Cell & Environment* **22**(12): 1497-1513.
- Roden JS, Lin G, Ehleringer JR. 2000.** A mechanistic model for interpretation of hydrogen and oxygen isotope ratios in tree-ring cellulose. *Geochimica et Cosmochimica Acta* **64**(1): 21-35.
- Sanchez-Bragado R, Serret MD, Marimon RM, Bort J, Araus JL. 2019.** The Hydrogen Isotope Composition $\delta^2\text{H}$ Reflects Plant Performance. *Plant Physiology* **180**(2): 793-812.
- Sternberg LdSL 1989.** Oxygen and hydrogen isotope ratios in plant cellulose: mechanisms and applications. *Stable Isotopes in Ecological Research*: Springer. 124-141.
- Wieloch T, Grabner M, Augusti A, Serk H, Ehlers I, Yu J, Schleucher J. 2022.** Metabolism is a major driver of hydrogen isotope fractionation recorded in tree-ring glucose of *Pinus nigra*. *New Phytologist* **234**(2): 449-461.
- Yakir D, DeNiro MJ. 1990.** Oxygen and hydrogen isotope fractionation during cellulose metabolism in *Lemna gibba* L. *Plant Physiology* **93**(1): 325-332.
- Zhang B-L, Billault I, Li X, Mabon F, Remaud G, Martin ML. 2002.** Hydrogen isotopic profile in the characterization of sugars. Influence of the metabolic pathway. *Journal of Agricultural and Food Chemistry* **50**(6): 1574-1580.

Acknowledgements

I would like to start by thanking the major contributors to this work, my three supervisors, **Nina Buchmann**, **Marco M. Lehmann**, and **Arthur Gessler**.

Also, I would like to add a special acknowledgment to my closest supervisor **Marco M. Lehmann**, who gave me the opportunity with this PhD and letting me developing my own scientific ideas and expertise in the field of plant ecophysiology and stable isotope research.

Jim Ehleringer from the University of Utah, I greatly appreciate the reviewing my thesis and co-examining my defense.

I am very grateful for the great former and current members of the isotope lab at WSL, **Matthias Saurer**, **Haoyu Diao**, **Elsa Östlund**, **Oliver Rehmman**, **Philipp Spiegel**, and especially **Valentina Vitali** and **Manuela Oettli**, who all supported me on my way throughout the last four years, teaching me various methods in the lab, helping me with many analysis in R, and by being there for emotional support. I especially want to thank **Margaux Didion-Gency** for becoming such an awesome friend and office mate: I am looking forward for many more fantastic moments with you in the future; I even consider to come back to Bremgarten at one point (but I am hoping for Barcelona). I want to deeply thank **Charlotte Grossiord** and **Leonie Schönbeck** for not only teaching me how to conduct ecophysiological measurements during endless weeks in the basement of ETH, but also for becoming highly appreciated friends. I would like to thank **Jonas Gessler** for all his technical expertise and the amazing support he is providing with the LiCor devices. I want to thank **Oliver Rehmman** for his support in the climate chamber and in the lab. I want to thank to all the great former and current members of the **Forest Dynamics Group** at WLS, especially **Elisabet Martinez-Sancho**, **Evrin Ayse Sahan**, **Yanli Zhang**, **Yann Vitasse**, **Maria Elvira Murazzi**, **Stefan Klesse**, **Antoine Cabon**, **Kerstin Treydte**, **Paula Ballikaya**, **Marçal Argelich Ninot**, **Petra D`Odorico**, **Frederik**

Baumgarten, Maihe Li, Georg von Arx, Stefan Hunziker, Anouchka Perret-Gentil, Flurin Sutter and Marcus Schaub.

I want to thank the members of the **Grassland Sciences group** at ETH, I always enjoyed your feedback about my work during the Grassland Seminars, and especially **Anna Gilgen** for all the helpful information and support she provided.

I am especially deeply grateful to **Lucas Cernusak** and his amazing group at James Cook University in Cairns, **Kali Middleby, Alex Cheesman, Arun Singh and Iftakharul (Russell) Alam**, for introducing me to the wet tropics of Australia, for showing me the amazing region during and after work, and bringing back my love for tropical ecosystems. But most importantly, for becoming friends! I also want to thank my dear friends from JCU PGC **Siddharth (Karens) Singh, Zhuoqun (Nero) Liu and Elena Ohara**. I am missing a lot to hang out with you, buying amazing food at Rusty's, and exploring Cairns area. I am grateful to **Janine Evans**; it was always a pleasure to talk with you about the various aspects of Australian plants, and to **Sophie Zwartsenberg**, it was amazing to core with you all these tropical trees, to check out JCU campus and to explore Cairns Botanic Gardens.

I am grateful to the EPFL group, **Eugénie Mas, Christoph Bachofen, Thibaut Juillard, Alex Tuñas Corzon, Laura Mekarni, Janisse Deluigi, Alice Gauthey** for all the fun times we had at WSL and in Pfynwald.

A special thanks to the gardeners at WSL, **Gabor Reiss, Claudio Cattaneo, Peter Schweizer, and Peter Suter**, for all their support they are providing all year round regarding the organisation and taking care of plants and related infrastructure.

I am grateful for all the other amazing people I have met at WSL, especially the entomologists **Doris Schneider, Maja Ilic, Michael Eisenring, and Bastiaan Drost**.

I would also like to thank all my beloved friends who are accepting me the way I am, some even letting me infiltrating their children with my love for nature and science as a godfather.

I am very grateful for my husband **Thomas**: for all your support during my studies, for taking care of all my plants during the time I was away, for all the love you gave me and for putting up with me for so long.

Ich danke auch von ganzem Herzen meinen Eltern für ihre Liebe, Akzeptanz und Unterstützung all die Jahre, meinen Geschwistern für die jahrelange Abhärtung, und meiner Grossmutter für all die Liebe und schönen Erinnerungen, die ich an sie habe.

Curriculum Vitae



Philipp Schuler

Swiss Federal Institute for Forest, Snow and Landscape Research WSL

Address: Zürcherstrasse 111, 8903 Birmensdorf, Switzerland

Contact: Tel. +41 76 377 4228 E-Mail: philipp.schuler@wsl.ch

Date of birth: 29.10.1986

Nationality: Swiss

ORCID-ID: 0000-0002-5711-2535

Research Gate: <https://www.researchgate.net/profile/Philipp-Schuler>

Google Scholar: <https://scholar.google.com/citations?user=P4mHAMAAAAJ&hl=de>

I am a plant-ecophysiologicalist, focussing on the biochemical and physiological drivers of stable (hydrogen) isotope fractionation. My goal is to learn how stable (hydrogen) isotopes are imprinted in plant carbohydrates, how this is interacting with the carbon balance of a plant, and how this is responding to changes in the environment.

Education:

- | | |
|----------------|--|
| 2019 - present | Doctoral student at ETH Zurich and WSL Birmensdorf |
| 2018-2019 | MSc in Environmental Geosciences, University of Basel |
| 2013-2018 | BSc in Biogeography and Environmental Geosciences, University of Basel |
| 2002-2005 | Apprenticeship as Lab Technician, Novartis Pharma AG |

Employment History

2006-2018 Scientific Associate, Biotechnology, Novartis Pharma AG

2005-2006 Lab Technician, Genetic Toxicology, Novartis Pharma AG

Supervision of Graduate Student

2020-2022 Co-supervisor of the Master-student Oliver Rehmann

Research abroad

2022-2023 Visiting the Terrestrial Ecology group of Prof. Lucas Cernusak of the Centre for Tropical Environmental and Sustainability Science at James Cook University in Cairns, Australia for 6 months

Contribution to Conferences

2023 *Unravel the metabolic drivers of ²H fractionation in plant carbohydrates to enable the triple isotope (²H/¹⁸O/¹³C) approach for tree-ring research.* TRACE Tree Rings in Archaeology, Climatology and Ecology annual meeting

2023 *Novel insights into the biochemical drivers shaping hydrogen isotope values of sugar and cellulose within a plants' leaf.* EGU General Assembly Conference

2022 *The phylogenetic impact on photosynthetic and post-photosynthetic hydrogen isotope fractionation in 73 tree species.* AEIC Australasian Environmental Isotope Conference

2022 *Decrypt the fundamental processes behind the $\delta^2\text{H}$ -fractionation in plant carbohydrates.* TRACE Tree Rings in Archaeology, Climatology and Ecology annual meeting

2022 *The phylogenetic impact on photosynthetic and post-photosynthetic hydrogen isotope fractionation in 73 tree species.* EGU General Assembly Conference

- 2021 *Development of an accurate and precise water-vapor equilibration method for hydrogen isotope analysis of plant non-structural carbohydrates and first applications.* Annual Meeting of the Ecological Society of America
- 2020 *New method for hydrogen isotope analysis of non-structural carbohydrates.* EGU General Assembly Conference

Major Collaborators

Marco M. Lehmann (WSL, Switzerland), Nina Buchmann (ETH, Switzerland), Arthur Gessler (WSL and ETH, Switzerland), Valentina Vitali (WSL, Switzerland), Matthias Saurer (WSL, Switzerland), Charlotte Grossiord (EPFL and WSL Switzerland), Leonie Schönbeck (EPFL Switzerland and University of California, U.S.A.), Haoyu Diao (WSL, Switzerland), Manuela Oettli (WSL, Switzerland), Lucas Cernusak (JCU, Australia), Margaux Didion-Gency (EPFL and WSL Switzerland)

Publication List

Published

Schuler P., Cormier M-A., Werner R. A., Buchmann N., Gessler A., Vitali V., Saurer M., Lehmann M. M. (2022). A high temperature water vapor equilibration method to determine non-exchangeable hydrogen isotope ratios of sugar, starch, and cellulose. *Plant, Cell, and Environment* **45**(1): 12-22

Schuler P., Vitali V., Gessler A., Buchmann N., Saurer M., Lehmann M. M. (2023). Hydrogen isotope fractionation in carbohydrates of leaves and xylem tissues follows distinct phylogenetic patterns: a common garden experiment with 73 tree and shrub species. *New Phytologist* **239**(2): 547-561

Lehmann M.M., Vitali V., **Schuler P.**, Leuenberger M., Saurer M. (2021). More than climate: Hydrogen isotope ratios in tree rings as novel plant

physiological indicator for stress conditions. *Dendrochronologia* 65, 125788

Schönbeck L. C., **Schuler P.**, Lehmann M. M., Mas E., Mekarni L., Pivovarov A. L., Turberg P., Grossiord C. (2022). Increasing temperature and vapor pressure deficit lead to hydraulic damages in the absence of soil drought. *Plant, Cell & Environment* 45(11): 3275-3289

Diao H., **Schuler P.**, Goldsmith G. R., Siegwolf R. T. W., M Saurer M., Lehmann M. M. (2022). On uncertainties in plant water isotopic composition following extraction by cryogenic vacuum distillation. *Hydrology and Earth System Sciences* 26(12): 5835-5847

Vitali V., Peters R. L., Lehmann M. M., Leuenberger M., Treydte K., Büntgen U., **Schuler P.**, Saurer M. (2023). Tree-ring isotopes from the Swiss Alps reveal non-climatic fingerprints of cyclic insect population outbreaks over the past 700 years. *Tree Physiology* 43(5): 706-721

Lehmann M.M., **Schuler P.**, Cormier M-A., Allen S. T., Leuenberger M., Voelker S. (2022). The stable hydrogen isotopic signature: From source water to tree rings. Chapter in: Siegwolf R. T., Brooks J. R., Roden J., Saurer M. (2022). *Stable isotopes in tree rings: Inferring physiological, climatic and environmental responses*. Springer: 331-359

Further publications from experiments I have conducted during my doctoral. thesis, not yet published

Schuler P., Rehmann O., Vitali V., Cernusak L., Oettli M., Gessler A., Buchmann N., Saurer M., Lehmann M. M. *Hydrogen isotope fractionation in plants with C₃, C₄, and CAM CO₂ fixation*

Schuler P., Didion-Gency M., Diao H., Vitali V., Oettli M., Gessler A., Buchmann N., Saurer M., Lehmann M. M. *Hot and Hungry: High temperatures induced carbohydrate depletion in plant leaves - insights from triple isotope fractionations*

Schuler P., Schönbeck L. C., Grossiord C., Vitali V., Gessler A., Buchmann N., Saurer M., Lehmann M. M. *The impact of temperature, VPD, and drought on plant internal hydrogen isotope fractionation and how this is imprinted in tree ring cellulose*